" A STUDY OF THE ANODIC BEHAVIOUR OF ALUMINIUM ALLOYS IN ALKALINE ELECTROLYTES."

A Thesis submitted for
the Degree of Doctor of Philosophy.
by

Barry Neil Walters.

Chemical Energy Research Centre,
Department of Chemistry,
City University,
Northampton Square,
London EC1V OHB.

This work was carried out under the supervision of
Professor A.C.C. Tseung, and sponsored by
the S.E.R.C.

October 1988.

* It was pointed out by the examiners that the exchange current density is a measure of the speed of the electrode reaction at its reversible potential. As the half cell tests carried out result in an irreversible reaction, then it is the rate constant k_2^o that is actually measured.

Dedication.

I would like to dedicate

this work to

Lynette Walters

whose love, support and

understanding provided the

foundations of all my

achievements.

ACKNOWLEDGEMENT.

During the period of my research I have been fortunate enough to receive the support of many people and it is impossible to mention them all. However, I would like to take this opportunity to express my gratitude to a certain few who, in various but equally important ways, were extremely supportive during these years.

I would like to offer my sincere thanks to Prof. A.C.C. Tseung for his continuous encouragement and guidance throughout this project. Also I would like to extend my gratitude to Prof. Z.G. Lin for his enthusiasm and interest in my work during my stay at Xiamen University.

I am greatly indebted to Dr. Sam Elbeik for his patience and encouragement during my first year. Also I appreciate the time spent by Dr. Sanping Jiang and Dr. Lyn Bevan in discussing ideas and reading this thesis. My thanks also go to all lecturers and colleagues at both the Chemical Energy Research Centre, City University, and the Electrochemistry group at Xiamen University, who have taken an interest in my work. I would like to thank Mr. Mike Phillips and Mr. Fa Yang Wang of the Electron Microscope Centres at City and Xiamen University respectively, for their efforts, and I also acknowledge the help of Mr. Nigel Jones in X-ray Diffraction Analysis and Mr. Adrian Taylor in Atomic Absorption, City University.

I would like to express my gratitude to my Father for his continuous support throughout my time in higher education. Finally, I would like to say a big thank-you to my family and close friends especially Simon, Rachel, Nicky, Paul and Chris, for putting up with me during the last three years!

Barry Walters

October 1988.

ABSTRACT.

Recent studies on the discharge performance of aluminium alloys in alkaline media have led to improved alloys with significantly lower corrosion rates and more anodic potentials. Performance of various alkaline electrolytes have also been examined and considerable progress has been made in this area. A review of the available literature reveals a list of several elements which are suitable for alloying with aluminium as regards reducing corrosion and overpotential. Previous work at the Chemical Energy Research Centre, City University, showed that with an aluminium alloy Q4, which contained additives of bismuth, lead, magnesium, titanium and zinc, improved characteristics were obtained on comparison to the performance of bulk manufactured aluminium. Furthermore, on discharging the alloy in a novel electrolyte developed at City, which consisted of a 1:1 mixture of 50% (w/v) sodium hydroxide and 30% (w/v) potassium hydroxide, improvements in performance were observed when compared to the results obtained from discharge in the traditionally used 30-40% (w/v) potassium hydroxide. Firstly, in full cell discharge (where the aluminium anode was coupled with an oxygen reduction cathode), the operating life of the cell was considerably longer (up to as much as 50%). Secondly, and probably more important, was the fact that the

power output was also significantly greater. As for reducing hydrogen evolution, several alloying elements had this effect. However, work done showed that the most effective means of minimising corrosion was to use electrolyte additives. The most suitable electrolyte additive was found to be mercuric oxide. The presence of mercury as an electrolyte additive has a distinct advantage over alloying the metal with aluminium. In the case of the latter, the amalgam formed results in the oxide layer being broken down and the alloy becomes unstable in the atmosphere. Saturation of the electrolyte with mercuric oxide poses no such problems. Also as the solubility of mercury in alkaline solution is so small (ca. 5×10^{-7}wt% in 5M potassium hydroxide) there is no significant toxicity problem.

Four commercially available aluminium alloys of varying compositions were obtained from aluminium companies involved in the research and development of aluminium air batteries. It was decided to extend the examination of the mixed alkaline electrolyte to these alloys and study the performances using various electrochemical techniques. The role of mercuric oxide on the discharge process was also further investigated.

Study of the anodic behaviour of the aluminium alloys was achieved using the traditional electrochemical half cell tests employing various alkaline electrolytes. Half cell tests indicated that the most negative potential and the highest limiting current density values were actually obtained using

potassium hydroxide electrolyte. However, this tended to be overshadowed in the full cell tests by the considerably longer operating life of the cells employing the mixed electrolyte. The overall results indicate the superior performance of alloys containing significant quantities of tin and titanium. Also, the full cell performance of the alloy New Q4, containing the same additives as Q4 but in different quantities, was also extremely attractive. These elements are believed to form a layer on the electrode surface during discharge, thereby controlling the dissolution of the aluminium and preventing excessive hydrogen evolution and cause an anodic shift in potential.

Evidence of the formation of these layers on the electrode surface was not easily obtained. EDAX mapping of the electrode surface revealed some interesting micrographs in which the quantities of some these elements on the electrode surface appeared to increase after discharge. This evidence was inconclusive however, as the element to aluminium ratio was too small for any value to be recorded. This did suggest though that certain elements like tin and titanium did form a layer on the surface. It was then decided to carry out ESCA work on the electrode surfaces both prior to and after discharge. ESCA did reveal that certain elements were present on the electrode surface after discharge, and thus suggests that the formation of a layer of an element on the electrode surface during discharge is likely.

Some preliminary ellipsometry experiments were performed to study the effect of the various alloying elements on the oxide film present on the aluminum surface. Initial experiments revealed interesting information in that the alloys behaved differently. It seems that the surface structure is extremely sensitive to the composition of the alloy. Further work in this area could lead to more information about the oxide film and the most suitable alloying elements for rapid breakdown of the layer on commencing discharge.

The various electrolytes used for the experiments resulted in a different reaction product structure on precipitation of aluminium hydroxide. With potassium hydroxide electrolyte a fine white precipitate is obtained which completely smothers the electrode surface. With the electrolyte mixture, a granular precipitate is obtained which may allow the diffusion of ions to and from the electrode surface after passivation has occurred. This coupled with the greater solubility that the electrolyte mixture has for aluminate, results in longer operating life of the full cell system. Another factor is that the granular electrolyte is easily removed from the cell by washing, unlike the precipitate from use of potassium hydroxide. This enables the actual cells to be used for longer periods as the active sites on the cathode are not covered by this fine white precipitate. Also the stability of the mixed electrolyte after passivation is of benefit as complete precipitation from the electrolyte does not occur. With potassium hydroxide electrolyte, complete precipitation occurs

as soon as passivation commences.

Use of mixed electrolyte in full cell tests always resulted in longer operating life for every alloy. However, only two of the four alloys under test showed a significant power output increase. It must be noted though that the build up of precipitate during the operation of the cell affects the performance. Use of a pump enabling the electrolyte to circulate through the cell and an external reservoir would be expected to reveal the effect of the higher solubility of the mixed electrolyte to a greater extent. The alloys which did show greater power output from use of the mixed electrolyte were numbers 2 and 3, the former being a low corrosion alloy and the latter containing significant proportions of tin and titanium. However, the stability and reaction product structure make it desirable for all alloys in aluminium air cells to be discharged in a mixed electrolyte of sodium and potassium hydroxide rather than the traditionally used potassium hydroxide.

Finally the effect of adding mercuric oxide to the electrolyte was examined using a novel electrode microzone scanning current measurement technique. This technique allowed the in situ examination of the current distribution on the electrode surface to be measured. Conclusive new evidence was found regarding the effect of mercury on corrosion current, current distribution and the superior characteristics of the material as an electrolyte additive rather than an alloying element.

CONTENTS

List of Figures.

List of Tables.

CHAPTER 1.

INTRODUCTION.

1. Introduction.

There exists an opening in the electrochemical power source market for a high energy density, low cost system. A major potential use is in the field of portable equipment, where there is no ideal power source for computers, television video cameras and power tools. Another area which could be exploited is submersible equipment. The use of aluminium as a battery anode is extremely attractive because of its high electrochemical equivalent and theoretical specific energy values. Aluminium has a high energy content (free energy of formation of $Al_2O_3.3H_2O$ equals - 2295 kJ/mol)[1]. Comparisons between aluminium and other metals are made in Table 1.1.

Table 1.1 Electrochemical Comparison of Various Metals.

Metal	Electrochemical Equivalent Ah/g	Theoretical Cell Voltage* V	Theoretical Specific Energy Wh/g	Operating Voltage V
Lithium	3.86	3.4	13	2.4
Aluminium	2.98	2.7	8.1	1.6
Magnesium	2.20	3.1	6.8	1.4
Calcium	1.34	3.4	4.6	2.0
Zinc	0.82	1.6	1.3	1.2
Iron	0.96	1.3	1.2	1.0

* Voltage when coupled with an oxygen electrode.

Another property of aluminium is that the metal is

amphoteric and so the cell can operate over a wide range of pH values. Aluminium's low price, related to the fact that it is the most common metal found in the earth, and it's good handling characteristics are further attractive features.

The idea of using aluminium as an anodic material is not new. Indeed the first patents were filed in the late 1850's on systems using aluminium anodes, carbon cathodes and nitric acid electrolytes [2,3]. Since this period, a great deal of research has been carried out, resulting in the filing of many patents during the first half of the twentieth century eg. [4-10], on the use of aluminium as a battery anode. An excellent historical review of the available literature covering the systems using aluminium anodes and employing various cathodes and electrolytes is given by Quarshie [11].

Efforts in the latter half of this century have led to the coupling of aluminium with an air (oxygen) electrode because of the latter's low weight and infinite capacity. Also the boom period of fuel cell research has resulted in advances in technology yielding high current density air electrodes suitable for use with alkaline electroloytes.

The first reported aluminium air system was by Zaromb [13] in the 1960's, who claimed that current densities on aluminium of up to 1 A/cm^2 were feasible. Since then

several prototypes have been proposed and this research work has been carried out by many research groups in various countries. One of the major research groups is an aluminium company, Alcan International. With the decline in price of aluminium during the 1970's, the company looked to alternative uses for it's product. The research group has grown internationally with centres in Canada and the U.K. with links to several University groups. Alcan have marketed an emergency light using aluminium air cells, though the electrolyte employed is neutral chloride. Much of the work carried out by Alcan and it's associates has been related to the search for suitable aluminium alloys for discharge in both saline and alkaline electrolytes. However, they have also worked on a project on electrolyte management of alkaline battery systems for the U.S. Department of Energy, and on the development of a saline aluminium air power pack capable of being refuelled and used in combination with a lead acid cell as an electric vehicle power source, for the Canadian government [14].

The Norwegian Defence Research Establishment have built a 120 Watt prototype to power communications equipment. Their present objective is to construct a 500W, 12V, 600Ah battery for the Norwegian Army, with a weight less than 20kg [15].

Aluminium Air cells can use both alkaline and saline electrolytes. The saline electrolyte, typically sodium chloride results in an energy density of up to 160Wh/kg, and

a power density of 20W/kg. Use of an alkaline electrolyte however, results in significantly higher values, with an energy density of 400Wh/kg and a power density of 170W/kg [16].

There are major technological problems however, which have hindered the progress of the development of commercially available aluminium air cells. The high standard electrochemical potential is not achieved in practice, probably due to the presence of an oxide layer on the metal surface [17]. Alloying the aluminium with certain elements certainly reduces this problem and an anodic shift in potential is observed. However, this potential remains significantly lower than the theoretical value.

Another problem is wasteful cathodic corrosion of aluminium [18]. This is a well known phenomenon and various attempts have been made to inhibit hydrogen evolution by alloying the aluminium with suitable elements [14] or by using certain electrolyte additives [11,12]. Whilst this has the effect of minimising corrosion it cannot completely eradicate it. Today, researchers are looking towards the use of hydrogen oxygen recombination systems to further minimise the effects of corrosion.

Production of copious amounts of reaction product is another factor which has to be taken into account. When the alkaline electrolyte (typically 30-40% potassium hydroxide)

becomes saturated with aluminate, it precipitates out as a white solid and clogs the cell. This has led many researchers to use sodium hydroxide electrolyte which results in a granular precipitate, which is easily flushed out of the cell. However, conductivity is lower in sodium hydroxide, and a slightly lower potential is observed.

Research at City University on aluminium air has in recent years been focussed on the alkaline electrolyte system, believing that the future of the cell lies in it s exceptionally high energy and power density values. Attempts have been made to minimise some of the previously mentioned problems, and significant progress has been made. Quarshie [11], discovered that by mixing sodium and potassium hydroxide electrolytes a dramatic increase in solubility of aluminate is achieved (see Figure 1.1) This enabled an aluminium air cell to function for a period up to 50% longer, thereby having a significantly greater power output. This work was performed on an aluminium alloy with trace amounts of zinc, lead, bismuth and gallium added. Further work by Quarshie showed that saturation of the electrolyte with mercuric oxide, greatly reduces hydrogen evolution. As the solubility of mercuric oxide in alkali is extremely low (ca. 5×10^{-7} wt% in 5M potassium hydroxide) it is not a toxicity problem. This work has subsequently been filed as a patent [19].

The aims of this work were to further investigate the effect

Figure 1.1 Comparison of the Solubility of Reaction Product in Electrolyte Mixture with the Solubility in Conventional Alkaline Electrolyte.

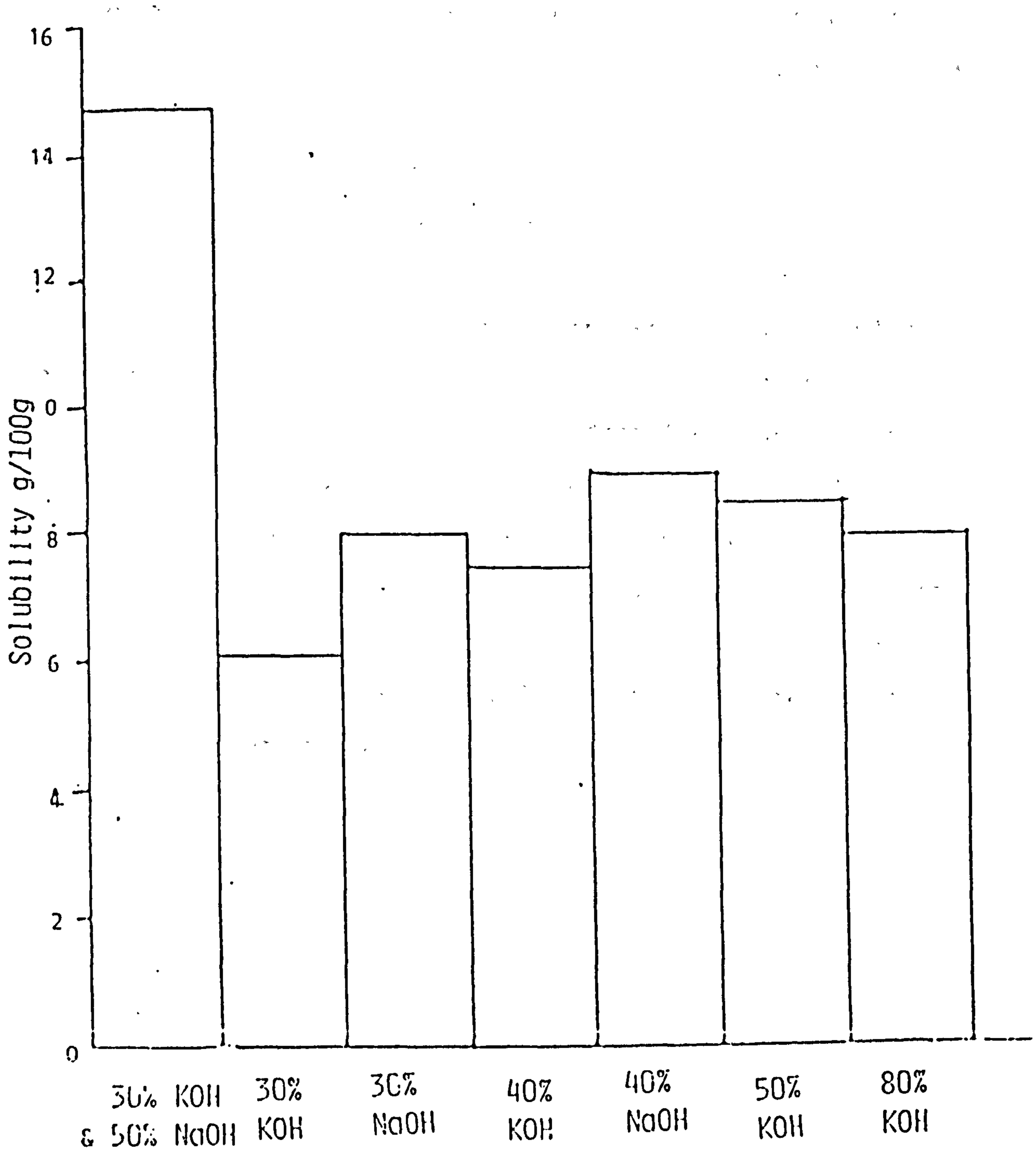

of the mixed electrolyte on the dissolution of aluminium and to extend the examination to a range of commercially available alloys of differing compositions. Progress has been made at City University to overcome some of the previously mentioned problems that are associated with aluminium air. This work attempts to explain how the improvements made to the system actually work.

Firstly, the effect of mercury was investigated, in order to determine the role of the material in the discharge process. The structure of the reaction product from use of mixed electrolyte was also further examined, and the possible role that this has in increasing the operating life of the cell is also discussed. Preliminary investigations were also carried out to study the effect of alloy composition on the aluminium surface. Finally full cell tests were performed to establish which alloys performed best under stated conditions.

CHAPTER 2.

PRINCIPLES OF CELL OPERATION AND ELECTRODE PROCESSES.

2.1 Principles of the Aluminium Air Cell.

An electrochemical cell converts the energy of chemical reactions into direct current electricity. All cells consist of a positive electrode, the cathode, a negative electrode, the anode, and also an electrolyte. During discharge, oxidation and reduction reactions take place. Electrons are formed by oxidation of the anode and travel via an external circuit to the cathode where they are absorbed. Reduction therefore occurs at the cathode and electric current passes from cathode to anode in the external circuit. The electrolyte provides the medium in which the electrochemical reaction of the cell occurs.

2.1.1 The Anode.

On discharge in alkaline electrolyte aluminium is oxidised as follows ;

(2.1) $Al + 4OH^- \dashrightarrow Al(OH)_4^- + 3e$

The standard electrochemical potential of aluminium in alkaline media is given as -2.35V [20].

However, this high reversible potential of aluminium is never achieved in practice due mainly to the following two reasons ;

(i) The overpotential required for anodic dissolution of

aluminium is extremely high due to the presence of a protective oxide layer on the surface [21]. Even at open circuit a large part of the potential is lost because of this resistive layer causing a potential shift in the positive direction. This fact has been cited by several authors [20, 22, 23, 24, 25].

(ii) Some aluminium is dissolved by wasteful corrosion to evolve hydrogen [21, 22, 24, 26, 27, 28, 29, 30]. This reaction may be regarded as the sum of reaction (2.1) and ;

(2.2) $2H_2O + 2e \text{ -------> } 2OH^- + H_2$

which both occur at the anode. The overall corrosion reaction is given by ;

(2.3) $2Al + 6H_2O \text{ -------> } 2Al(OH)_3 + 3H_2$

and occurs even when no current is being passed. As the potential is driven in the positive direction in dissolving the aluminium alloy, hydrogen evolution increases with increasing current, and the anodic efficiency is considerably reduced. The efficient use of aluminium as an anode material depends on the ability to inhibit reaction (2.3).

As polarisation occurs, the potential generally increases with respect to time (see Figure 2.1). This is due to the

electronic resistance of the electrode and the rate of diffusion of reactants and products in the electrolyte. Finally, passivation occurs at a particular current density value known as the limiting current density.

2.1.2 The Cathode.

At the air electrode oxygen is electrochemically reduced to form hydroxyl ions ;

(2.4) $O_2 + 2H_2O + 4e \text{ -------> } 4OH^-$

The use of such an electrode is distinctly advantageous due to its 'infinite' capacity, which exists due to the abundance of oxygen in the atmosphere.

The air electrode [31, 32] consists of an outer hydrophobic layer of polytetrafluoroethylene (henceforth PTFE) and carbon. Nickel mesh is present as a current collector and is coated with either cobaltous oxide or platinum on carbon catalyst, graphite and PTFE (see Figure 2.2).

Figure 2.1 Polarisation Curve for Aluminium.

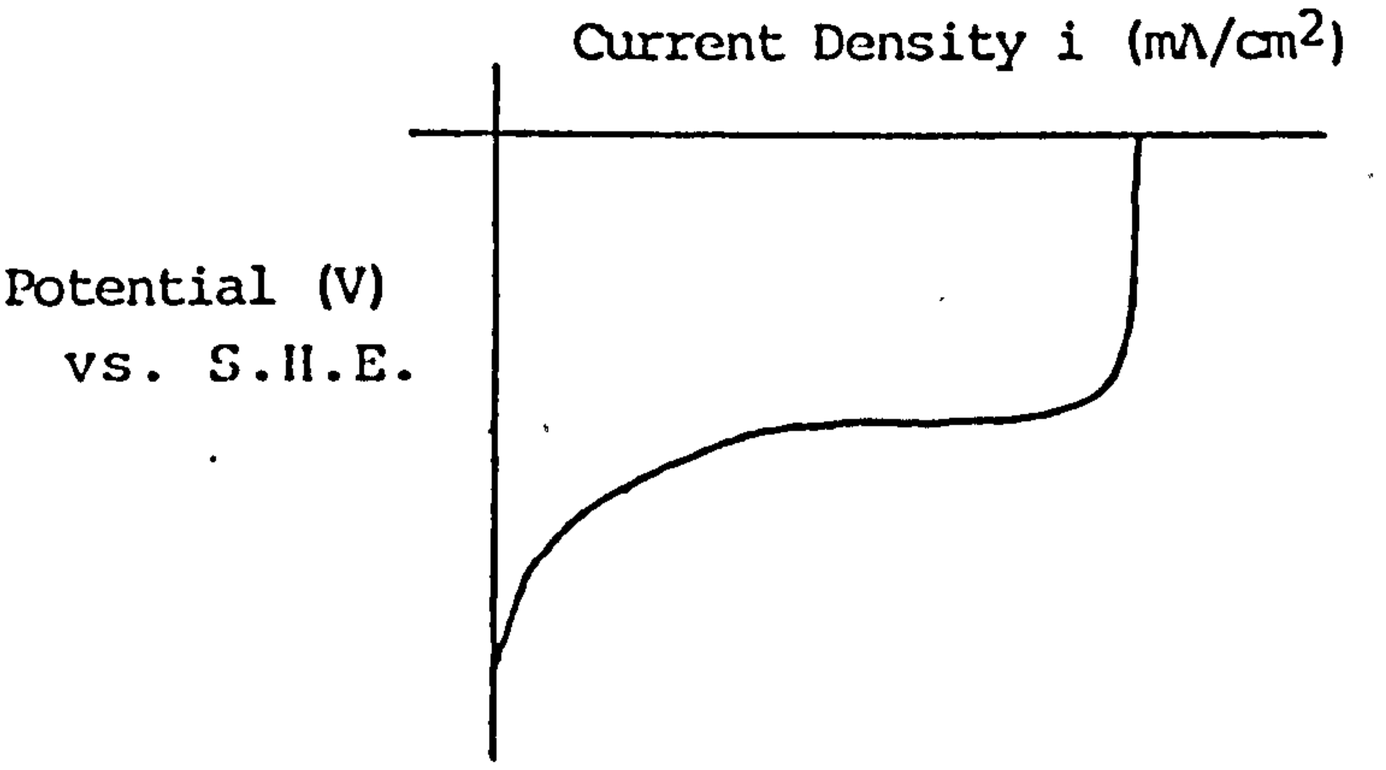

Figure 2.2 Structure of Air Electrode.

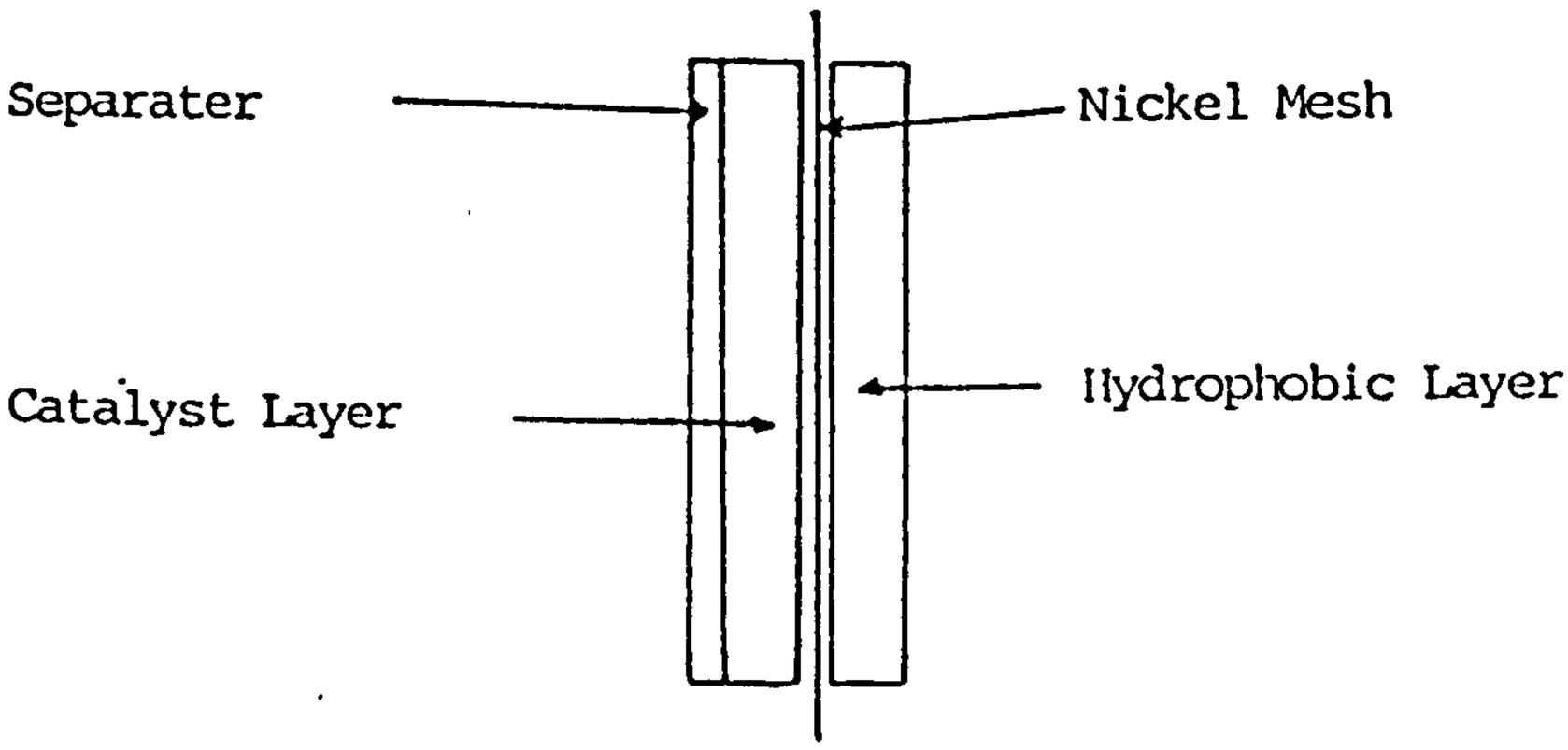

Figure 2.3 Polarisation Curve for the Air Electrode.

1.23 Theoretical Potential

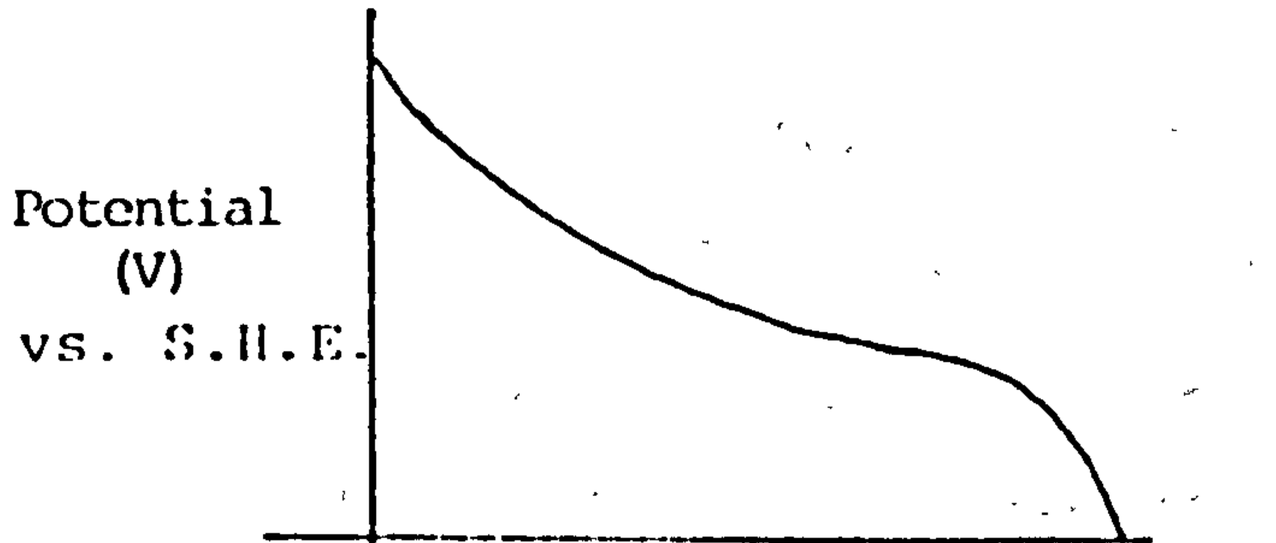

The electrode reaction occurs in the vicinity of three adjacent phases. The oxygen from the atmosphere in the gaseous phase, the electrolyte in the liquid phase and the electronic conductor is solid.

The function of the PTFE and carbon is to stabilise the gas liquid interphase. Electrolyte is permitted to enter the air electrode by capillary action through the small PTFE pores. However, the large PTFE particles act as wet proofing agents by raising the contact angle between the electrolyte and the particles. Whilst this prevents leakage, it allows oxygen to enter and make contact with the entire area of the catalyst present. 5% platinum on carbon is the active catalyst employed as it promotes the electron transfer reaction for the reduction of oxygen. However, in a commercial environment, a more economically feasible catalyst, cobaltous oxide would be used. Both catalysts are resistant to attack from the electrolyte. The nickel mesh acts as a structural membrane as well as a current collector. Finally a zirconium layer is painted onto the interior of the air electrode and acts as the separator.

The cathodic reaction therefore only occurs on the surface of a conducting, catalytic electrode in contact with both oxygen and electrolyte. A major requirement of the design of an air electrode is thus the accommodation of a system which stabilises the interfaces between the gas, liquid and solid

phases and maximises the overall area of contact.

The polarisation curve for the air electrode is shown in Figure 2.3. The theoretical potential in alkaline electrolyte for the reduction of oxygen is given as 0.401V [33]. As current is drawn the cell suffers a further loss of voltage, possibly due to a concentration difference in gas supply and to the rate of electron transfer. As in anodic polarisation, the current reaches a value where increase results in a dramatic decrease of potential and this is the cathodic limiting current.

2.1.3 The Electrolyte.

Electronic current does not pass between the electrodes via the electrolyte. The electrolyte acts as an ionic conductor enabling the ionic species produced at one electrode to travel to another.

The electrolyte used in the aluminium air cell can be either acid or alkali, due to the amphoteric nature of the electrode reactions. Both are feasible though both have particular disadvantages. Acid electrolytes may corrode the current collector and catalyst, making necessary the use of the more expensive platinum. Alkali electrolytes tend to become carbonated on exposure to air, and as the carbonate concentration increases it may precipitate out in the pores thus damaging the air electrode structure ;

(2.5) $CO_2 + 2KOH \text{ ------> } K_2CO_3 + H_2O$

However, alkali electrolyte is generally used for a high power aluminium air cell.

2.1.4 The Full Cell.

Therefore, in an aluminium air cell, the air electrode is the cathode and the aluminium is the anode. The electrolyte employed in this system is alkali. All cell reactions and potentials are given below. The potential values are with respect to the standard hydrogen potential at 25^oC, 1 atmosphere pressure in a 1 molar solution of hydrochloric acid.

Anode

(2.1) $Al + 4OH^- \text{ ------> } Al(OH)_4^- + 3e$ $\qquad E_o = -2.35V$

Cathode.

(2.4) $O_2 + 2H_2O + 4e \text{ ------> } 4OH^-$ $\qquad E_o = 0.401V$

Overall Cell Reaction

(2.6) $4Al + 3O_2 + 4OH^- + 6H_2O \text{ ----> } 4Al(OH)_4^-$ $\quad E = 2.75V$

Electrolyte Regeneration

(2.7) $Al(OH)_4^-$ -------> $Al(OH)_3 + OH^-$

Net Reaction of Full Cell

(2.8) $4Al + 3O_2 + 6H_2O$ -------> $4Al(OH)_3$

Corrosion Reaction occurs as a result of equation (2.1) and ;

(2.2) $2H_2O + 2e$ -------> $2OH^- + H_2$ E_o =-0.83V

to give ;

(2.3) $2Al + 6H_2O$ -----> $2Al(OH)_3 + 3H_2$ E = 1.50V

Thus for efficient cell operation the following are required ;

(i) a ready supply of reactants for reactions (2.1) and (2.4),

(ii) regeneration of the electrolyte, reaction (2.7), and

(iii) inhibition of reaction (2.3) [27].

In general the aluminium air cell has been categorised as a primary system, or as a mechanically rechargeable cell in which a sheet of aluminium anode once discharged is replaced

Figure 2.4 Schematic Diagram of Full Cell.

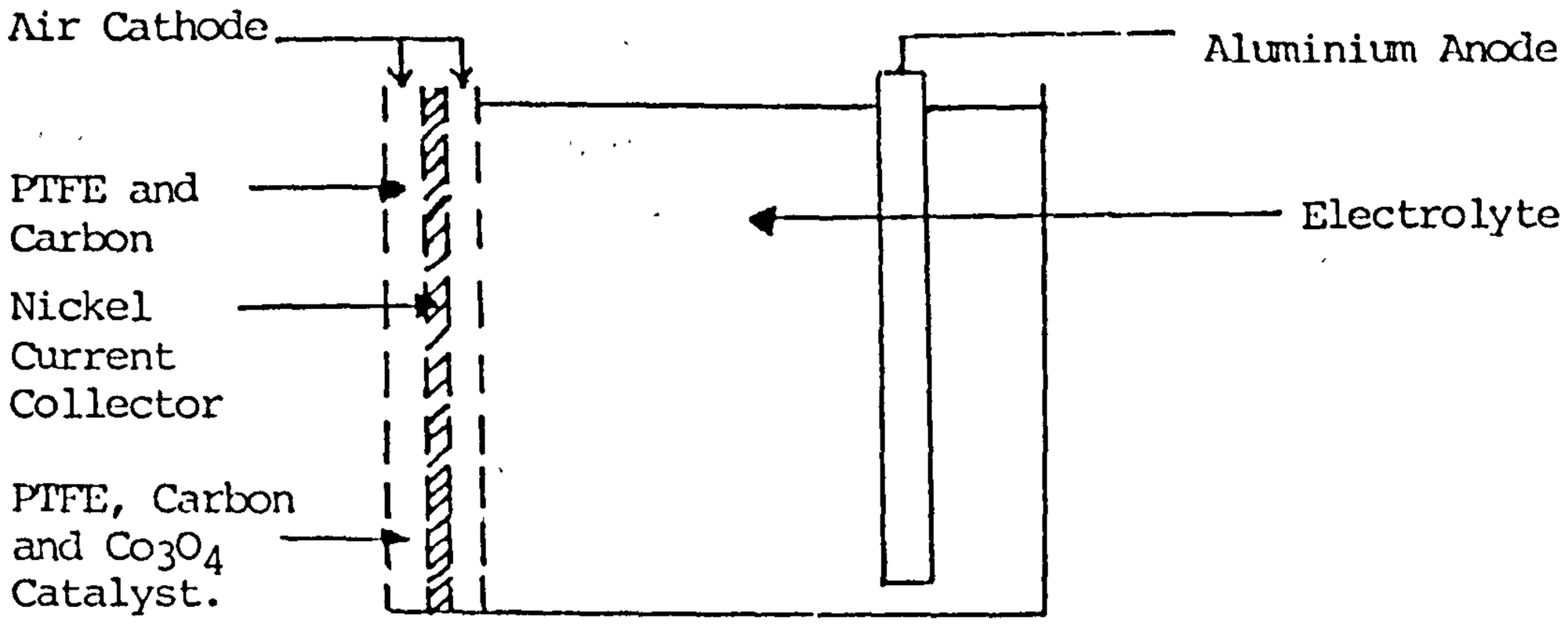

by a new one [34]. Perhaps a more accurate definition is that it is a hybrid cell, using fuel cell technology as well as material from within the cell. A fuel cell may be defined as a cell in which the reactants are continuously fed into the system. Aluminium air cells incorporate fuel cell technology as oxygen from the atmosphere is reduced at the cathode, and as the supply is inexhaustable, it may be provided continuously. A schematic diagram of the cell is given in Figure 2.4.

2.2 Electrode Processes.

2.2.1 Electrode Kinetics.

Equilibrium Electrode Potentials.

If a metal is partially immersed in a solution of its ions, a potential difference is established between the metal and the solution. Some metal atoms are ionised ;

(2.9) $M \text{ ------> } M^{n+} + ne$

In solution some metal ions will take electrons from the metal and deposit as metal atoms ;

(2.10) $M^{n+} + ne \text{ ------> } M$

Eventually an equilibrium will be set up between the two processes ;

(2.11) $M \quad <=======> \quad M^{n+} + ne$

The final potential that is established by the metal can be determined by coupling with a standard hydrogen electrode. The latter has a potential which is arbitrarily taken as zero and this enables the standard electrode potential of the metal to be determined.

The Nernst Equation.

The van't Hoff reaction equation expresses the free energy change (ΔG) for a chemical reaction in the form ;

$$(2.12) \quad \Delta G = \Delta G^{o} + RT\ln \frac{(\text{activity of products})}{(\text{activity of reactants})}$$

where ΔG^{o} is the Standard Free Energy Change

R is the Gas Constant

F is the Faraday.

Thus with respect to equation (2.11), equation (2.12) can be written in the form ;

$$(2.13) \quad \Delta G = \Delta G^{o} + RT\ln \frac{a_M}{a_M{}^{n+}}$$

The free energy change of a reversible electrode reaction is related to the electrode potential by ;

$$(2.14) \quad \Delta G = -nFE$$

or for the standard state ;

$$(2.15) \quad \Delta G^{o} = -nFE_{o}$$

Substituting the equation (2.15) and (2.14) into (2.13) ;

$$(2.16) \quad nFE = nFE_{o} + RT\ln \frac{a_M^{n+}}{a_M}$$

and

$$(2.17) \quad E = E_{o} + \frac{RT}{nF} \ln \frac{a_M^{n+}}{a_M}$$

or in general ;

$$(2.18) \quad E = E_{o} + \frac{RT}{nF} \ln \frac{[O]}{[R]}$$

which is known as the Nernst Equation.

It is generally assumed that the activity coefficients of O

and R species are unity so that concentrations rather than activity may be used in the Nernst Equation.

At equilibrium potential there is no net current flowing and so there is no overall chemical change. This means that the exchange current density i_o is equal to the current densities of both forward and backward reactions ;

$$(2.19) \quad i_o = i_a = i_c$$

Non Equilibrium Potentials.

If a potential is applied to an electrode process so that a large current flows, the electrode equilibrium is affected. This means that if the current is to be maintained a shift in potential must occur (in a more positive direction than E_o for an anodic process and a more negative direction for a cathodic process), and the electrode process becomes unidirectional and is said to be irreversible. The difference between the shift in potential and E_o is known as the overpotential η ;

$$(2.20) \quad \eta = E - E_o$$

For the process

$$(2.21) \quad O + ne \underset{k_2}{\overset{k_1}{<=======>}} R$$

k_1 and k_2 are the rate constants for the forward and backward reactions respectively.

At any potential the measured current density is given by ;

$$i_o = i_a + i_c \qquad (2.22)$$

The values of i_a and i_c are dependent on ;

(i) the rate constant for that particular reaction,

(ii) the concentration of the reduced/oxidised species at the electrode surface.

thus,

$$i_c = -nFk_1[O]$$

$$i_a = nFk_2[R] \qquad (2.23)$$

The rate constants actually vary with the applied electrode potential and are related in the following manner ;

$$k_1 = k_1^{o} \exp\left(-\alpha_c \frac{nFE}{RT} \right)$$

$$k_2 = k_2^{o} \exp\left(\alpha_a \frac{nFE}{RT} \right) \qquad (2.24)$$

where α_a and α_c are the transfer coefficients for the respective reactions.

Equations (2.19), (2.20), (2.24) and (2.25) can be used to mathematically derive the Butler Volmer Equation [35];

$$(2.25)\quad i = i_o\left[\exp\left(\frac{\alpha_a nF\eta}{RT} \right) - \exp\left(- \frac{\alpha_c nF\eta}{RT} \right) \right]$$

This is one of the most basic equations of electrode kinetics and gives the relationship between the current density and the exchange current density, overpotential and transfer coefficients.

The Tafel Equation.

There are limiting forms of equation (2.25) ;

(i) If the overpotential η is small, equation (2.25) can be simplified to

$$(2.26)\quad i = i_o \frac{nF\eta}{RT}$$

(ii) At high overpotentials with respect to the cathodic reaction, equation (2.25) can be expressed as ;

$$(2.27)\quad \log -i = \log i_o - \frac{\alpha_c\, nF}{2.303RT}\,\eta$$

or

$$(2.28)\quad \eta = \frac{2.303RT}{\alpha_c nF}\,\log i_o - \frac{2.303RT}{\alpha_c nF}\,\log i$$

(iii) For large overpotentials with respect to the anodic reaction, equation (2.25) can be expressed as ;

$$(2.29)\quad \log i = \log i_o + \frac{\alpha_a\, nF}{2.303RT}\,\eta$$

or

$$(2.30)\quad \eta = \frac{-2.303RT}{\alpha_a nF}\,\log i_o + \frac{2.303RT}{\alpha_a nF}\,\log i$$

Equations (2.28) and (2.30) can be expressed as ;

$$(2.31)\quad \eta = a + b \log i$$

and this is known as the Tafel Equation.

From equation (2.31), (2.30) and (2.28) it can be seen that;

$$(2.32)\quad -a/b = \log i_o$$

The overpotential for the aluminium electrode is determined

for various current density values and a graph of η (iRfree) versus log i can be plotted. The Tafel equation constants a and b can be obtained from the intercept and slope of the graph respectively. Thus the exchange current density may be calculated using equation (2.32).

2.2.2 Overpotential.

As previously stated the difference between the reversible and irreversible electrode process is known as the overpotential. Overpotential can be associated with two principal causes ;

(i) Ohmic polarisation. This occurs in the almost linear region of the characteristic voltage current curve (see Figure 2.5 c)) and is caused by;

(a) the `iR' drop between the luggin capillary and working electrode in a half cell, or between the two electrodes in a full cell system, and

(b) the resistance caused by products of cell reactions.

(ii) Polarisation from electrode process losses. The discharge of ions at an electrode involves three main stages ;

(a) transport of ions to the electrode surface,

(b) discharge of ions to form atoms,

(c) conversion of atoms to a stable form.

The passivation caused by (a) is termed concentration overpotential, and that which arises from (b) and (c) is termed activation overpotential. Activation overpotential can be seen in the rapid fall in cell potential at low current drain (see Figure 2.5 a)). The majority of overpotential in the dissolution of metals comes from concentration overpotential and this can be seen in Figure 2.5 b).

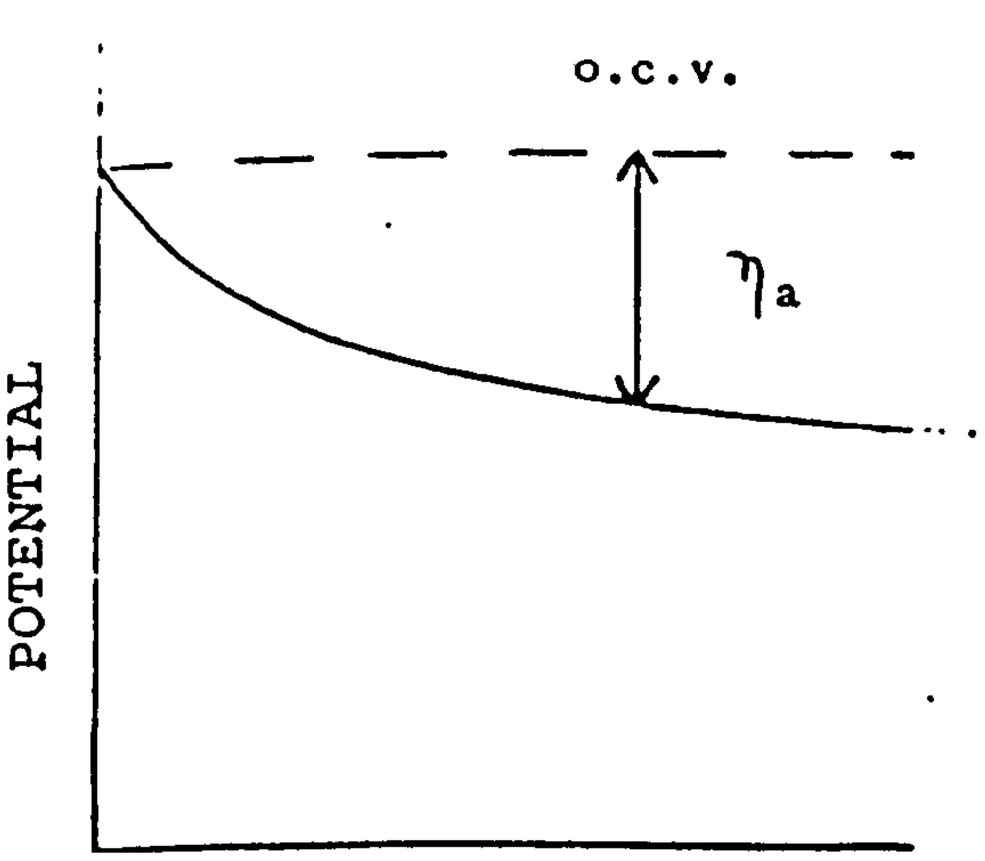

(a) ACTIVATION OVERPOTENTIAL

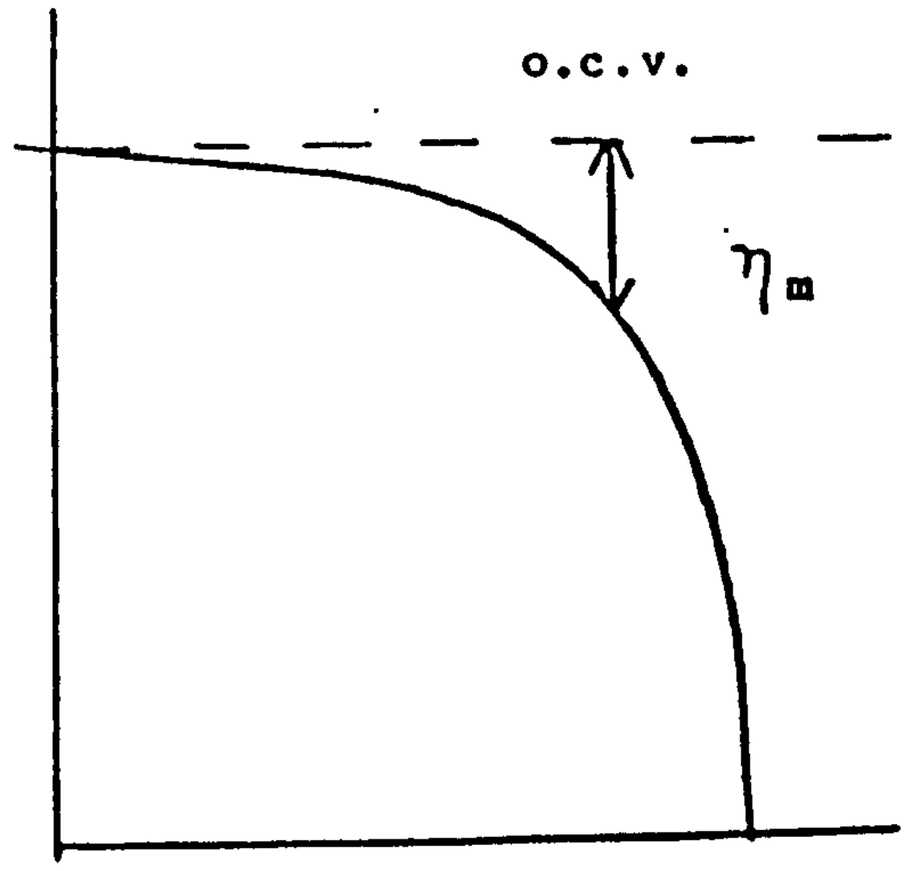

(b) MASS-TRANSFER/CONCENTRATION OVERPOTENTIAL

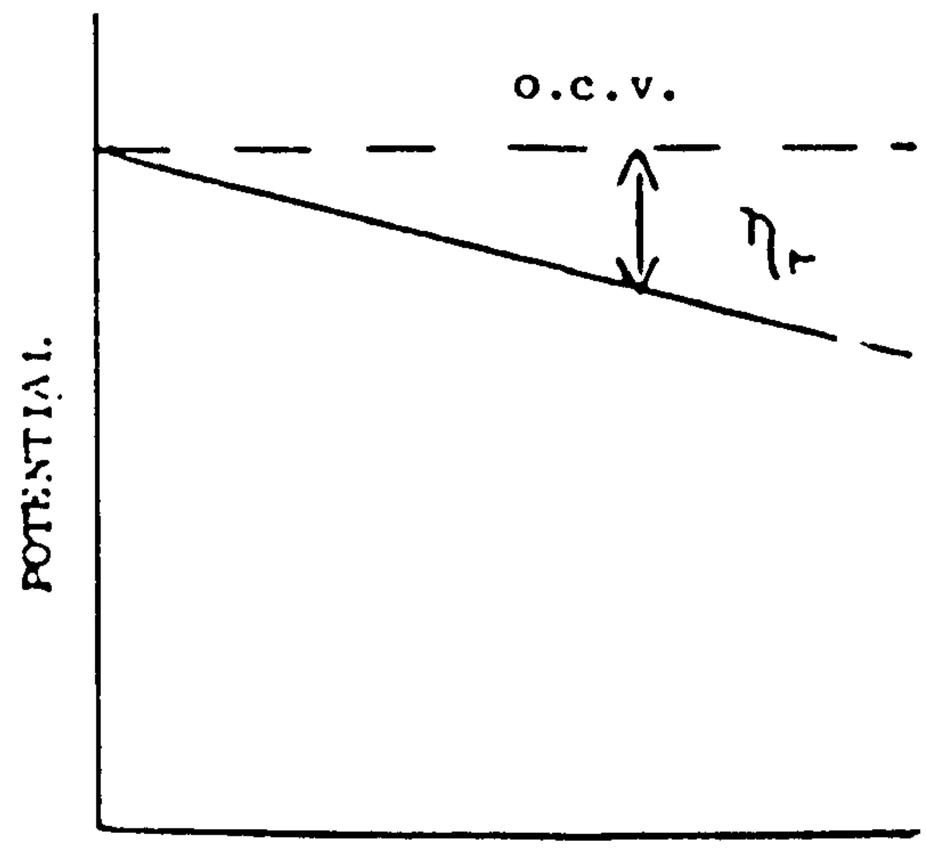

(c) OHMIC OVERPOTENTIAL

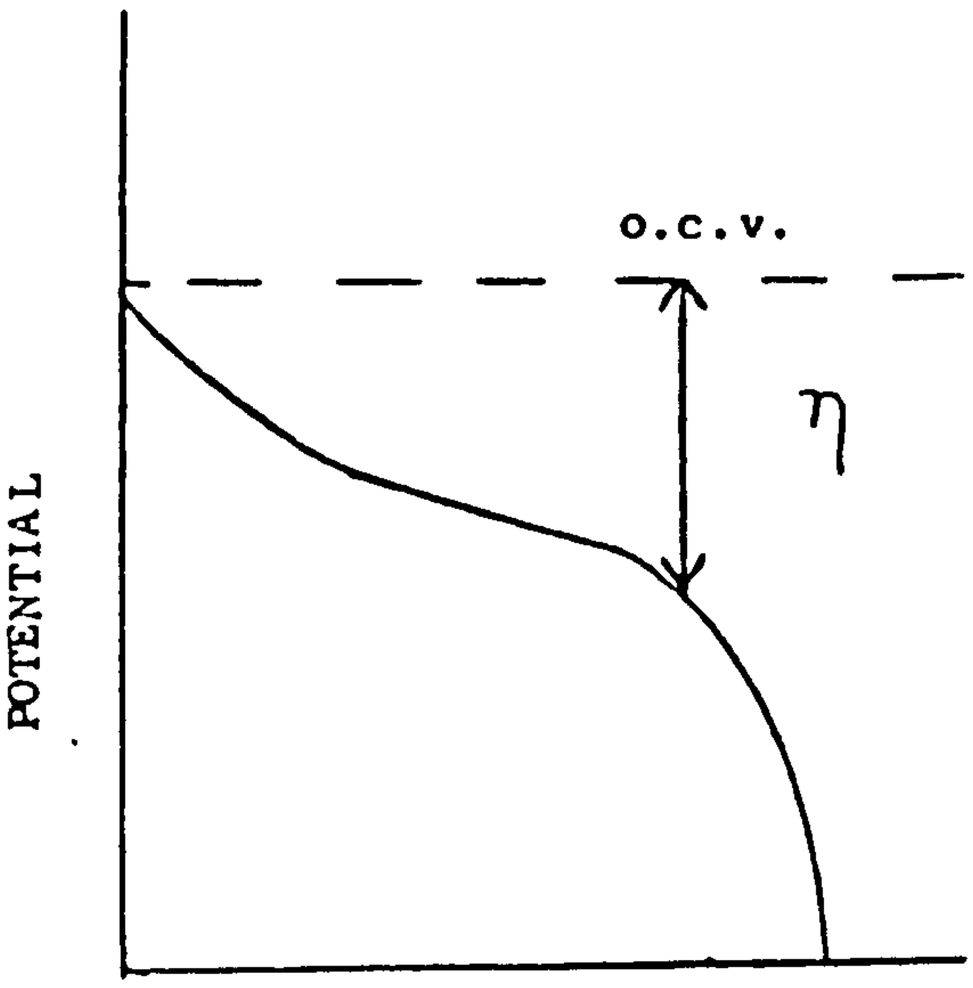

(d) CELL CHARACTERISTIC

Figure 2.5 Contributions to Cell Polarisation.

CHAPTER 3.

ANALYTICAL, EXPERIMENTAL AND PREPARATION TECHNIQUES.

This chapter describes the analysis and experimental techniques employed during the course of this research.

3.1 Analytical Techniques.

3.1.1 Atomic Absorption Spectrophotometry.

Elements present in the aluminium alloys were determined by atomic absorption spectrophotometry [36, 37].

To obtain a solution of metallic salts the alloys were dissolved in concentrated HCl, and then diluted to a level which enabled absorbances within the linear range given by the standard to be obtained.

The principle of atomic absorption is as follows. On aspiration of a solution of metallic salts into a flame, vapour containing metal atoms may be formed. Radiation characteristics of the particular metal may be emitted, but most atoms will remain in an unexcited state. These atoms are capable of absorbing radiant energy of their own specific resonance wavelength. Thus if light of resonance wavelength is passed through the flame containing the relevant atoms , some of the light will be absorbed. The extent of the absorption is proportional to the number of unexcited atoms in the flame.

3.1.2 Scanning Electron Microscopy.

Scanning electron microscopy, or SEM, is an extremely powerful and useful technique for study of the surface of solid samples [38].

Electrons are generated by thermionic emission from a tungsten filament and accelerated through a potential E. Work done for this project employed accelerating voltages in the order of 20-40keV. Three condenser lenses form the electrons into a fine beam or probe, and the probe scans the specimen surface in the form of a square raster, by means of scanning coils. The low energy secondary electrons emitted from the specimen surface are detected above the sample and an image is reproduced on a Cathode Ray Tube. The intensity of each point on the CRT is a reflection of the number of electrons collected from the corresponding point on the sample surface. The result is a reproduction of the specimen surface on the CRT.

The JEOL JEM 100B and the HITACHI S 520 Electron Microscopes were used for scanning purposes. Micrographs were obtained which gave information regarding the morphology of the specimen surface.

3.1.3 Energy Diffraction Analysis of X-Rays (EDAX).

A Phillips EDAX 9100/60 was used for X-ray spectroscopy

work. This technique involves the bombardment of samples by high energy electrons. When this occurs inner shell electrons may be ejected from atoms, and the outer shell electrons move into the vacated inner shell postions. As this occurs the excess energy is released in the form of X-radiation, each element having a characteristic X-ray emission spectrum which consists of a series of peaks. From the positions of the peaks elements can be identified, and from the intensity of these peaks, a quantitative analysis can be made. Finally the intensities of the X-ray emission can be superimposed on a surface scan to give a reflection of the distribution of an element in the sample, in effect a `distribution map'.

3.1.4 Electron Spectroscopy for Chemical Analysis (ESCA).

An ESCALAB MK II was used to carry out analysis of electrode surfaces.

ESCA provides information about a thin surface layer [39, 40]. A monochromatic radiation source (MgK α/AlK α, 1254eV and 1487eV respectively), is used to irradiate a sample. Electrons in the atomic shells of elements may be ionised. The kinetic energy (k.e.) of the ionised electron is equal to the difference between the energy of the incident radiation (hf), and the binding energy (E_B) of the electron and is given by ;

(3.1) k.e. $= hf - E_B$

For any atom a range of binding energy values is obtainable, representing the various electrons from inner and outer atomic shells. These binding energies are characteristic for each individual element.

The kinetic energy of the photoelectron that emerges from the sample surface is measured using an electron spectrometer, which is basically an electrostatic or magnetic analyser. The double pass cylindrical mirror is amongst the most popular in commercial instrumentation. The system consists of two stages of coaxial cylinders with a negative potential applied to the outer cylinder. The potential applied between the inner and outer cylinders creates a cylindrical retarding potential. Electrons from the sample pass through an annular defining slit, into the radial field between the cylinders to be focussed back onto the axis by the negative potential. The electrons pass into the second cylindrical mirror analyser to be focussed onto an electrical multiplier. The output of the multiplier is a series of pulses that are fed to a pulse amplifier then to a digital to analog converter and finally to a computer for storage.

Samples were analysed both as introduced into the instrument, and also after etching the surface with argon. Argon etching was used to remove the oxide layer present so

as to enable the actual alloy surface to be examined.

From the analysis, wide scan photoemission spectra are obtained (binding energy vs. intensity). The photoelectron lines are matched up with the known binding energies of the characteristic element, and this provides identification of the elements present on the sample surface.

3.1.5 X-Ray Powder Diffraction.

The Debye-Scherrer method [41] was used to identify the crystal structure of the various reaction products obtained on discharge of aluminium alloys in various alkaline electrolytes. Both photographic film and chart paper were used, (the former to calculate the d spacing and the latter to calculate the relative intensities) from which a set of lines and peaks were obtained. The position of the lines and intensities of the peaks are characteristic of a particular substance, and substances were identified using The Powder Diffraction File [42], by comparing the eight most intense lines.

3.2 Preparation of Electrodes.

3.2.1 Aluminium Alloy Anodes.

Aluminium alloys were cut and rolled to a thickness of 2mm. They were then polished using Bondaglass-Voss ltd. metal polishing liquid so as to leave a fine finish. The alloys were then machine cut into electrodes of the following dimensions ;

(a) 2mm x 10mm x 20mm, and,

(b) 2mm x 5mm x 20mm.

The alloys were then degreased with acetone using an ultrasonic bath, and then thoroughly washed with distilled water.

Electrode areas of $2cm^2$, $1cm^2$ and $0.5cm^2$ were required, and the areas of the electrodes not undergoing test were painted with two coats of lacomit. In half cell tests electrical contact was made with a crocodile clip, and the contact point carefully covered with teflon tape so no metal other than the test area was exposed to the electrolyte. See Figure 3.1

Full cell anodes were prepared as shown in Figure 3.2, again lacomit being used to seal areas other than the test area.

3.2.2 The Counter Electrode.

Nickel mesh was used as the counter electrode in all half cell work done. Nickel wire was spot welded onto a piece of

Figure 3.1 Aluminium Electrodes for Half Cell Tests.

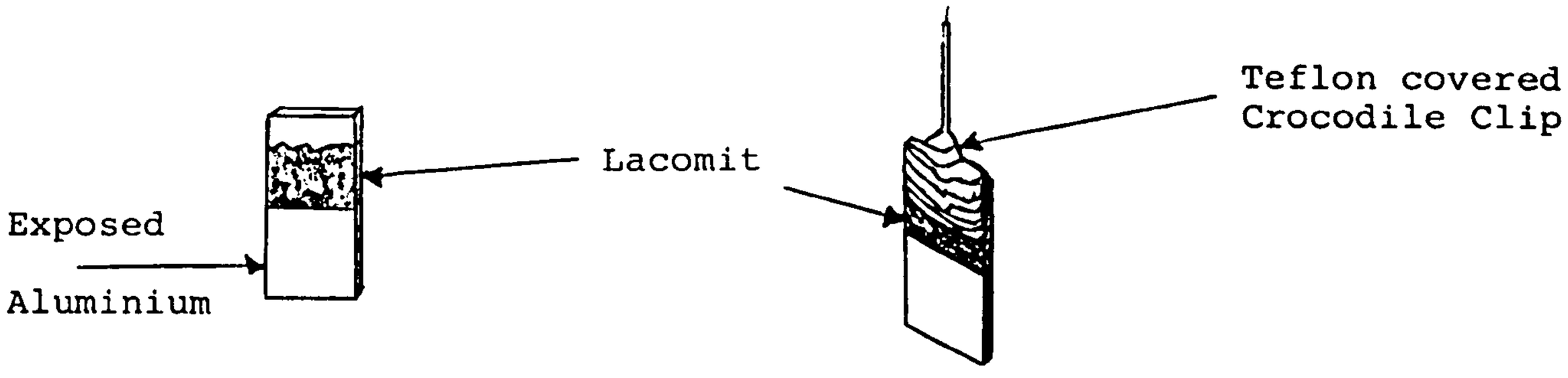

Figure 3.2 Aluminium Electrodes for Full Cell Tests.

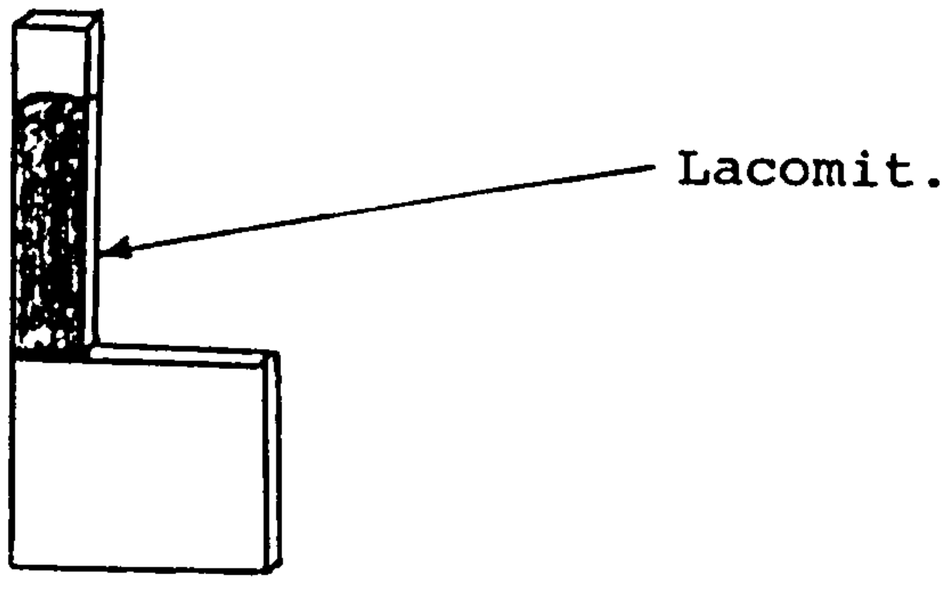

Figure 3.3 Nickel Mesh Counter Electrode.

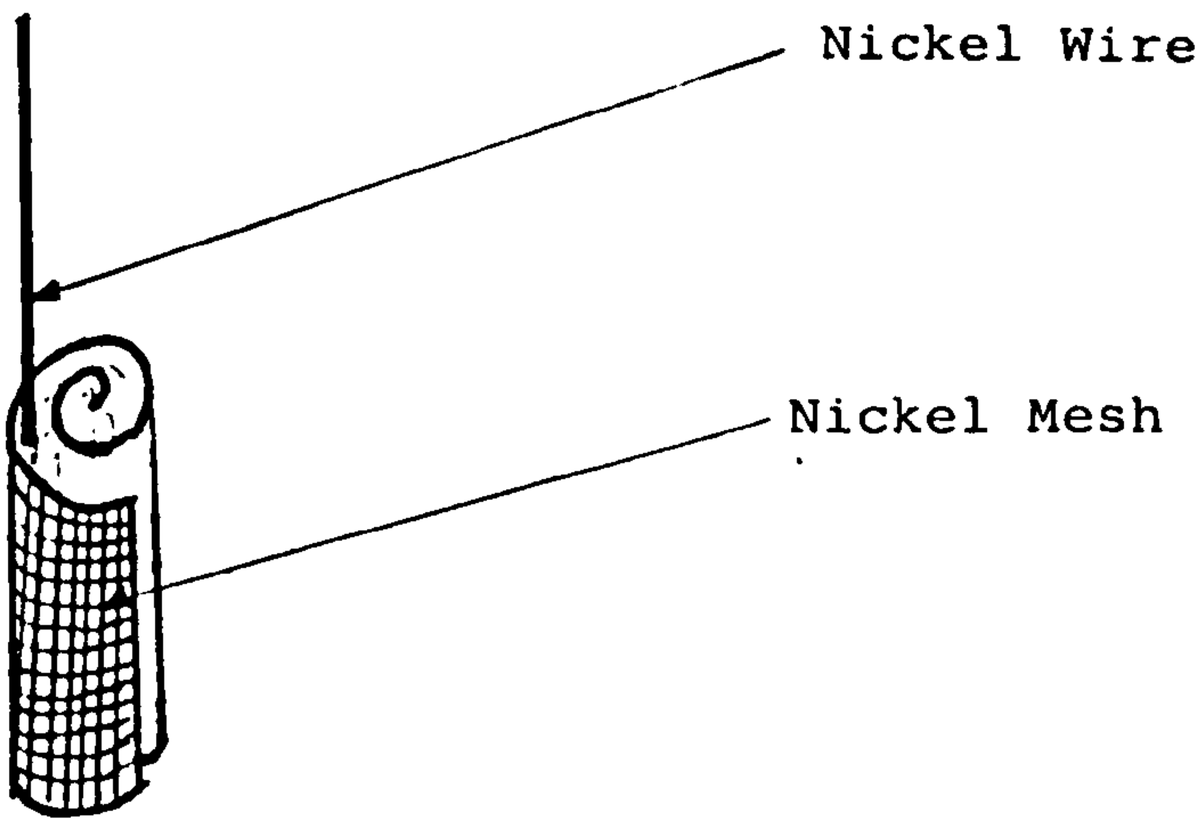

mesh which was then rolled, so as to enable the electrode to fit in the counter electrode section of a three compartment cell. See Figure 3.3.

3.2.3 The Reference Electrode.

The Hg/HgO reference electrode was used throughout this project. The electrode was prepared in the following manner. First a glass tube was prepared as shown in Figure 3.4. Through the side arm A, platinum wire was placed and this was sealed using epoxy. The tip of the wire reached into the cavity B. This was then covered with a layer of mercury. It was ensured that the tip of the platinum wire did not protrude through the mercury. This was then covered with a layer of mercuric oxide, and 40% potassium hydroxide was then drawn up the tube. The system was allowed to settle for several hours before being calibrated versus a Reference Hydrogen Electrode. The potential was recorded and if the value was in the region of 925-930mV the electrode was regarded as being acceptable [43]. Thereafter, the potential of the reference electrode was regularly checked and if the potential deviated from the previously accepted value, a new one was prepared.

3.2.4 The Oxygen Electrode (for Full Cell Tests).

The structure of the oxygen electrode can be seen in Figure 3.5, and was prepared as follows [44].

Figure 3.4 Hg/HgO Reference Electrode.

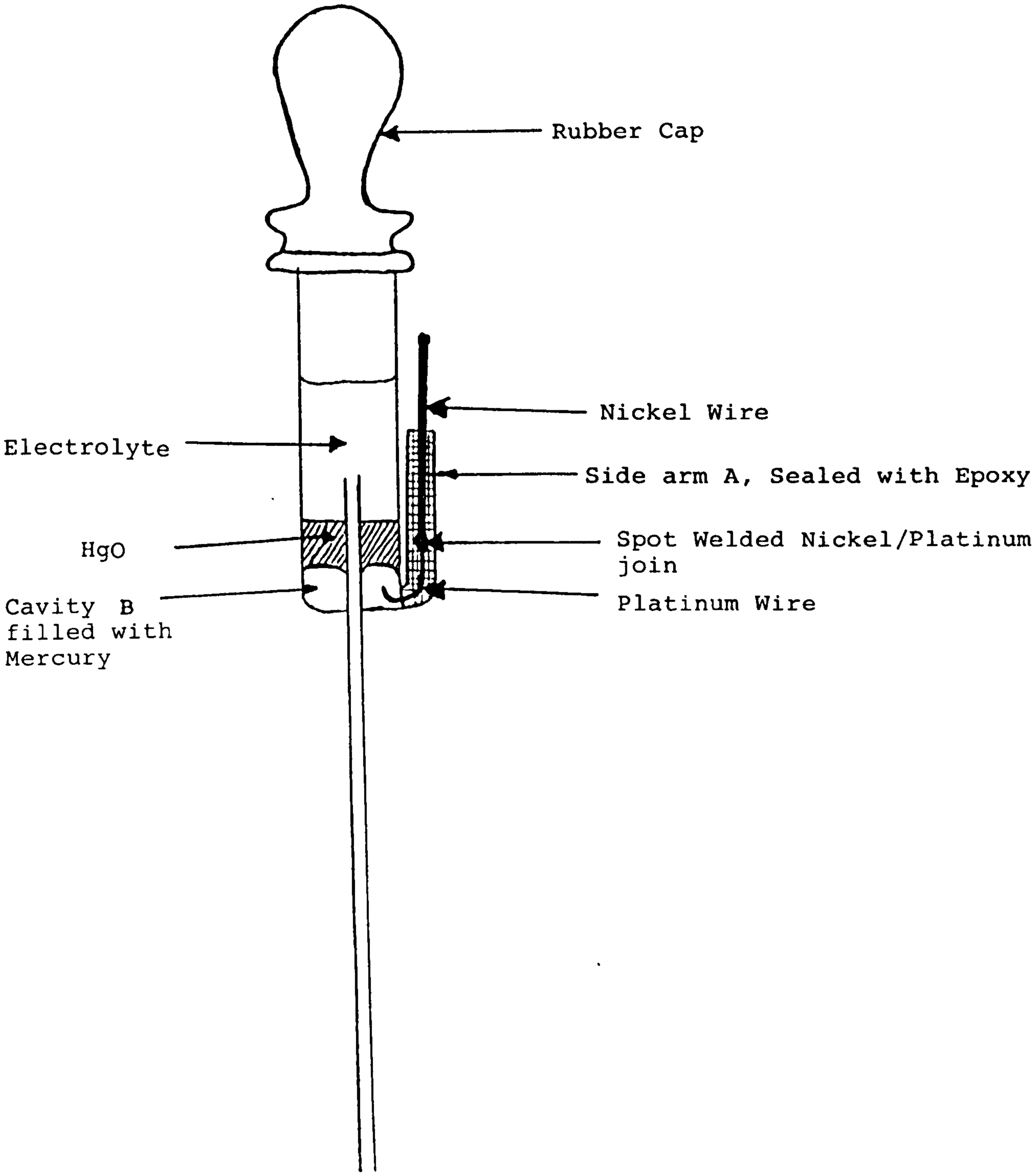

Figure 3.5 Structure of the Oxygen Electrode.

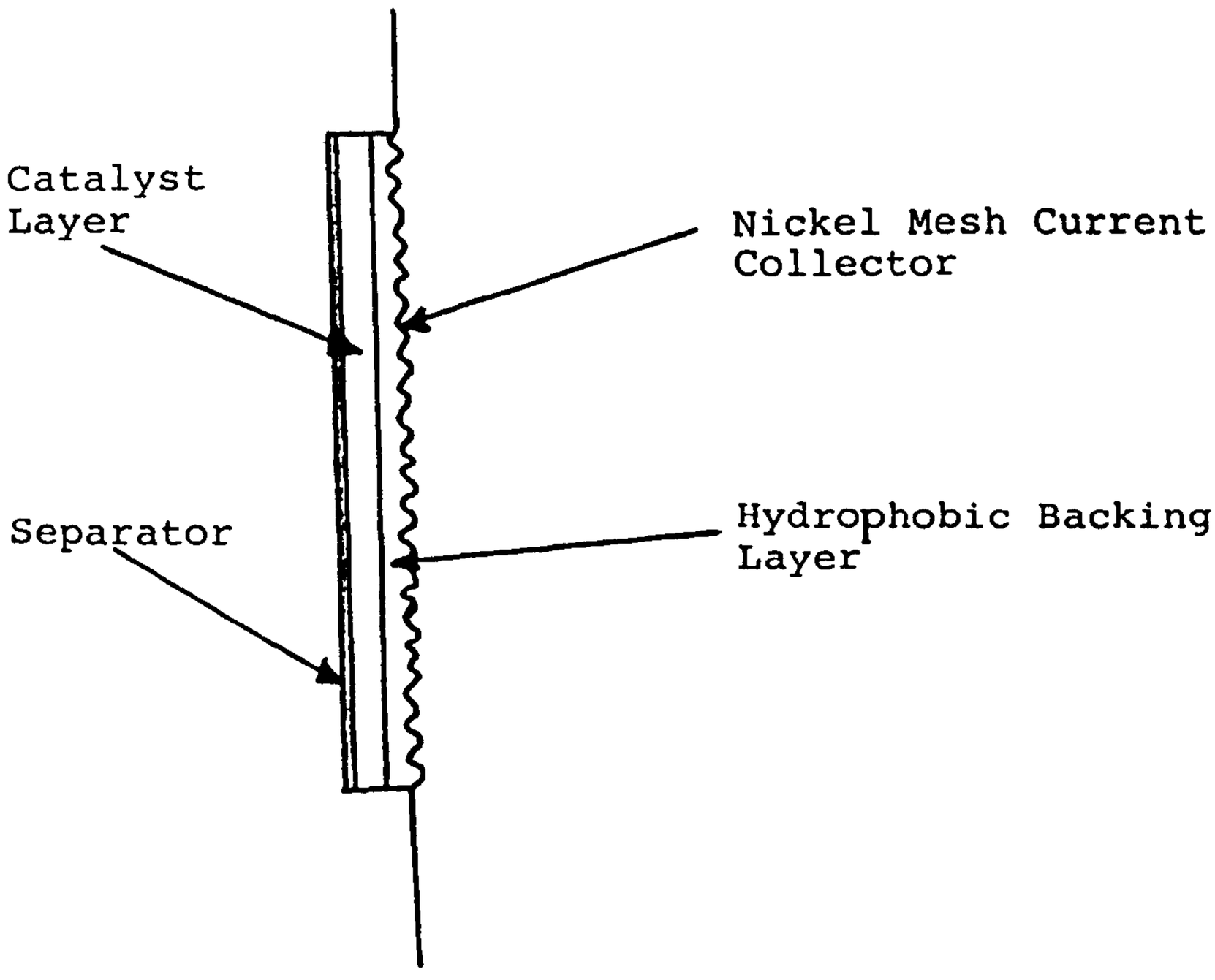

First, nickel mesh was cut out to exactly the shape and size required to make the air electrodes. (Strips of 6cm x 3.6cm and 8cm x 3.6cm). The strips were degreased in acetone and washed in soapy water. The diffusion layer was prepared by mixing 10g of lampblack, 25g teflon dispersion, 2.5g of crushed ammonium carbonate (for pore building) and 14cm^3 of ethanol until a dough like substance was obtained. The mixture was then placed between the two rollers, which were several millimeters wide. The substance was rolled and folded several times whilst reducing the distance between the two rollers. After rolling to a thickness of 1.4mm, the material was stored in a jar containing a little ethanol.

The catalyst layer was prepared by mixing 5g of 5% platinum on carbon, 2.5g of teflon dispersion, 3cm^3 water and 7cm^3 ethanol. The material was then rolled as previously described to a thickness of 0.7mm. The catalyst and backing layer were then taken and rolled together to a thickness of 1.05mm. The material was then cut with a scalpel to the size of the nickel mesh pieces, and these were then pressed together at a pressure of 0.3 tonnes per cm^2 for 10 seconds.

The final layer of the oxygen electrode was prepared by mixing 3g of zirconia oxide (ZrO_2), 0.75g of teflon dispersion and 10cm^3 of water. The zirconiumlayer was painted onto the catalyst layer using a soft brush.

After preparing the electrodes in this manner, they were heated in an oven for one hour at 100°C, one hour at 140°C and finally one hour at 200°C. After cooling, the oxygen electrodes were mounted on perspex frames and sealed using epoxy. The design of the cell can be seen in Figure 3.6.

3.3 Electrochemical Techniques.

The electrochemical techniques that have been employed during the course of this research project are listed below. Some techniques are briefly outlined and are further expanded upon in the relevant chapter.

3.3.1 Half Cell Tests.

Currents and electrode potentials are measurable quantities, and a great deal of useful information can be gathered from a graphical representation of such data [45]. Current / potential characteristics can be obtained from half cell tests. As this research project is concerned with studying the anodic performance of aluminium alloys, such a test would be set up employing an aluminium working electrode, a nickel counter and a reference electrode. The reference electrode is of a known fixed potential to which the potential of the working electrode can be related. The electrodes are placed in the appropriate compartments of a three compartment cell, and the system is controlled by means of a potentiostat.

Figure 3.6 Design of Cell.

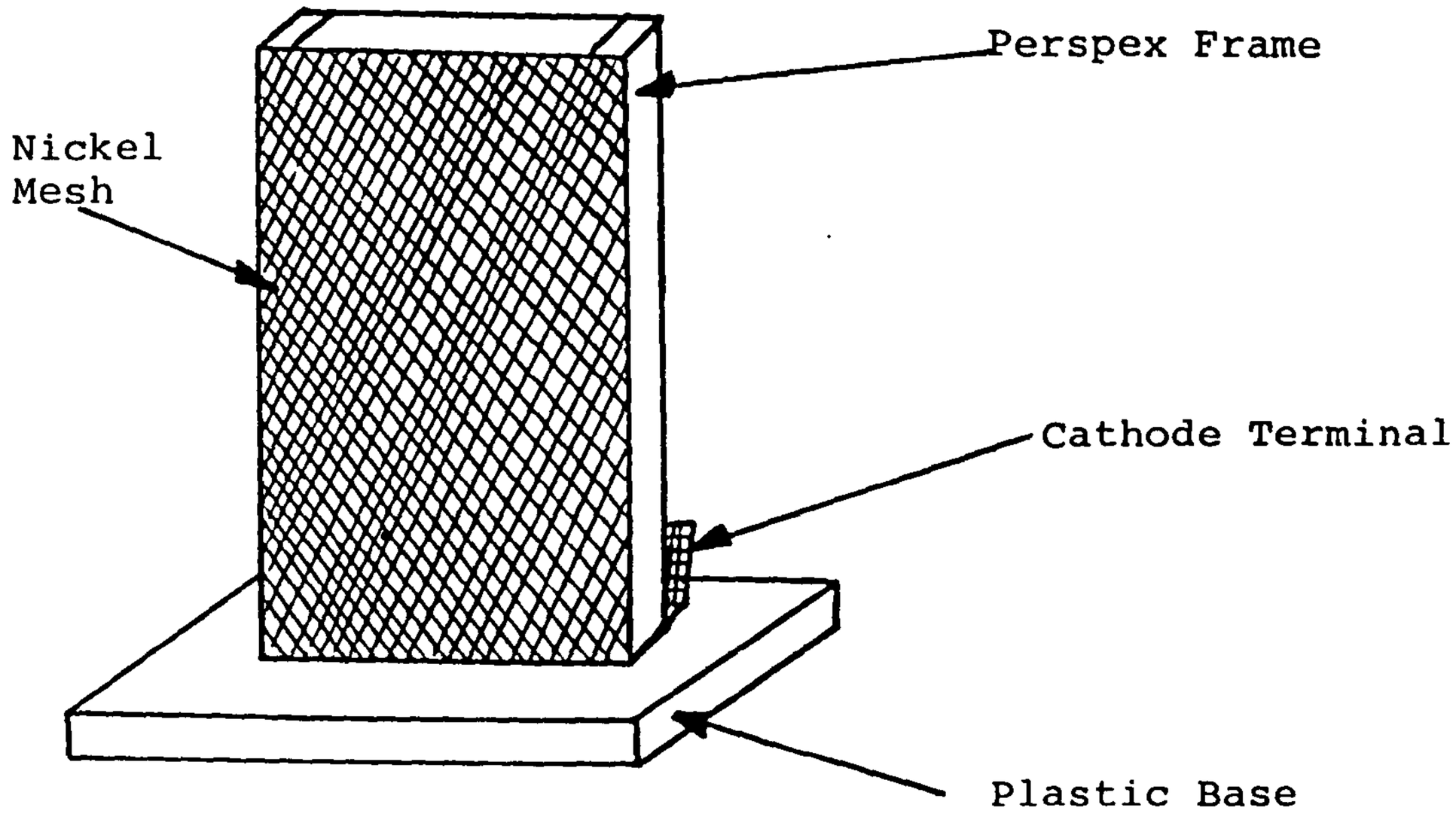

(a) Steady State Polarisation.

Automatic control of potential is achieved using a potentiostat. This enables the potential between the working and reference electrodes to be controlled at a fixed and selected potential whilst values of the current can be recorded. Steady state characteristics can also be determined by galvanostatic polarisation. In this case, a fixed current passes between the working and reference electrodes and the potential can be recorded. Therefore, the current / potential data is controlled by the electrochemical reaction on applying a fixed current / potential to a system. However, mass transfer effects become increasingly significant with time, and eventually, a `steady state' situation is achieved. Figure 3.7 shows the system for a) galvanostatic polarisation and b) potentiostatic polarisation.

(b) Transient Measurements.

The use of cyclic voltammetry enables a potential that is applied to a working electrode to change with time at a constant rate. The corresponding current is measured as a function of potential and and plotted on an XY recorder. See Figure 3.8. Use of this technique means that the possibility of an electrode surface changing during the course of an experiment and the effects of mass transfer,

Figure 3.7 System for ;

a) Galvanostatic Polarisation

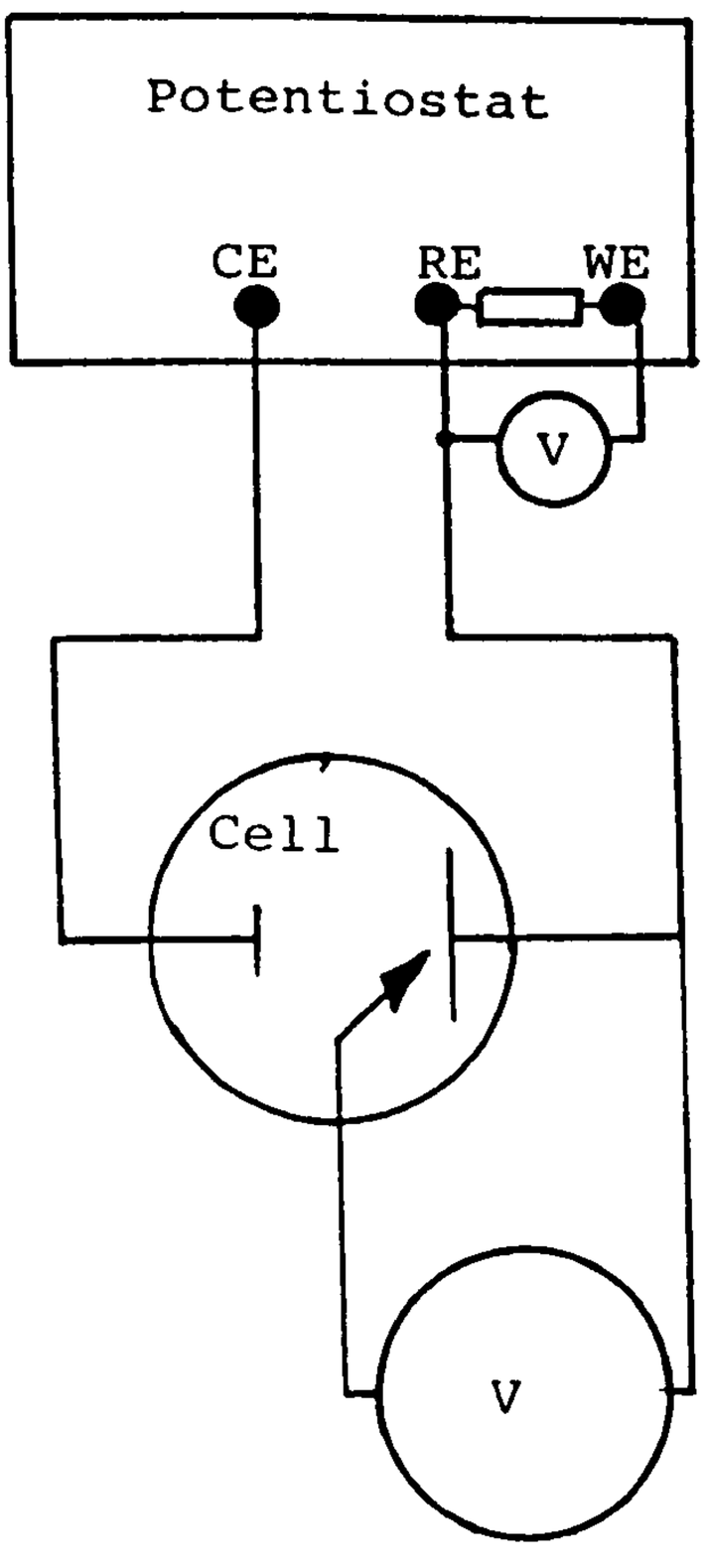

b) Potentiostatic Polarisation

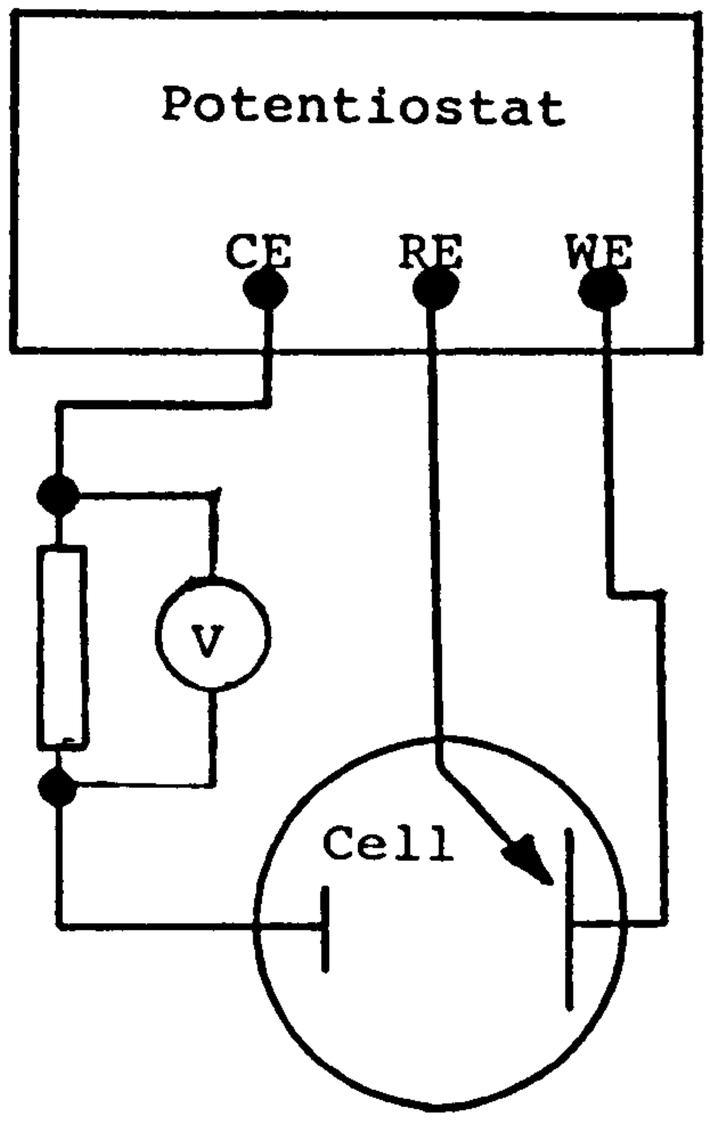

Figure 3.8 Circuit for Linear Sweep Voltammetry in Potentiostatic Mode.

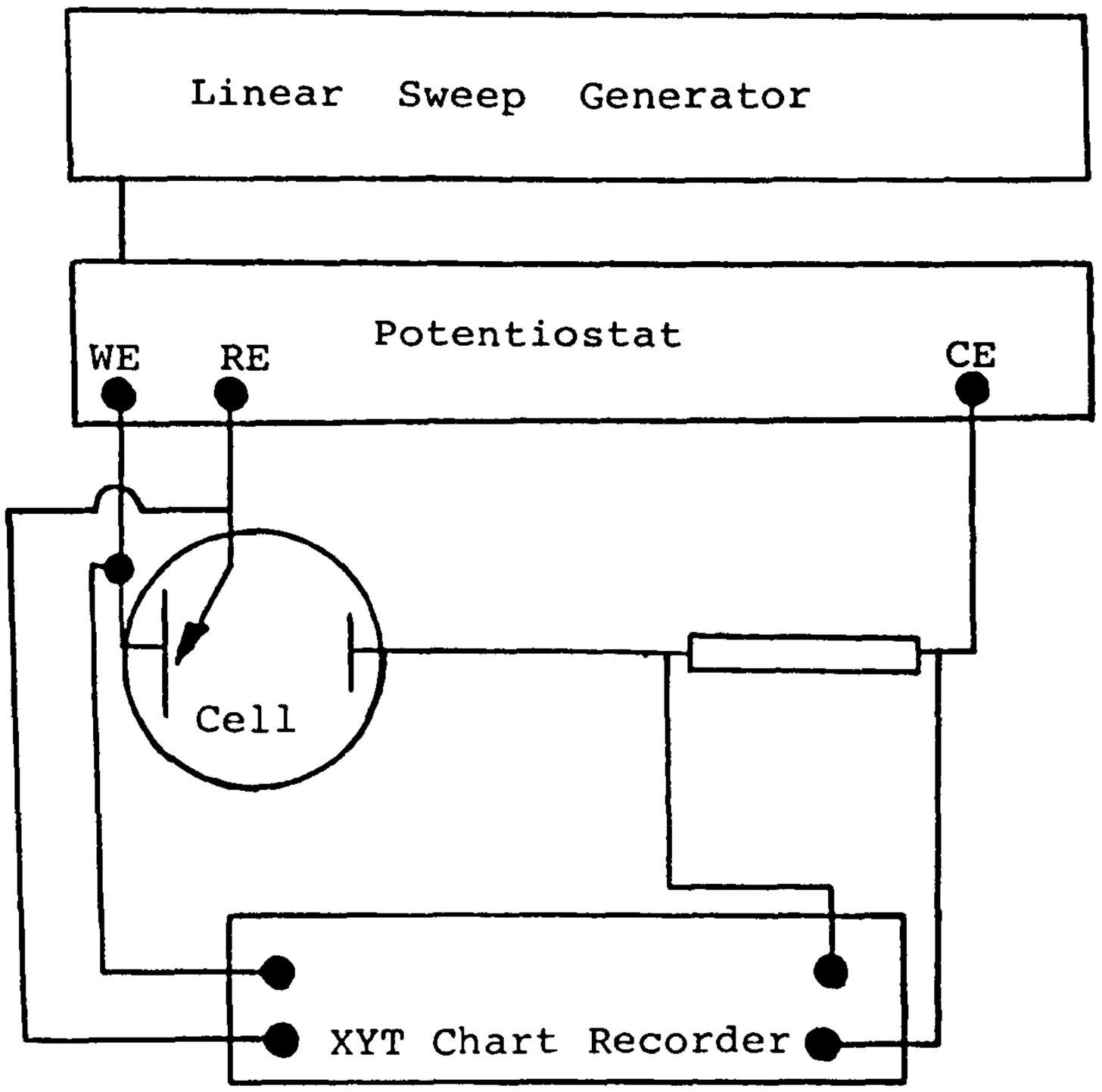

can be considerably reduced.

(c) Experimental Set Up.

Half cell tests were conducted in a three compartment glass cell. The working and counter electrodes were held rigid by nickel connecting wires which were passed through rubber bungs. The reference electrode was placed in the appropriate compartment of the cell, see Figure 3.9. Temperature controlled experiments were achieved using a thermostatically controlled water bath.

Steady state measurements were conducted using a Ministat Precision Potentiostat, and the current or potential values applied to the test system were read using a standard digital multimeter. The corresponding potential / current responses were recorded either from a digital multimeter or a JJ CR 600 chart recorder. Ohmic polarisation which is present in half cell tests due to the working to reference electrode gap, was measured and recorded using the interruptor technique [46].

3.3.2 Electrode Microzone Current Density Measurement.

At Xiamen University, a novel electrode microzone scanning technique has been designed which allows the examination of active and passive centres of metal surfaces during discharge [47, 48]. Use of this instrument enabled

Figure 3.9 Experimental Half Cell System.

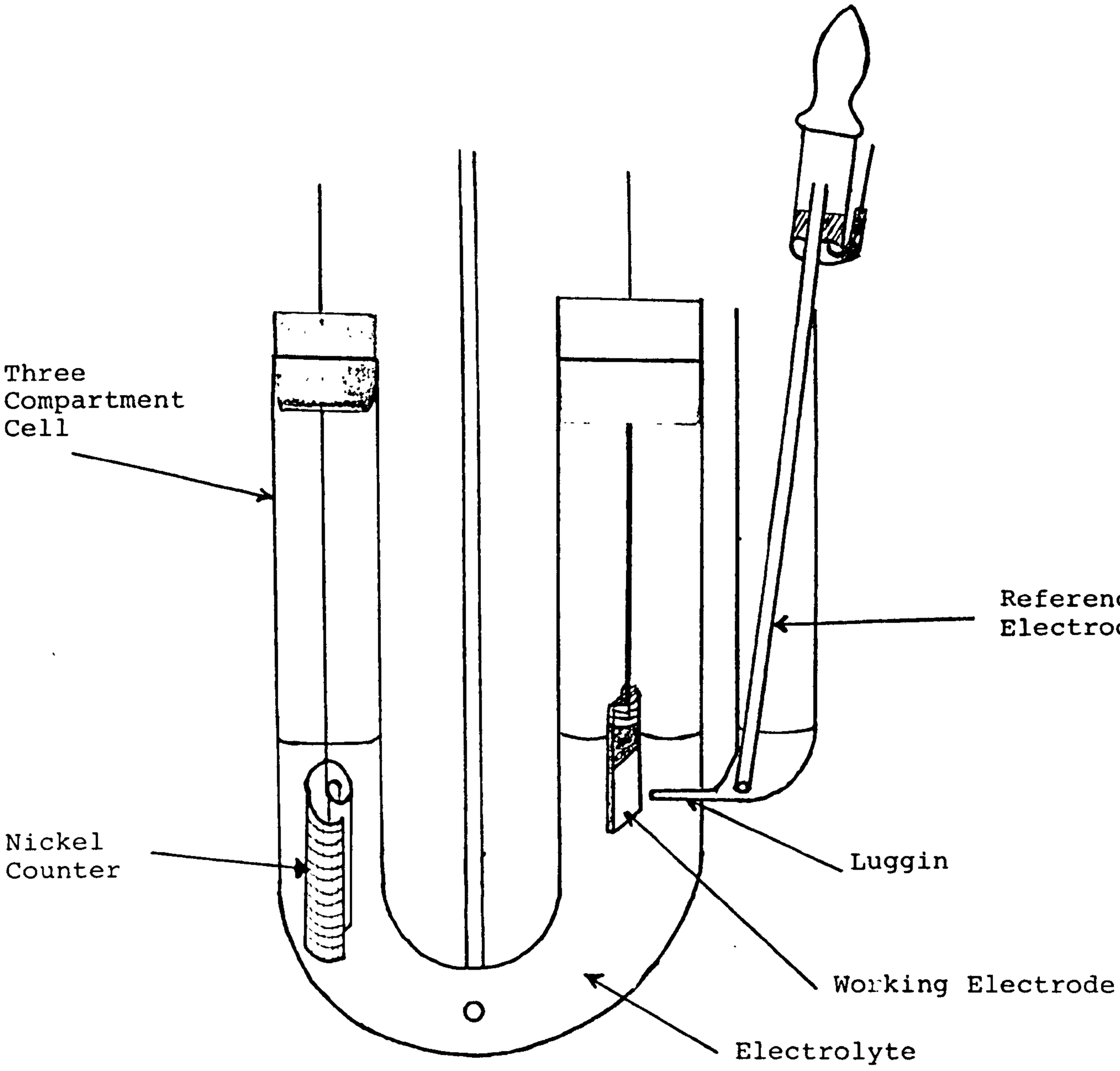

information to be gathered regarding the uniformity of current distribution, and also allowed the role of mercury as an electrolyte additive to be further investigated.

3.3.3 Ellipsometry.

Some preliminary investigations of the behaviour of aluminium alloys was carried out using an Ellipsometer type TC-2 (Xian Factory). Ellipsometry is an optical technique which has been applied to the study of electrode surfaces for many years. The technique involves the determination of the change in polarisation state of an incident light beam upon reflection at a surface [49, 50]. The instrument consists of a polariser, compensator and analyser, from which readings can be taken which can reveal information about a surface under examination.

CHAPTER 4.

ALUMINIUM ALLOYS AS BATTERY ANODES.

4.1 Introduction.

The idea of using aluminium as a battery anode is extremely attractive because of it s high electrochemical equivalent and theoretical specific energy values [51]. However, despite these characteristics, it is well established that in practice anodic performance is reduced by the presence of the oxide film on aluminium and that some aluminium is used up in the corrosion process [51- 58]. It was realised early in the research into aluminium as a battery anode that it was beneficial to alloy the aluminium with suitable elements so as to reduce these problems. There is a wealth of literature available relating to suitable alloying elements and several patents have been filed [51-54, 60-79]. Any element that is to be alloyed with aluminium must be soluble in the solid solution of aluminium at equilibrium. Also, the element must have a high hydrogen overpotential so as to reduce corrosion. Considerable research has been carried out on various alloys and a brief resume of some of the work done is given.

A thorough analysis of suitable alloying elements for anodic dissolution of aluminium was reported by Reding and Newport in 1966 [74]. Their results showed that gallium, mercury and indium cause significant shifts in anodic potential. Zinc, cadmium, magnesium and barium also caused the potential to become more negative, though not to the same extent. Pryor et al [63-71] also carried out studies on the

performance of various aluminium alloys, notably with tin. Murai et al [80] studied the behaviour of an aluminium anode which was alloyed with zinc, tin, bismuth and gallium. Scamans et al [81] and Despic et al [54] have studied aluminium tin, aluminium gallium and aluminium indium alloys. At City University, Quarshie studied the effect of various quantities of zinc in aluminium anodes and compared their performance with that of a commercially available alloy [11].

Research has also shown that a number of elements were clearly unsuitable for alloying. Reding and Newport [74] found that the presence of manganese and copper result in a more cathodic potential and Murai et al [80] showed that copper, silica and iron have a deleterious effect on anodic efficiency and cell potential.

Results of this research have thus led to a list of alloying elements which when added to aluminium in trace amounts cause an anodic shift in potential, activating the electrode. These are mercury, gallium, indium, tin, bismuth, magnesium, barium, zinc, lead and cadmium. Undesirable elements for anodic dissolution are iron, copper and silicon.

For this project, four aluminium alloys of various compositions were obtained. To study the role of the alloying elements, several experiments were performed.

Preliminary corrosion tests were carried out at OCV in alkaline electrolytes, and half cell experiments were also performed and the behaviour of the four alloys compared. The alloys were also examined under the electron microscope and the EDAX system used to investigate surface composition both prior to and after discharge.

Inconclusive evidence was obtained of the possible build up of alloy elements on the electrode surface during discharge. A scan of the surface revealed a plain aluminium surface, due to the weight % of additives being very small. However, on studying the distribution map both prior to and after discharge, the diagrams suggested a quite dramatic increase in alloy sites on the electrode surface in the latter. Whilst it was realised that this is by no means conclusive evidence of elements on the aluminium surface, it did suggest that this was likely. ESCA work was then performed in an attempt to obtain further evidence.

4.2 Aluminium Alloys.

Four aluminium alloys were obtained, three from Alcan International U.K. and one from Alupower Inc. New Jersey, U.S.A. These alloys were specially prepared for discharge in aluminium air cells, and contained various element additives in order to activate the aluminium. High purity aluminium is used in which the amounts of impurity iron and

copper have been reduced to trace quantities so as to reduce corrosion.

4.3 Analysis of Alloys.

Composition of the alloy samples was determined by Atomic Absorption Spectrophotometry (see section 3.1.1). Table 4.1 gives the various compositions of the alloys.

Table 4.1 Composition of Alloys.

	w/w % of Element in Alloy			
	Alloy			
Element	New Q4 1	Sea Water 2	Low Corrosion 3	High Power 4
Bi	0.018	0.150	0.030	0.05
Cu	0.003			0.01
Fe	0.006	0.036	0.029	0.02
Ga	0.056	0.118		0.10
Hg		0.291	0.162	0.36
In		0.011	0.052	0.02
Mg	0.0001	0.298	0.271	0.43
Mn	0.0002		0.114	
Pb	0.180	0.007	0.014	
Sn		0.335		0.95
Ti	0.001	0.595	0.770	
Tl		0.046	0.043	0.01
Zn	0.0005			

Analysis of the alloys leads to the following conlusions of the samples. Alloy 1 is very pure aluminium with trace iron and other impurities being lower than the quantities present in any other alloy. The activating elements in this alloy are bismuth, lead, gallium and zinc. Alloy 2 contains a high percentage of tin activating element and titanium, which is well known as a corrosion inhibitor [82]. The alloy also contains mercury, indium and bismuth which act as both hydrogen evolution inhibitor and activating elements. The alloy also contains gallium, magnesium, lead, and thallium. Alloy 3 is a low corrosion alloy with mercury bismuth and indium and titanium corrosion inhibitor elements added. Also, the fact that the alloy does not use gallium as an activating element is significant as corrosion rate with gallium is very high [83]. Alloy 4 is the high power alloy which contains significantly high quantities of tin. It also contains bismuth, mercury, gallium, indium and magnesium. The presence of gallium and the high percentage of tin whilst leading to significantly high potentials, results in a greater hydrogen evolution problem than for other alloys as can be seen in the preliminary corrosion tests reported in section 4.4.

It is necessary to discuss the effect of these alloying elements in more detail. The function of the activating elements is to cause a change in anodic behaviour from that of highly pure aluminium with an oxide film to that of a film free metal with more negative potentials.

Typical preparation of aluminium alloys is to heat the aluminium at elevated temperatures e.g. for aluminium tin alloys (like alloy 2) this is typically 620°C for a sufficient period to dissolve the tin. The other alloy elements are also added at this point, and they must be soluble in the solid solution of aluminium. After heating, the sample is rapidly cooled by immersion in water. Tin in aluminium acts as an activating agent thus causing an anodic shift in potential. Preparation of the alloy in this manner has the function of increasing the amount of tin retained in solid solution and uniformly distributes the metal throughout the alloy [67].

The other metals to be found in the alloys are present for two reasons ;

(i) To modify the properties of the alloy. The bismuth, indium, gallium, magnesium additives act as aluminium lattice expanders. Generally, lattice expanders stabilise the activating element in retained solid solution and permits high galvanic currents to be drawn from the alloy.

(ii) Because of the method of preparation of the alloy and association of impurity elements with aluminiumin ore, trace amounts of e.g. iron, nickel, copper and silicon are to be found in the alloys. These are insoluble elements which have little or no effect on current output. However,

accumulation of such elements results in a reduced efficiency of the anode by acting as secondary cathode sites and causing local corrosion. Obviously, it is desirable to keep quantities of these elements to a minimum.

4.4 Corrosion of Aluminium Alloys.

4.4.1 Experimental Procedure.

Known masses of each aluminium alloy were placed in containers with $100cm^3$ of the following electrolytes ;

1:1 50w/v% KOH & 30w/v% NaOH (saturated with mercury), henceforth - **Electrolyte A.**

1:1 30w/v% KOH & 50w/v% NaOH (saturated with mercury), henceforth - **Electrolyte B.**

40w/v% KOH, henceforth - **Electrolyte E.**

The experiment was conducted in a water bath and the temperature controlled at 25^oC. Every thirty minutes the alloys were removed from the solutions, washed and dried, and the mass of each recorded. Each experiment was run five times and the average total mass /mg lost for the alloys in each electrolyte was plotted versus time /minutes.

4.4.2 Results and Discussion.

The corrosion results in electrolytes A and E are given in Figures 4.1 and 4.2. Figure 4.3 compares the corrosion of bulk manufactured aluminium with two of the aluminium alloys in electrolyte B. The results clearly show that alloy 3 corrodes the least in all electrolytes. This can be attributed to the high percentage of titanium in the alloy, the presence of mercury and also the fact that gallium is not used as an activating element. Alloy 4 corrodes the most in all cases, and this can be related to the fact that the only corrosion inhibitor present is mercury. As regards alloys 1 and 2, it is interesting to note that before 70 minutes, alloy 2 has the greatest corrosion, whereas after 100 minutes alloy 1 does in all electrolytes. Alloy 1 uses high purity aluminium, whereas alloy 2 contains titanium corrosion inhibitor, which appears to be more effective for the initial period. Figure 4.3 shows the benefit of alloying. Bulk aluminium (BDH 99.9% purity) was used with the same experimental procedure as previously outlined and the graph shows the dramatic increase in corrosion as compared to alloys 3 and 4 in electrolyte B.

4.5 Steady State Polarisation of Aluminium Alloys.

4.5.1 Half Cell Tests.

Figure 4.1 Corrosion of Alloys at OCV vs. Time

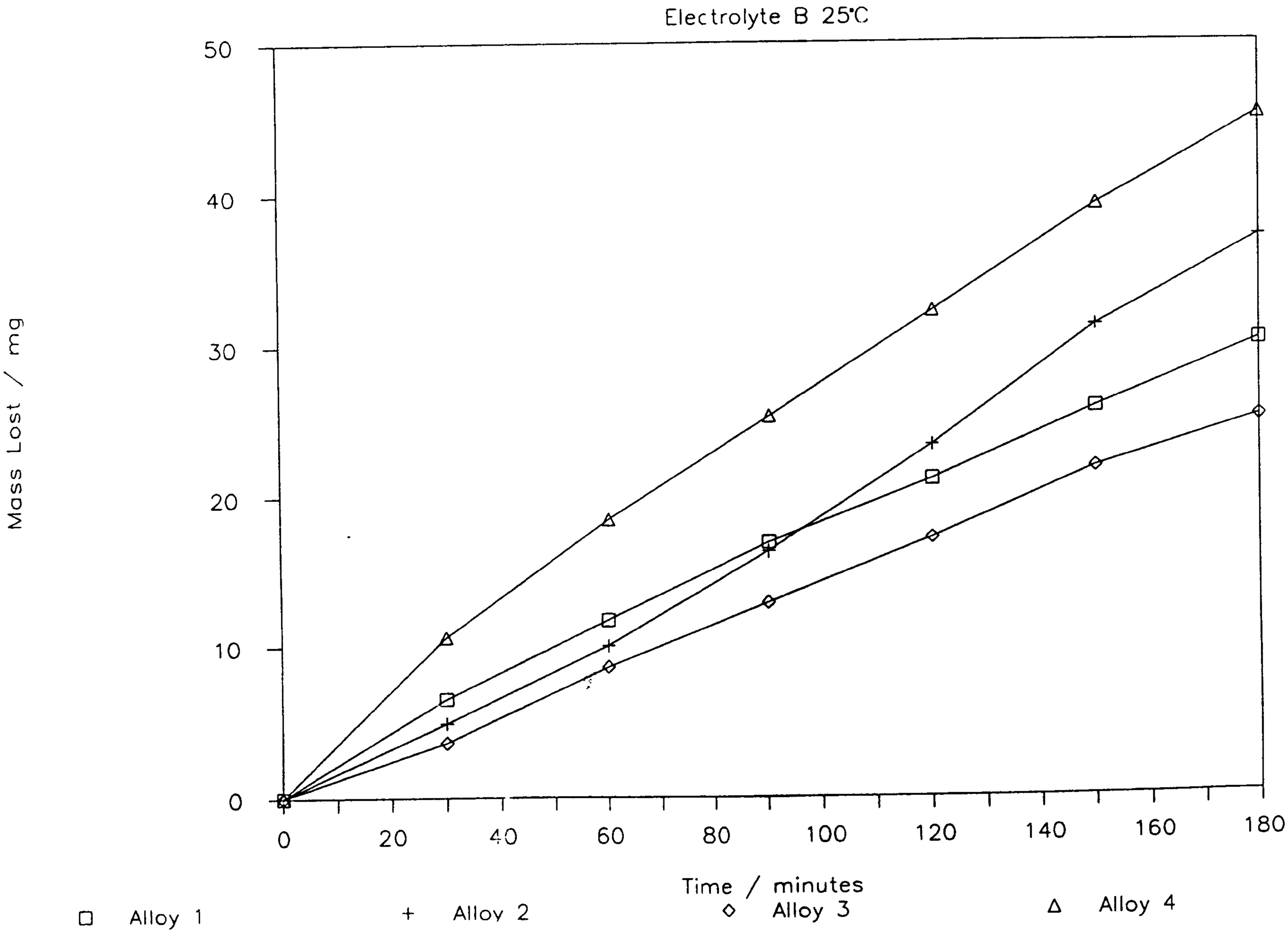

Figure 4.2 Corrosion of Alloys at OCV vs. Time

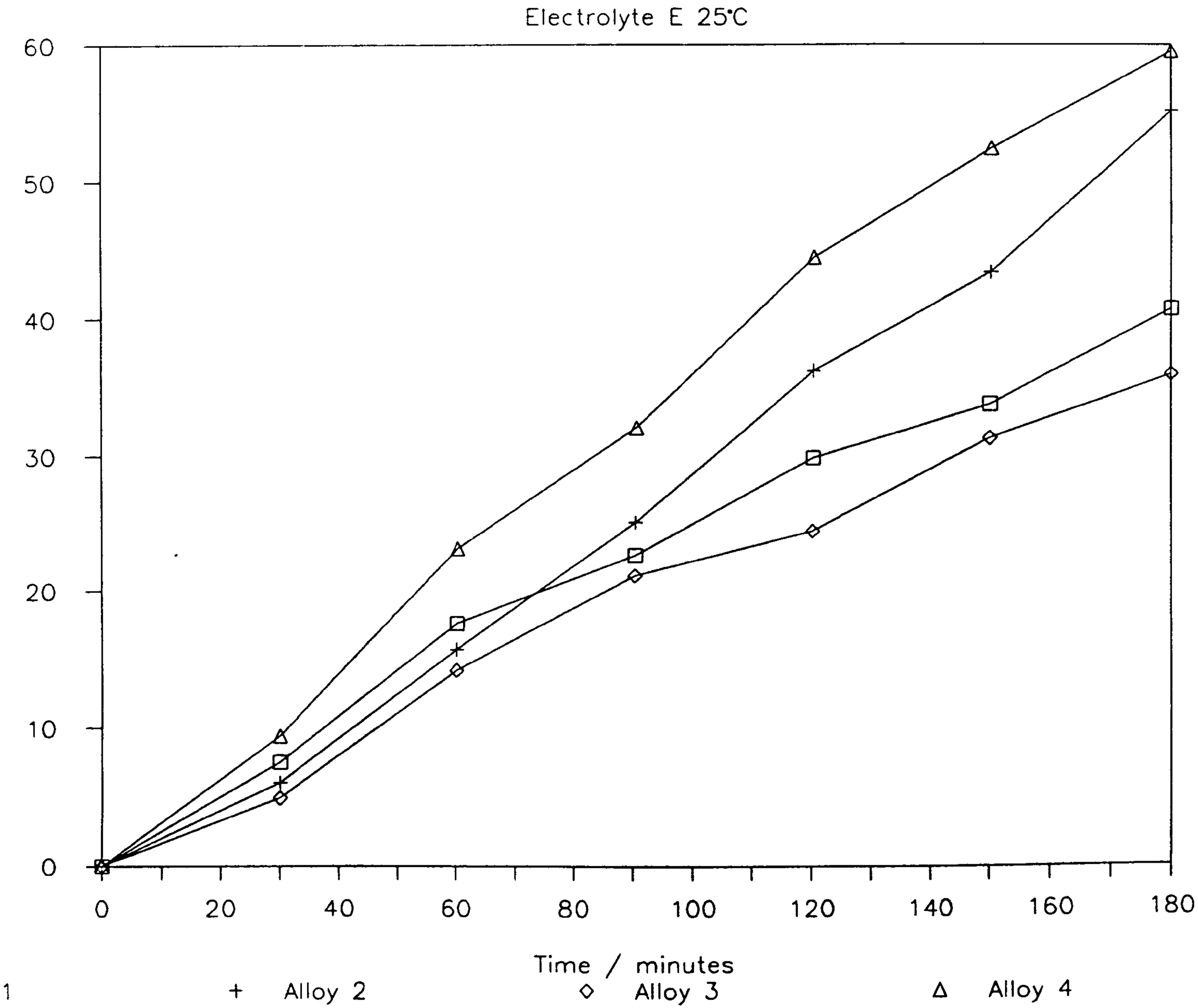

Figure 4.3 Corrosion of Bulk Manufactured Al

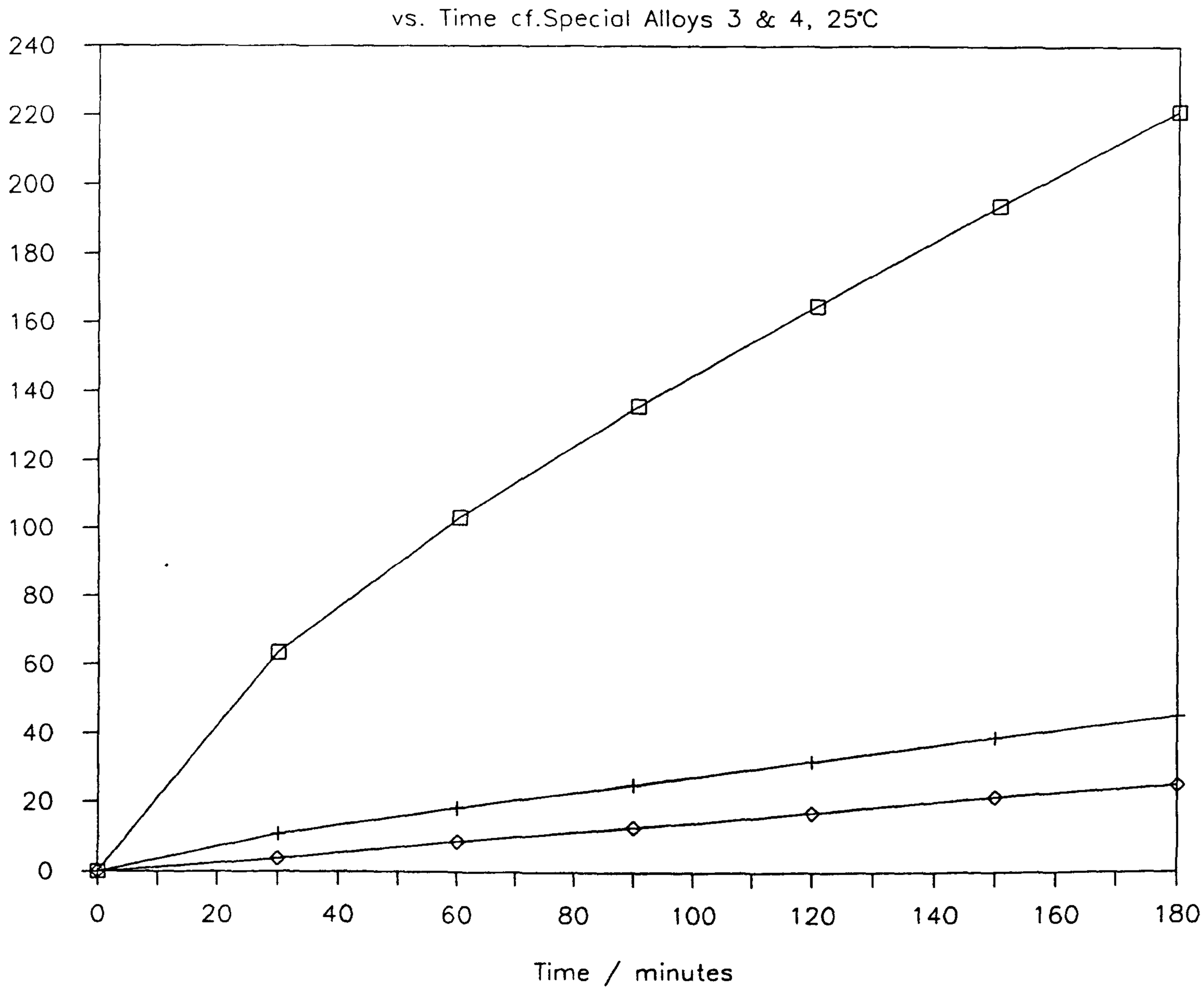

$1cm^2$ aluminium alloys were discharged with the potentiostat in the galvanostatic mode (as described in section 3.3.1). Temperature for the experiments was maintained at 25^oC by means of a water bath. Readings were taken one minute after fixing the current in order to allow the potential to stabilise. Each alloy was discharged in $80cm^3$ of electrolyte, and the experiments repeated five times for each alloy in all three electrolytes A,B and E.

4.5.2 Results and Discussion.

Figures 4.4 to 4.7 show the potential (`iR' free) versus current density plots. Figures 4.4 and 4.5 give the total current density range to passivation point of alloys 1-4, in electrolytes B and E respectively i.e. the point where a slight increase in current density leads to a dramatic cathodic shift in potential. The graphs show that alloy 4 has considerably less overpotential between approximately $20mA/cm^2$ to it s limiting current density. The alloy cannot cope with the higher current density values that alloys 1 and 2 can. In the electrolyte mixture B, the limiting current density is lower for every alloy, but most significantly for alloy 3. Alloys 1 and 2 behave quite similarly in electrolyte B, the potential at $100mA/cm^2$ being ca. -1400mV for alloy 1 and -1430mV for alloy 2 with respect to Hg/HgO. In electrolyte E, the potential for

Figure 4.4 Potential vs. Current Density Curves

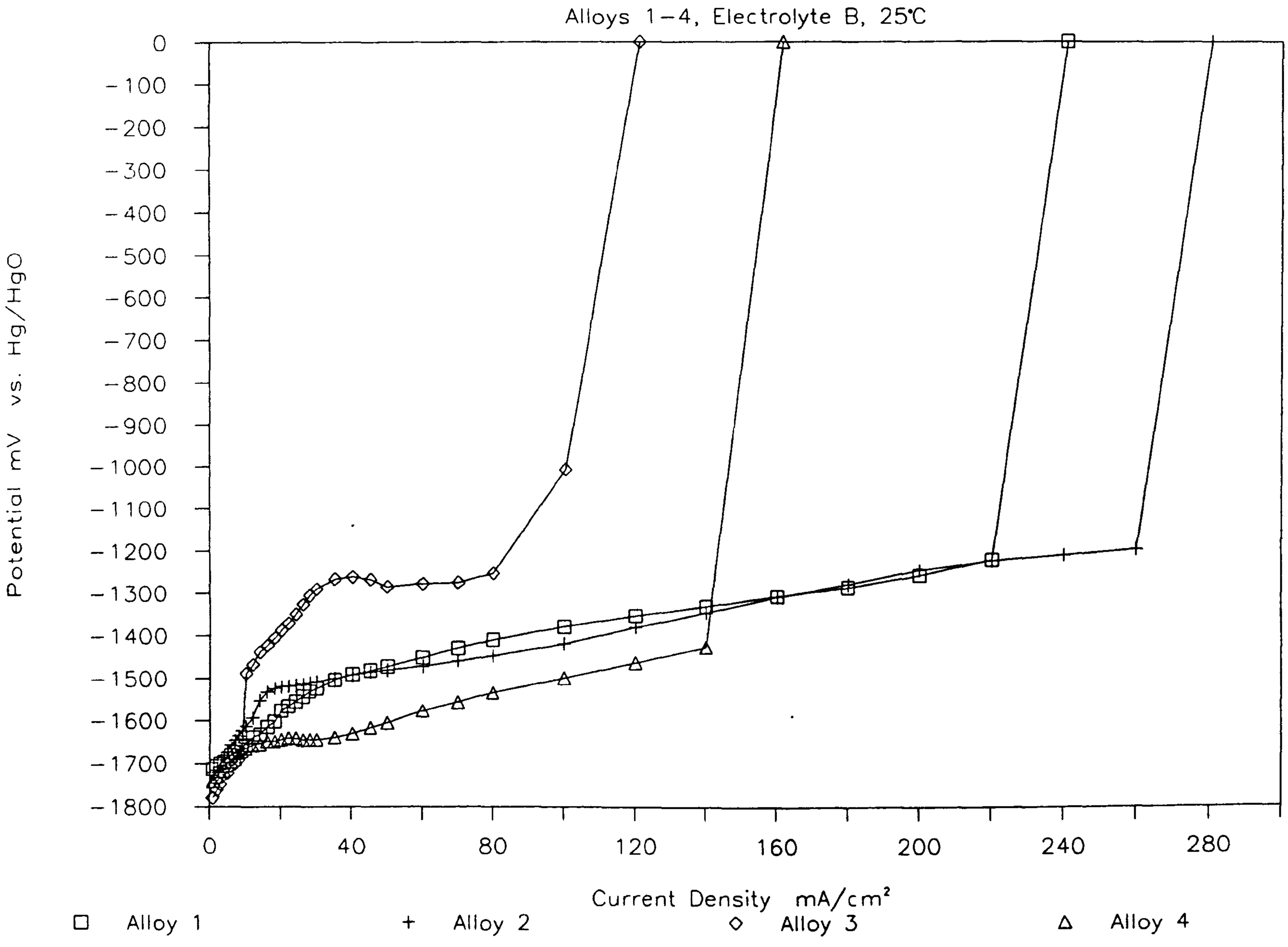

Figure 4.5 Potential vs. Current Density Curves

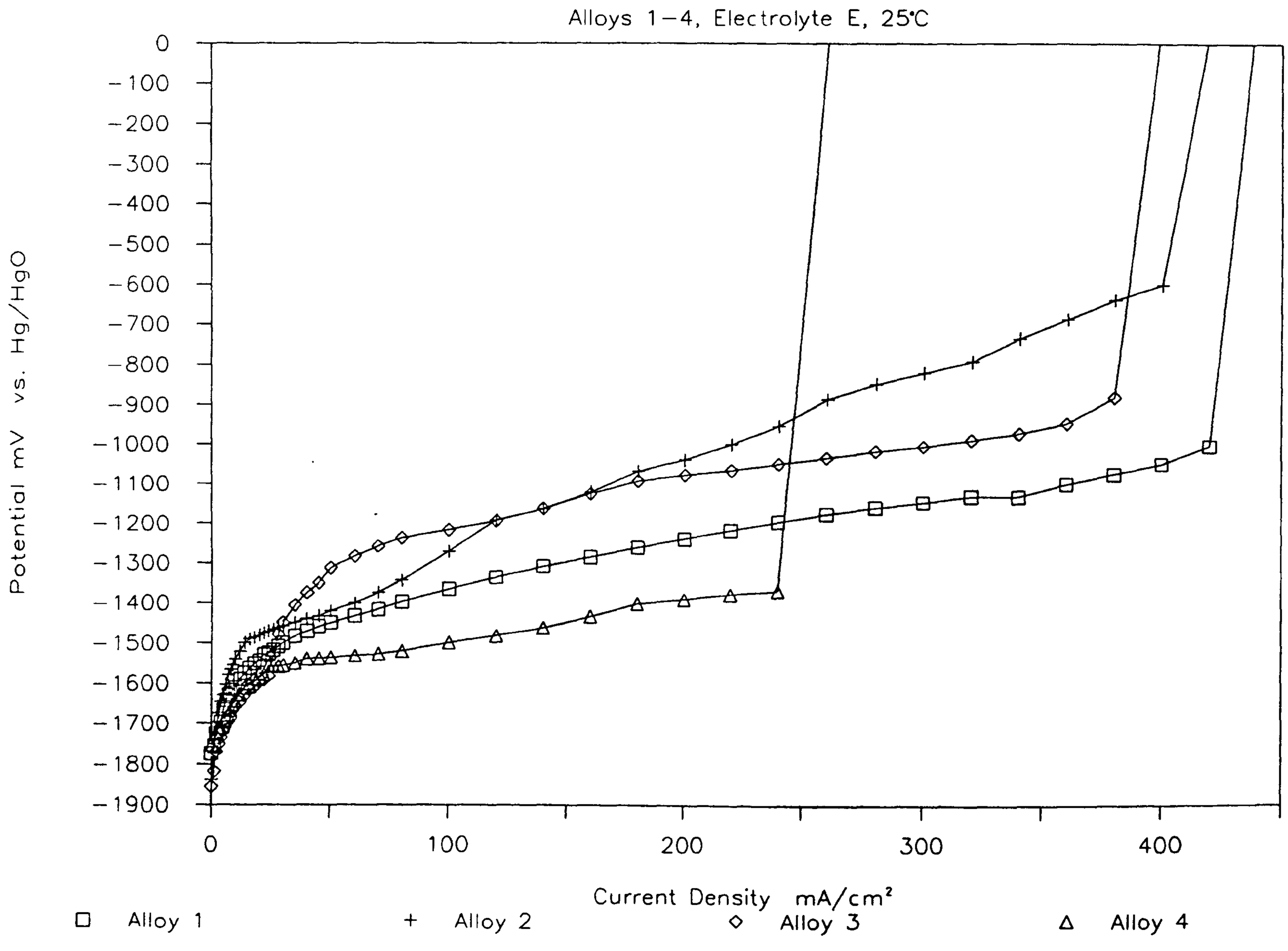

Figure 4.6 Potential vs. Current Density Curves

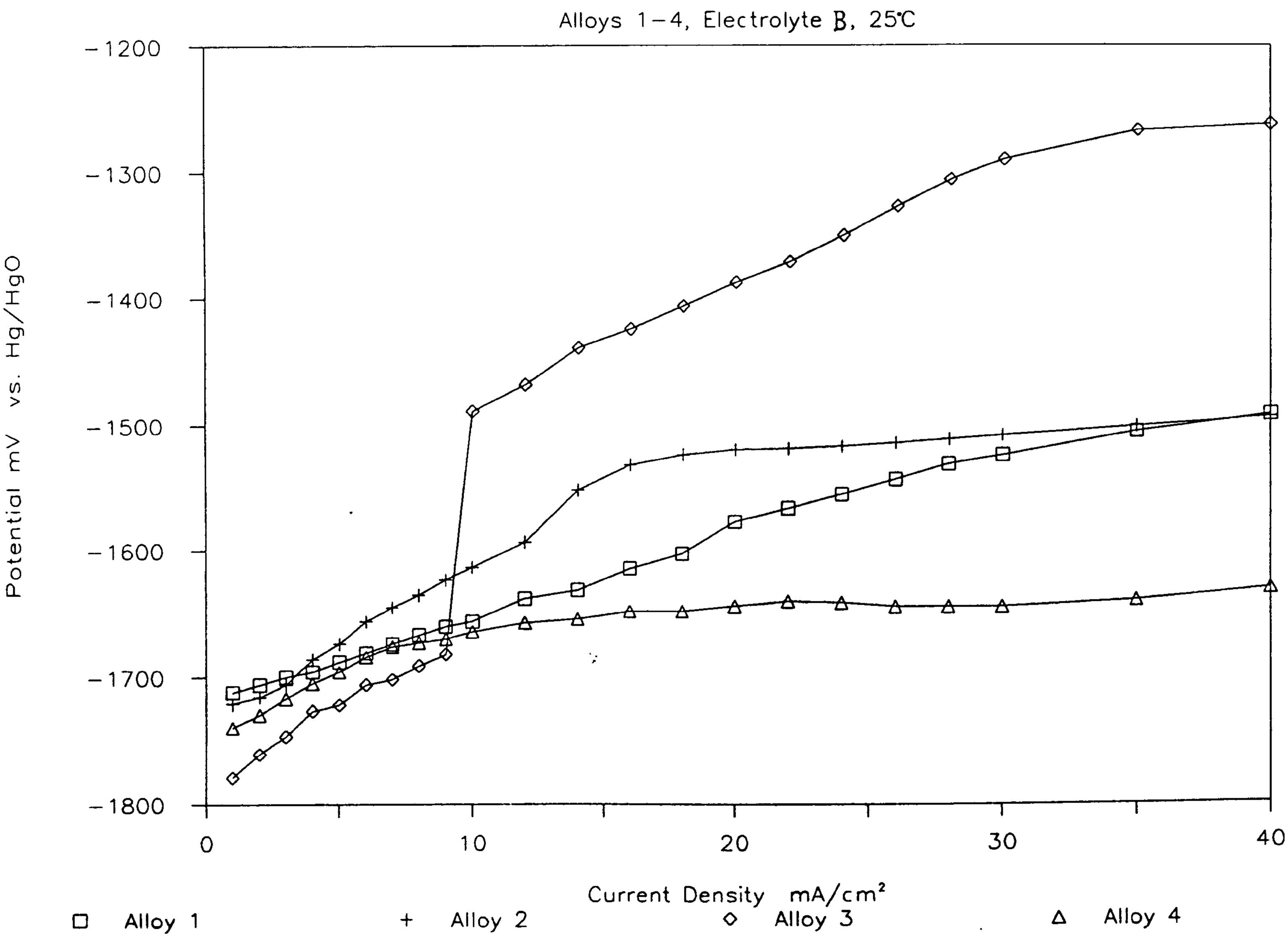

Figure 4.7 Potential vs. Current Density Curves

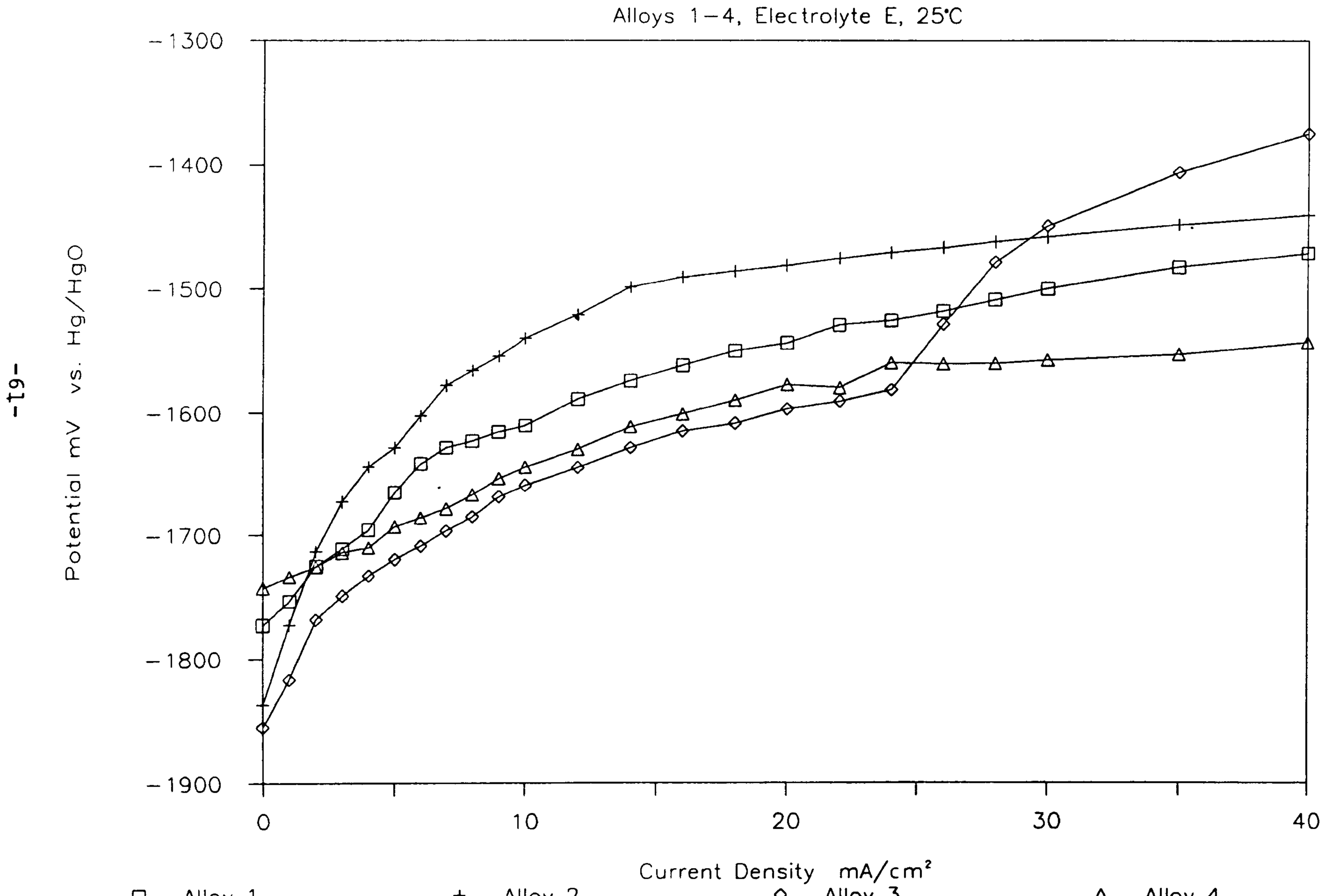

alloy 1 is similar ca. -1400mV at the same point, and for alloy 2 it is ca. 100mV more positive. The potential for alloy 2 remains more negative until limiting current density with electrolyte B, but for alloy 1 the reverse is true, it's potential being ca. -1330mV at 200mA/cm^2 in electrolyte E and -1280mV in electrolyte B. Figures 4.6 and 4.7 show the potential current density curves at low current density values. It is interesting to note that at these low current density values, the best performance comes from alloy 3, with it s low corrosion characteristics. The results show that alloy 3 has lower overpotential at higher current density values in electrolyte E than in the mixed electrolyte. At the current density 10mA/cm^2 alloy 4 takes over as the alloy with the lowest overpotential in electrolyte B, but in electrolyte E this does not occur until 25mA/cm^2. Table 4.2 gives the OCV values for the alloys in the various electrolytes at 25^{o}C.

Table 4.2 OCV Values (vs. Hg/HgO) in mV of Alloys 1-4 in Electrolytes A,B and E.

	Electrolyte		
Alloy	A	B	E
1	-1705	-1738	-1771
2	-1707	-1710	-1817
3	-1820	-1825	-1852
4	-1707	-1730	-1752
Aluminium	-1308	-1283	-1524

Each reading in the above table was taken after ca. 4 minutes in order for the potential to stabilise.

In every case the higher OCV value is obtained from using electrolyte E. The alloy which is affected the most from use of a mixed electrolyte (apart from bulk aluminium) is alloy 2, which loses ca. 100mV at OCV. The remaining three alloys have OCV values of 20 to 35mV more positive in mixed electrolyte B than electrolyte E.

At OCV the effect of alloying aluminium becomes quite clear. The presence of these elements in the aluminium causes anodic shifts of 397mV in electrolyte A, 427mV in electrolyte B, and 228mV in electrolyte E.

4.5.3 Tafel Plots.

From the voltage / current data recorded it was possible to construct Tafel plots of current density versus overpotential. Study of Tafel plots enables the exchange current density to be calculated. The exchange current density is a measure of the speed of the electrode reaction at it s reversible potential. The higher the value of the exchange current density the faster the electrode reaction. Correspondingly, the lower the value, the slower is the electrode reaction and the greater is the shift from reversible potential when a small current is flowing through the system. Basically, if the exchange current density

* It was pointed out by the examiners that the exchange current density is a measure of the speed of the electrode reaction at its reversible potential. As the half cell tests carried out result in an irreversible reaction, then it is the rate constant k_2^o that is actually measured.

value is high, then an electrode can pass high currents at low overpotentials. Exchange current densities typically fall in the range of 10^{-2} to 10^{-16} A/cm^2 [85].

Table 4.3 gives typical values of rate constants for the anodic reaction obtained for alloys 1-4 in electrolytes A,B and E.

Alloy/Electrolyte	Average k_2^o Value
1A	1.38
1B	1.67
1E	1.17
2A	2.22
2B	2.27
2E	0.78
3A	1.52
3B	1.03
3E	0.81
4A	1.08
4B	1.70
4E	1.54

For alloys 1 and 2 the rate constant k_2^o is highest in electrolyte B and lowest in electrolyte E. Alloy 3 displays different characteristics with electrolyte A having the highest value and again electrolyte E the lowest value. Alloy 4 is unique in that electrolyte A has the lowest value with electrolyte B again having the largest value. So with alloys 1, 2 and 4 use of electrolyte B results in the highest value for k_2^o. Thus use of electrolyte B with these alloys enables currents to be passed for lower overpotentials.

Study of the various Tafel slopes reveals interesting data other than the exchange current density. In each example three distinct curves are obtained. The first slope (marked (1) in Figure 4.8) is at low values of log i, and the electrode process can be said to be kinetically controlled in this region. The second slope (marked (2)) shows the diffusion influenced region of the electrode reaction, and finally, the slope marked (3) is obtained as the system approaches passivation.

Figures 4.9 and 4.10 show the Tafel slopes obtained for alloy 1 in electrolytes E and B. What is of interest here is the gradual increase in overpotential obtained in Figure 4.9, and the sharp change in slope that is obtained between the first and second curves in Figure 4.10.

Alloys 2 and 4 also give interesting results, both contain

similar amounts of gallium and mercury activating elements. They both also contain bismuth, indium, magnesium and thallium. Alloy 2 contains a significant amount of titanium and also tin. Alloy 4 has no titanium but it does contain almost three times as much tin as alloy 2. Figures 4.11 and 4.12 show the Tafel slopes for alloy 2, discharged in electrolytes E and B. Again it can be observed that the change from the electron transfer to diffusion influenced region for the electrode reaction is much more dramatic with the mixed electrolyte B than for electrolyte E. Also, the change in the slope occurs at a lower log i value for electrolyte B than it does for electrolyte E. Figures 4.13 and 4.14 represent alloy 4 in electrolytes E and B repectively. The most interesting point here is that in the diffusion influenced region, the overpotential is virtually constant with increasing log i and a plateau is observed in both electrolytes. The overpotential in this region is also considerably lower than the other alloys. As alloy 2 has similar additives, it is likely that the behaviour observed is related to the relatively high weight percentage of tin in the alloy.

Finally, Figures 4.15, 4.16 and 4.17 show the Tafel slopes obtained for the discharge of alloy 3 in electrolytes E, A and B respectively. These results show an extremely sharp increase in overpotential in the region 0.8-1.4 log i mA/cm^2 which is not observed to the same extent in any other alloy. This again is more pronounced for mixed electrolytes than

for electrolyte E. It is certain that the alloying elements are playing a significant role in this dramatic shift in overpotential. Alloy three contains a very high weight percentage of titanium. It is possible that during discharge, a layer of titanium forms on the electrode surface but as the current increases the layer begins to break down and we observe the dramatic increase in overpotential. Also this dramatic increase in overpotential occurs at much higher current density values for electrolyte E than for the mixed electrolytes. It can also be observed from study of the Tafel plots that in the electron transfer controlled electrode reaction region alloy 3 has the lowest overpotential.

In order to further investigate the sharp change of slope in overpotential observed for alloys 1, 2 and 4 in the mixed electrolytes, half cell tests were carried out using 40 wt/v % sodium hydroxide saturated with mercury. The experimental conditions were as previously described and Tafel plots were obtained. Figure 4.18 shows the Tafel slope for alloy 1 and is a typical example of results obtained. What we observe is an increase in overpotential and then a sudden change in slope at 1.2 log i mA/cm^2. For alloy 1 in electrolyte E (see Figure 4.9), the increase in overpotential is gradual and occurs at much lower values of overpotential. The higher overpotential values and sudden change in Tafel slope at 1.2 log i mA/cm^2 in Figure 4.18 must therefore be due to the use of sodium hydroxide electrolytes as increases in

Figure 4.8 Tafel Plots

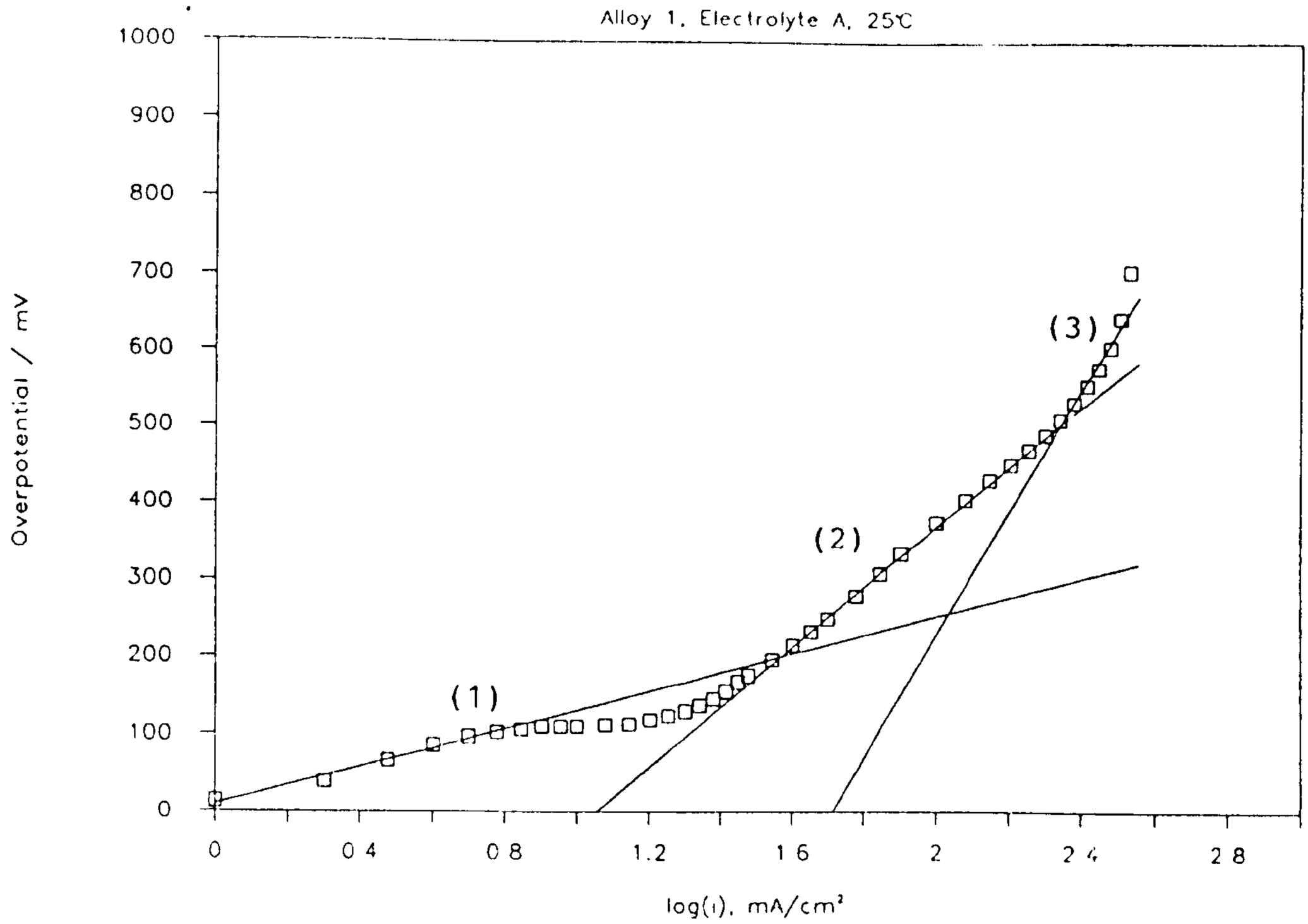

Figure 4.9 Tafel Plots

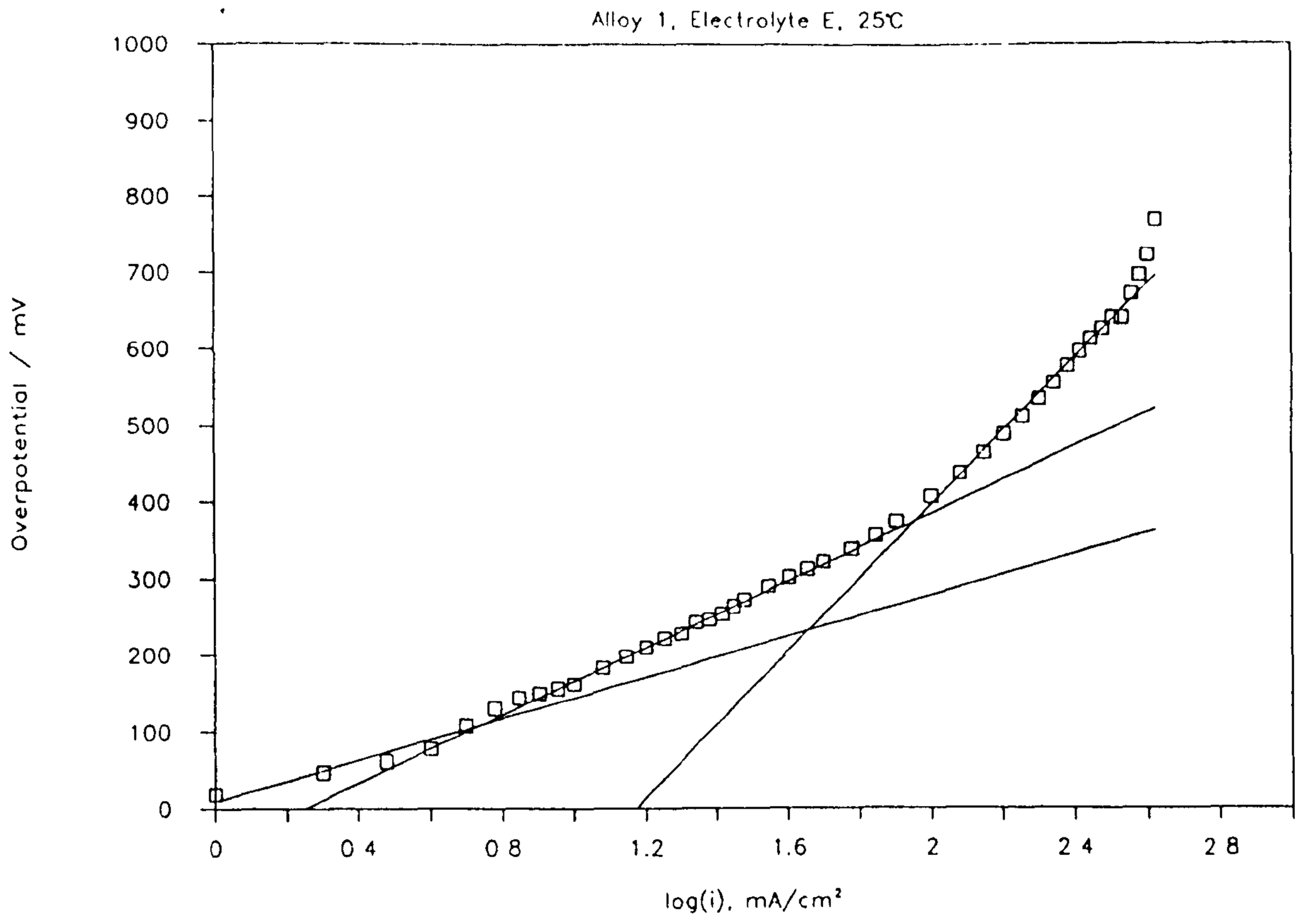

Figure 4.10 Tafel Plots

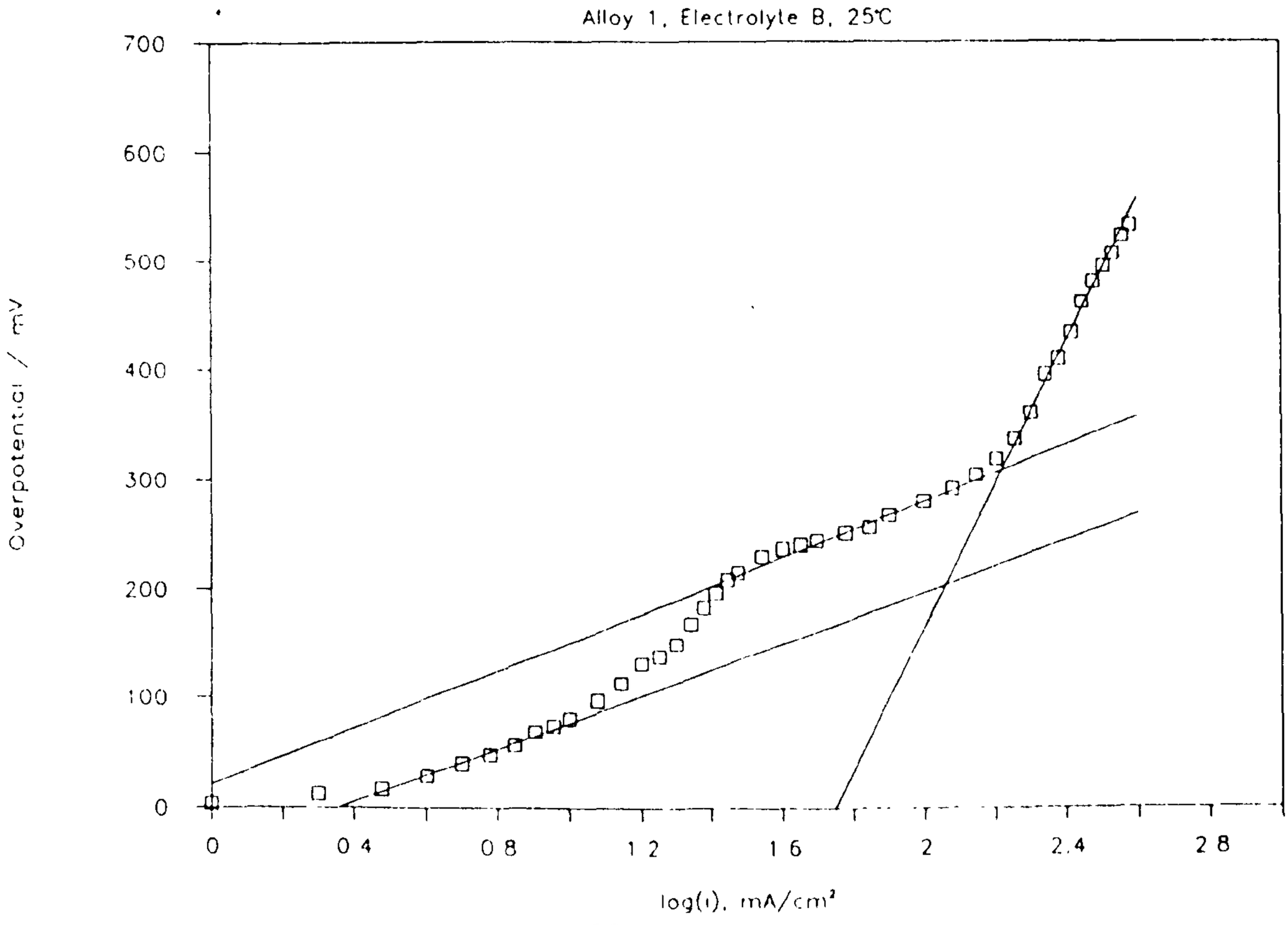

Figure 4.11 Tafel Plots

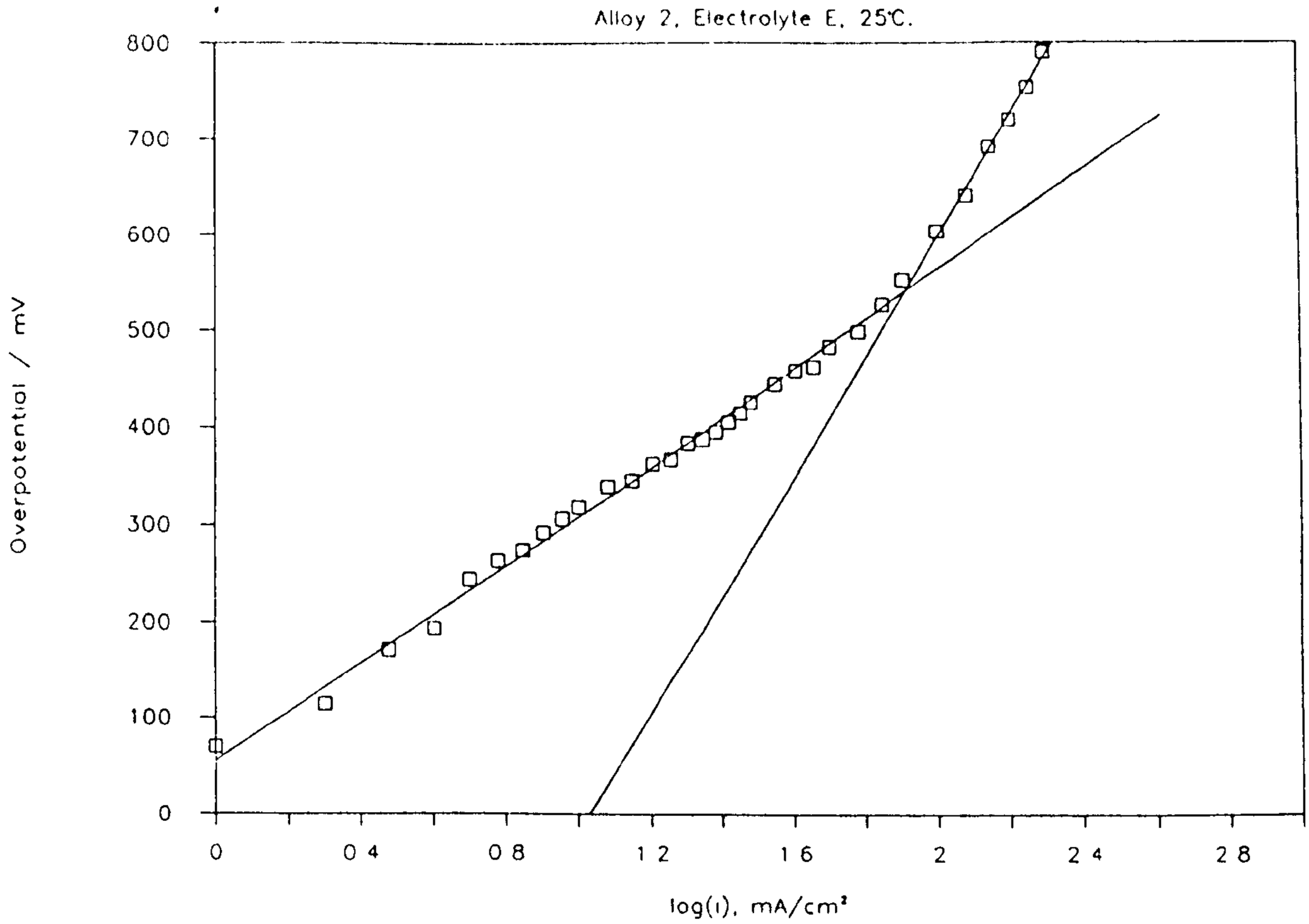

Figure 4.12 Tafel Plots

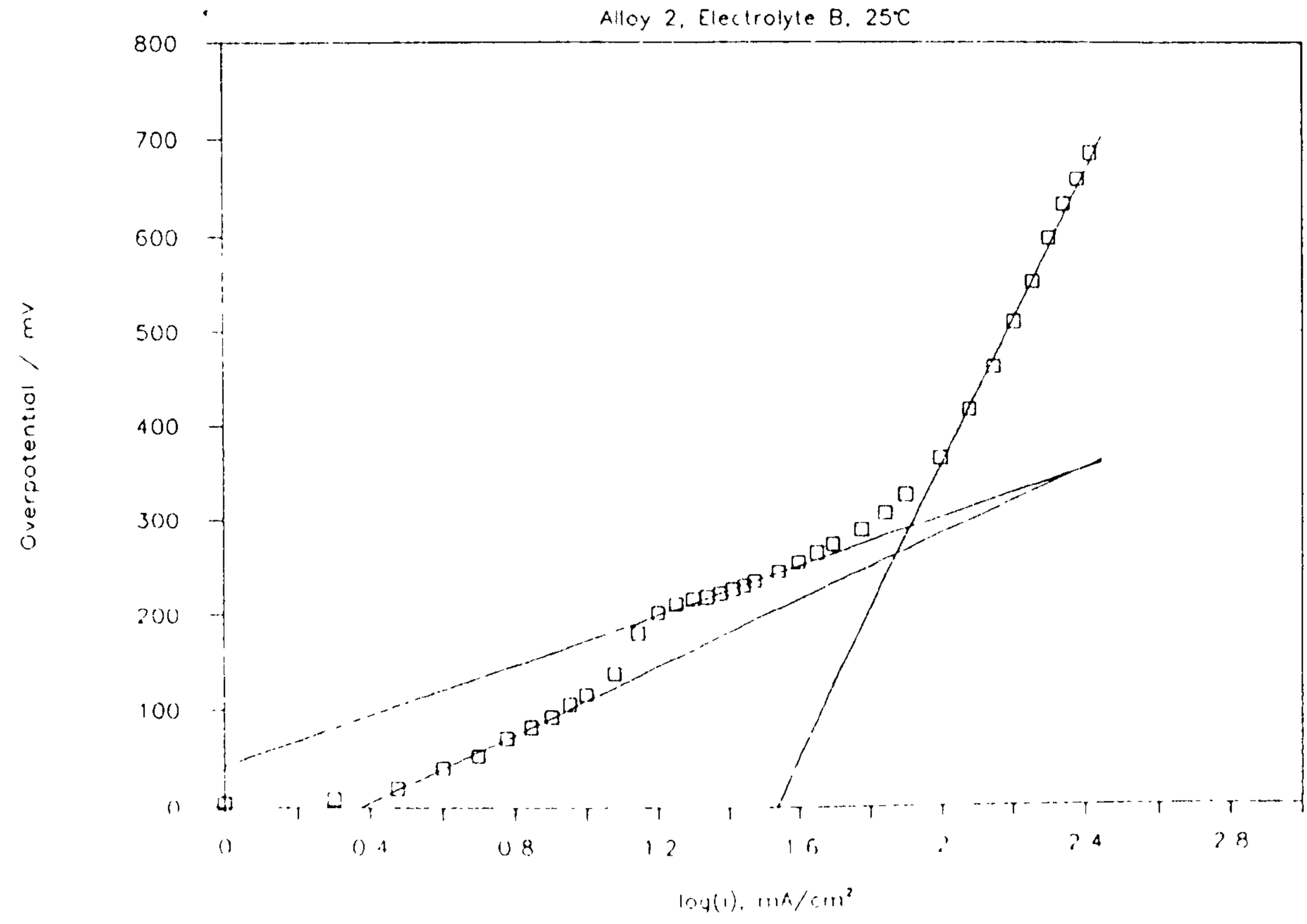

Figure 4.13 Tafel Plots

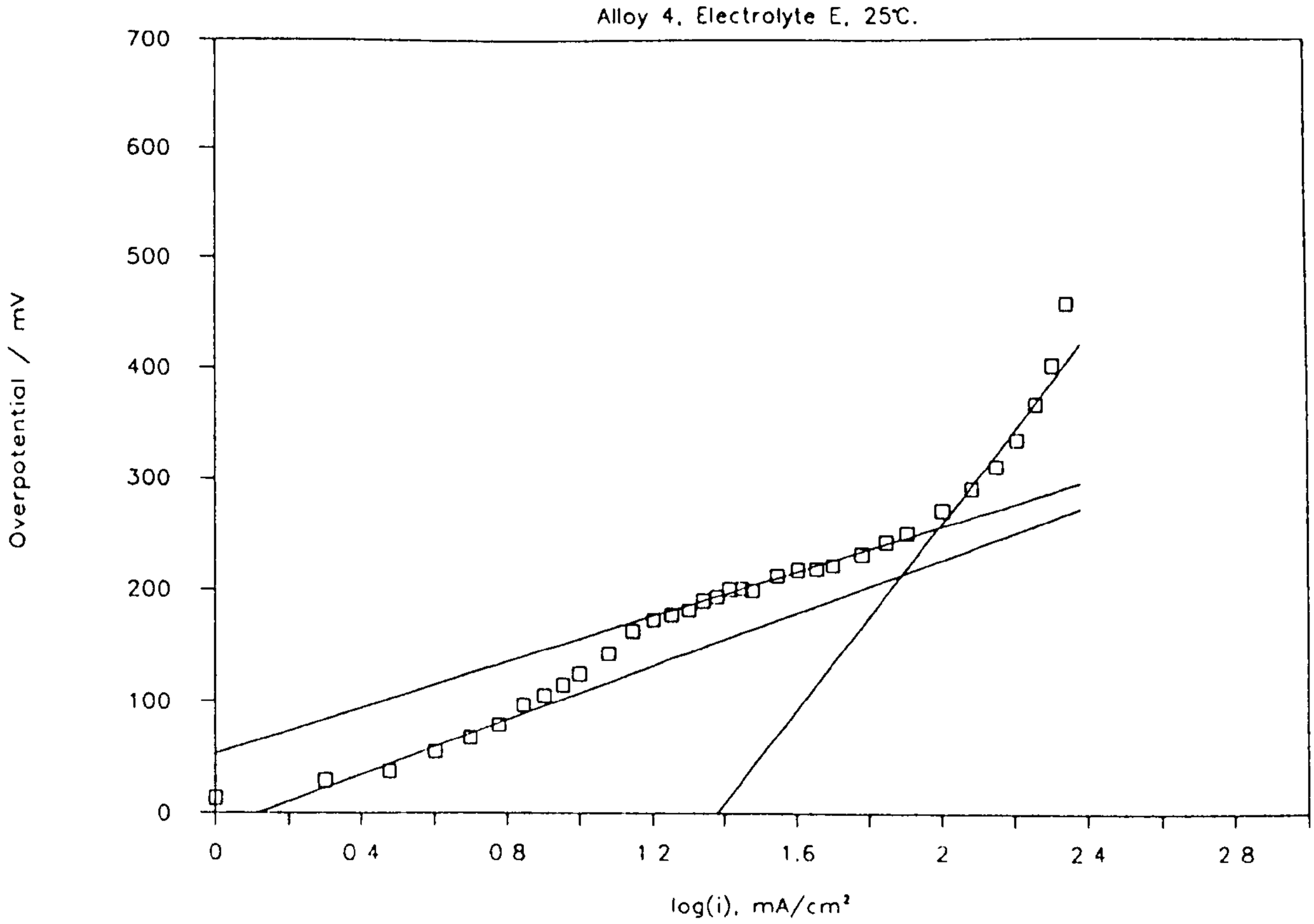

Figure 4.14 Tafel Plots

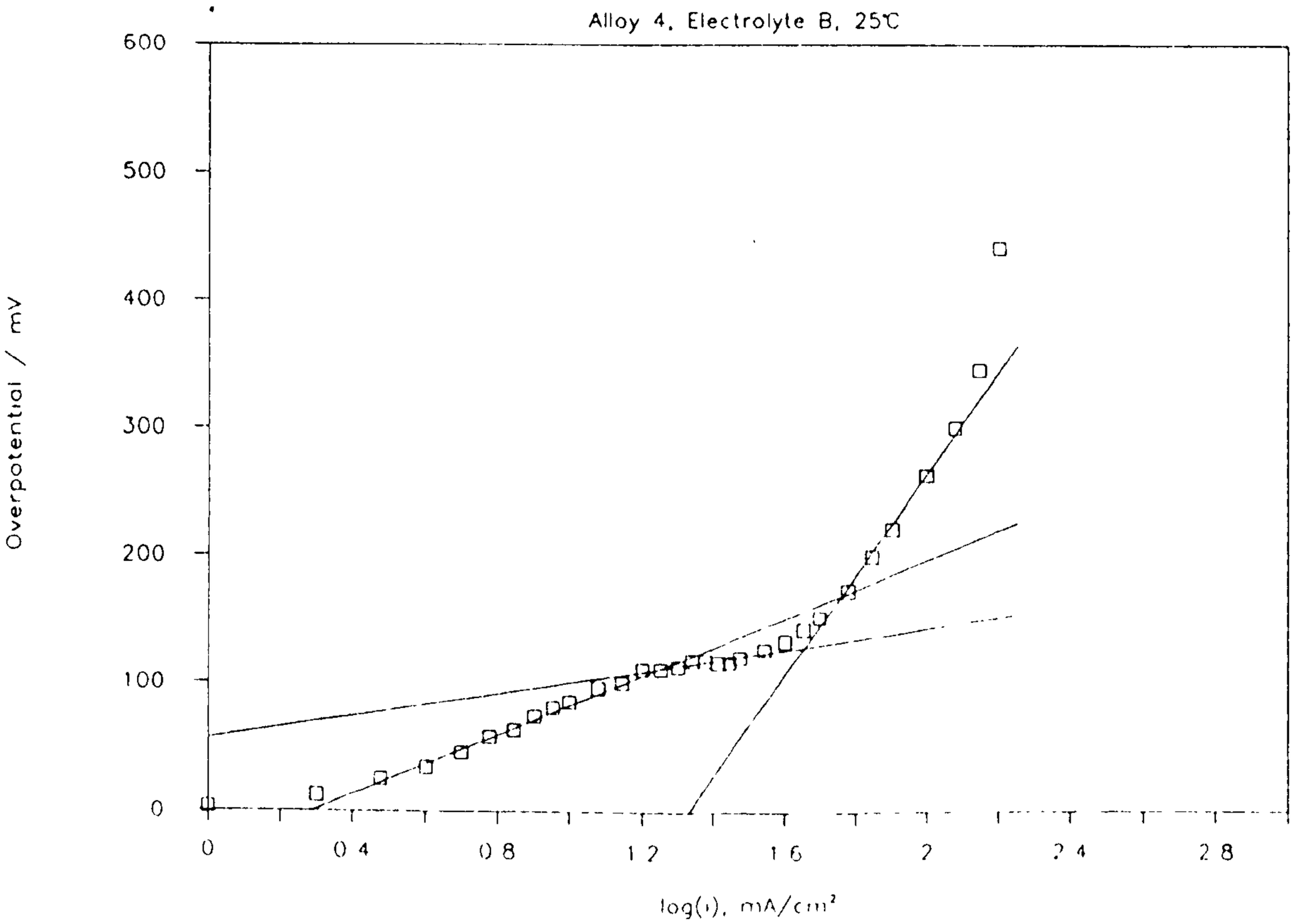

Figure 4.15 Tafel Plots

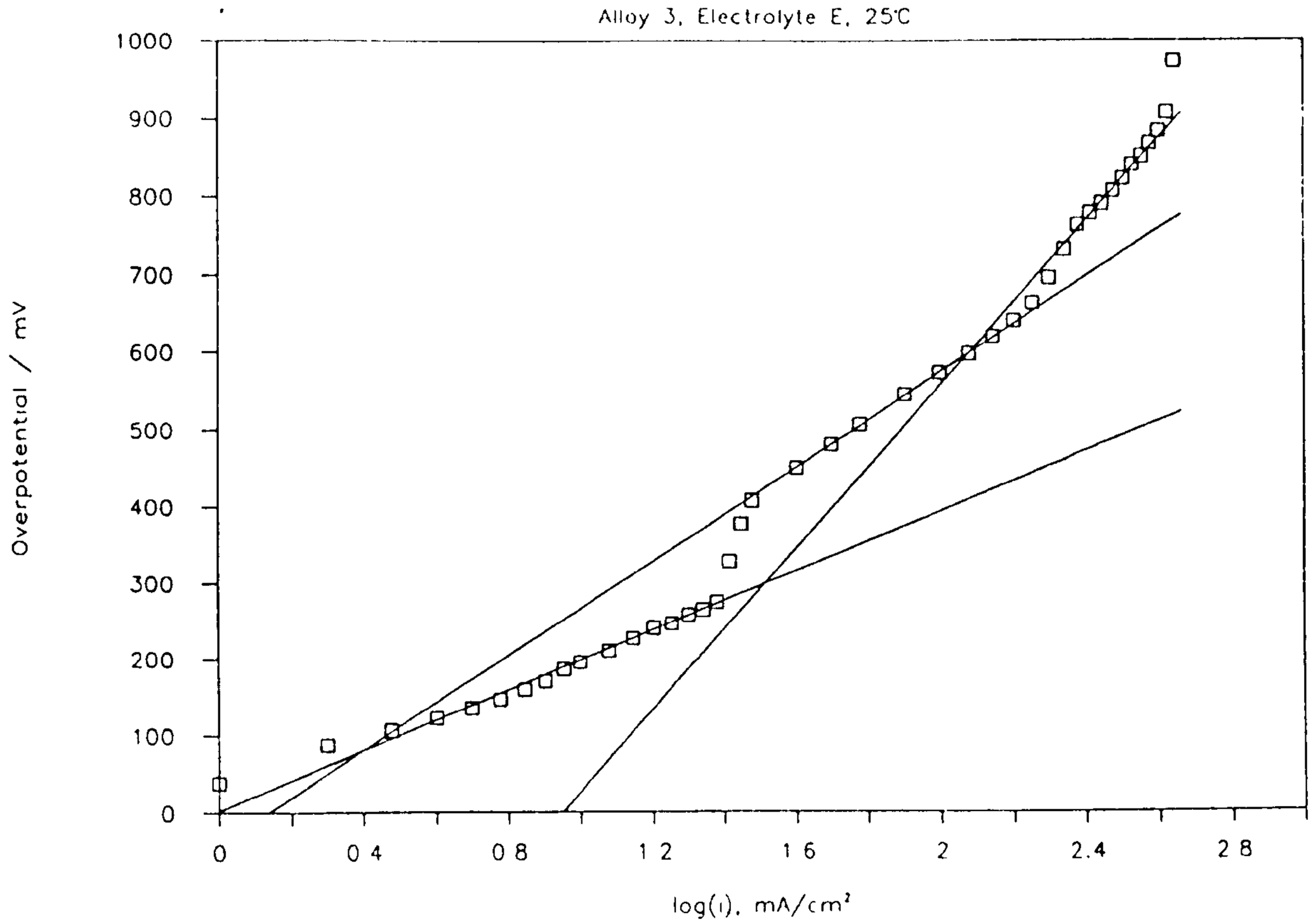

Figure 4.16 Tafel Plots

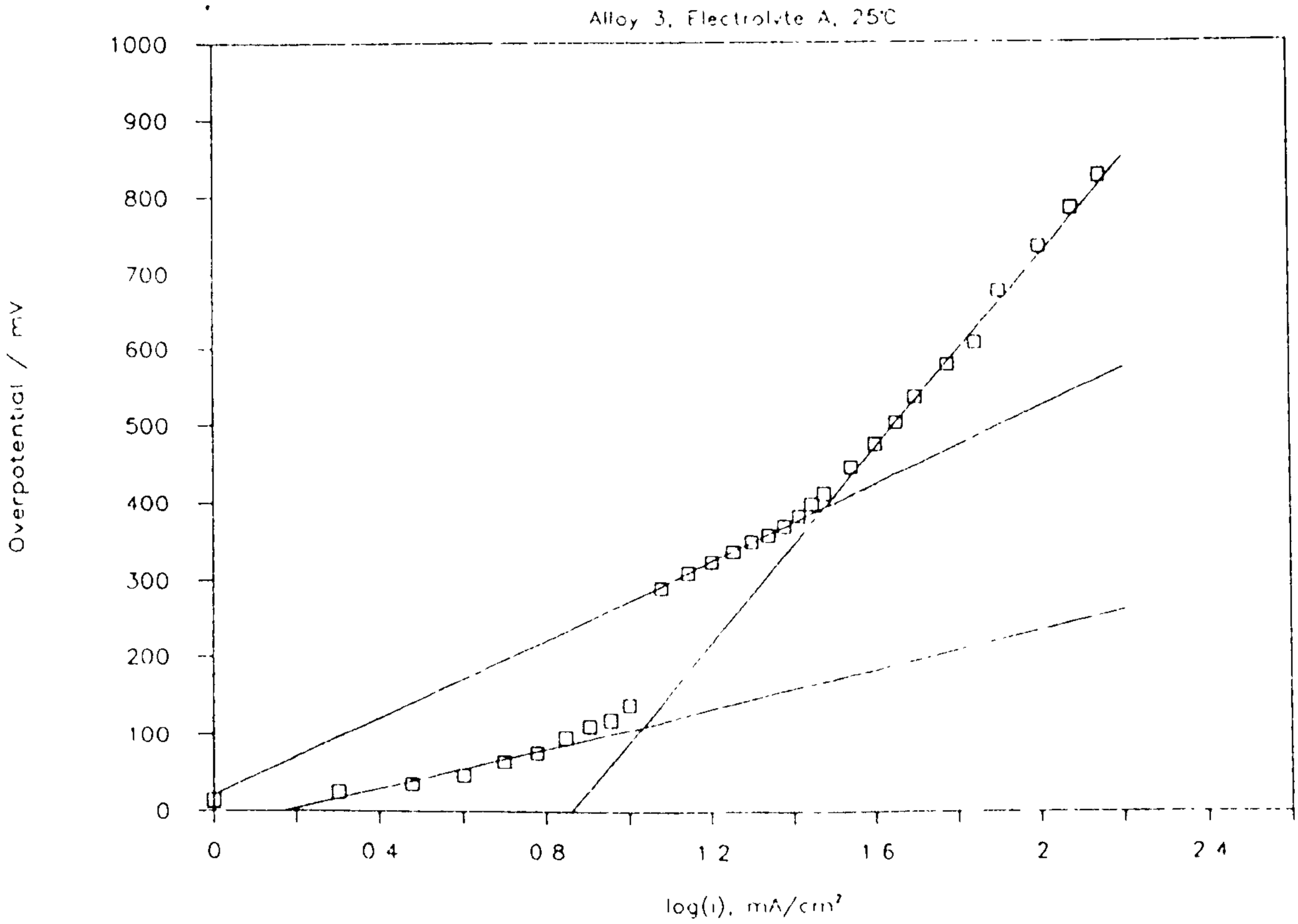

Figure 4.17 Tafel Plots

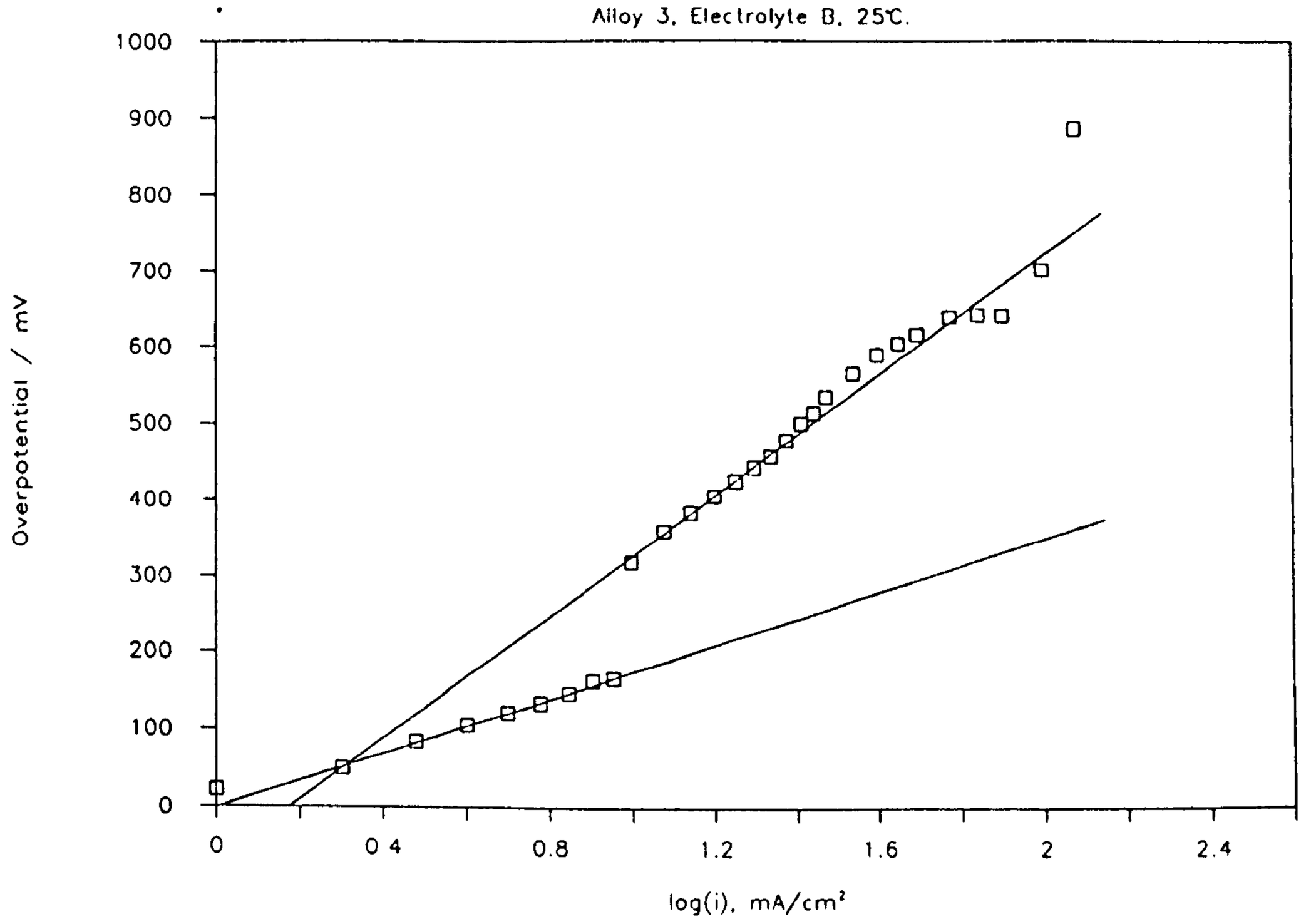

Figure 4.18 Tafel Plots

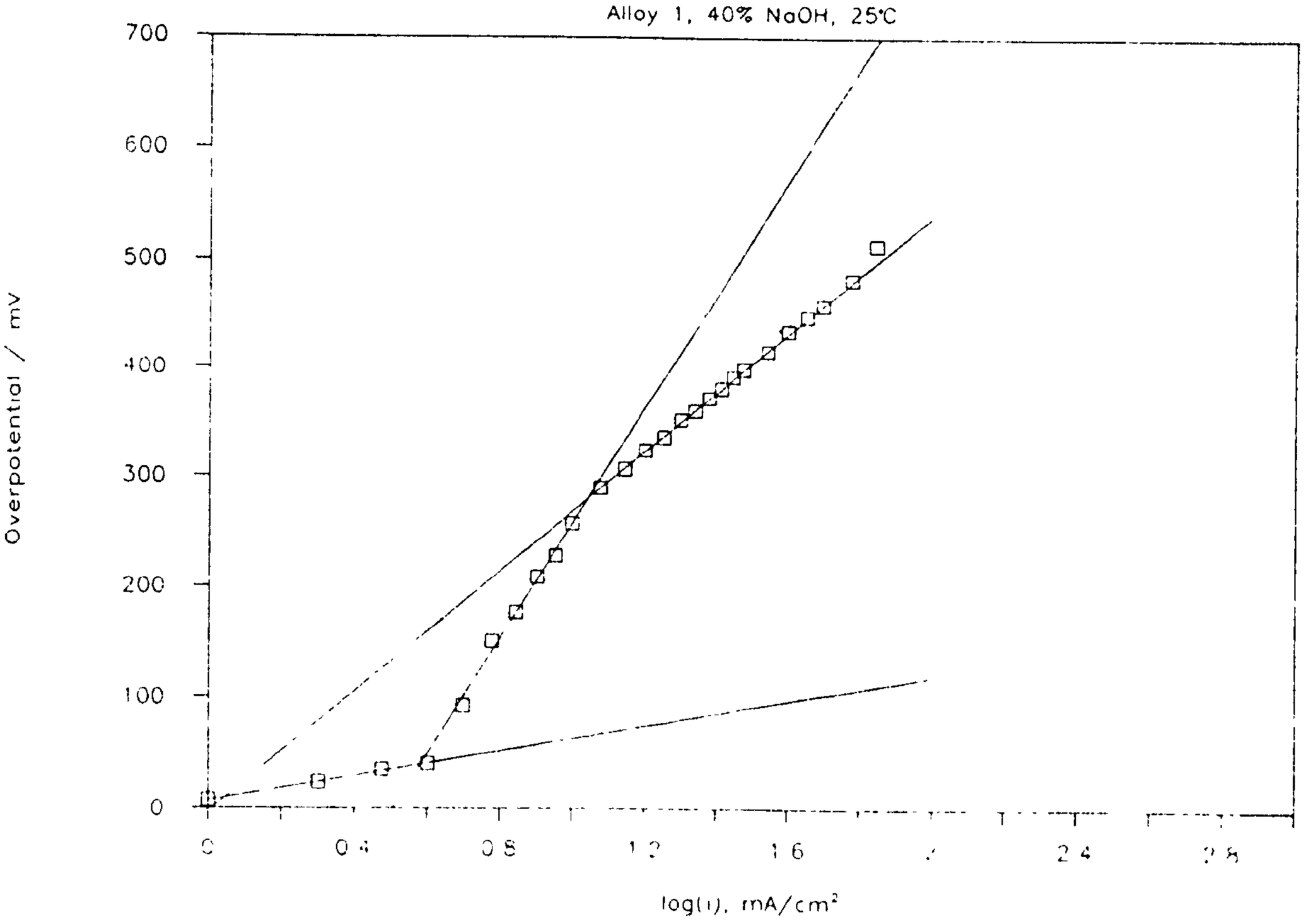

overpotential are not observed to the same extent with electrolyte E nor the sudden change in Tafel slope so apparent. This characteristic must therefore be related to the presence of sodium hydroxide electrolyte.

4.5.4 Discussion.

In comparing all the results it is noticeable that in the mixed electrolytes, there is a prominent change in slope as the electrode process changes from being kinetically controlled to diffusion influenced. See alloy 4 electrolyte B (Figure 4.14), alloy 2 electrolyte B (Figure 4.12), and alloy 3 electrolytes A and B (Figures 4.16 and 4.17 respectively). With electrolyte E, this dramatic shift between the two regions is not so pronounced, and is in fact a much more gradual process. See alloy 1 electrolyte E (Figure 4.9), alloy 2 electrolyte E (Figure 4.11) and alloy 4 electrolyte E (Figure 4.15). Also of significance, is that diffusion influenced region begins at higher values of log i in electrolyte E than it does in mixed electrolytes A and B.

In an attempt to explain these characteristics it is necessary to look at the results obtained from work done in chapter 5. Results from this chapter show that with the use of sodium hydroxide and sodium and potassium hydroxide electrolyte mixtures, the structure of the reaction product is in granule form. However, with use of potassium

Figure 4.19 Possible Initiation Stage of Precipitation on Electrode Surface After Discharge in ;

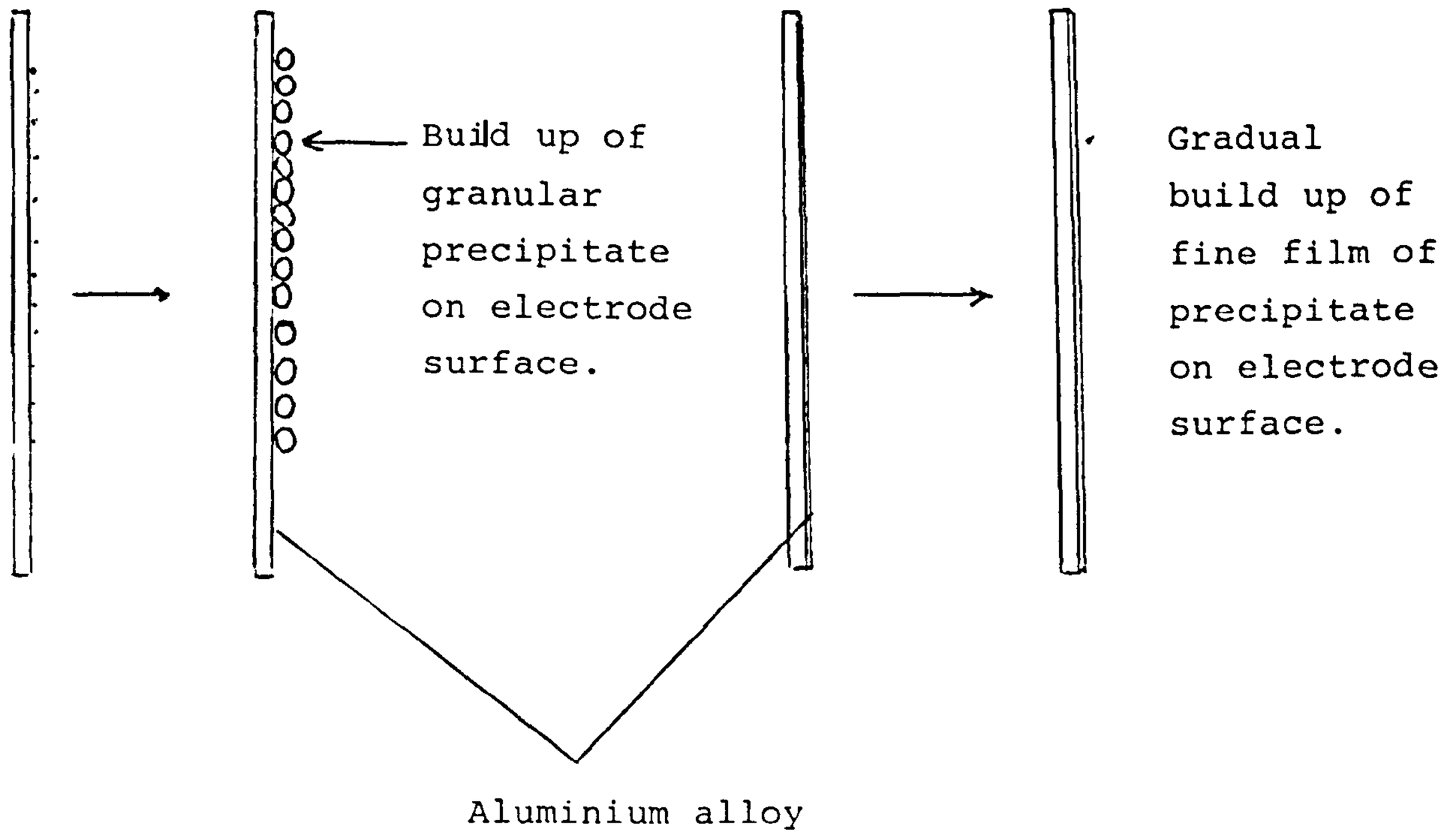

hydroxide electrolyte, the precipitate formed is a fine powder like structure. These findings could be related to the Tafel plot characteristics that have been pointed out. Figure 4.19 shows the possible initiation stage of precipitation occuring on the electrode surface.

It is possible that resistance to diffusion is greater for the initiation stage of granule formation than for thin film formation. This could explain why there is a gradual change from the kinetically controlled to the diffusion influenced process for electrolyte E i.e. the gradual build up of thin film precipitate is represented by the gradual increase in the Tafel slope. As for the mixed electrolyte which results in the formation of larger granules, there is a thicker spherical formation on the electrode surface which is reflected in the sharp change in the Tafel slope due to the sudden shift from the kinetically controlled to diffusion influenced electrode process.

4.6 Transient Measurements.

Experiments involving the transient polarisation of alloys 1-4 in electrolytes A, B and E were carried out as stated in section 3.3.1 (b).

Sweeps were carried out at rates of 2, 10 and 20 mV/s. On increasing the sweep rate there was no apparent change in slope of the voltage current curve obtained. Limiting

current did increase with increasing sweep rate.

Again with transient measurements, alloy 4 was found to have the most anodic potential up to limiting current density in all electrolytes. This alloy was followed by alloy 2 then alloy 1. Alloy 3 had the lowest potential and again this was consistent in all electrolytes. Also it was noted that all alloys had a greater limiting current density in electrolyte E rather than mixed electrolytes A and B.

Figure 4.20 Transient Polarisation, Alloys 1–4.

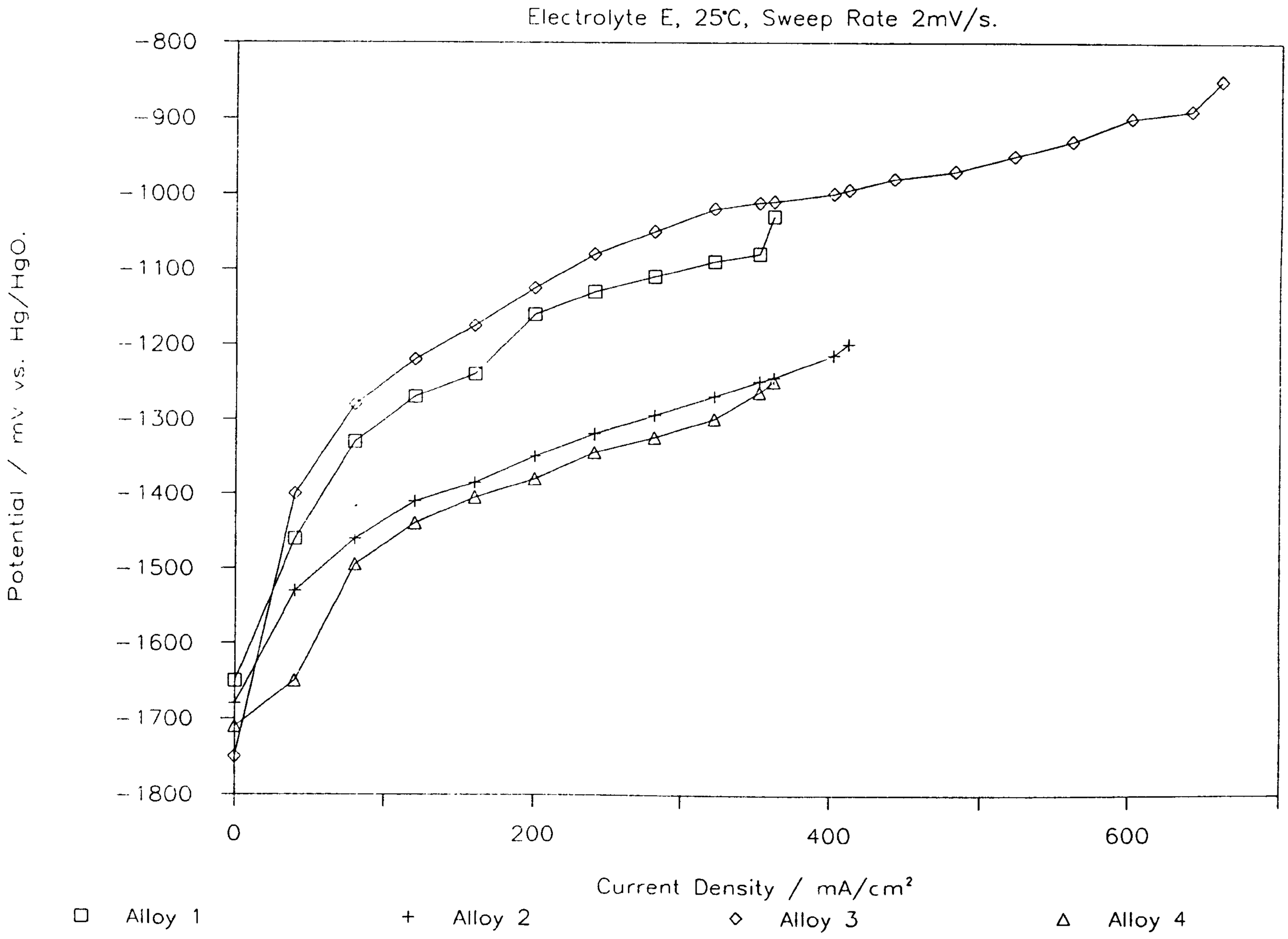

Figure 4.21 Transient Polarisation, Alloys 1–4.

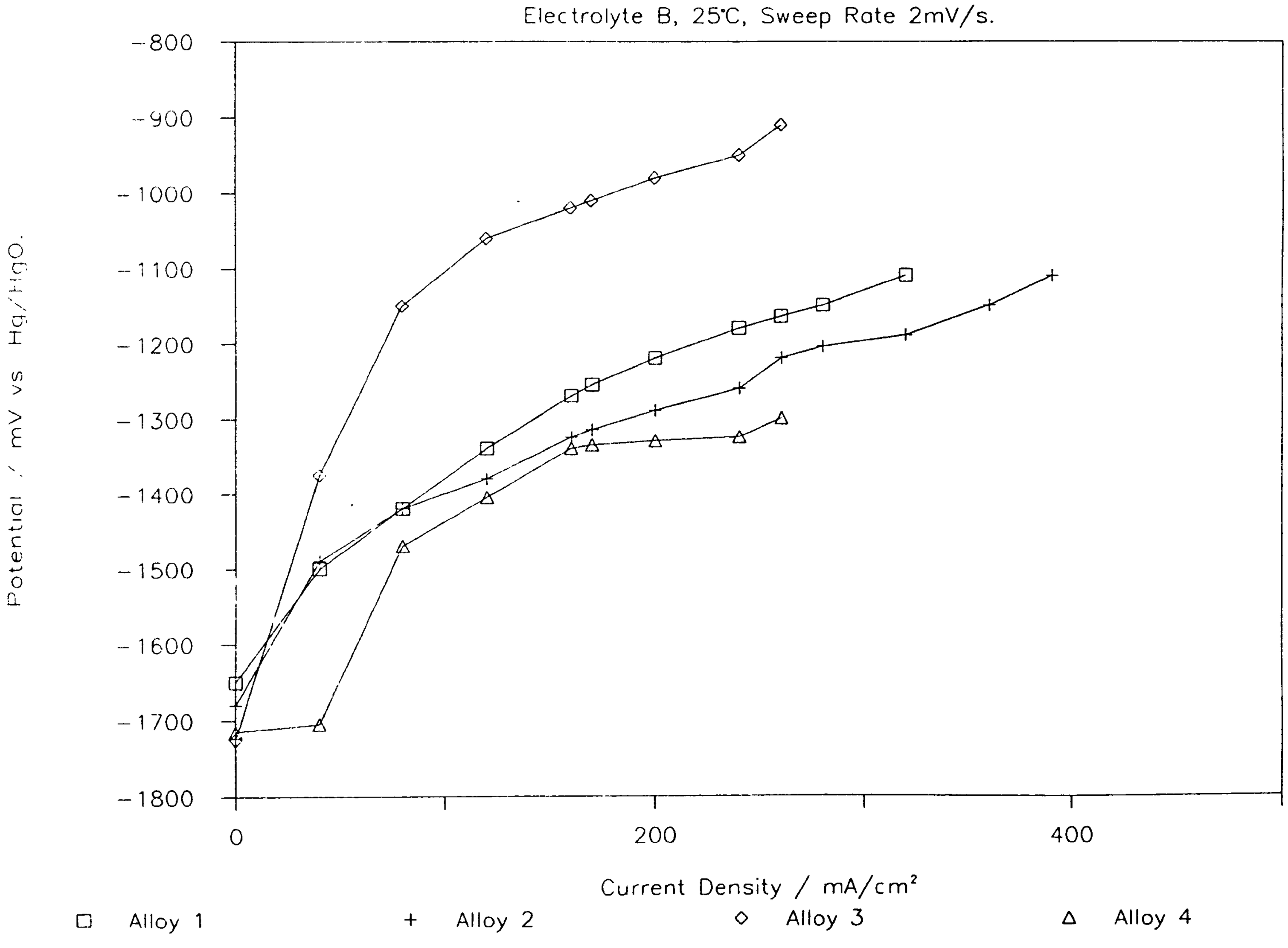

4.7 Scanning Electron Microscope Surface Examination of Alloys.

The scanning electron microscope was used to study electrode surfaces prior to, and after discharge in order to determine if the alloying elements build up on the surface during discharge in the electrolyte.

4.7.1 Experimental Procedure.

Alloys were discharged in electrolyte E using the half cell system described in section 3.3.1. The area of aluminium electrode exposed was $0.5cm^2$, and the current density $60mA/cm^2$. The electrodes were discharged for a period of one hour. The volume of electrolyte used was $10cm^3$, and the temperature controlled at 25^{o} C. The electrodes were then examined using the electron microscope and the distribution of the trace elements analysed using the EDAX distribution mapping system. Electron micrographs were taken and compared with those taken before discharge. All alloys were initially prepared as described in section 3.2.1.

4.7.2 Results and Discussion.

The results of the experiment are given in Table 4.4. A dramatic increase in alloy element centres was observed for certain elements, and these are marked as having increased in quantity on the electrode surface after discharge. Some examples of the distribution map micrographs are shown in

Table 4.4 Surface Composition Change After Discharge in Alkaline Electrolyte.

		Alloy		
	New Q4	Sea Water	Low Corrosion	High Power
Element	1	2	3	4
Bi	o	o	o	o
Cu	o			+
Fe	+	o	+	+
Ga	-	o		+
Hg		o	o	+
In		o	+	+
Mg	+	o	+	+
Mn	+		+	
Pb	o	o	o	
Sn		+		+
Ti	+	+	+	+
Tl		o	-	+
Zn	o			

key ;

o Little or no apparent change in quantity of element on electrode surface after discharge.

- Decrease.

+ Increase.

Figure 4.22 Electron Micrographs Showing the Distribution of Tin on the Surface of Alloy 2 a) Before and b) After Discharge. (20keV x 1.00k)

a)

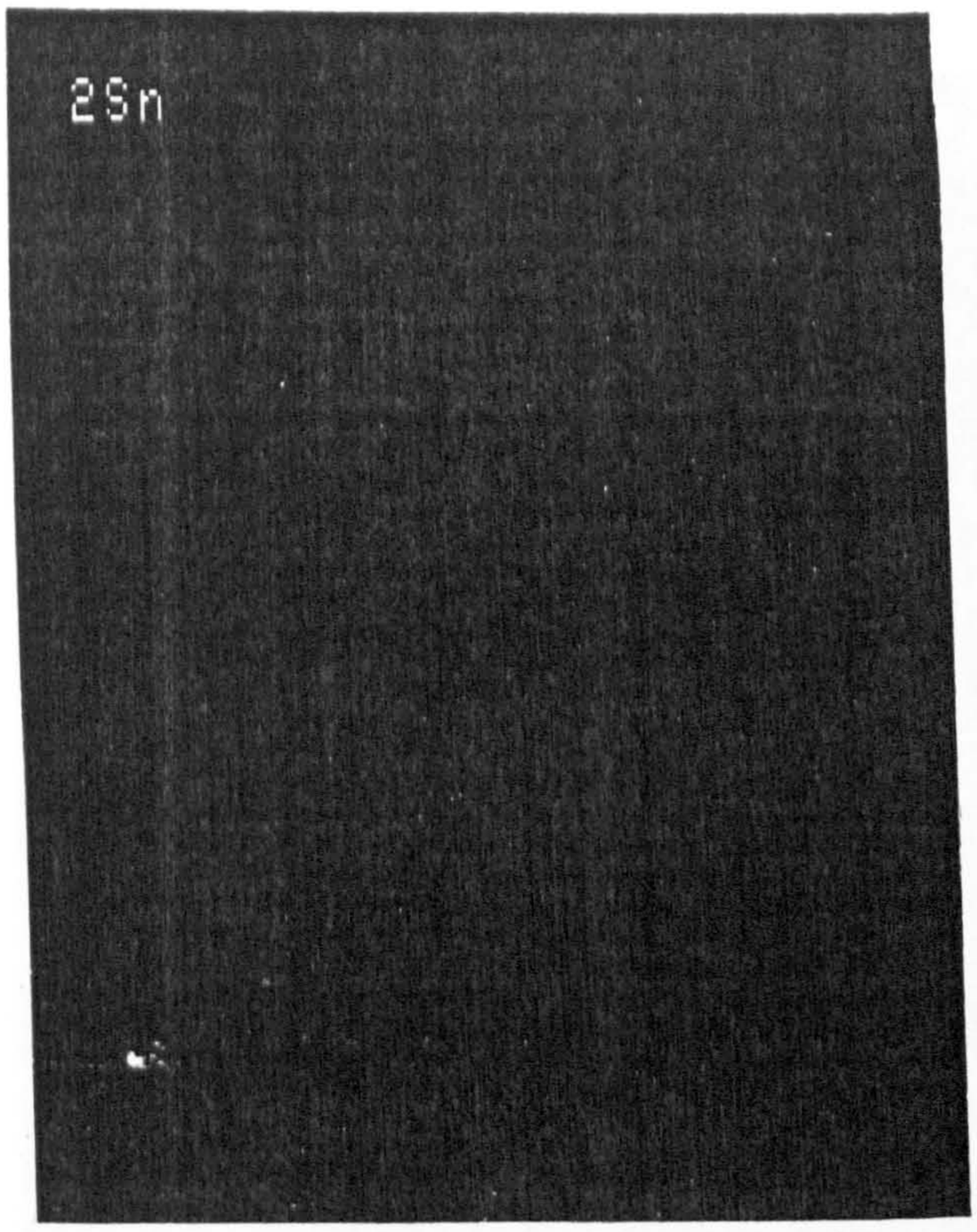

b)

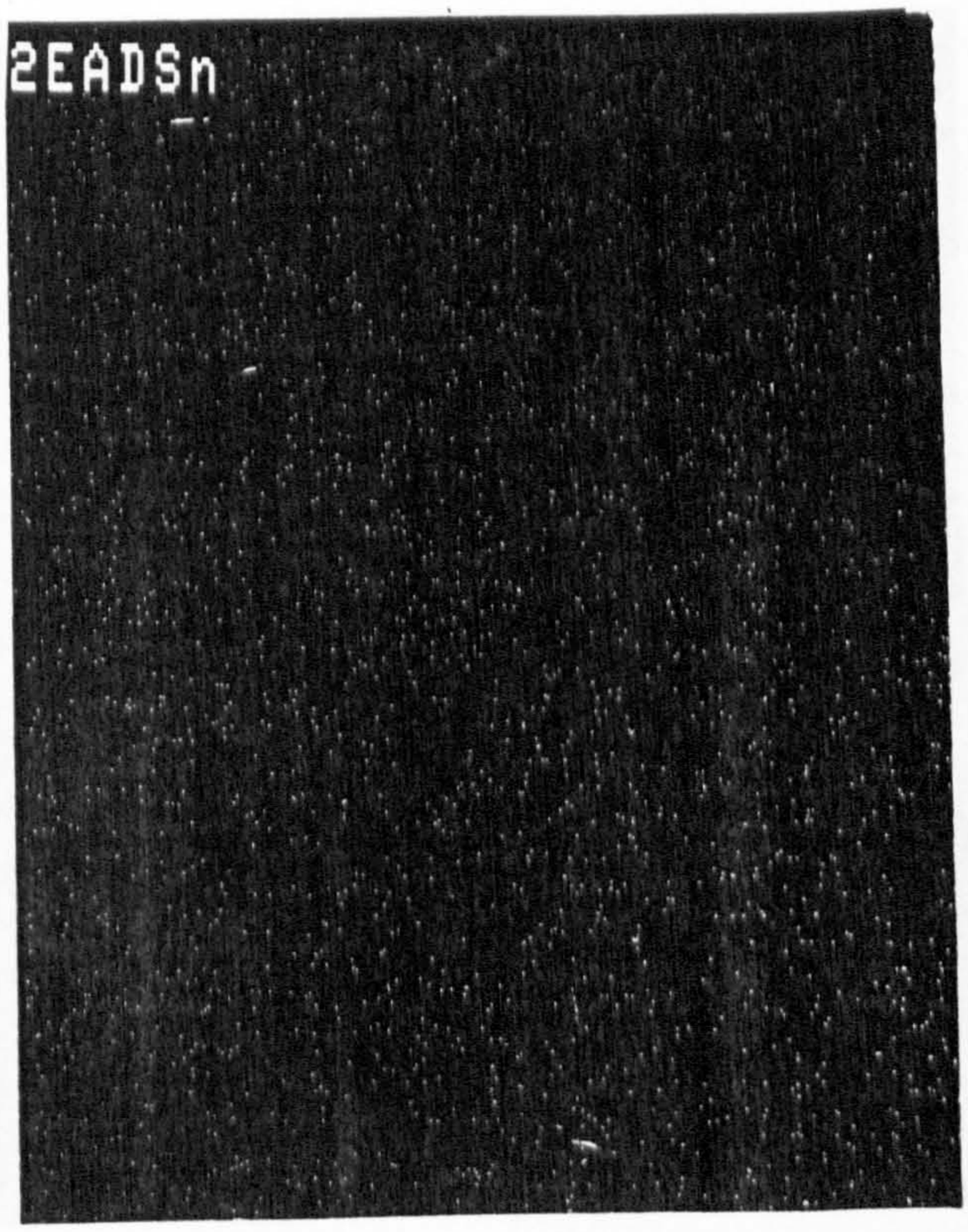

Figure 4.23 Electron Micrographs Showing the Distribution of Titanium on the Surface of Alloy 2 a) Before and b) After Discharge. (20keV X 1.00k)

a)

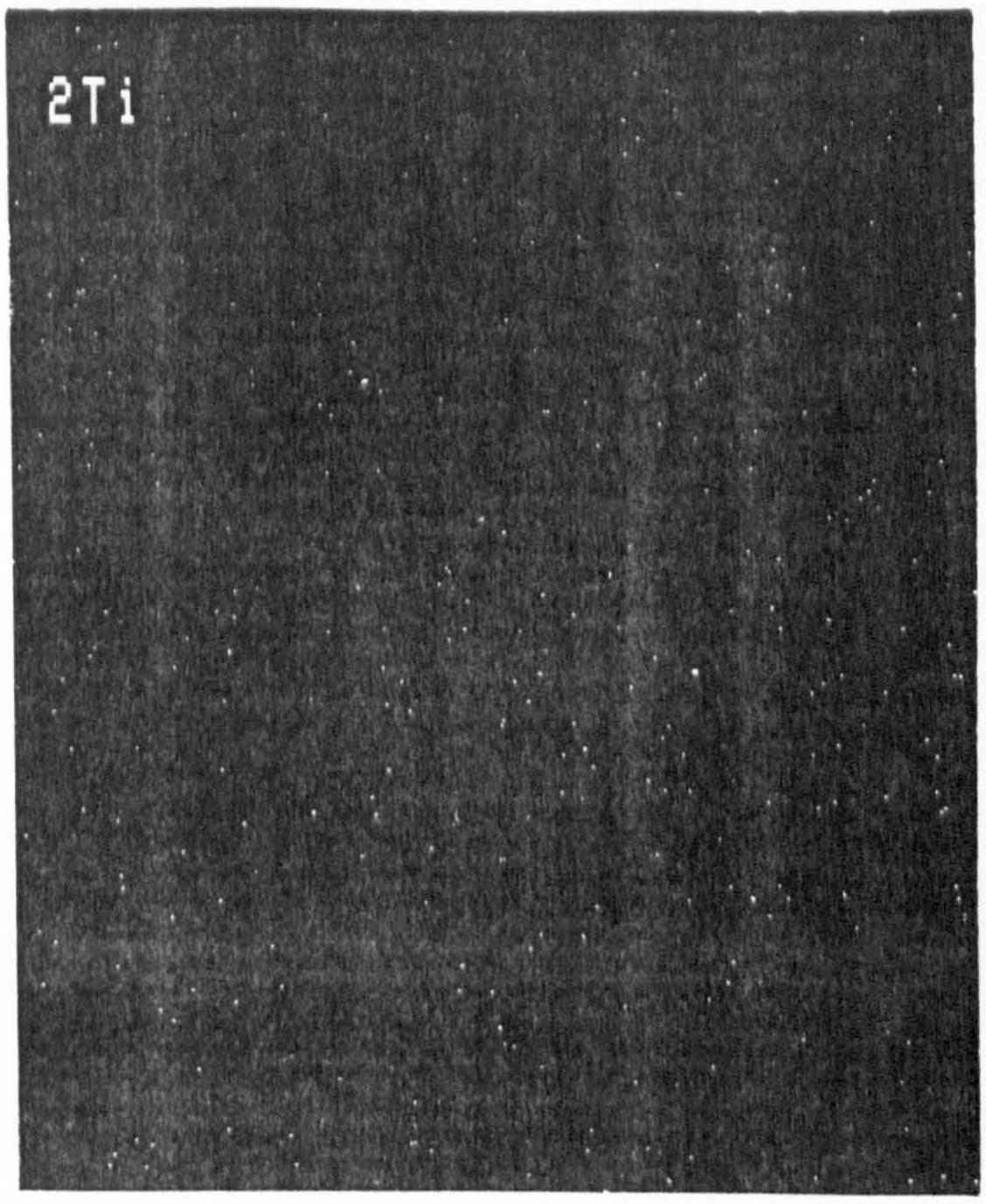

b)

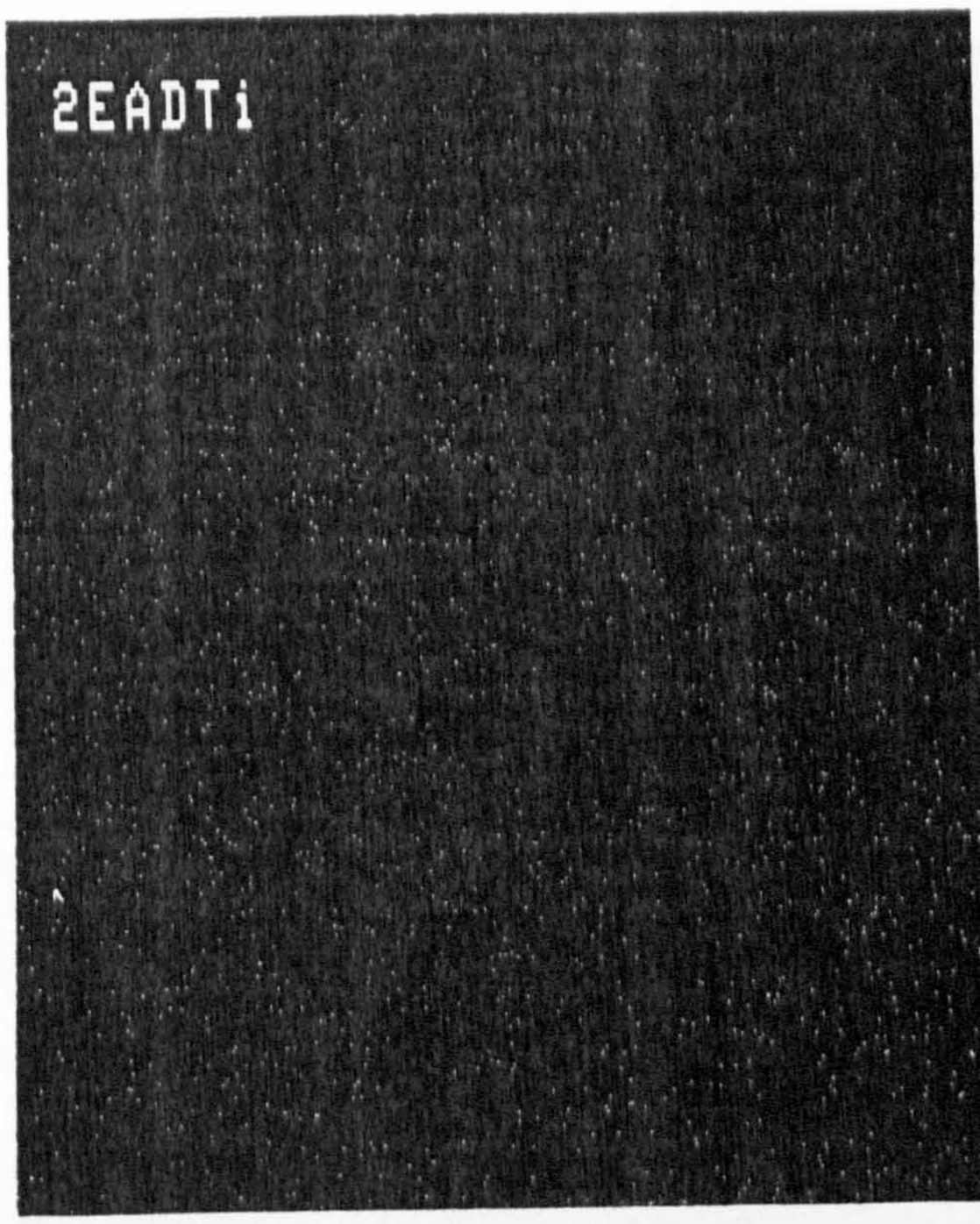

Figure 4.24 Electron Micrographs Showing the Distribution of Gallium on the Surface of Alloy 4 a) Before and b) After Discharge. (20 keV X 1.00k)

a)

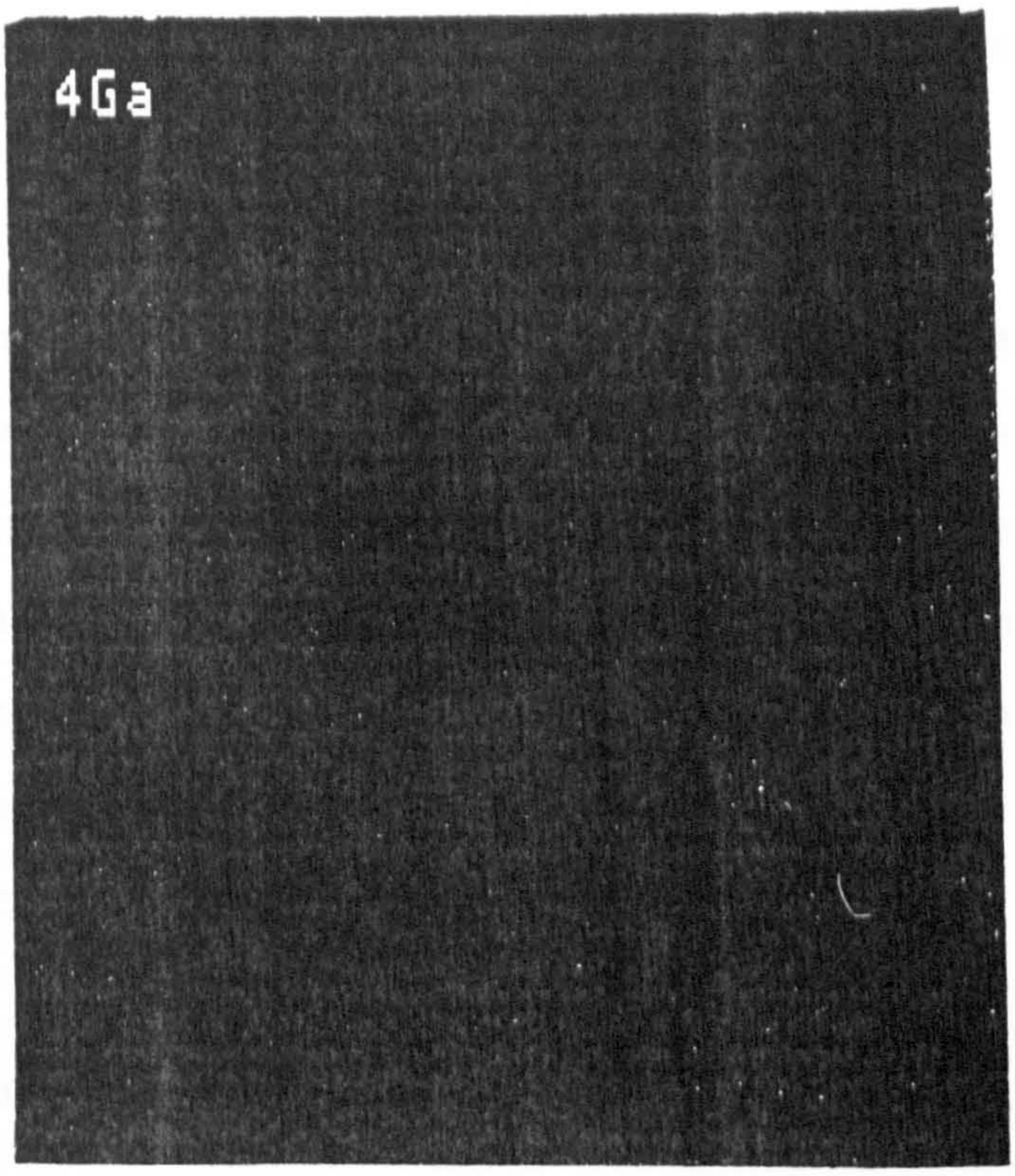

b)

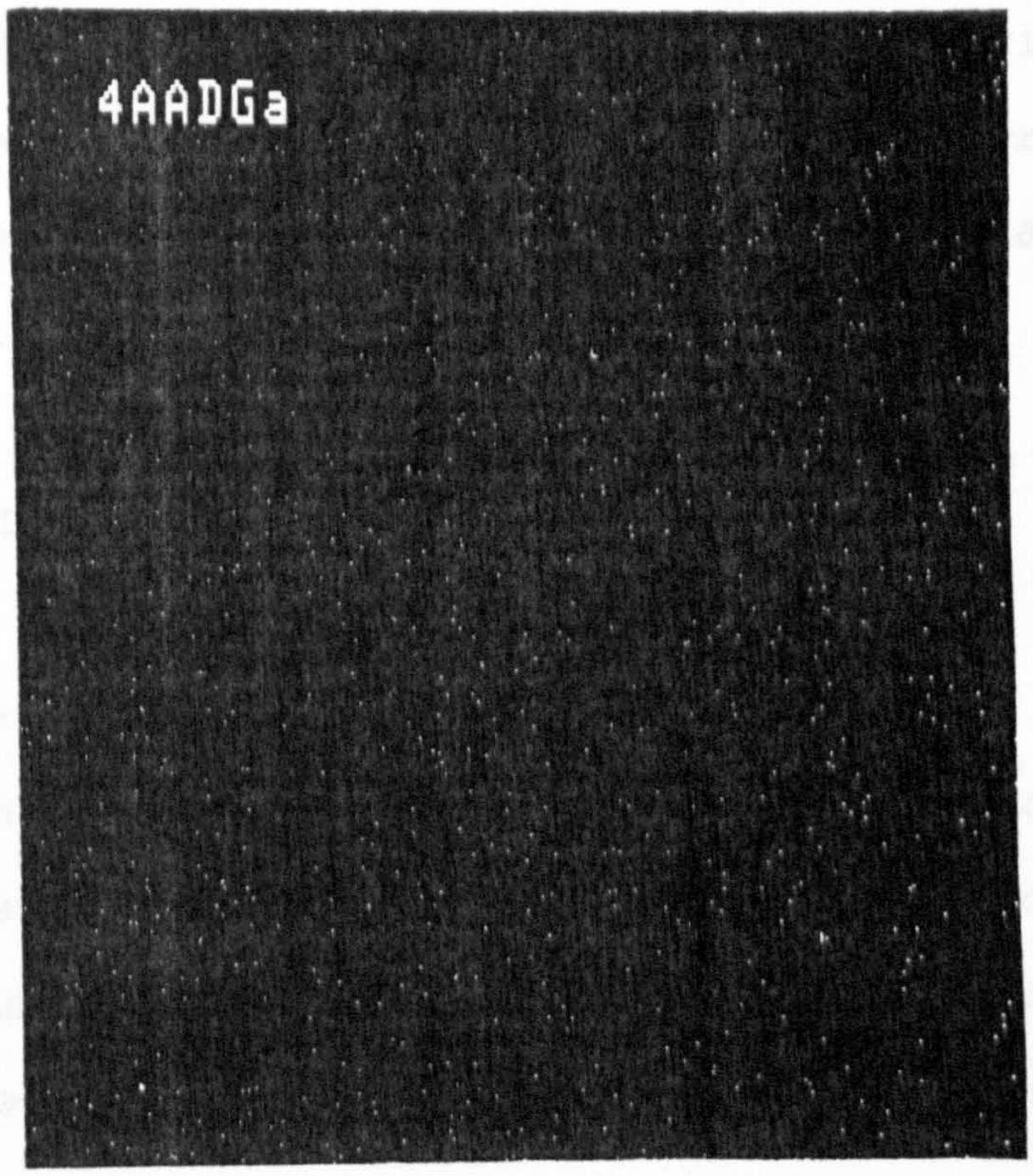

Figures 4.22-24. It might be reasonably argued that these micrographs do not provide conclusive evidence of an increase in alloy elements on the electrode surface after discharge beacause there is no aluminium / element ratio observed on the EDAX, due to the weight/weight % of the elements being so small. However, it does seem logical that certain elements would build up on the surface as preferential dissolution of the aluminium occurs. In further attempts to prove this, ESCA analysis of the electrode surfaces both prior to and after discharge, was carried out.

4.8 ESCA Analysis of Electrode Surfaces.

4.8.1 Experimental Procedure.

Alloys were prepared as previously described and the surfaces were compared both prior to and after discharge in electrolyte E. The conditions for discharge were as described in section 4.7.1.

4.8.2 Results and Discussion.

Alloys were studied before and after discharge to see if any increase in alloy elements occurred on the electrode surface during dissolution. It was found that for alloy 2, both tin and titanium, which were not observed prior to discharge on the electrode surface

Figure 4.25 ESCA Analysis of the Surface of Alloy 2 Before and After Discharge.

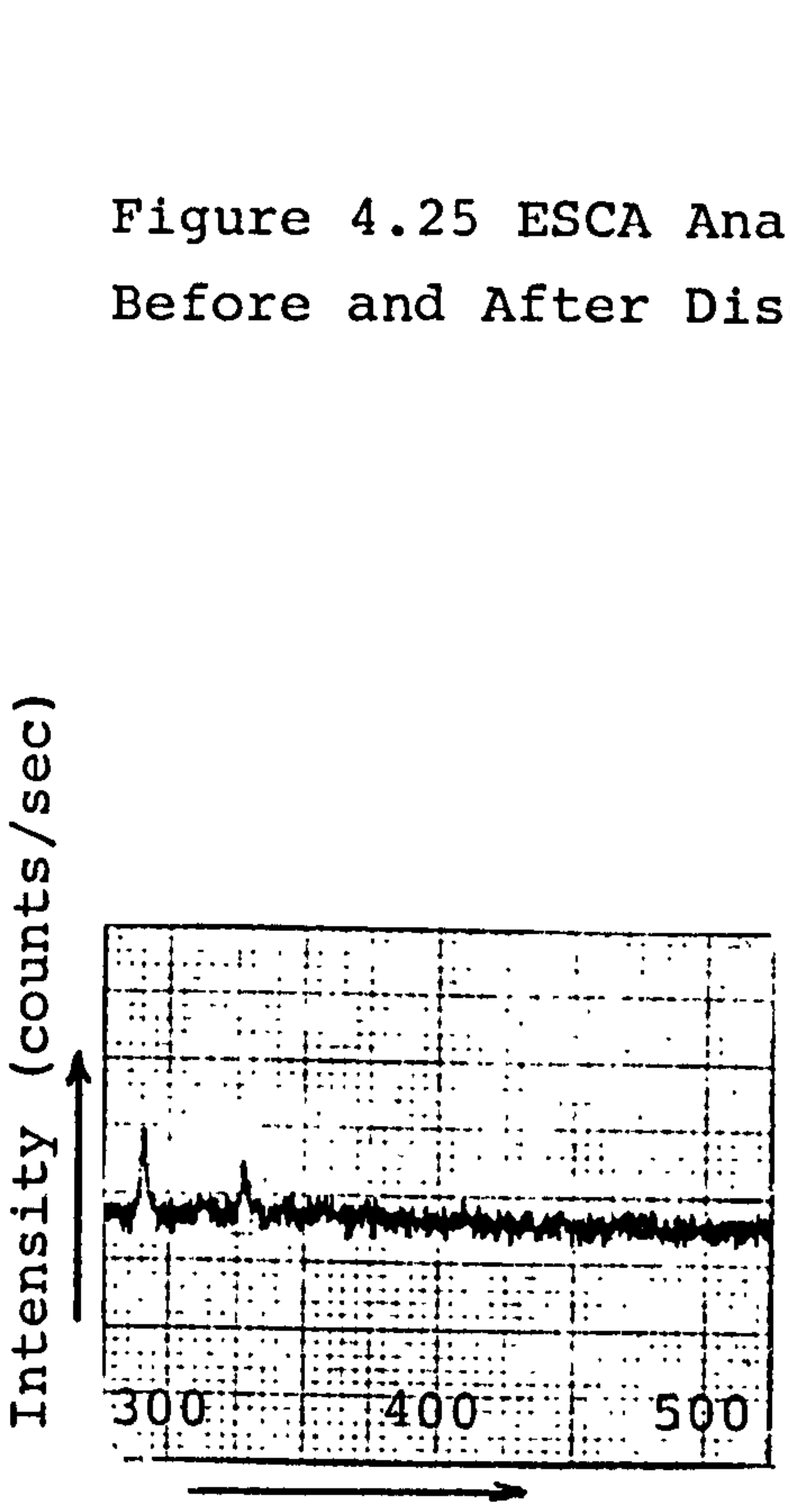

Alloy 2, before discharge, after Argon etching. No evidence of tin or titanium.

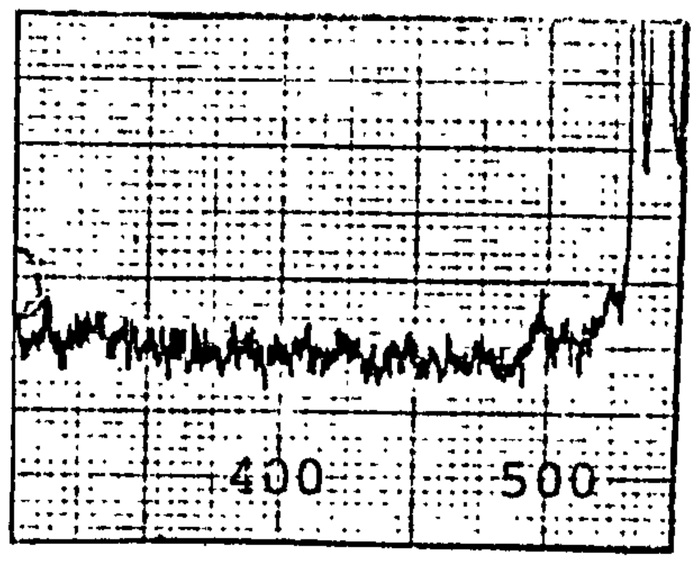

Alloy 2, after discharge evidence of tin at 496 eV. Literature value 486 eV.

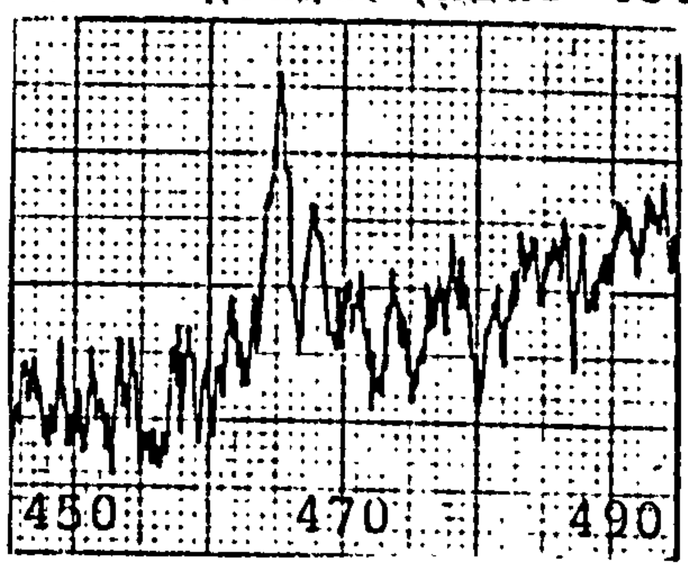

Alloy 2 after discharge and argon etching. Evidence of titanium at 465. Literature value 458 eV.

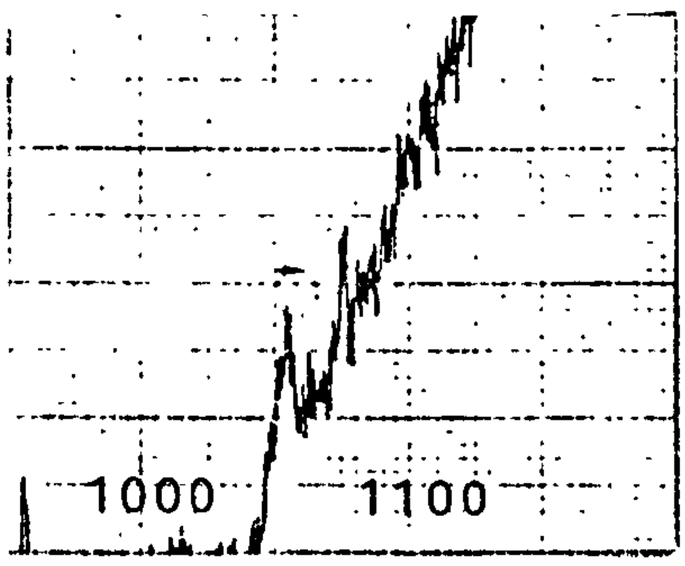

Alloy 2, before discharge after argon etching. No evidence of gallium.

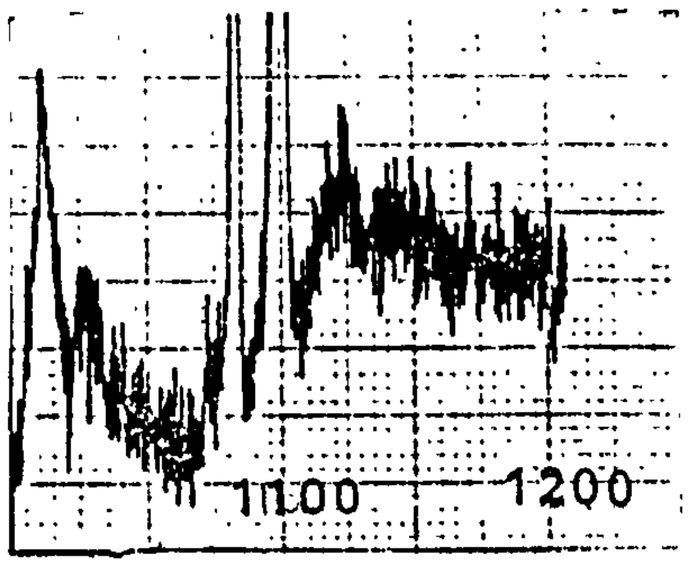

Alloy 2 after discharge and argon etching. Evidence of gallium at 1120 eV. Literature value 1117 eV.

Figure 4.26 ESCA Analysis of the Surface of Alloy 4 Before and After Discharge.

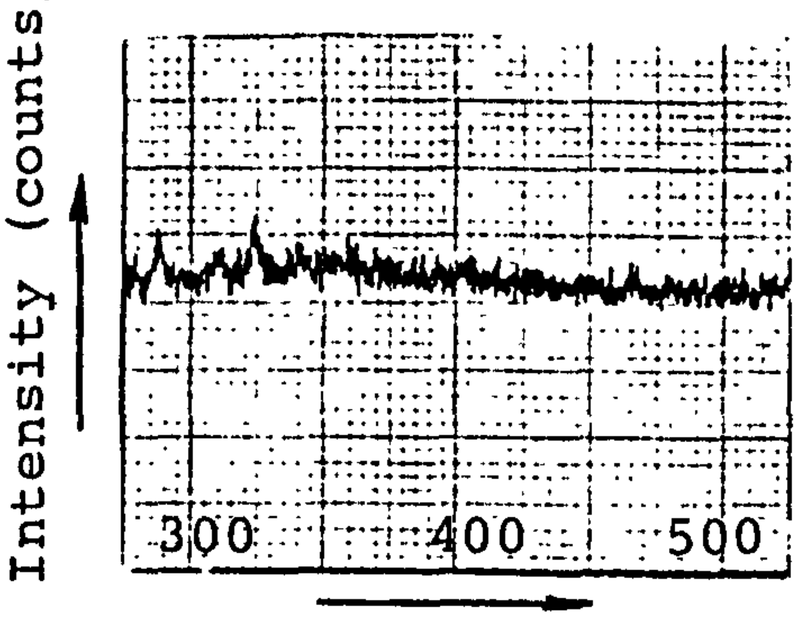

Alloy 4, before discharge and after argon etching. No evidence of tin.

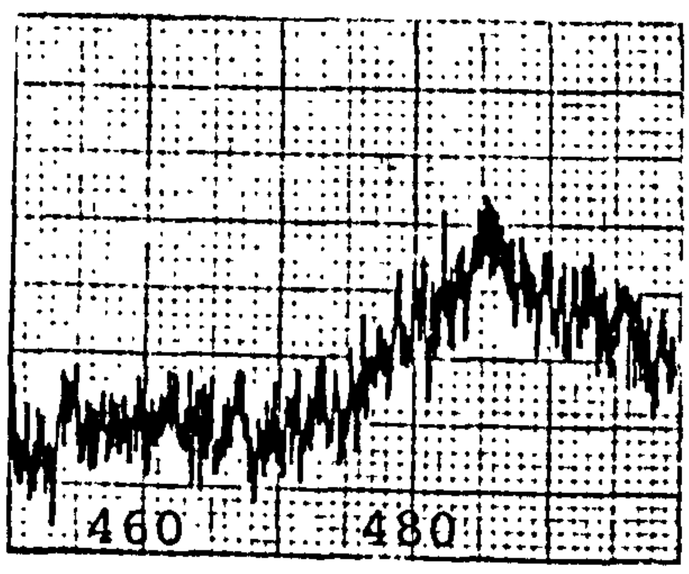

Alloy 4, after discharge.

Evidence of tin at 485 eV. Literature value 486 eV.

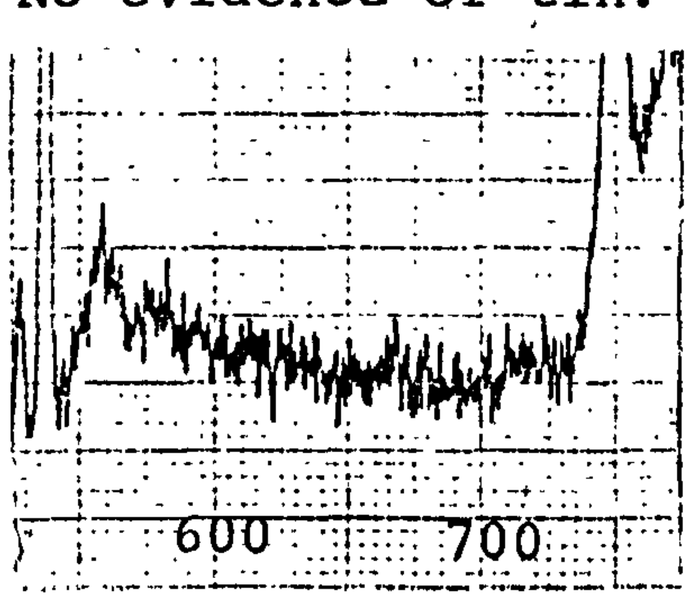

Alloy 4, before discharge and after argon etching. No evidence of iron.

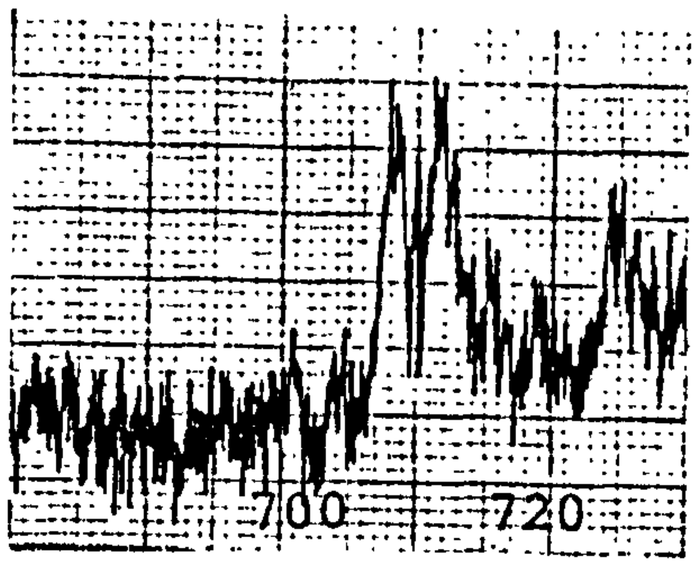

Alloy 4, after discharge. Evidence of iron at 710 eV. Literature value 710 eV.

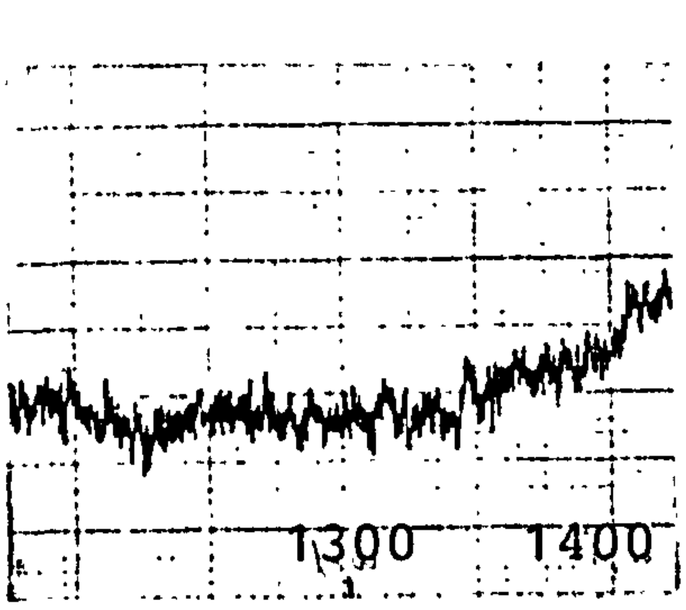

Alloy 4, before discharge and after argon etching. No evidence of magnesium. (Alkα)

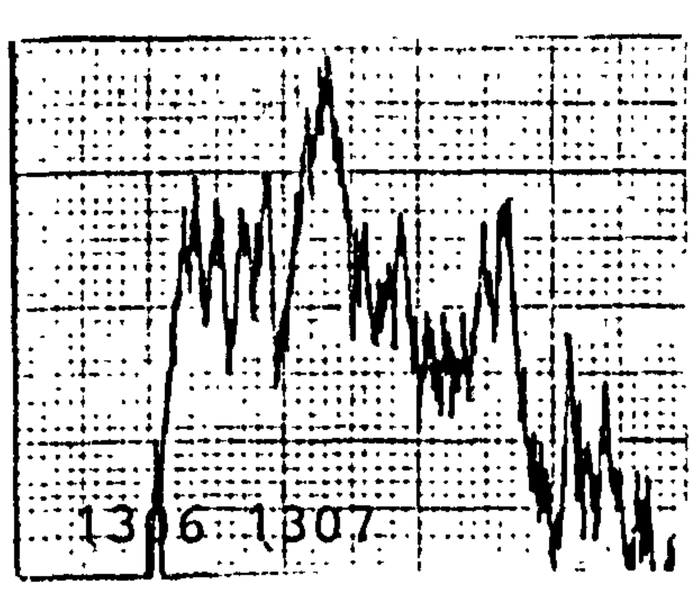

Alloy 4, after discharge and argon etching. Possible presence of magnesium at 1307 eV.

after discharge. It is also possible that gallium is present on the surface after discharge, but this is not so clear. As for alloy 3, titanium is present on the surface after dischaarge, but again it was not observed on the electrode before discharge. As for alloy 4, tin, iron and possibly magnesium were found on the electrode surface only after discharge. No other elements were found on the alloys either prior to or after the discharge process. The results from the ESCA analysis are summarised in Table 4.5.

Table 4.5 Elements Observed on Electrode Surface.

Alloy	Prior to Discharge	After Discharge
2	No elements observed	Ti, Sn possibly Ga
3	No elements observed	Ti
4	No elements observed	Fe, Sn possibly Mg

The experiments indicate that certain elements are present in greater quantity on the electrode surface after discharge. This was most clearly seen in the ESCA results in which tin and titanium were found on the surface of alloy 2, and tin and iron on the surface of alloy 4 after discharge (see Figures 4.25, 4.26). Results of this nature were expected after comparison of EDAX distribution maps of the alloy surfaces before and after discharge. Hasvold in an electrochemistry meeting [84] claimed that a film of tin forms on tin aluminium alloys in alkali media causing an anodic shift in potential. These results are in agreement

with this claim.

Use of ESCA does not conclusively prove that due to the discharge process, atoms of alloy elements migrate to the electrode surface. It might be reasonably argued that the increase in actual surface area due to the anodic dissolution process results in an increase in quantity of alloy elements on the electrode surface. However, it is likely that it is a combination of these two effects that lead to the increase in quantities of elements on electrode surfaces after discharge in alkaline media.

4.9 Conclusions.

Alloying aluminium with particular elements causes an anodic shift in potential. Most notable elements for this purpose are tin, gallium, indium, thallium, bismuth, mercury, lead and magnesium. Certain elements are good hydrogen evolution inhibitors eg. mercury and titanium. The four aluminium alloys used contained variations of the above elements in different quantities.

Simple corrosion tests were carried out at OCV and these showed that alloying aluminium with some of the previously mentioned elements considerably reduces corrosion, as compared to bulk aluminium. Also the results indicated that the presence of relatively large amounts of titanium leads to least hydrogen evolution.

Half cell tests showed that at low current densities, alloy 3, with a high percentage of titanium had the lowest overpotential. Above 10-20mA/cm^2 however, alloy 4 with it s significantly high percentage of tin, has the lowest overpotential. Alloy 4 passivates before the other electrodes in both mixed and potassium hydroxide electrolytes. The limiting current density for each alloy is also lower in mixed electrolytes. The anodic potential at higher current densities is slightly more negative for alloy 2 in electrolyte B. The potential of alloy 1 on the other hand, is slightly more anodic in electrolyte E. Alloys 3 and 4 have similar electrode potentials in both electrolytes.

The OCV values were found to to be greater for all alloys in electrolyte E.

A study of the Tafel slopes revealed interesting characteristics. Use of the mixed electrolyte results in a sharp change in the Tafel slope from the kinetically controlled region to the diffusion influenced region of the electrode process. Such a dramatic increase in overpotential was not observed for alloys in electrolyte E. A possible explanation for this phenomenon is that the diffusion resistance is greater at the initiation stage of the reaction product formation with mixed electrolytes than with potassium hydroxide. This is because the reaction

product with a mixed electrolyte are large granules, whereas with potassium hydroxide a fine thin film of hydroxide is formed on the electrode surface only gradually getting thicker leading to a gradual increase in diffusion resistance. Use of relatively large amounts of titanium leads to low activation overpotential (alloy 3), whereas relatively large amounts of tin, leads to a virtual plateau in the diffusion influenced region of the electrode process (alloy 4). It seems likely that thin films of tin and titanium are formed on the surface of the electrodes, which, as the current density increases, begin to break down resulting in a sharp increase in overpotential.

In attempts to examine the surface of the electrodes after discharge, EDAX and ESCA analysis techniques were employed. The former only showed increase in quantities of elements on the electrode surfaces on the distribution map, as the alloy elements were present in too low w/w percentages for aluminium / element ratios to be obtained. Use of ESCA led to more fruitful results, with definite increases in quantity of certain elements, most notably tin and titanium, on the electrode surface after discharge.

The increase in these elements on the surface cannot be completely attributed with migration of alloy elements to the surface, as the actual surface area increases on dissolution of aluminium.

CHAPTER 5.

THE STUDY OF PASSIVATION OF ALUMINIUM ALLOYS IN ALKALINE ELECTROLYTES.

5.1 Effect of Reaction Product Structure on Performance.

During the process of passivation, the following reaction takes place ;

(5.1) $Al(OH)_4^- \text{--------->} Al(OH)_3 + OH^-$

As aluminium passivates in potassium hydroxide, a fine white precipitate is formed which clogs up the cell. Use of sodium hydroxide however, enables this problem to be avoided as it forms a granular precipitate which is easily flushed out of the cell. This observation is not new [86]. Indeed Drazic et al [87], have studied the use of electrolyte additives which change the nature of the reaction product. However, as only Quarshie [88] has studied the use of mixed electrolytes, the role of the the reaction product formed in this case has not been investigated. As use of sodium hydroxide results in lower conductivity, previous researchers have looked to potassium hydroxide to maximise performance. However, as aluminium air technology advanced, researchers realised the greater importance of the granular precipitate and thus used sodium hydroxide electrolyte. Quarshie's use of a mixed electrolyte however, takes advantage of the properties that both sodium and potassium hydroxide offer.

It was therefore decided to carry out experiments to study the structure of the reaction product in each of the electrolytes A,B and E.

5.2 Experimental Procedure.

Discharge to passivation was carried out in two experiments, one of which had excess hydroxide ions so the concentration remained constant, the other with decreasing hydroxide concentration.

5.2.1 Constant Hydroxide Concentration.

The experiment in which the hydroxide ion concentration was kept constant involved the use of cyclic voltammetry as described in section 3.3.1. The experiment was carried out using a three compartment cell with $30cm^3$ of electrolyte, a nickel counter and a Hg/HgO reference electrode. The area of exposed alloy in each case was $0.25cm^2$. The sweep rate was 2mV/s from a potential of -1750mV to -500mV with respect to the reference. At the potential -500mV the electrodes were removed from the system and stored in a dessicator packed with silica gel until they were dry. The surfaces were then scanned using a Hitachi S-520 scanning electron microscope.

This experiments were repeated several times, both with one cycle and three cycles to the passivation peak before the electrodes were removed.

5.2.2 Decreasing Hydroxide Concentration.

Discharge to passivation in decreasing hydroxide ion concentration was achieved using full cell systems with limited electrolyte. The full cell was prepared as described in section 3.2.4. The dimensions of the full cell system are given in Figure 5.1 a) and b). The experimental apparatus was set up as shown in Figure 5.2. The potentiostat was set up in the galvanostatic mode and the cells discharged at 100mA/cm^2. The volume of electrolyte used was limited to 2.5cm^3 in each run. After passivation occurred the electrode surfaces were dried and examined as previously described.

Similar experiments to the above were also carried out using 40 wt/v% sodium hydroxide electrolyte saturated with mercury.

5.2.3 Results and Discussion.

It can be observed from the electron micrographs (Figures 5.3-5.8), that use of electrolyte E results in a fine white precipitate which completely smothers the electrode surface. This would prevent the diffusion of the electrolyte to the metal surface during the period of discharge when the reaction product just begins to precipitate out. Thus passivation of a cell would be expected to follow soon after precipitation commences. However, with the mixed electrolytes A and B, the structure of the reaction product is seen to be spherical in the constant hydroxide ion experiment. This would therefore prolong the ability of the

Figure 5.1 Full Cell System.

a) The Air Electrode.

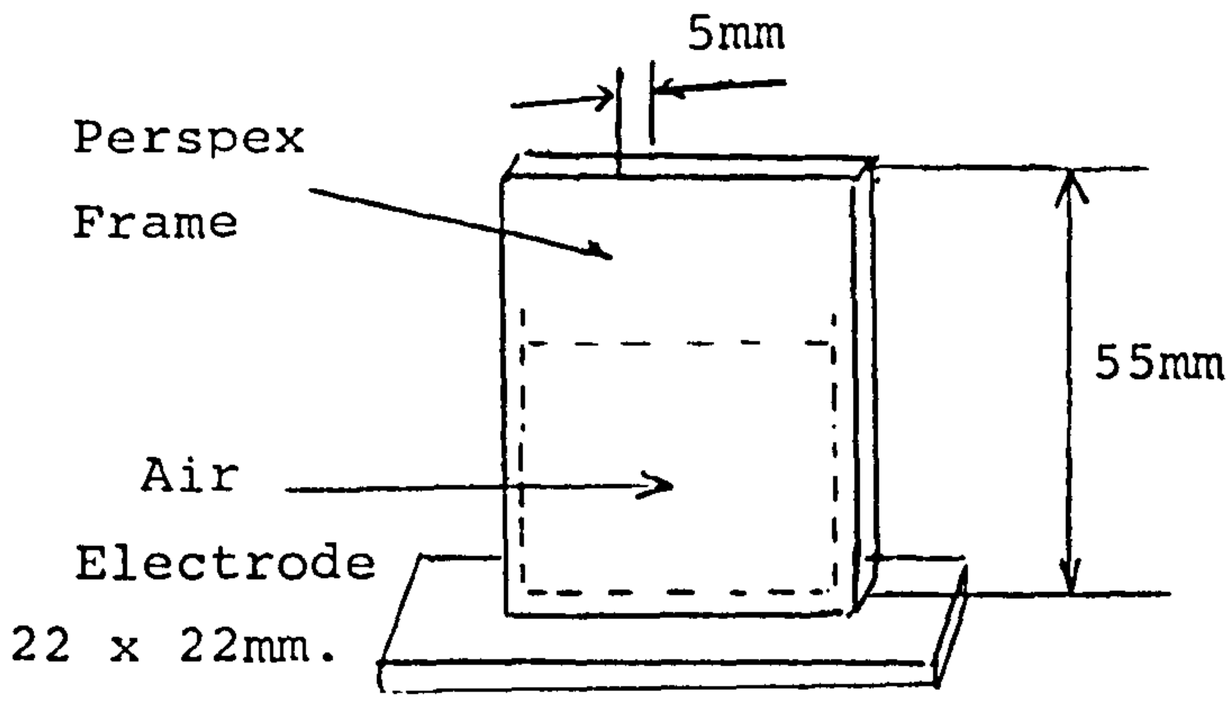

b) The Aluminium Alloy Electrode.

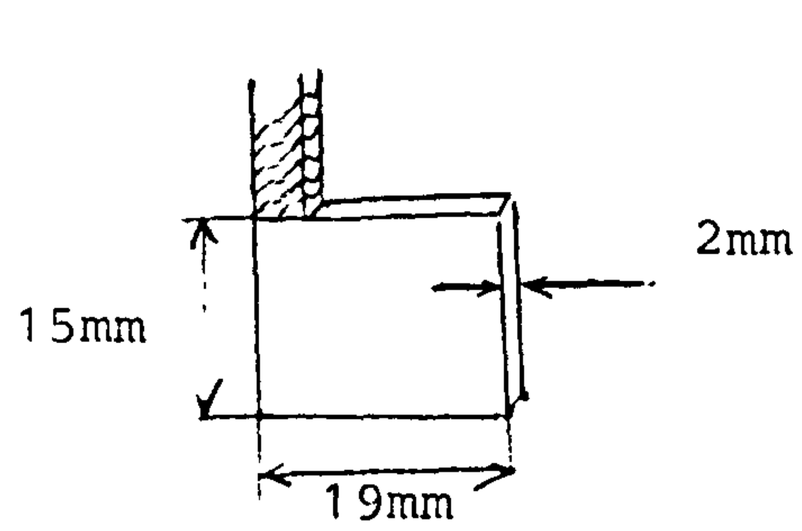

Figure 5.2 Circuit for Cell Discharge.

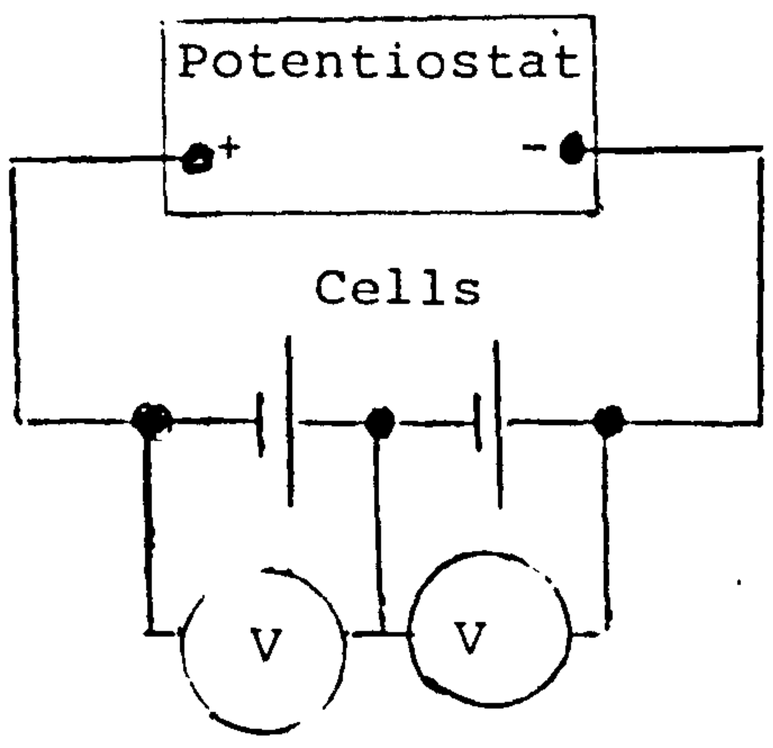

SEM micrographs of reaction product on electrode surfaces.

Figure 5.3 Linear sweep (1 cycle) to passivation peak.
Alloy 1 20keV x 2000.
(a) Electrolyte E.

(b) Electrolyte A.

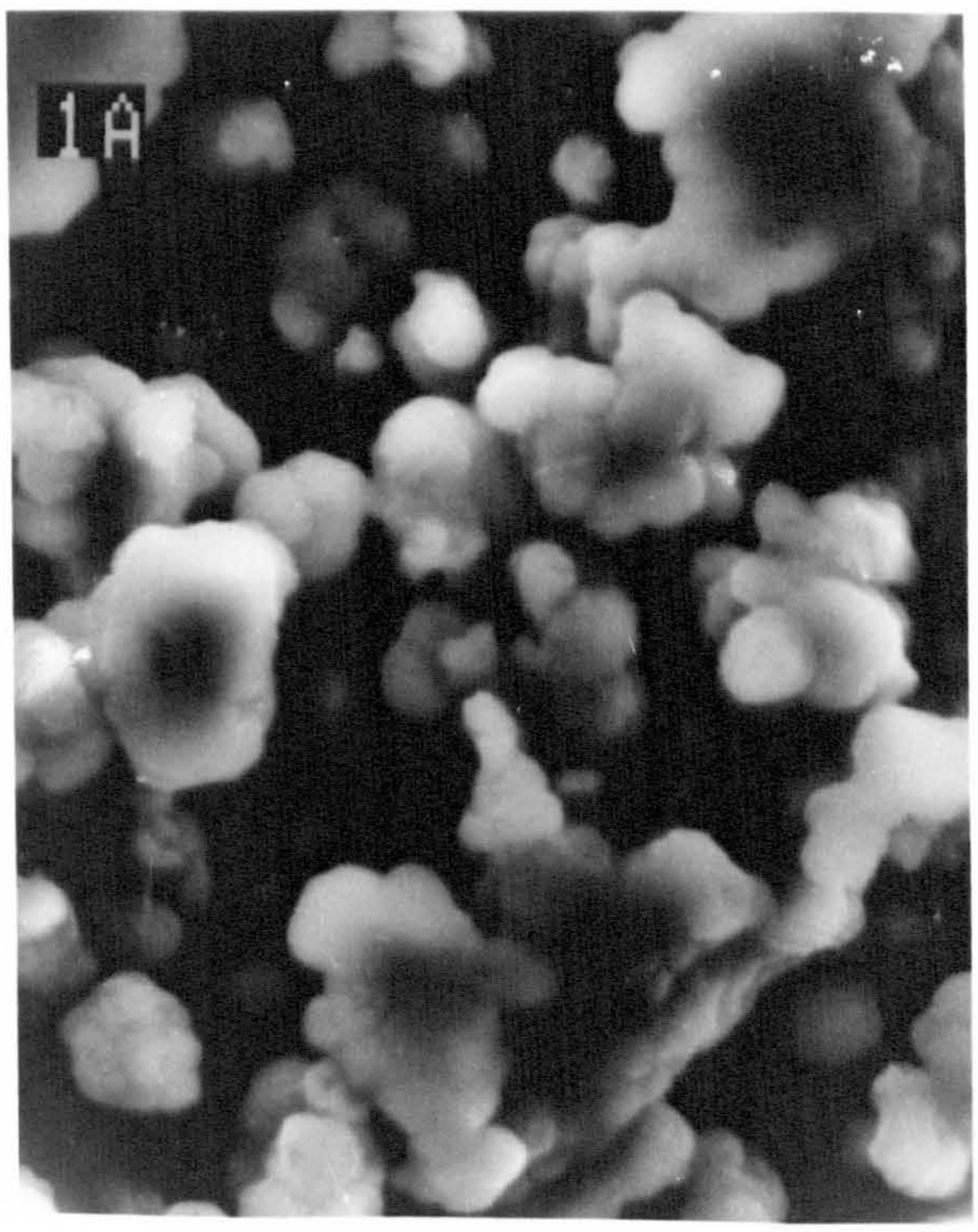

Figure 5.4 Linear sweep (1 cycle) to passivation peak.
Alloy 3 20keV x 2000.
(a) Electrolyte E.

(b) Electrolyte B.

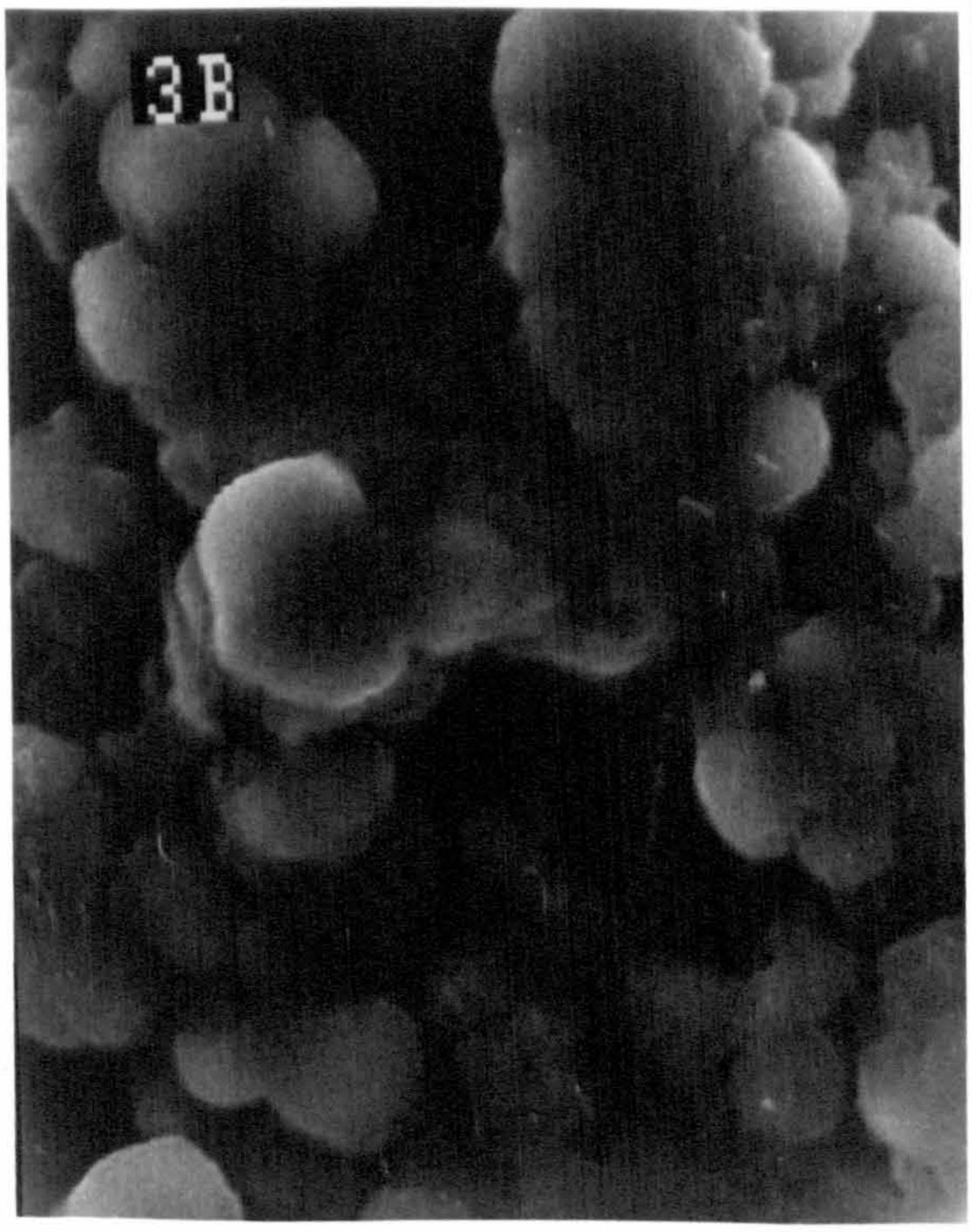

Figure 5.5 Linear sweep (1 cycle) to passivation peak.
Alloy 4 20keV x 2000.
(a) Electrolyte E.

(b) Electrolyte A.

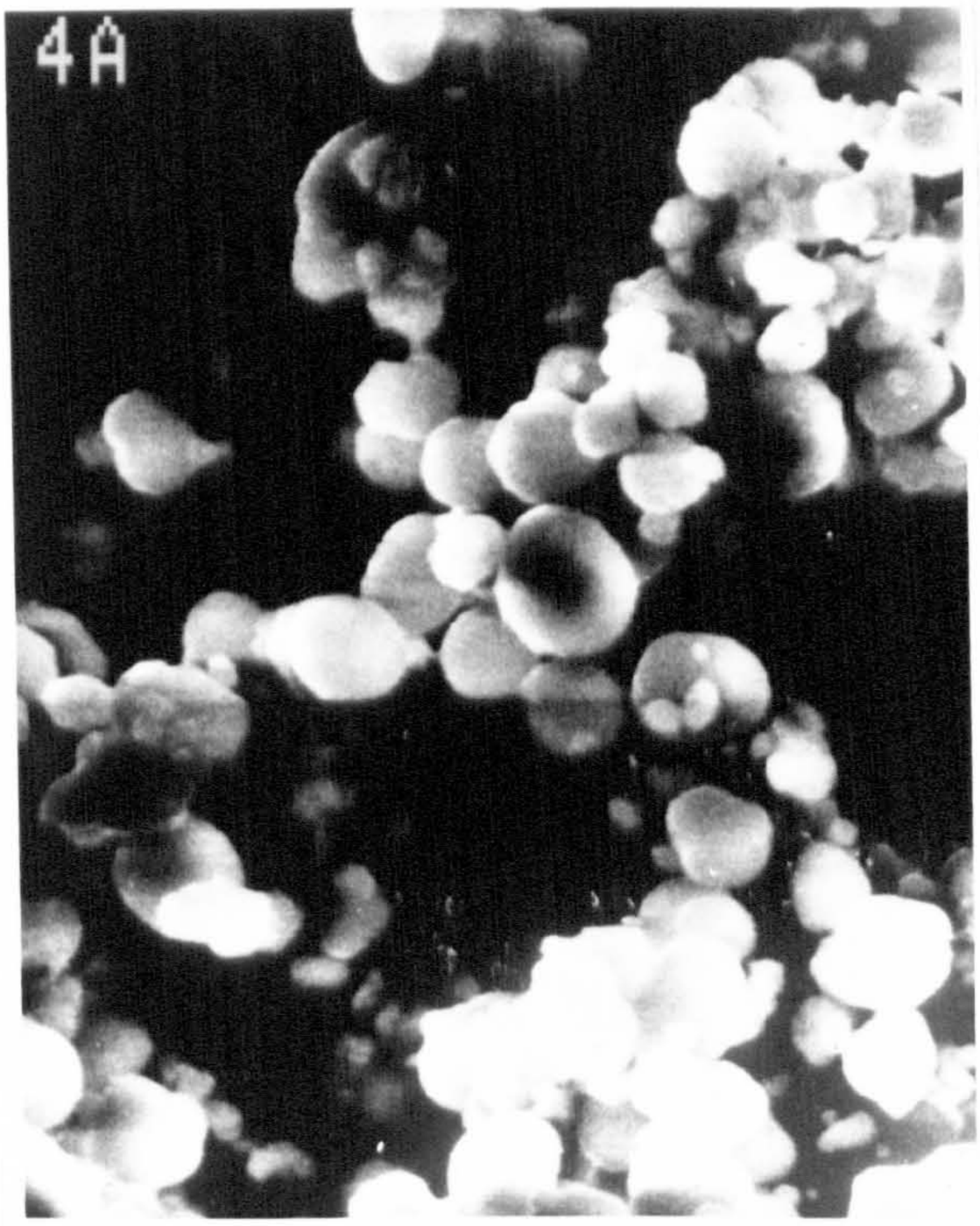

Figure 5.6 Linear sweep (3 cycles) to passivation peak.
Alloy 2 20keV x 2000.
(a) Electrolyte E.

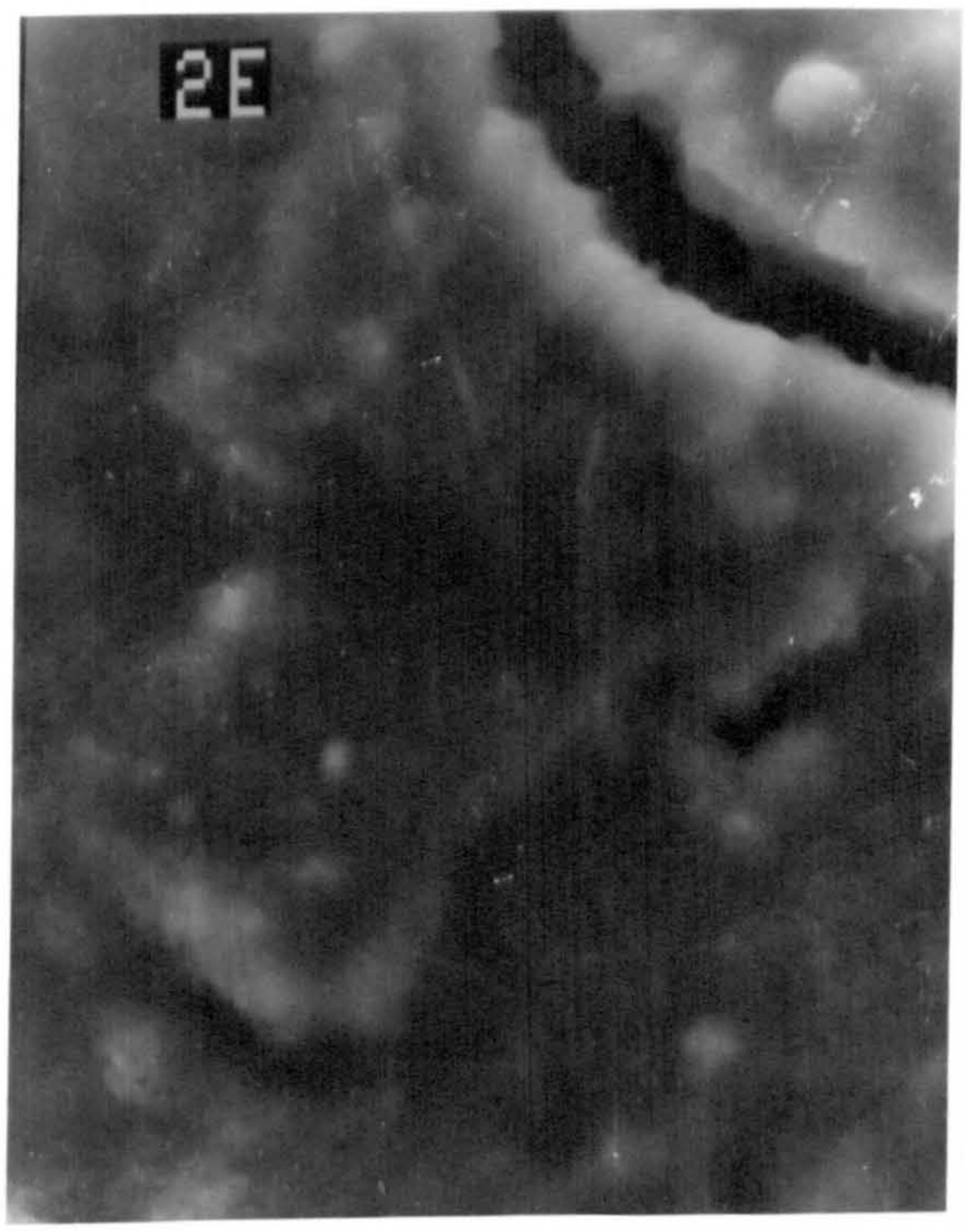

(b) Electrolyte B.

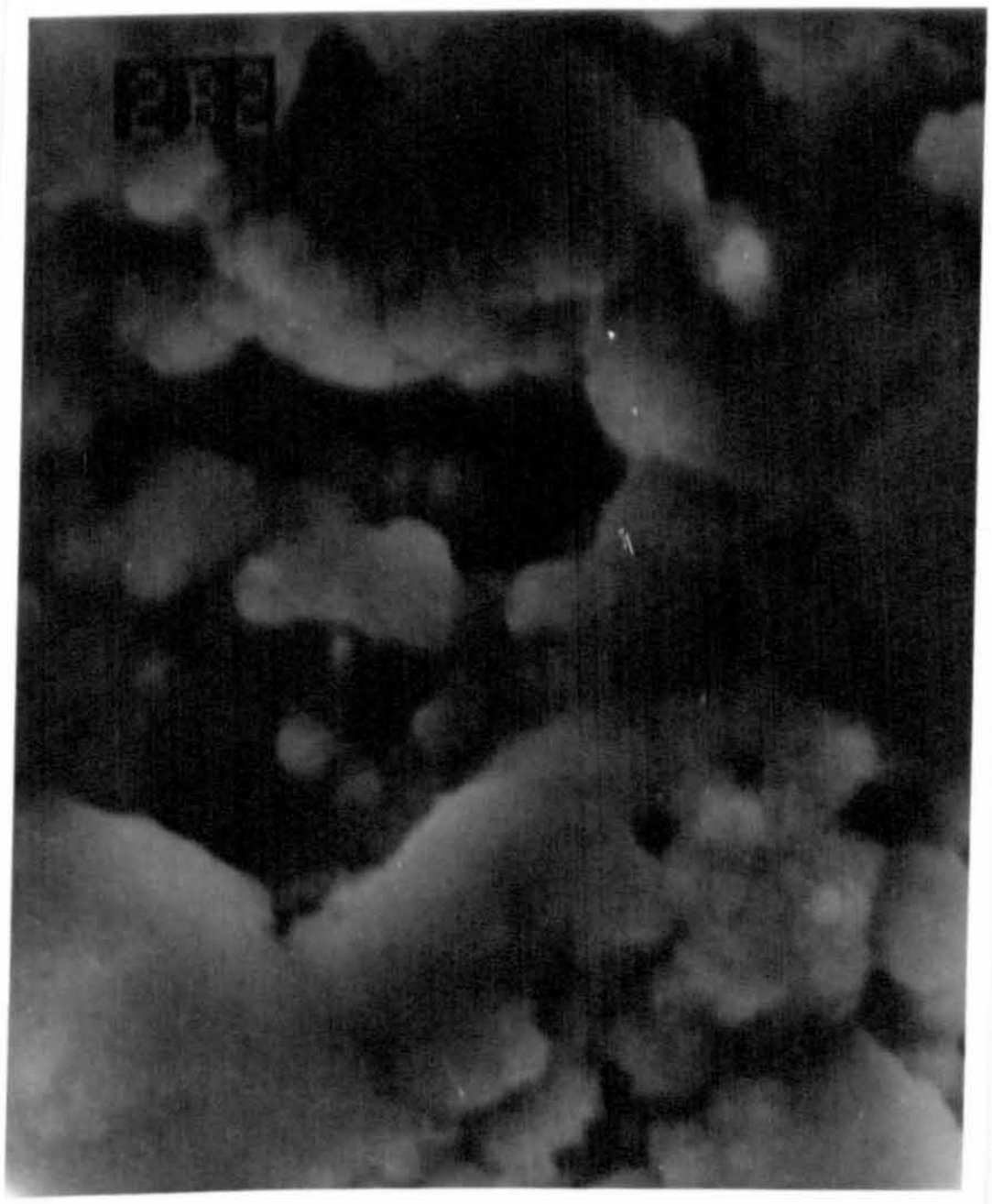

igure 5.7 Full cell discharge.
lloy 1 20keV x 2000.
a) Electrolyte E.

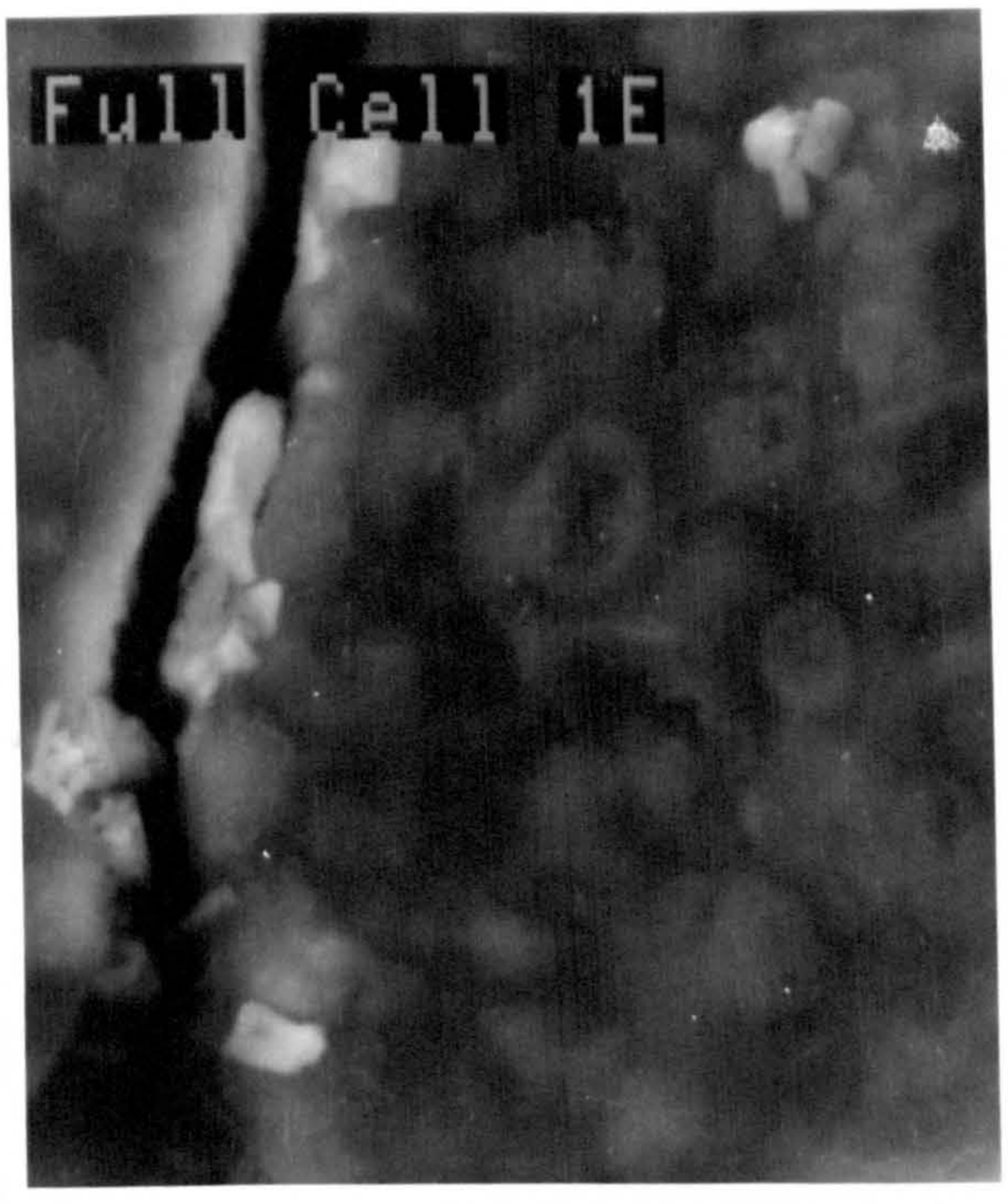

(b) Electrolyte A.

Figure 5.8 Full cell discharge.
Alloy 3 20keV x 2000.
(a) Electrolyte E.

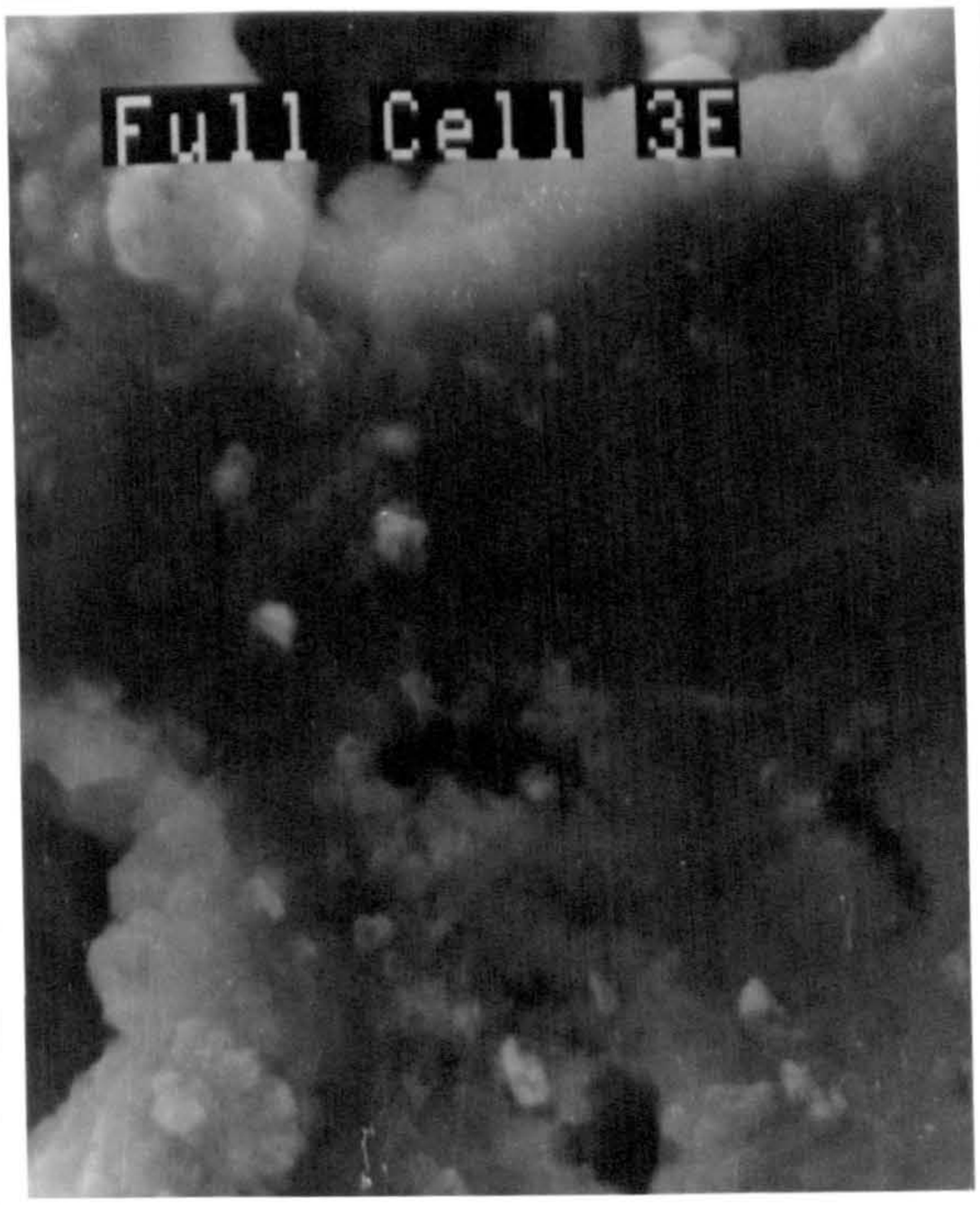

(b) Electrolyte A.

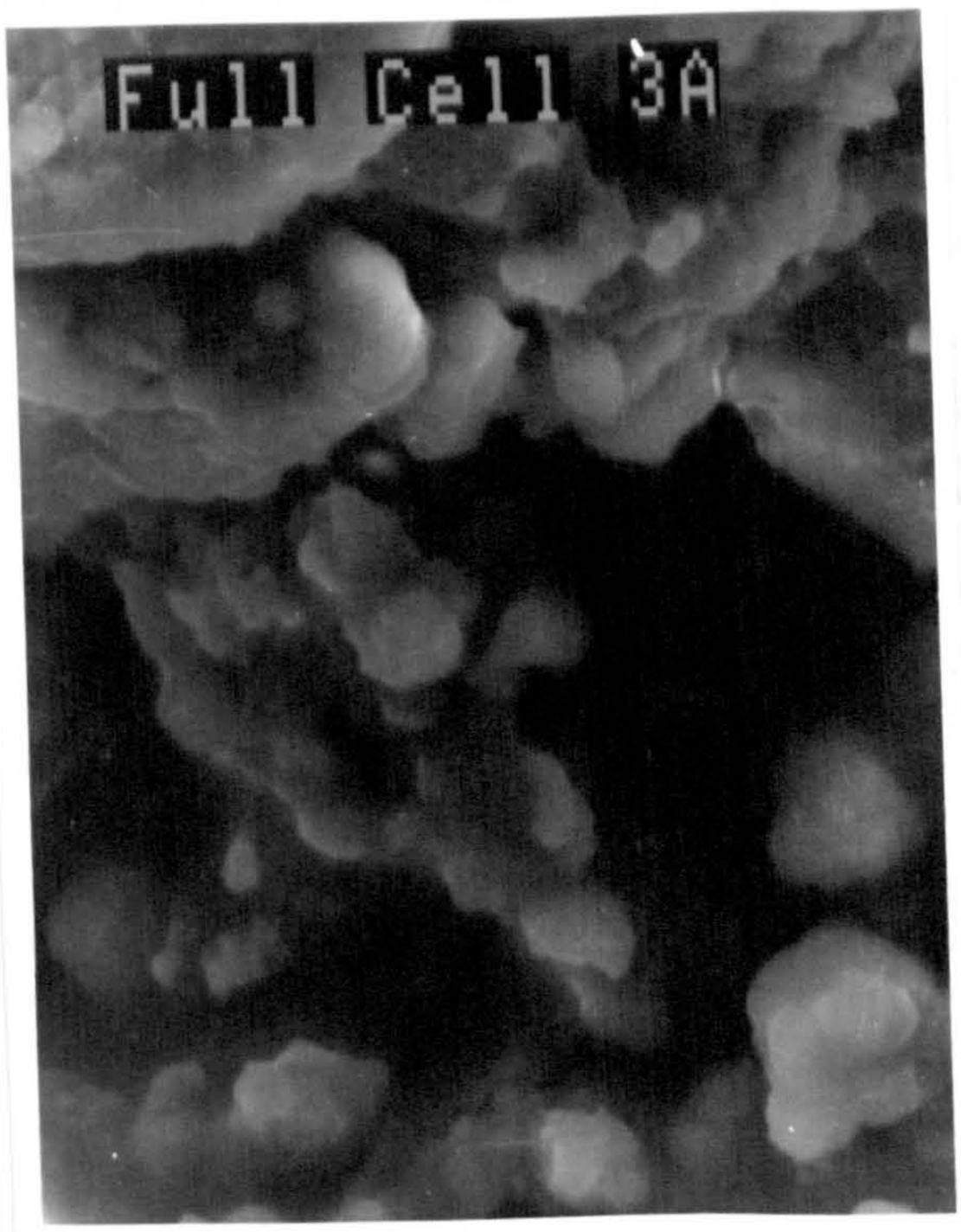

Figure 5.9 Linear sweep (1 cycle) to passivation peak.
Alloy 1 40keV X 3000.
Electrolyte - 40% Sodium hydroxide.

hydroxide ions to diffuse through to the metal surface and result in a longer period of discharge. In the voltammetry experiments involving three cycles and in the full cell tests, the electron micrographs do not so clearly show the granular precipitate with the mixed electrolyte, however, the porous nature of the precipitate is quite distinct.

The structure of the reaction product obtained from use of sodium hydroxide electrolyte can be seen in Figure 5.9. Clearly, the effect of the presence of NaOH results in the formation of spherical granules of aluminium hydroxide.

5.3 X-Ray Analysis of Reaction Product.

X-ray analysis as described in section 3.1.5, was carried out on samples of the reaction product obtained from use of electrolytes E and B. The use of electrolyte E resulted in the formation of aluminium hydroxide very similar in structure to that of gibbsite. The theoretical values for gibbsite are given in Table 5.1 below, as well as the values obtained for the reaction product from use of electrolyte E. 'd' spacings were calculated from photographic film using an Enraf Nonius ruler (Cu $K\alpha$) and the intensities calculated from chart paper.

Table 5.1 `d' Spacings and Intensity Values of Gibbsite and Reaction Product Obtained From Use of Electrolyte E.

Gibbsite	Reaction Product* (Electrolyte E)
d_I	d_I
4.82_x	4.80_x
4.34_4	4.40
4.30_2	$4.30_{2.5}$
3.35_1	3.35
2.44_2	2.45
2.37_2	2.40
2.03_1	2.05
1.98_1	2.00

* Intensity values only available for d spacings 4.80 and 4.30.

Analysis of a sample of reaction product obtained with use of mixed electrolyte B, revealed a substance which had similarities to the structure of Bayerite.

Table 5.2 'd' Spacings and Intensity Values of Bayerite and Reaction Product Obtained From Use of Electrolyte B.

Bayerite	Reaction Product (Electrolyte B)
d_I	d_I
4.71_9	4.70_9
4.35_7	4.30_x
3.20_3	3.20_3
2.22_x	2.20_5
1.72_4	1.70_2
1.46_1	1.45

The analysis reveals that different crystal structures of aluminium hydroxide are obtained with use of electrolytes E and B, and that the former electrolyte has a reaction product similar in structure to gibbsite and the latter a reaction product similar in structure to bayerite.

5.4 Study of Electrolyte Stabi lity After Passivation.

It has been observed that after passivation has occurred in electrolyte E, a white insoluble solid begins to precipitate out. This suggests that the electrolyte solution has reached saturation point. After passivation with the mixed electrolytes however, no solid can be seen to precipitate out. This suggests a stable supersaturated solution of

aluminate. Such a feature would be highly advantageous for the every day running of aluminium air cells, as cleaning of the system would be a relatively simple task. If however, copious amounts of thick white precipitate are obtained then the active sites on the air electrode will be covered, thereby reducing efficiency. It was decided to design a simple experiment to investigate the behaviour of the electrolytes after passivation.

5.4.1 Experimental Procedure.

To study the stability of the electrolyte after passivation of the electrode a circuit as shown in Figure 5.10 was set up. The cell was as shown in Figure 5.11. As soon as passivation of the system occured the electrodes were removed from the cell and a 100µl aliquot was taken from the electrolyte with a syringe, taking care not to disturb any solid that may have been present. The aliquot was then made up to 10mls with 0.4M HCl. From this solution a further 50µl was taken and diluted up to 10mls with 0.4HCl. The aluminium ions present in the sample were then in the order of 5-10ppm. The process was repeated at various time intervals and the samples stored for analysis.

The aluminium ions present in each sample indicated whether aluminium hydroxide had precipitated out or remained in the solution in the form of aluminate. The greater the ppm of aluminium present in the sample, the easier it is to retain

Figure 5.10Circuit for Half Cell Tests.

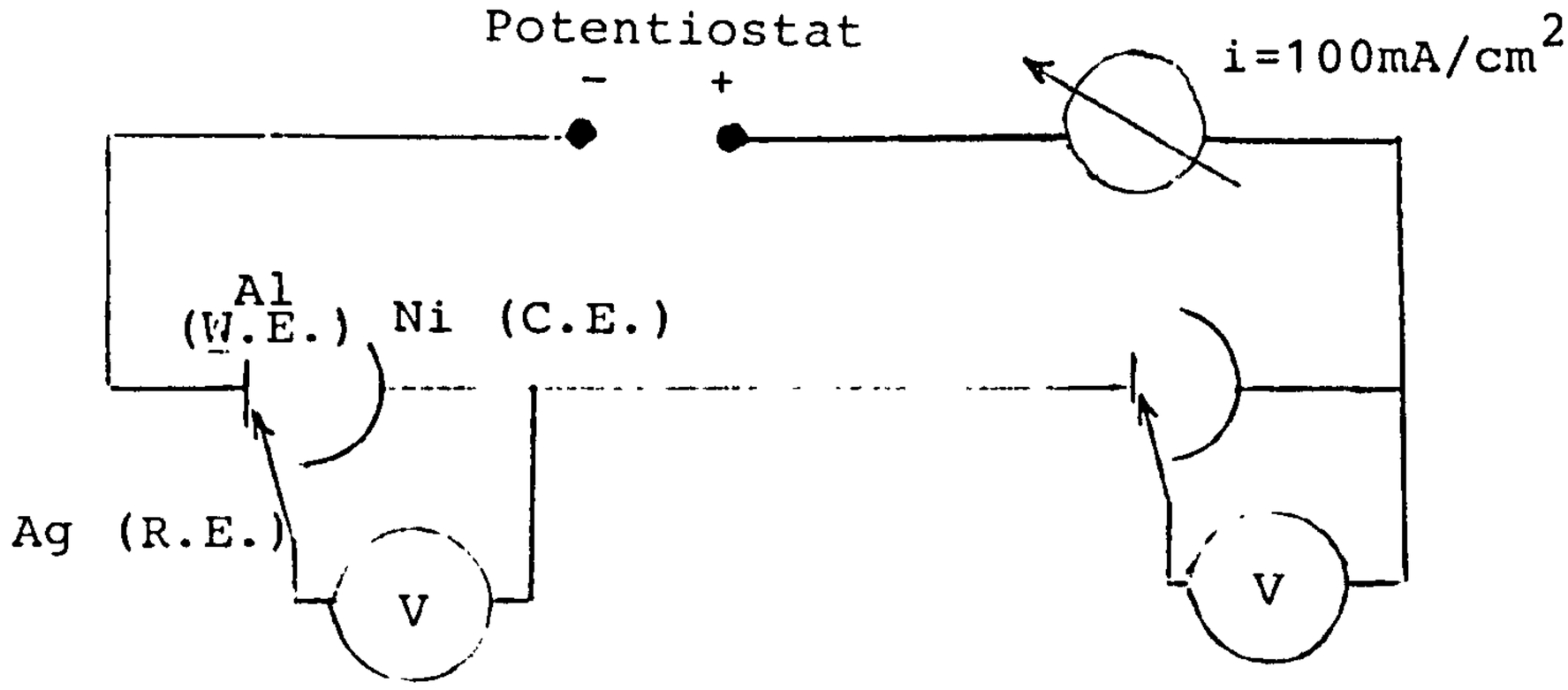

Figure 5.11 The Half Cell Design.

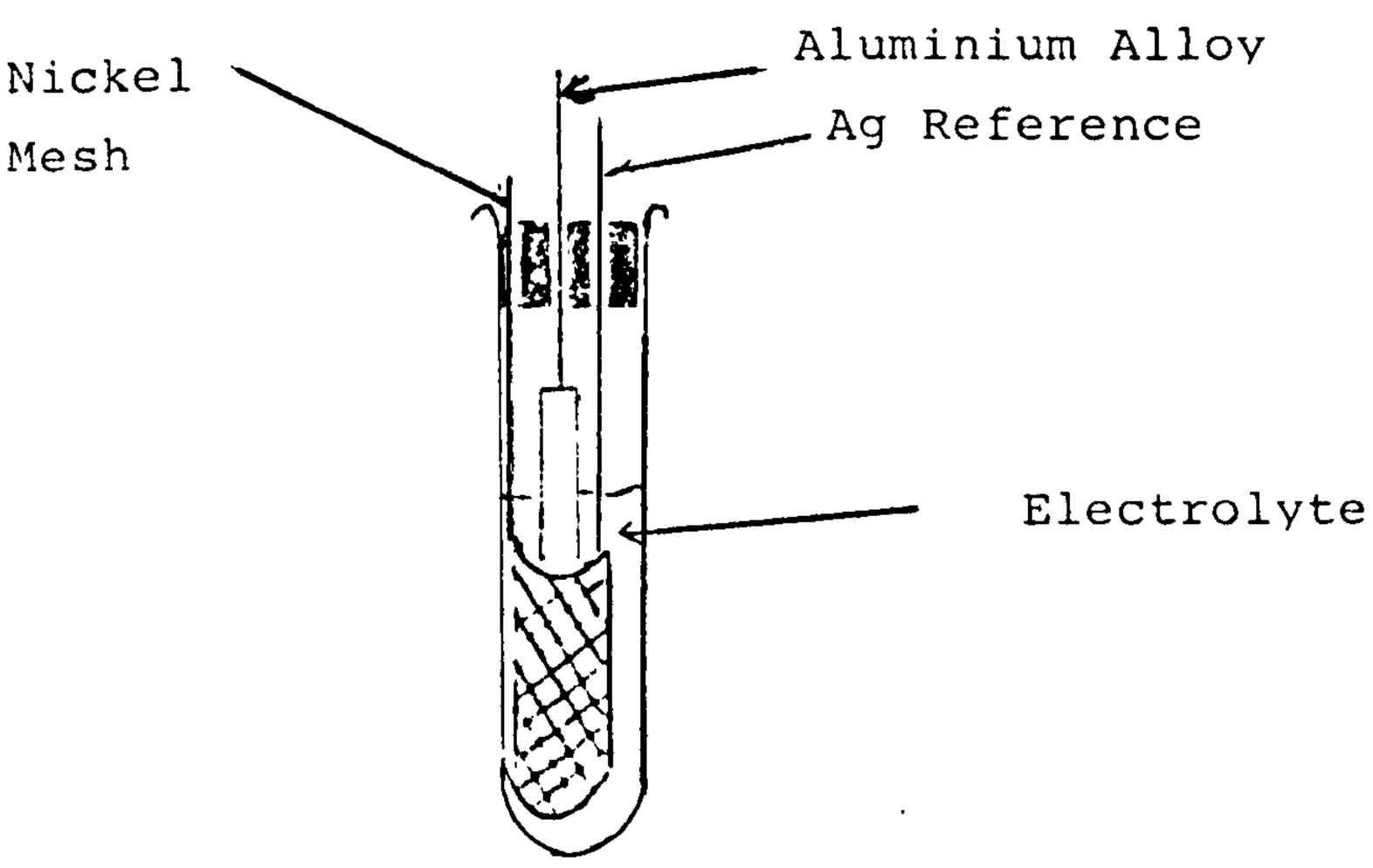

high efficiency levels in full cell systems.

5.4.2 Results and Discussion.

The solutions were taken for ICP (Inductively Coupled Plasma) [89, 90] analysis along with two aluminium standard solutions of 5ppm and 10ppm, which gave the aluminate content in the samples. Typical results are shown in Figure 5.12, which shows that immediately after passivation electrolyte E experienced a significant drop in aluminate content. This indicates that with electrolyte E, precipitation occurs as passivation takes place. This is in good agreement with the observed precipitation of the white insoluble solid. However, with the mixed electrolyte B, the cell operates for a longer period and on passivation bulk precipitation is not observed. This is reflected in the relatively high concentrations of aluminate found in the samples. It is possible that the mixed electrolytes with their higher solubility of aluminate, form a stable supersaturated solution of aluminate, as precipitation occurred in a matter of days after passivation not hours.

5.5 Conclusions.

It is clear that the morphology of the reaction product is different with the different electrolytes. The smooth reaction product that covers the alloy when electrolyte E is used prevents the mass transfer of hydroxide ions to the

Figure 5.12 PPM Aluminium in Electrolyte

Vs. Hours After Passivation.

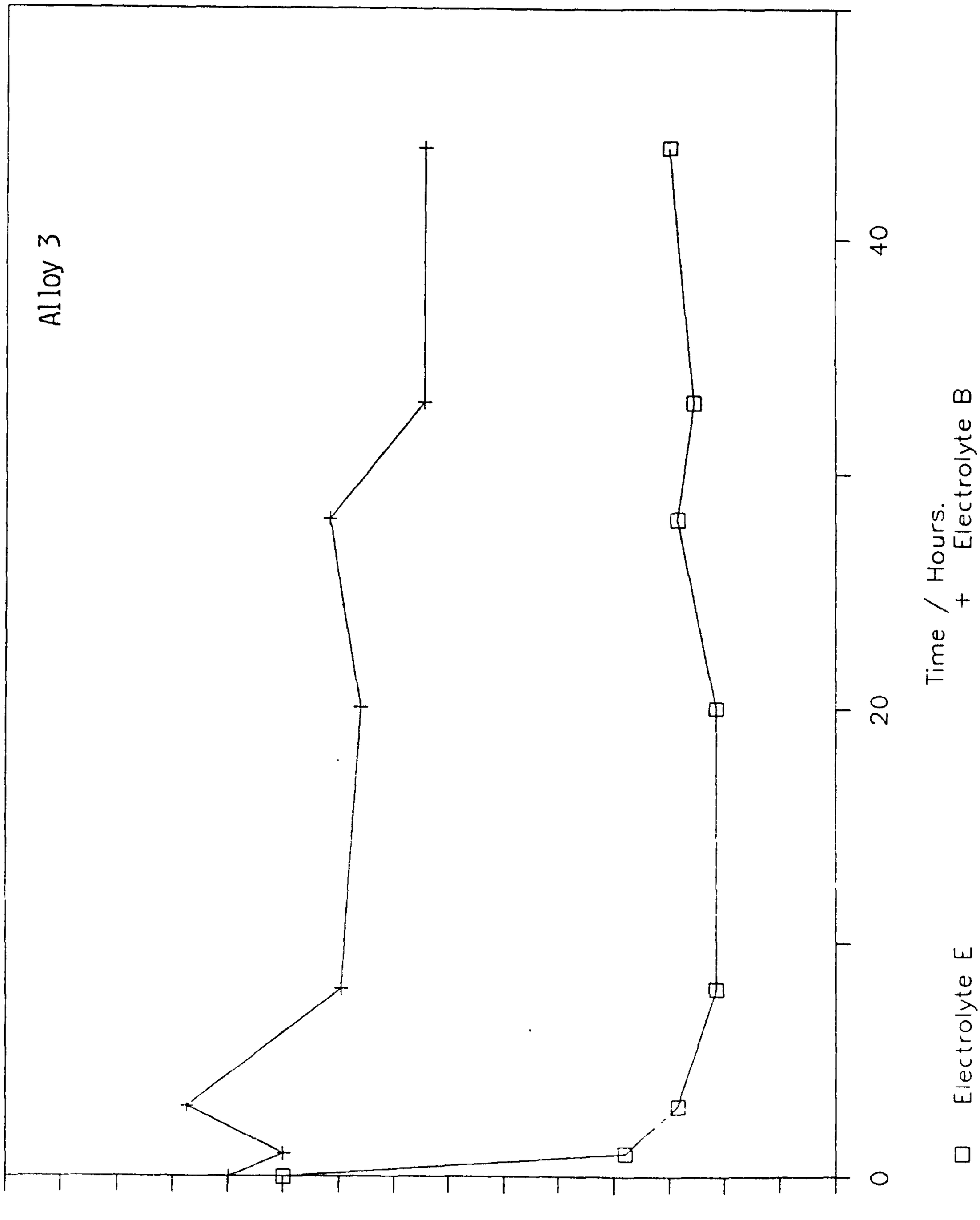

electrode surface. When there is limited hydroxide, the ability for the following reaction to occur is reduced and aluminium hydroxide is precipitated out.

(5.2) $Al^{3+} + 4OH^{-} \text{-------->} Al(OH)_4^{-}$

This aluminium hydroxide provides the crystal seed which causes the precipitation of the remainder of the reaction product. Use of a mixed electrolyte however, results in a porous structure which allows diffusion of hydroxide ions to the electrode surface after passivation has commenced, thereby prolonging the active life of the cell.

Combination of this fact with the greater solubility of aluminate in the mixed electrolyte, results in improved performance of full cells employing electrolytes A and B as compared with cells employing electrolyte E.

It is also interesting to note that after passivation occurs with electrolyte E, the aluminium hydroxide precipitates out as a thick white precipitate. However, with mixed electrolytes A and B, although passivation has occurred and the electrode is covered in a porous film of hydroxide, the aluminium forms a stable aluminiate solution and precipitation of all the hydroxide does not immediately follow. This is important as regards flushing out the reaction product from the cell. If the material is in the form of a stable saturated solution then cleaning the cell

becomes a relatively simple task, and the active sites on the air cathode do not become covered with hydroxide.

Thus the structure of the reaction product, and the ability for the electrolyte to form a stable saturated solution makes it distinctly advantageous to use a mixed electrolyte rather than the traditional potassium hydroxide electrolyte, in an aluminium air cell.

CHAPTER 6.

MEASUREMENT OF THE CURRENT DISTRIBUTION ON ALUMINIUM ALLOYS IN VARIOUS ELECTROLYTES.

6.1 Introduction.

At Xiamen University a novel microelectrode scanning instrument has been designed which enables the current at microzone centres on an electrode surface to be measured [91]. This technique provided new and interesting information about the behaviour of alloys in alkaline electrolytes, as previously used traditional techniques only reveal information about the total electrode surface.

6.2 Principle of System Used to Measure Microzone Current Distribution.

There is a potential distribution or current density distribution on the surface of the electrode when corrosion or discharge is occurring. If the distribution is uniform or even, then the potential distribution cannot be measured using the system.

However, consider the following example of corrosion ;

Figure 6.1 (a) Corrosion Site.

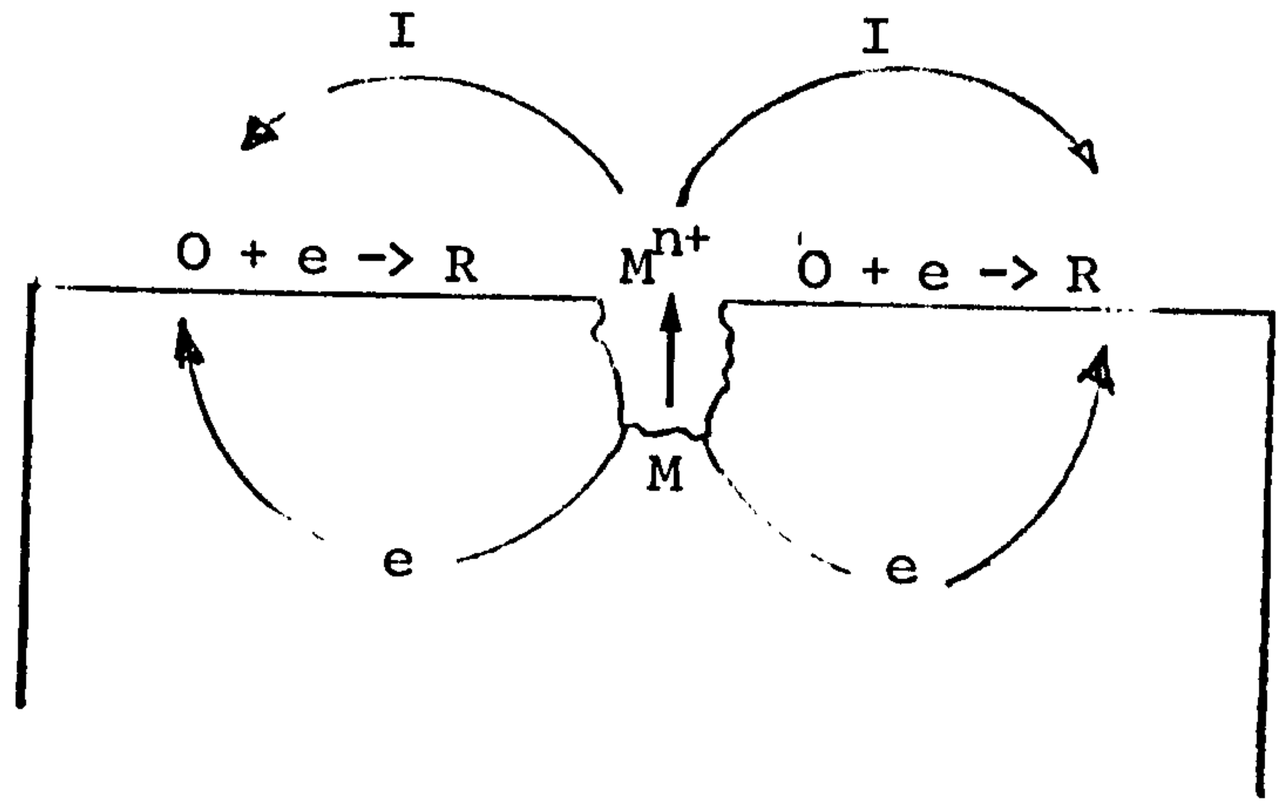

(b) Corrosion Current.

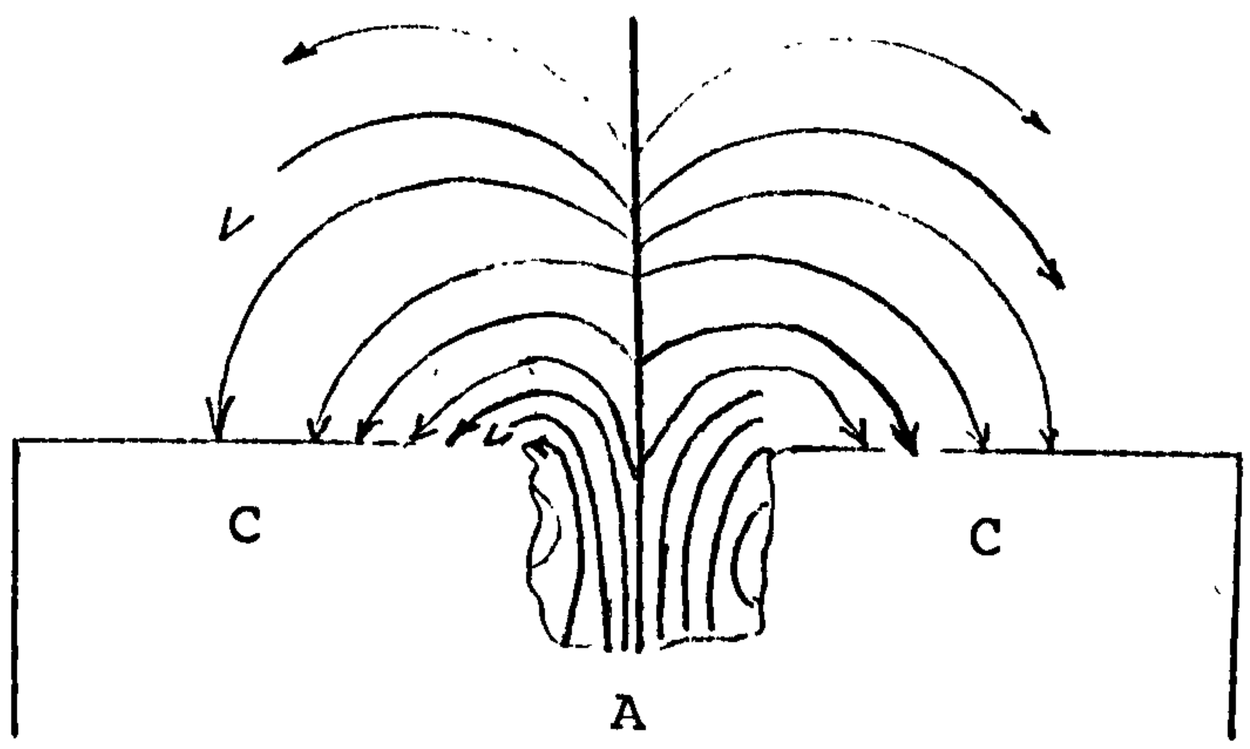

(c) The Potential Distribution.

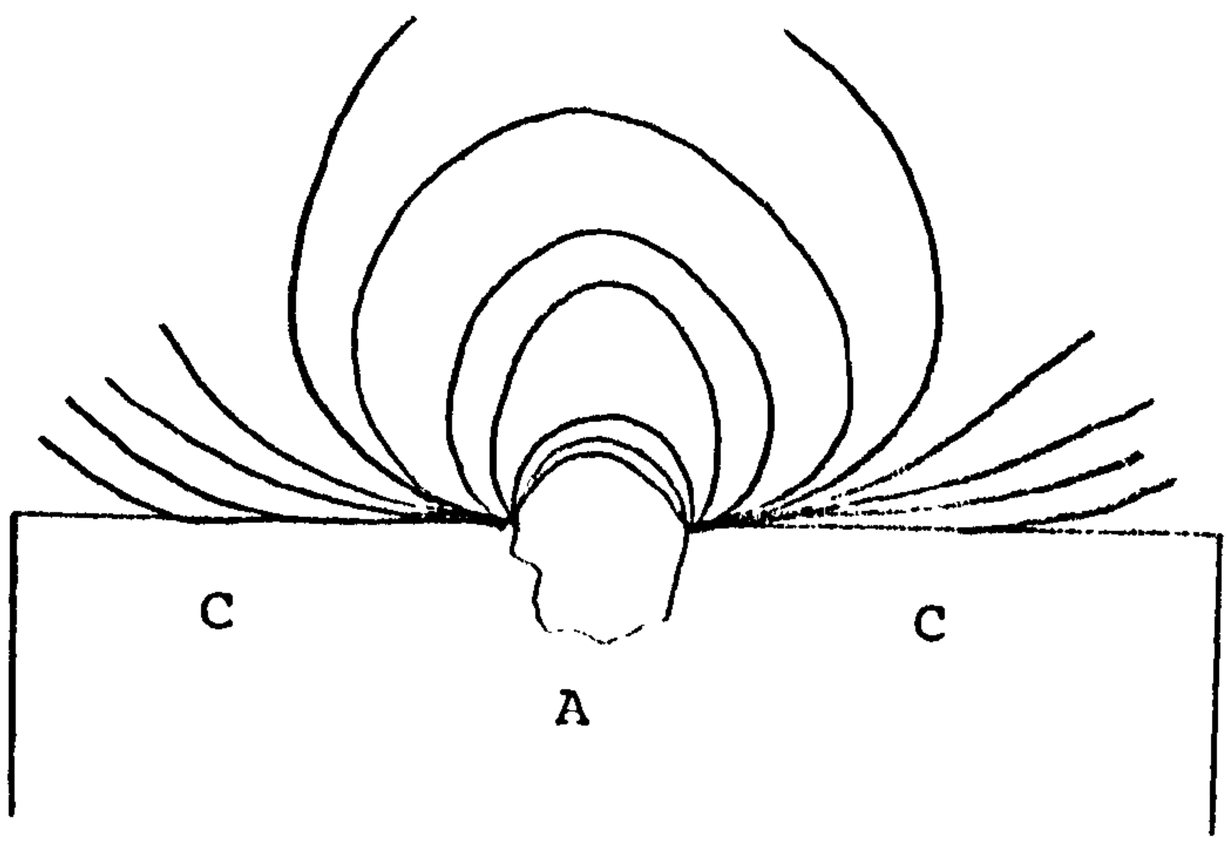

By scanning the metal surface with two microelectrodes, centres of corrosion or discharge, microzones, can be detected. The distribution of microzone current density is important in determining the overall efficiency of utilisation of the alloy. The measurement of current distribution clearly shows the change in corrosion current at OCV, and the in situ change in current density at the microzones during discharge. The measurement of the distribution of the microzone current density was achieved using a dual microelectrode system designed at Xiamen University Chemistry Department, by Prof. C. Lin [92].

Experimentally, the distribution of the microzone current density can be obtained by measuring the potential differences ($\triangle V$) at various positions at the electrode electrolyte interface, as the microzone current density is proportional to the surface current density.

According to the definition of electric field;

$$(6.1)\quad E=\triangle V/\triangle l$$

and applying ohms law;

$$(6.2)\quad i=-k(\triangle V/\triangle l)$$

E is the current density of the electric field,

$\triangle V$ is the potential between the two microelectrode tips,

i is the current density,

k is the conductivity of the medium.

6.2.1 The Microelectrode Structure.

Figure 6.2 shows the structure of the dual microelectrode system.

The diameter of the tip of each microelectrode is approximately 10μm. The distance between the two tips is approximately 400μm. These two microelectrodes are positioned in a vertical direction and scan the electrode surface at the same rate.

The density of the electric field is a vector quantity. Expressed in a three dimensional system its;

X component is $(\Delta V/\Delta X)^2$,

Y component is $(\Delta V/\Delta Y)^2$,

Z component is $(\Delta V/\Delta Z)^2$.

Therefore, the current density can be written as ;

$$(6.3)\quad (i) = -k\sqrt{(\Delta V/\Delta X)^2 + (\Delta V/\Delta Y)^2 + (\Delta V/\Delta Z)^2}$$

The technique described is concerned with the vertical components of the current density. Obviously if there is no current between the two tips of the microelectrodes, V=0. The potential between the microelectrodes is caused by the vertical components of the current passing through the two

Figure 6.2 The Dual Microelectrode System.

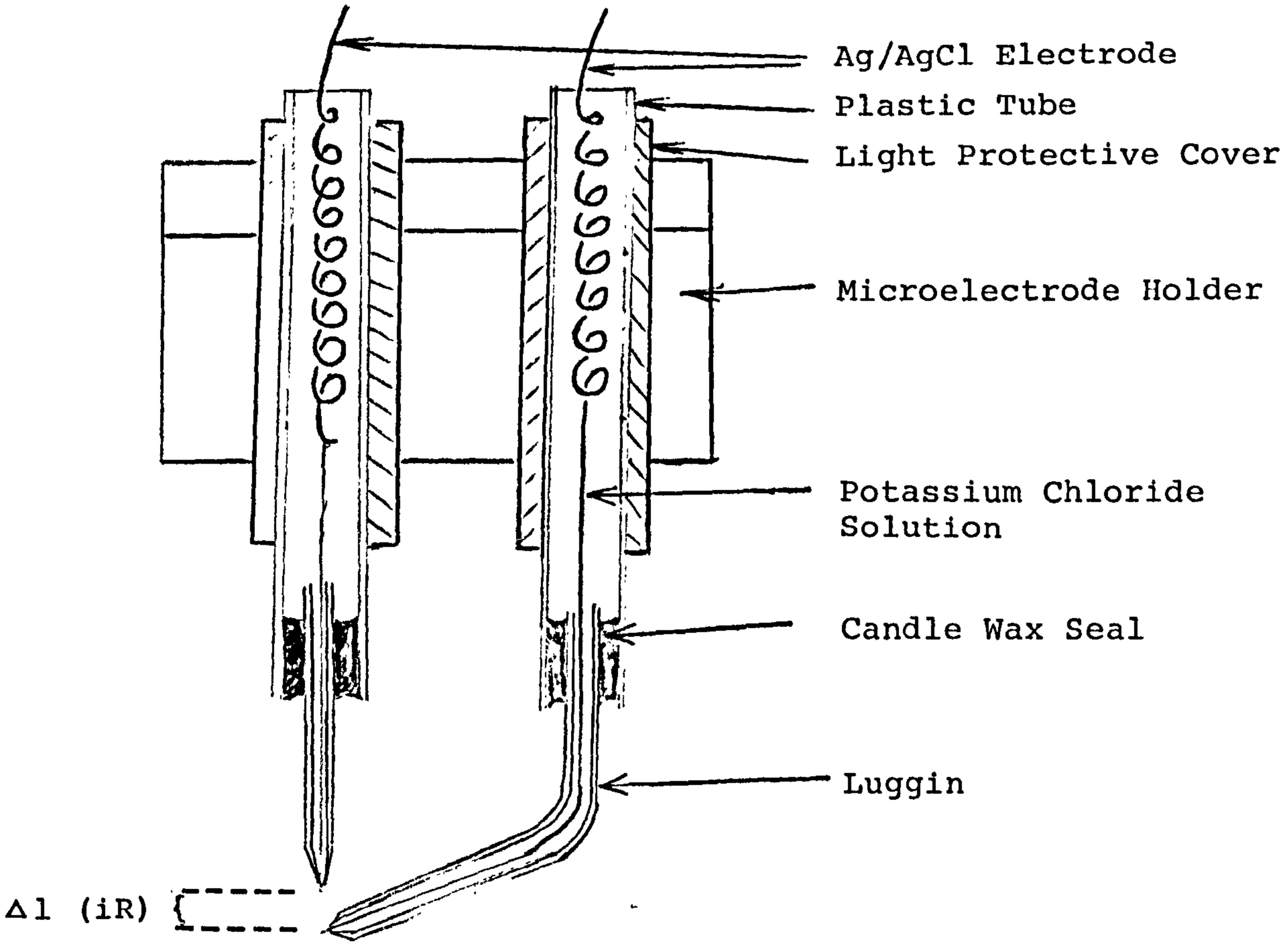

tips. At a discharge centre, the vertical components of the current passed reaches a maximum, which corresponds to a peak on the distribution diagram obtained by the complete scanning of the electrode.

6.2.2 Current Distribution Diagrams.

Figure 6.3 (a) is an example of a typical current density distribution diagram. As previously stated, the potential is proportional to the current density and so the potential peak in (a) corresponds to a current density peak. (b) shows the same distribution diagram from a different angle. (c) gives an equivalent potential diagram that can also be obtained.

6.2.3 Instrument Design.

The instrument design is as shown in Figure 6.4, and the hardware system for the scanning current distribution and signal detection is shown in Figure 6.5.

6.3 Experimental.

Aluminum alloys of approximately 1cm^2 were prepared as previously described. The alloys were set in a plastic container and contact made with the underside of the alloy and the external circuit using silver glue. The alloys were examined in two electrolytes, E and A, both at OCV and

Figure 6.3 Current Density Distribution Diagrams.
(a) Typical distribution diagram.

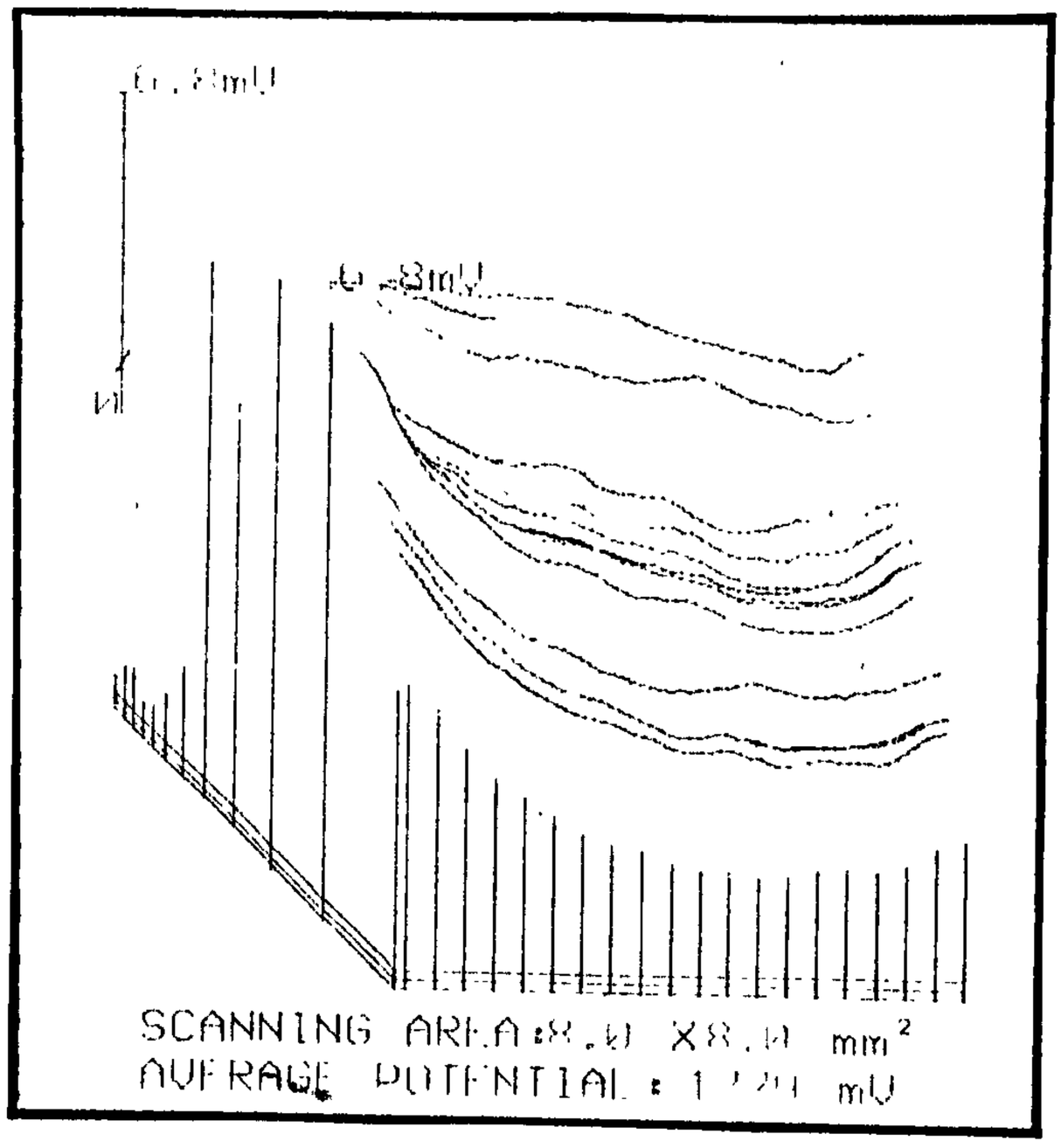

(b) Same diagram - different angle.

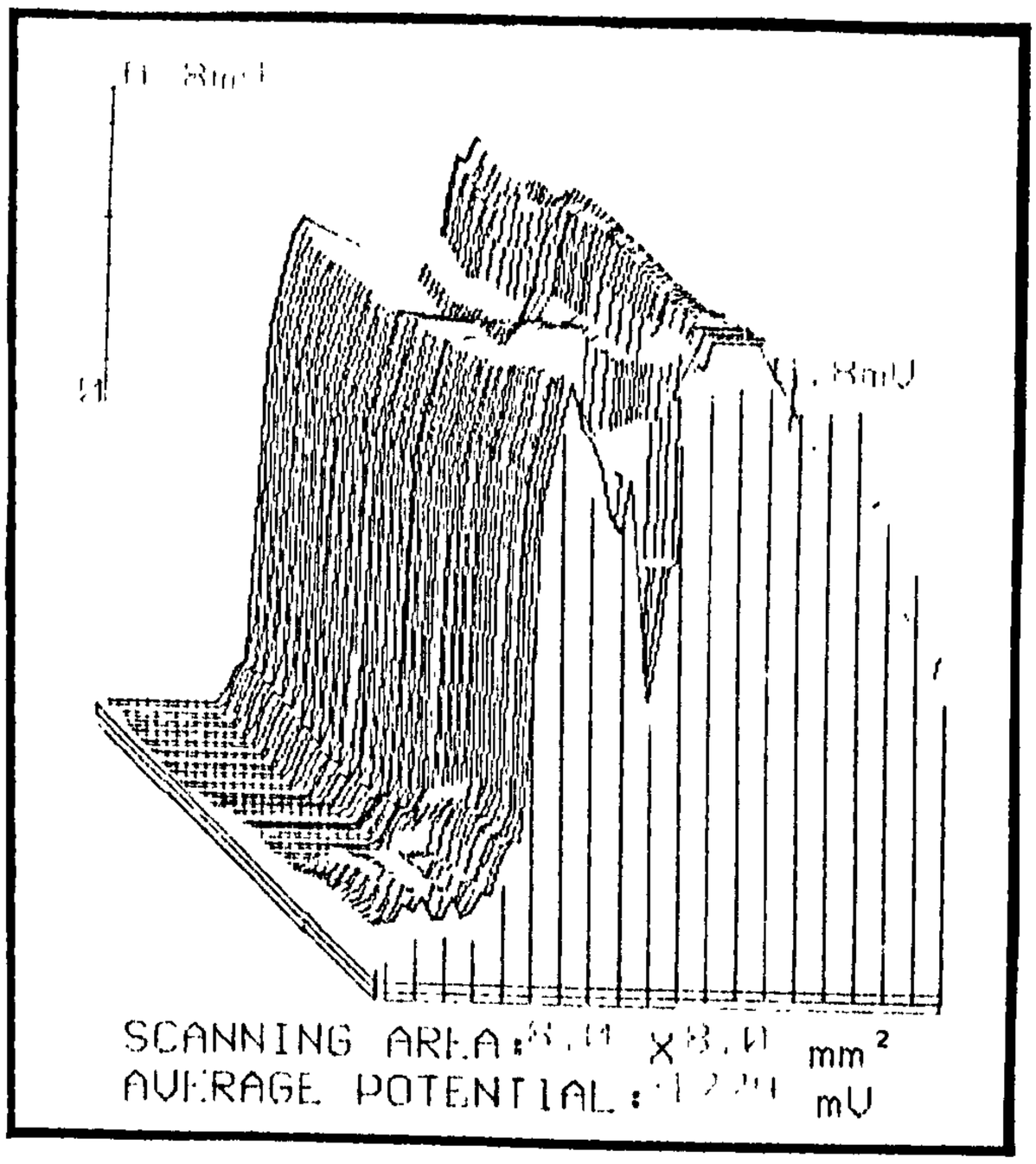

(c)

(i) Distribution diagram.

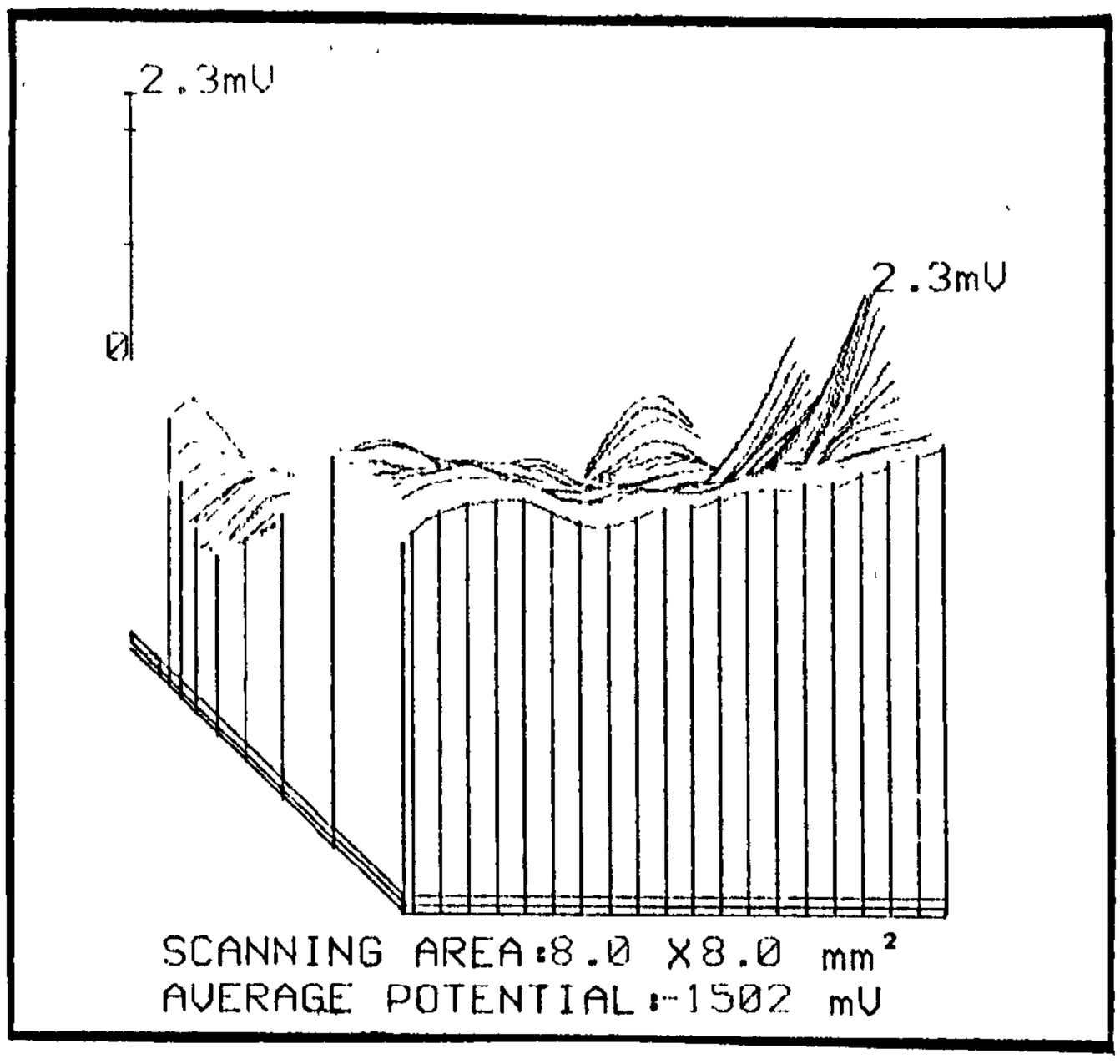

(ii) Equivalent potential diagram from (i) above. The points that are relatively close to each other represent peaks.

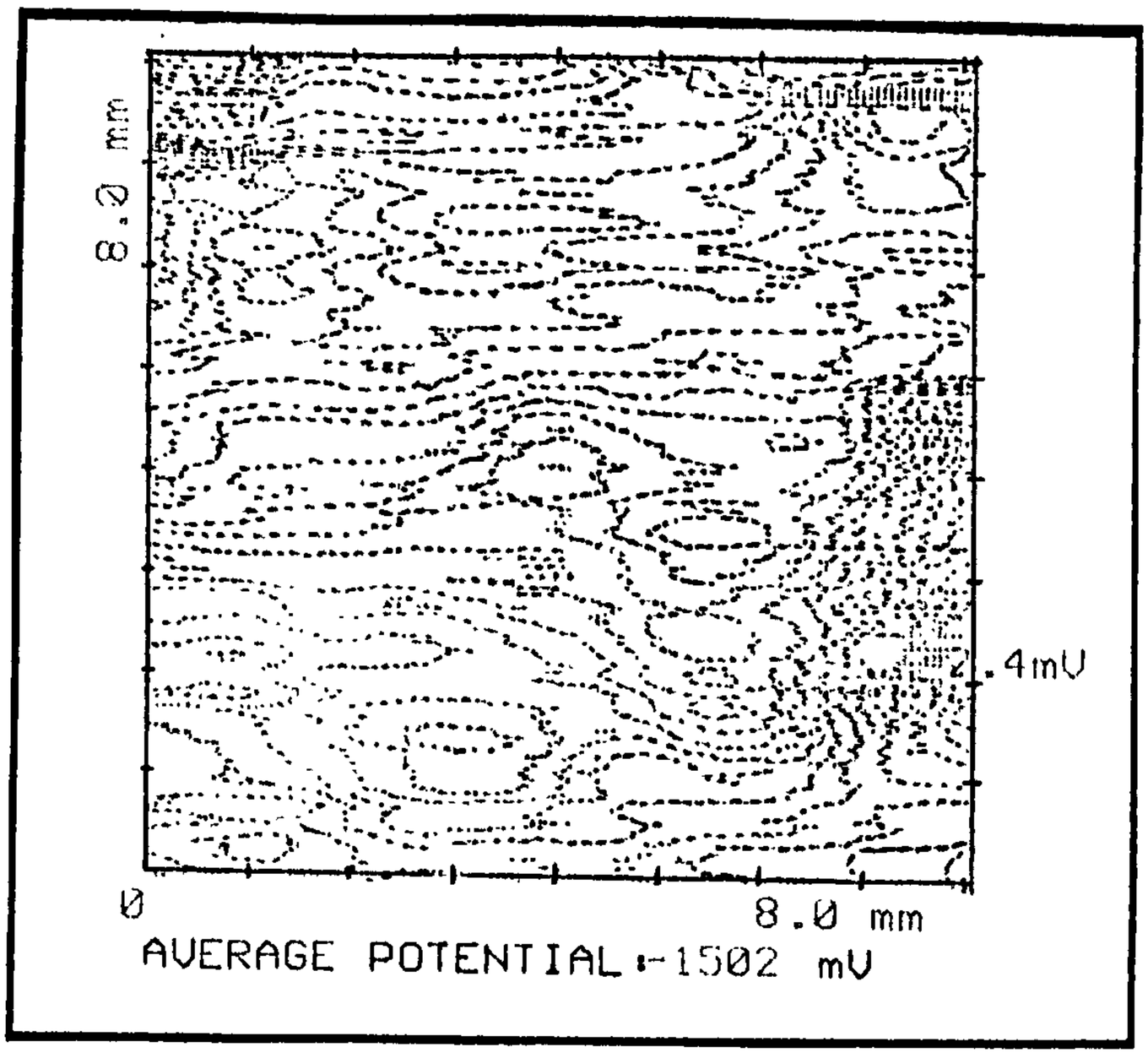

Figure 6 .4 Instrument Design for Measuring Current Distribution.

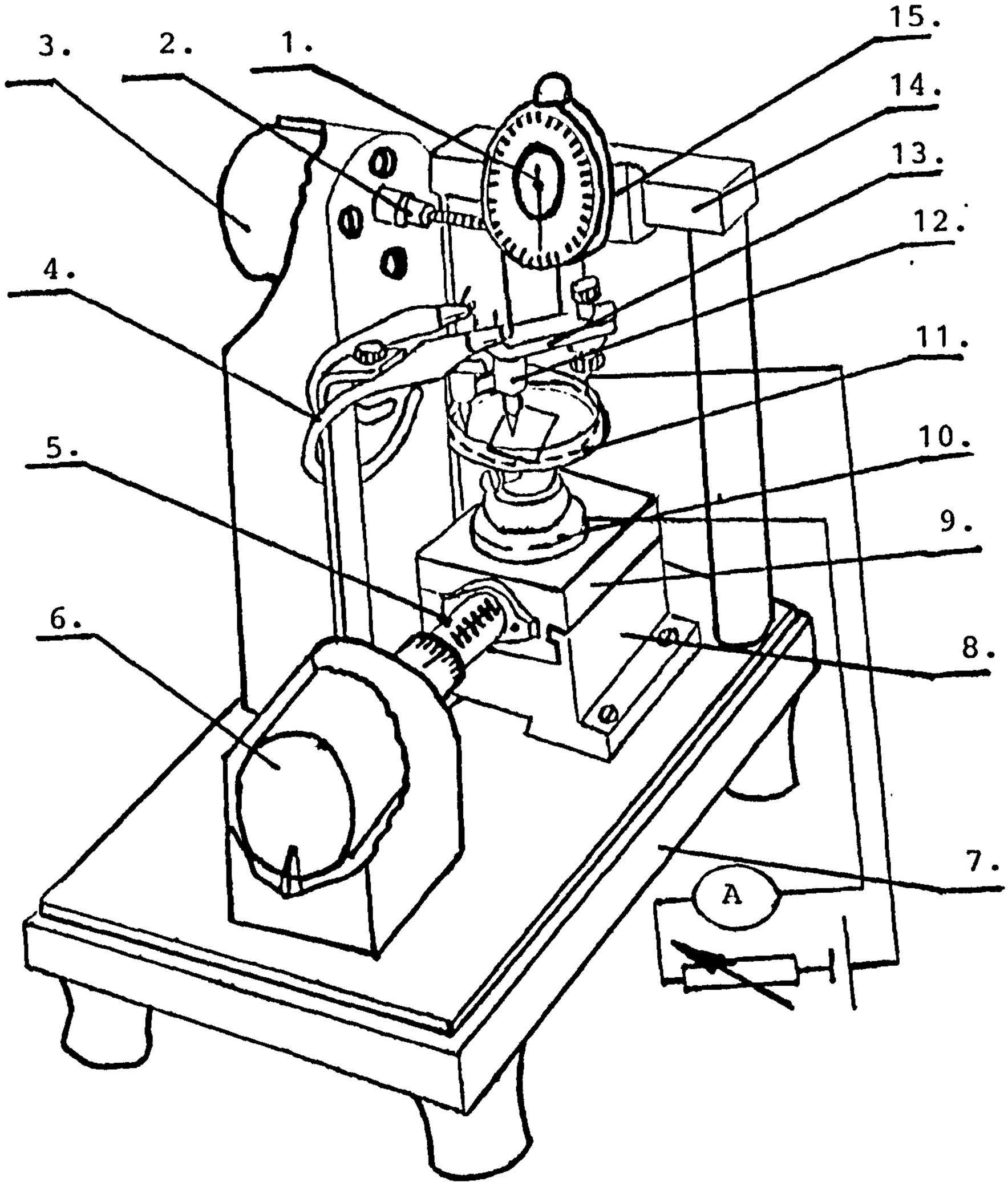

1. Micrometer
2. Y Axis Guider Screw
3. Y Axis Step Motor
4. Input Detector
5. X Axis Guider Screw
6. X Axis Step Motor
7. System Base
8. X Axis Slider Base
9. X Slider
10. Sample Holder
11. Electrochemical Cell
12. Microlectrode
13. Microelectrode Holder
14. Y Axis Slider Base
15. Y Slider.

Figure 6.5 Hardware System for Measuring Potential Distribution on Metal Surfaces.

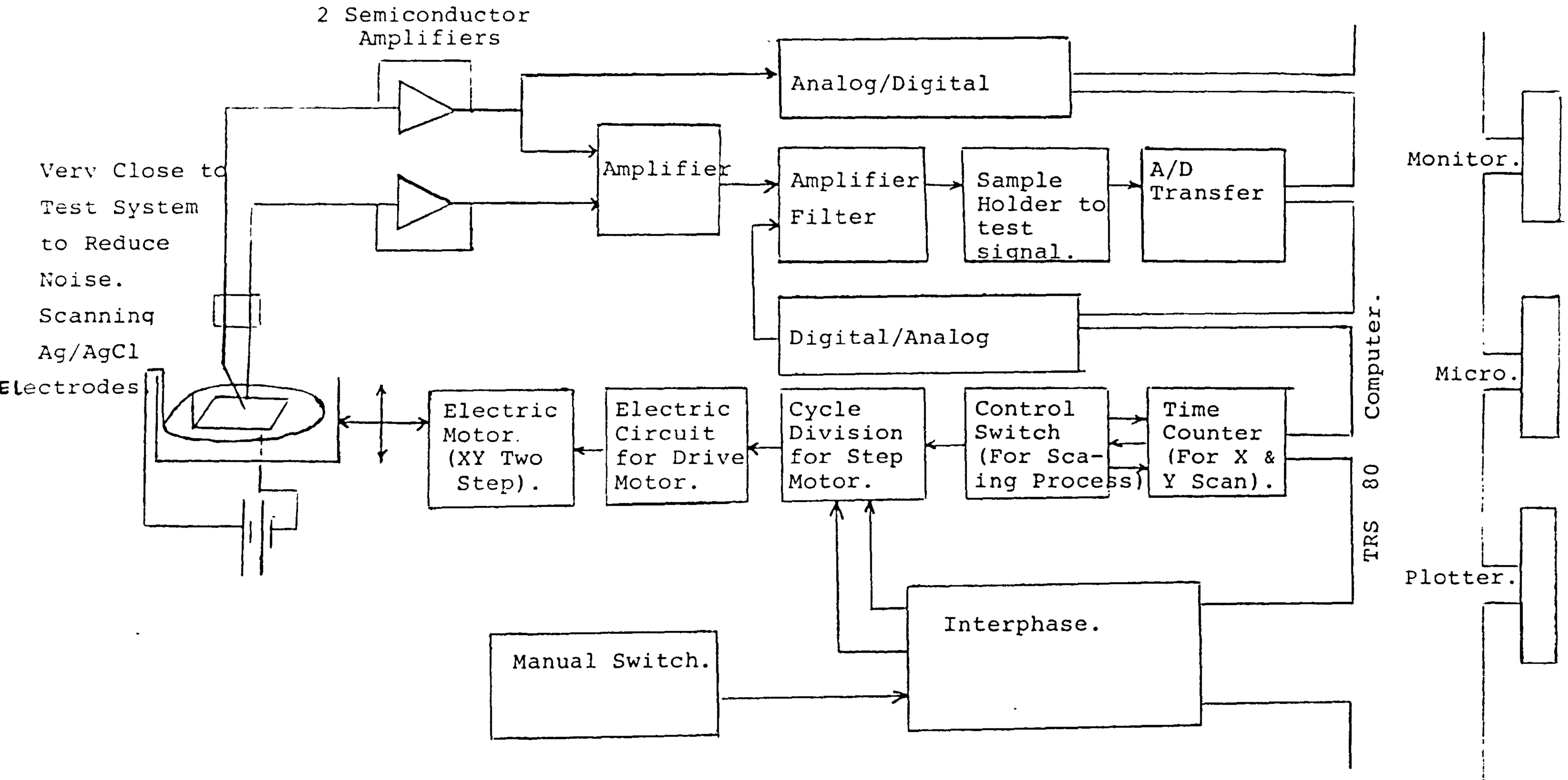

during discharge at selected current values.The electrodes were also discharged in electrolytes E and A to which no mercuric oxide was added. This enabled the role of mercury to be studied.

6.4 Results.

That the presence of mercury reduces corrosion of aluminium in alkaline media is well known. Previous experiments e.g measurement of hydrogen evolution, have clearly shown this is so [93]. The results shown in Figure 6.6 confirm this fact.

The surfaces of all four alloys were scanned at open circuit potential, and it can be seen from the distribution diagrams that for alloy 1, the corrosion current has greater peaks and the surface is more active in Figure 6.6 (a) which used electrolyte A with no added mercury than (b) electrolyte A plus mercuric oxide additive. So (a) without mercury has greater corrosion current at zones throughout the alloy than that of (b). Whilst there is a corrosion current in (b) it can be seen that the distribution is much more even than that of (a). Similar results were obtained with all four alloys.

Further studies were carried out at open circuit potential.

Figure 6.6

(a) Alloy 1, Electrolyte A (with mercury), OCV.

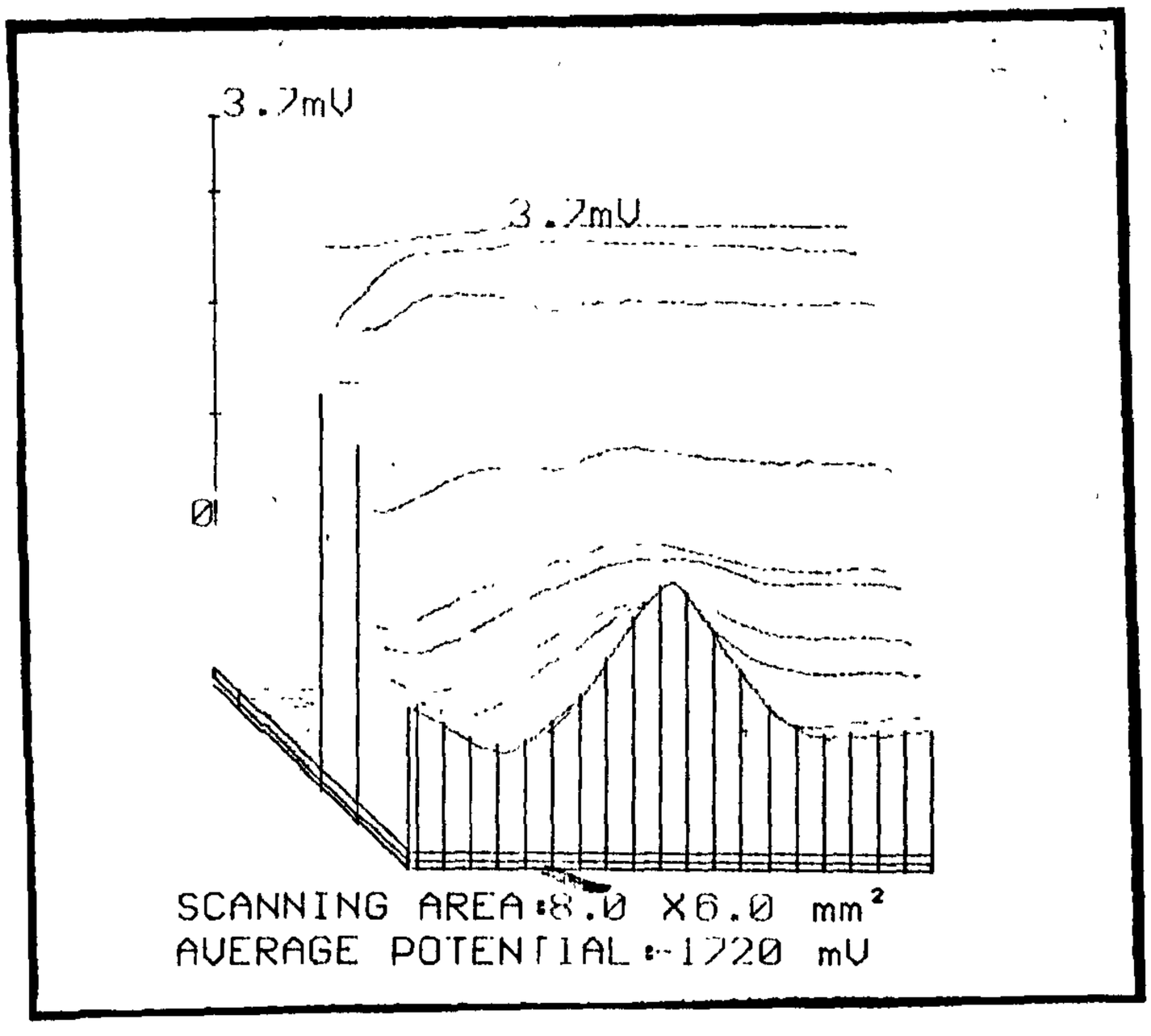

(b) Alloy 1, Electrolyte A (no mercury), OCV.

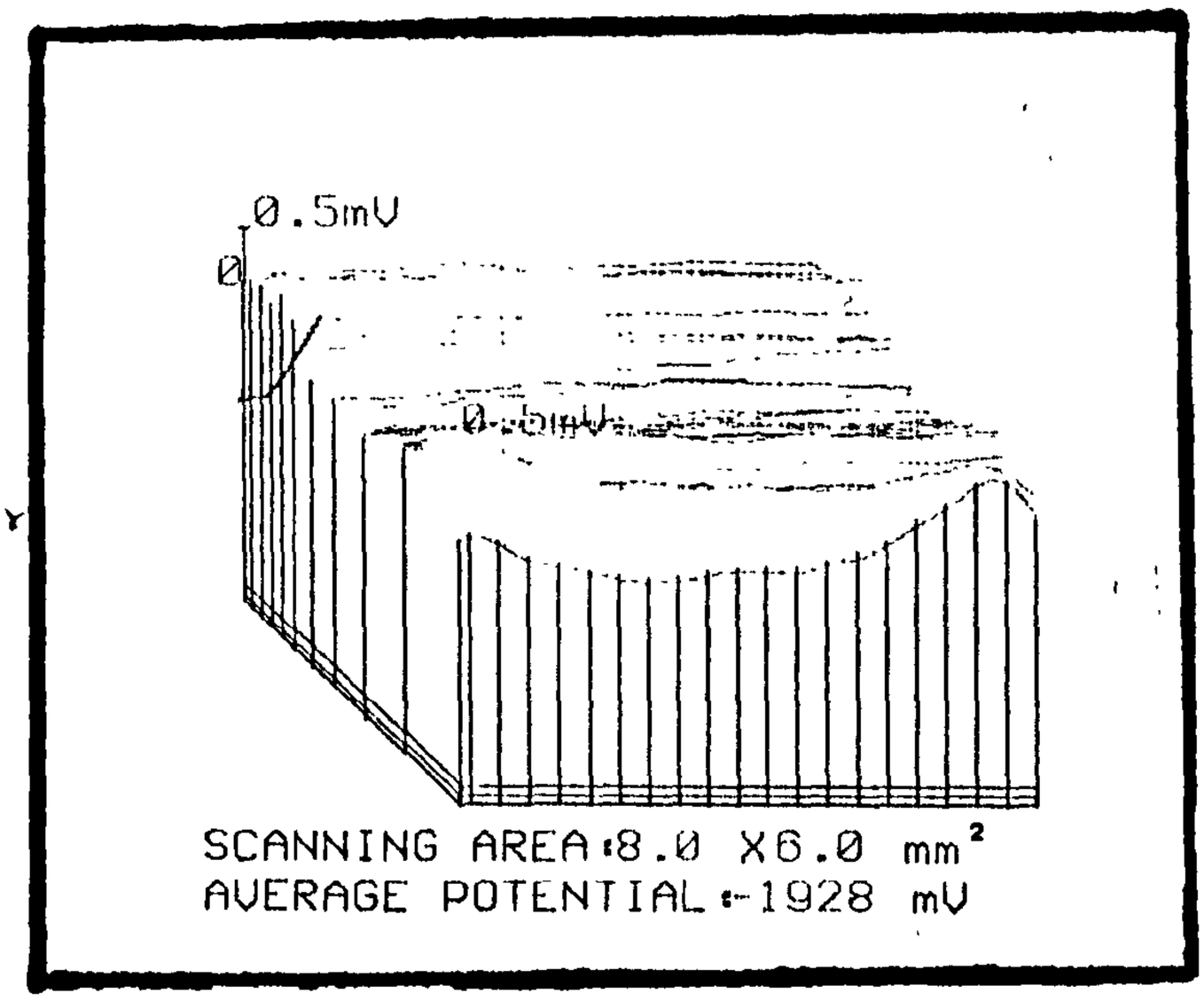

(c) After 60 minutes (t^6).

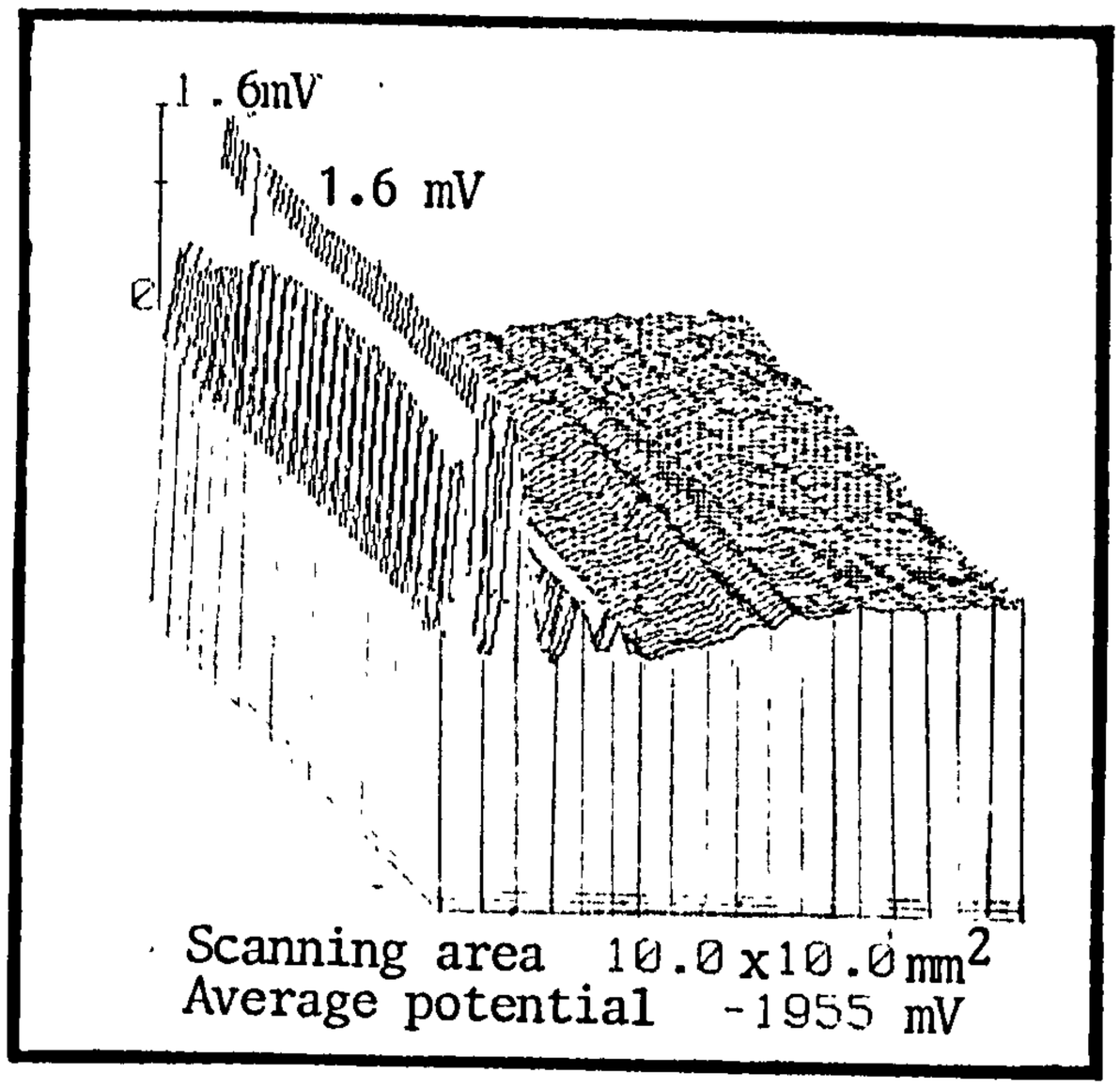

(d) After 90 minutes (t^9).

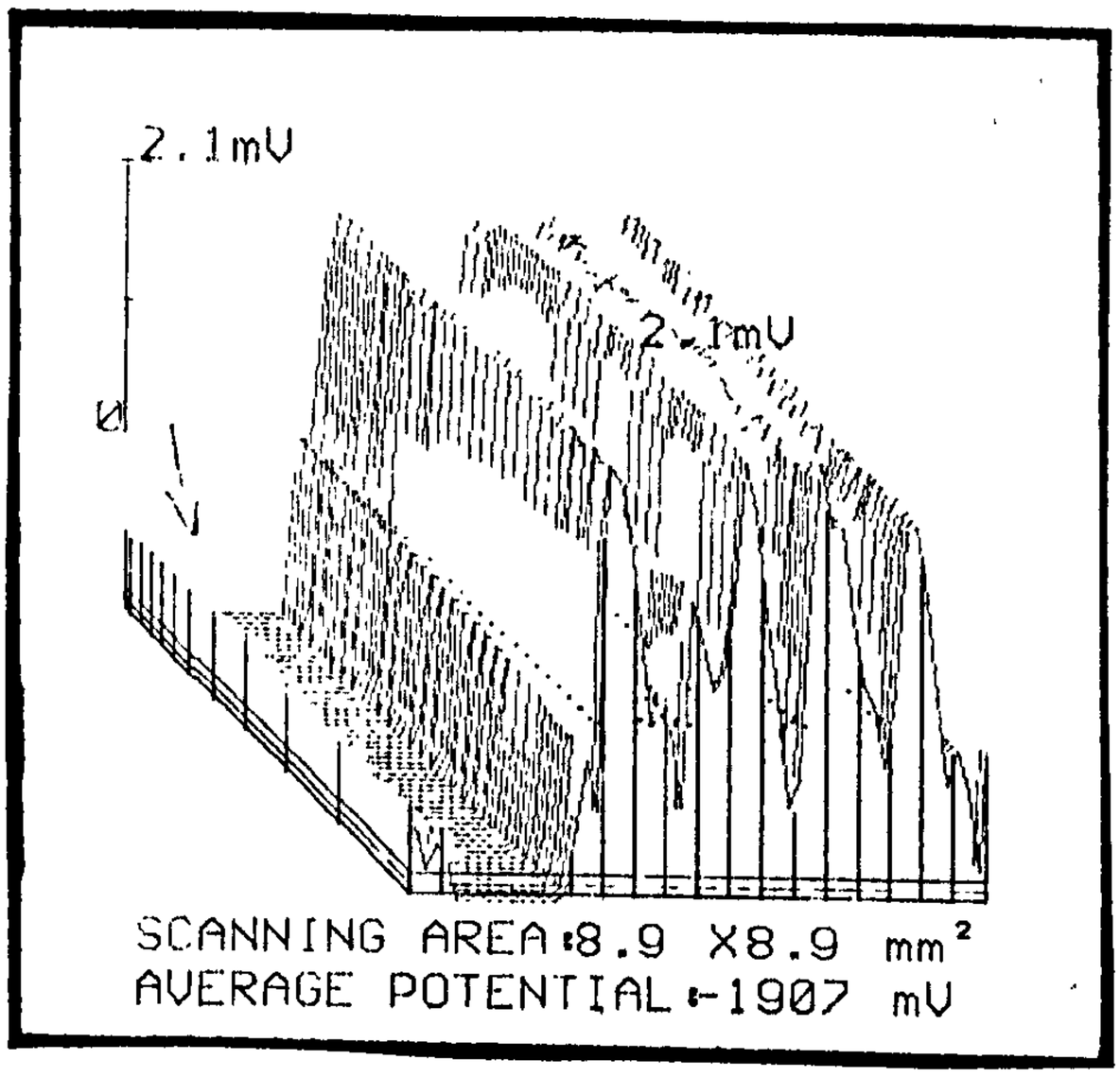

Figure 6.8 Alloy 2, Electrolyte E, no mercury, OCV.

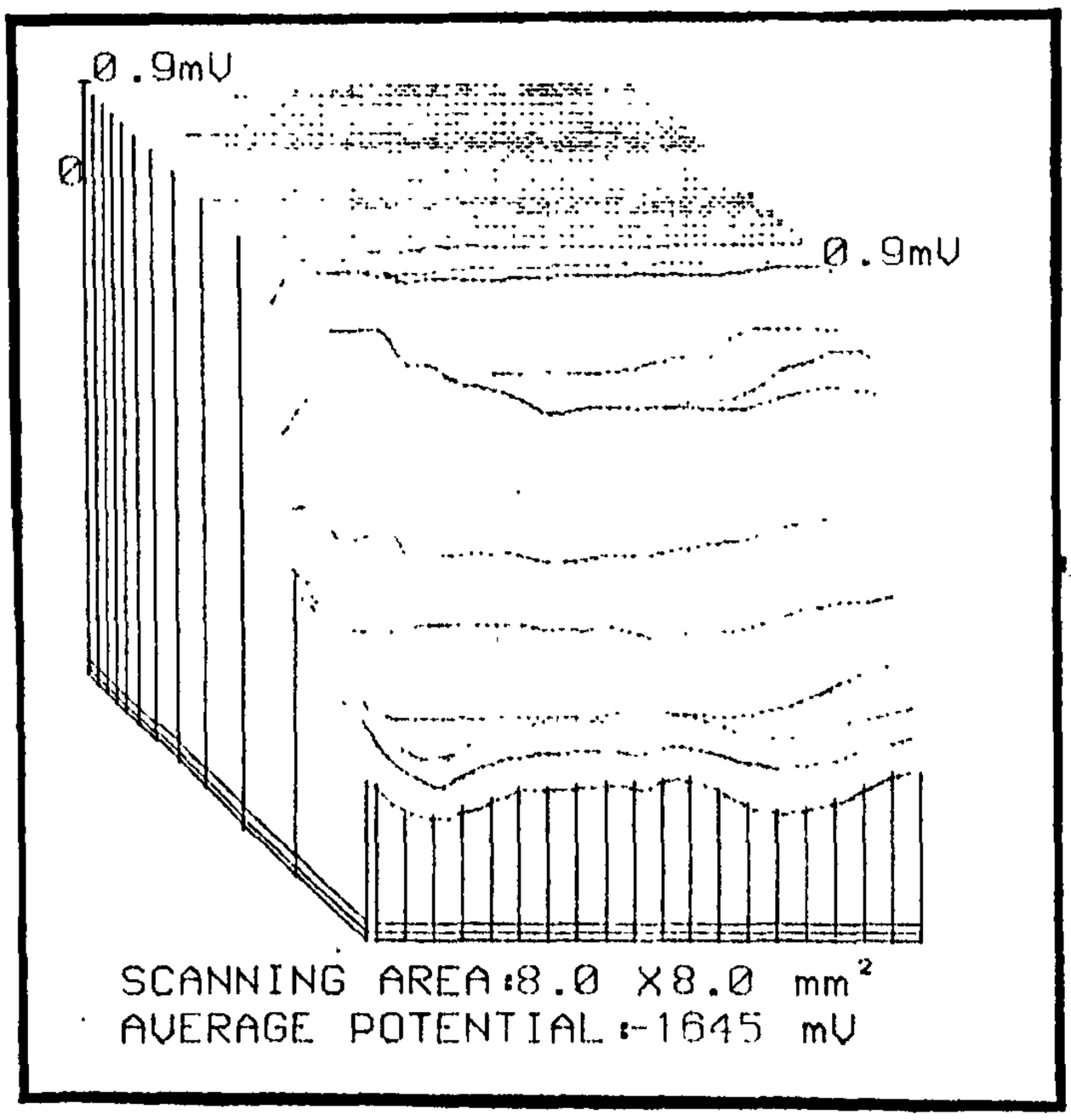

Figure 6.9

(a) (i) Alloy 3 discharged at 7mA in Electrolyte E, with mercury, at t = 0 mins.

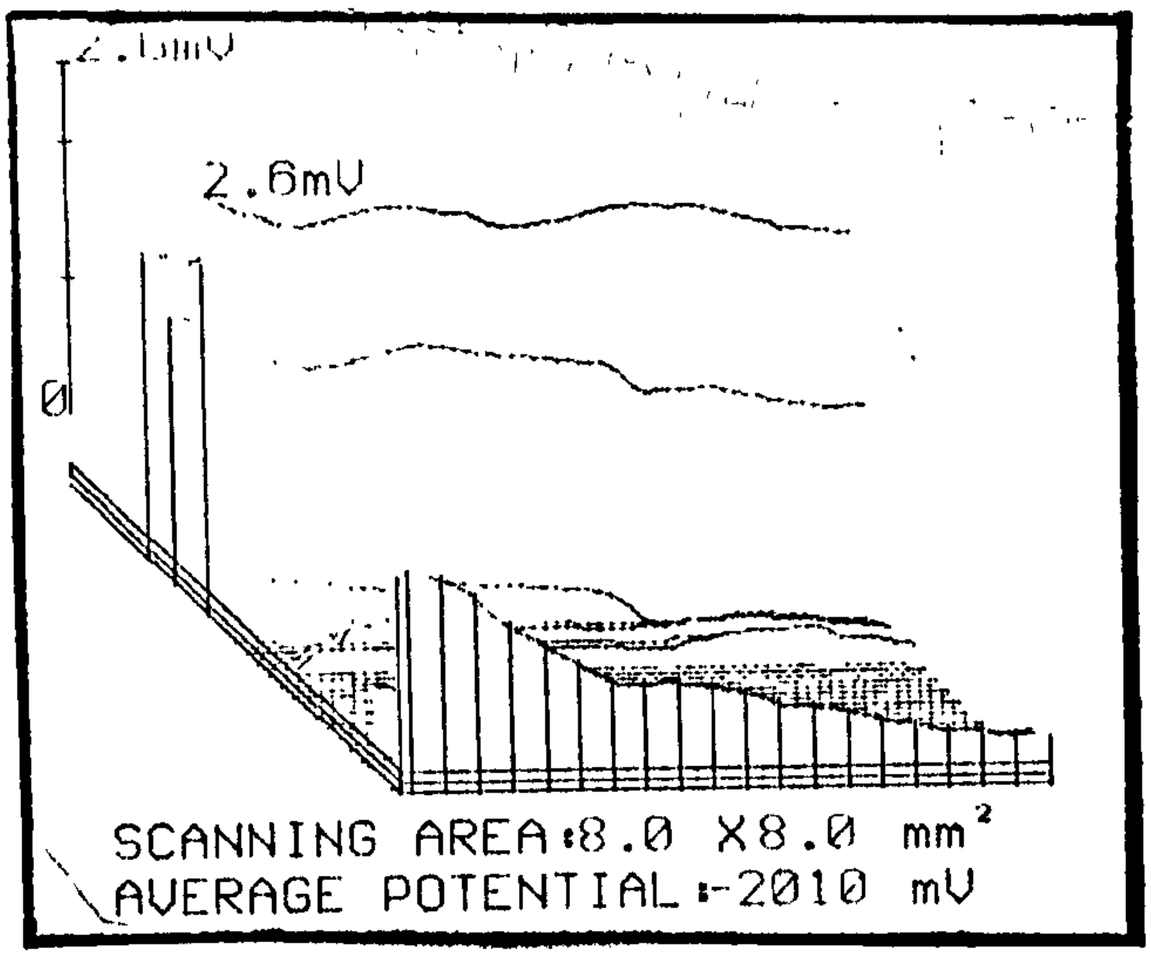

(ii) Different angle.

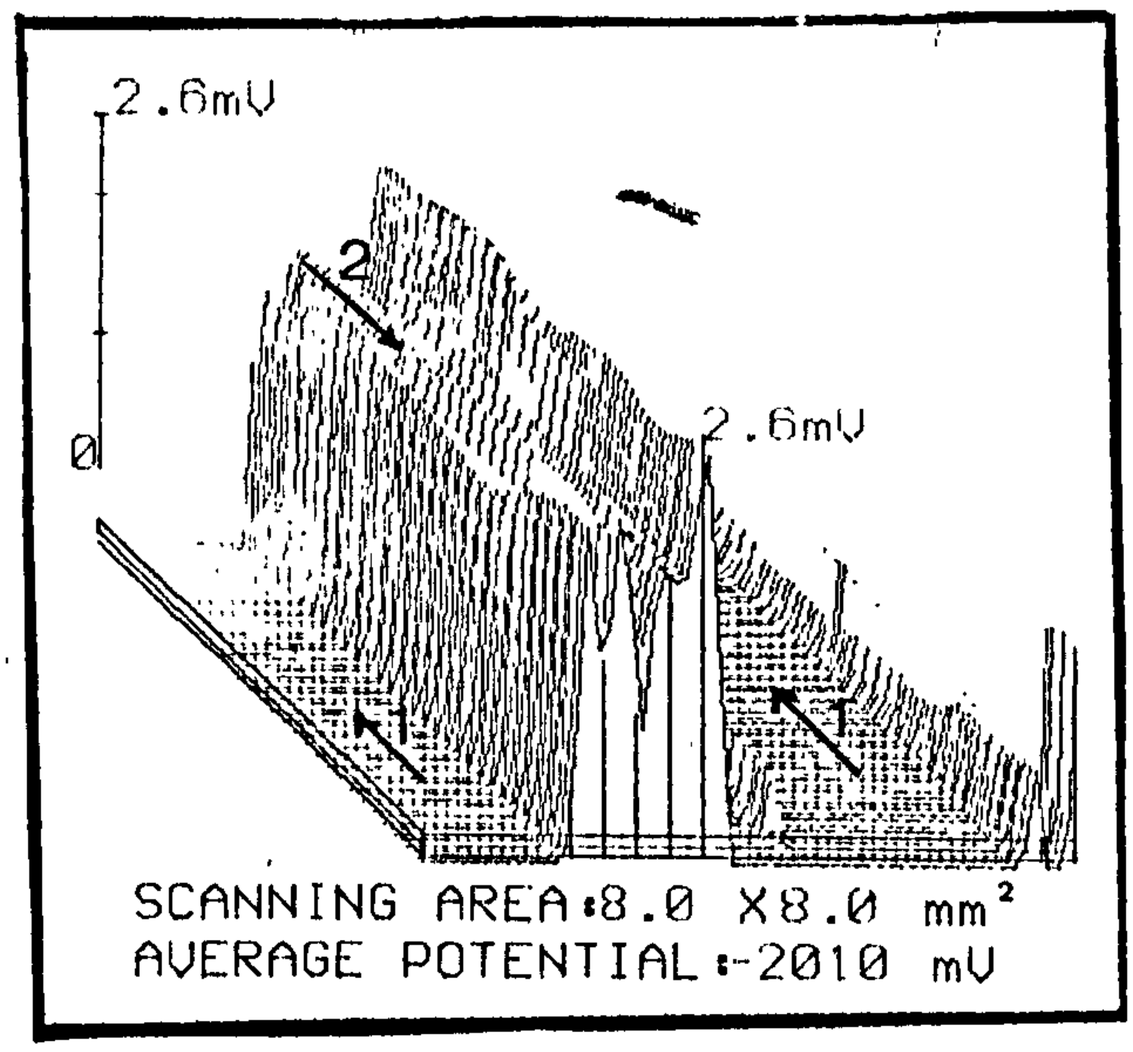

(b) (i) Alloy 3 discharged at 7mA at t = 30mins.

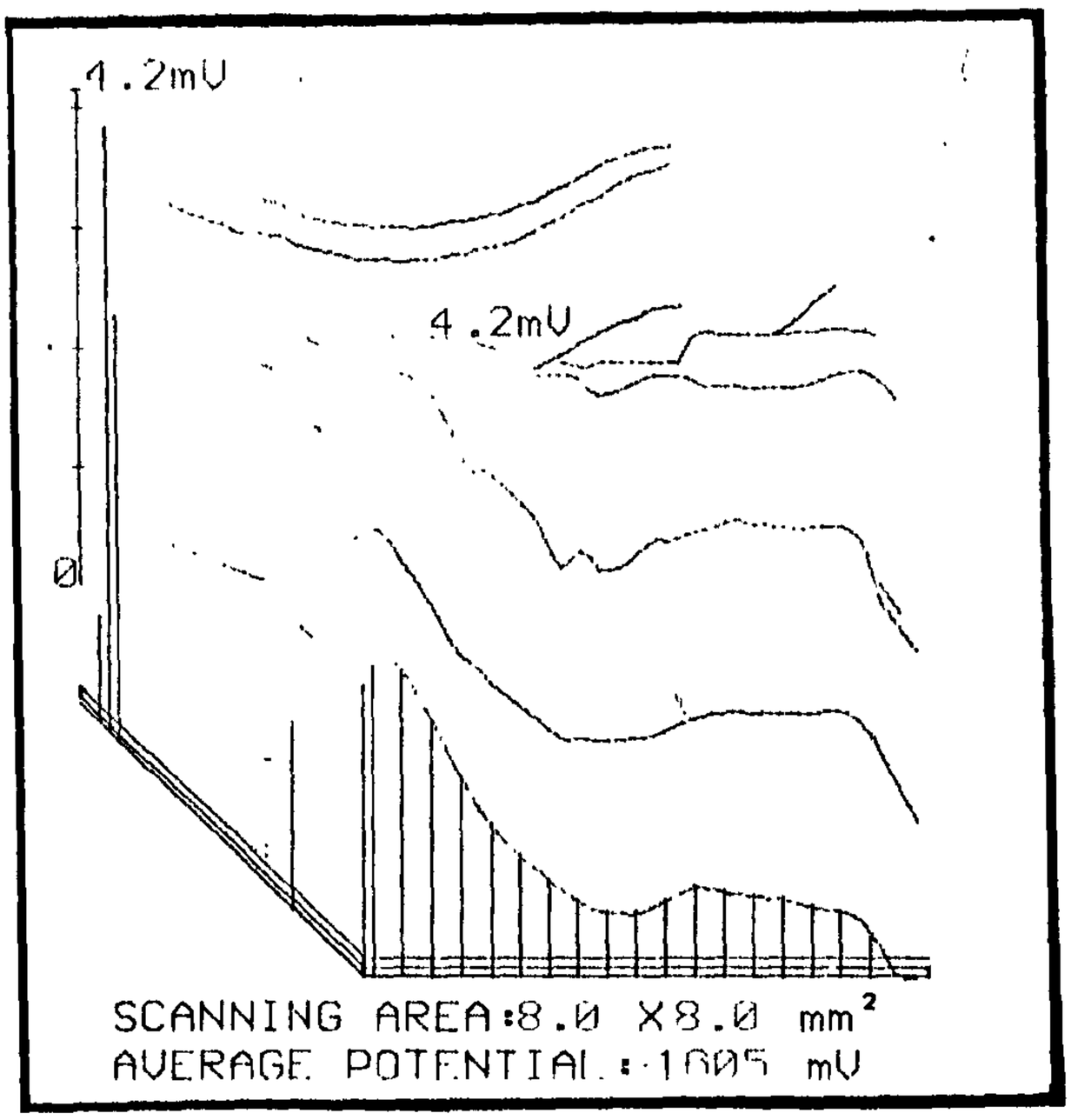

(ii) Different angle.

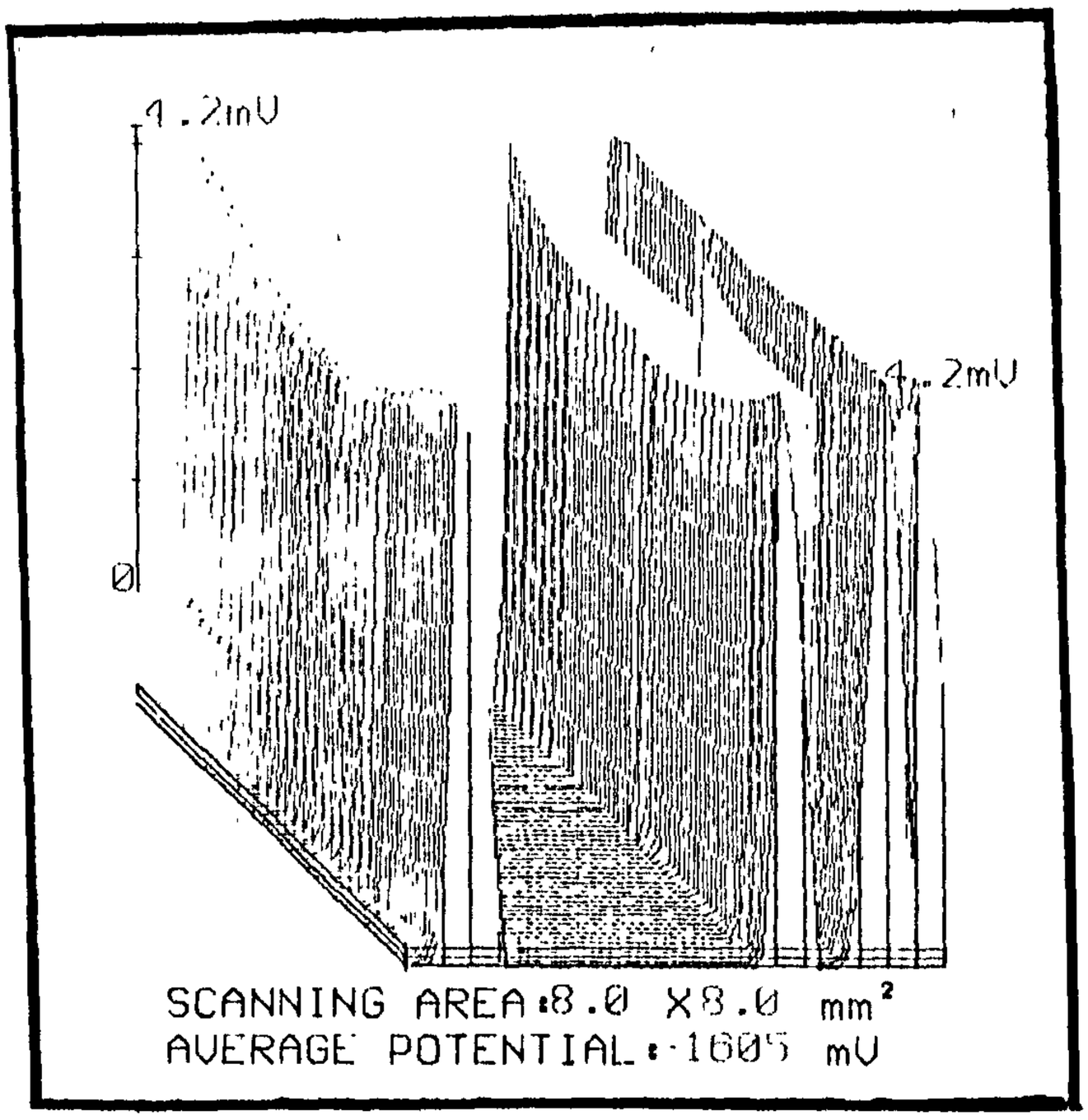

Figure 6.10

(a) (i) Alloy 3, Electrolyte E, discharged at 32mA. (Electrolyte saturated with mercury).

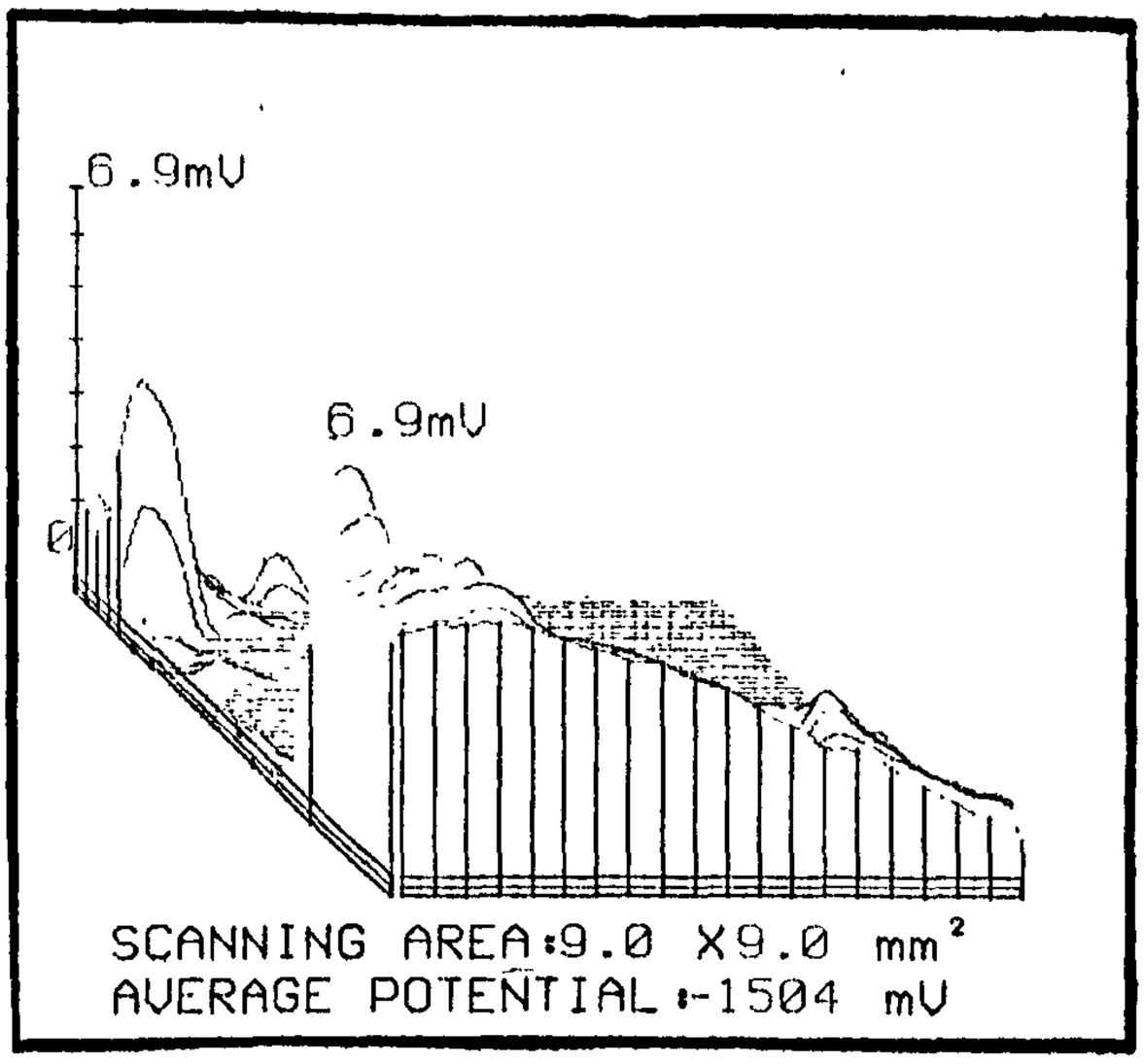

(ii) Discharged at 70mA.

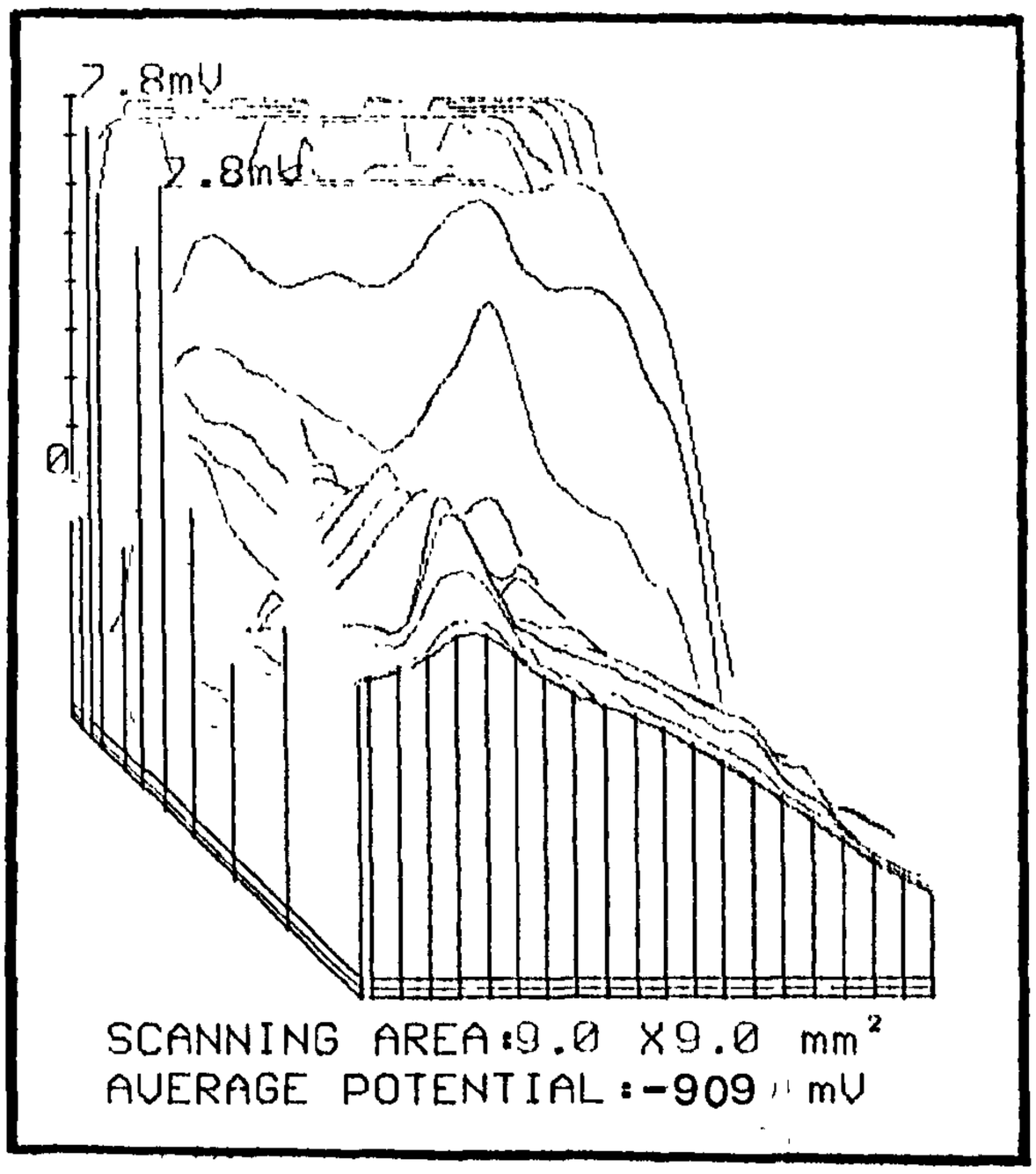

(b) (i) Alloy 4, Electrolyte A, discharged at 25mA.

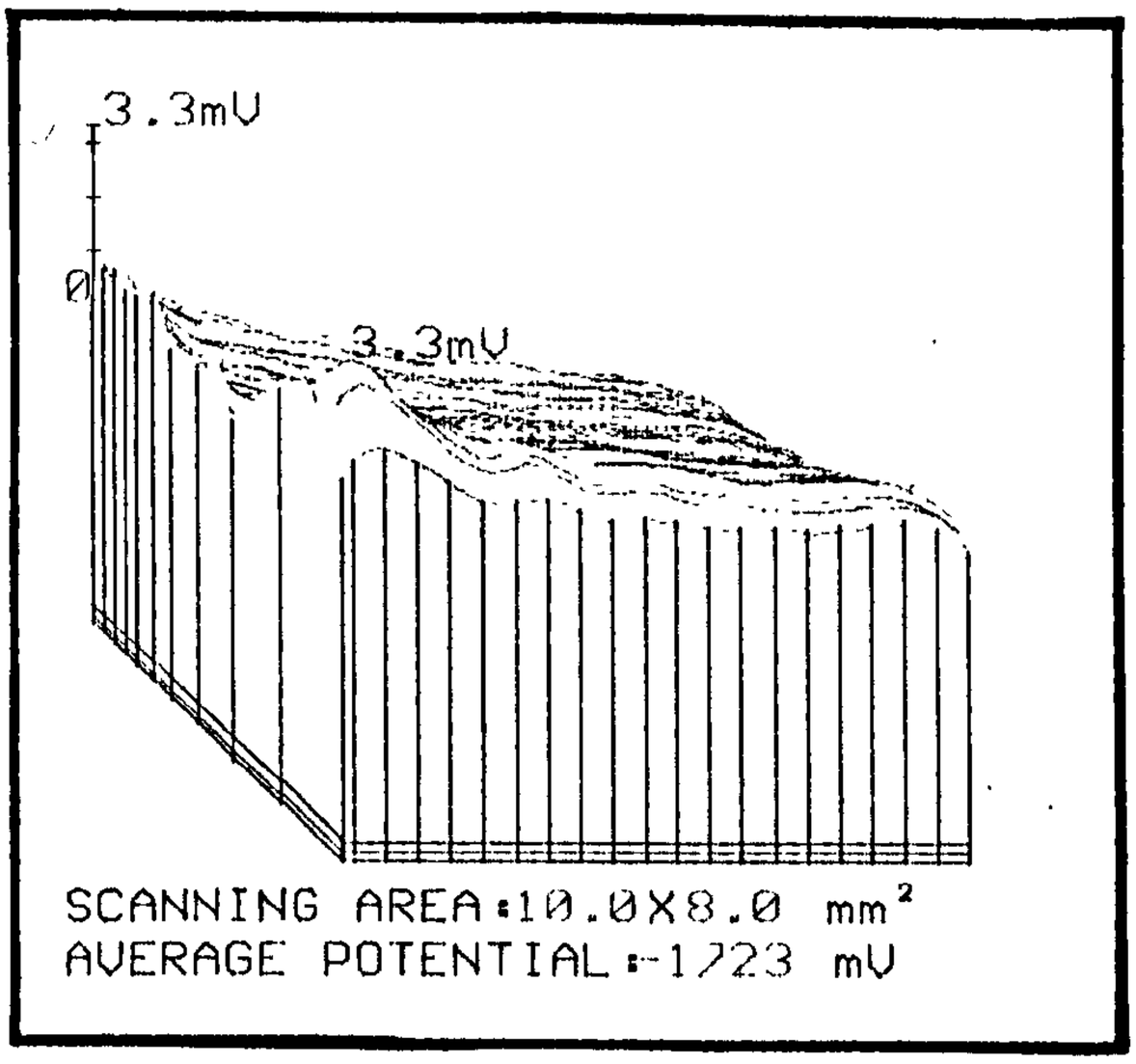

(ii) Discharged at 73mA.

Figure 6.11

(a) (i) Alloy 2, Electrolyte E with mercury, discharged at 60mA.

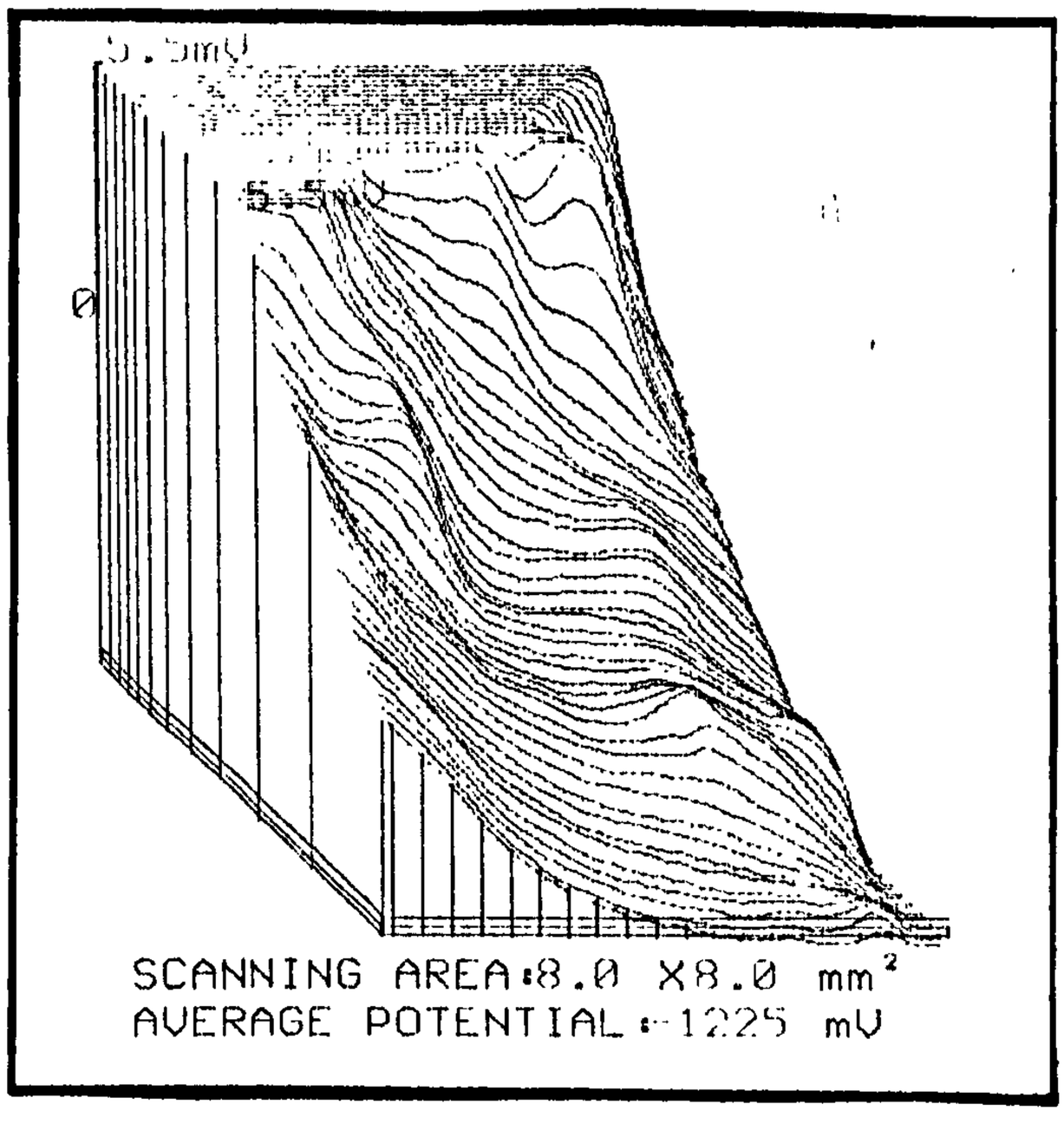

(ii) Equivalent potential diagram.

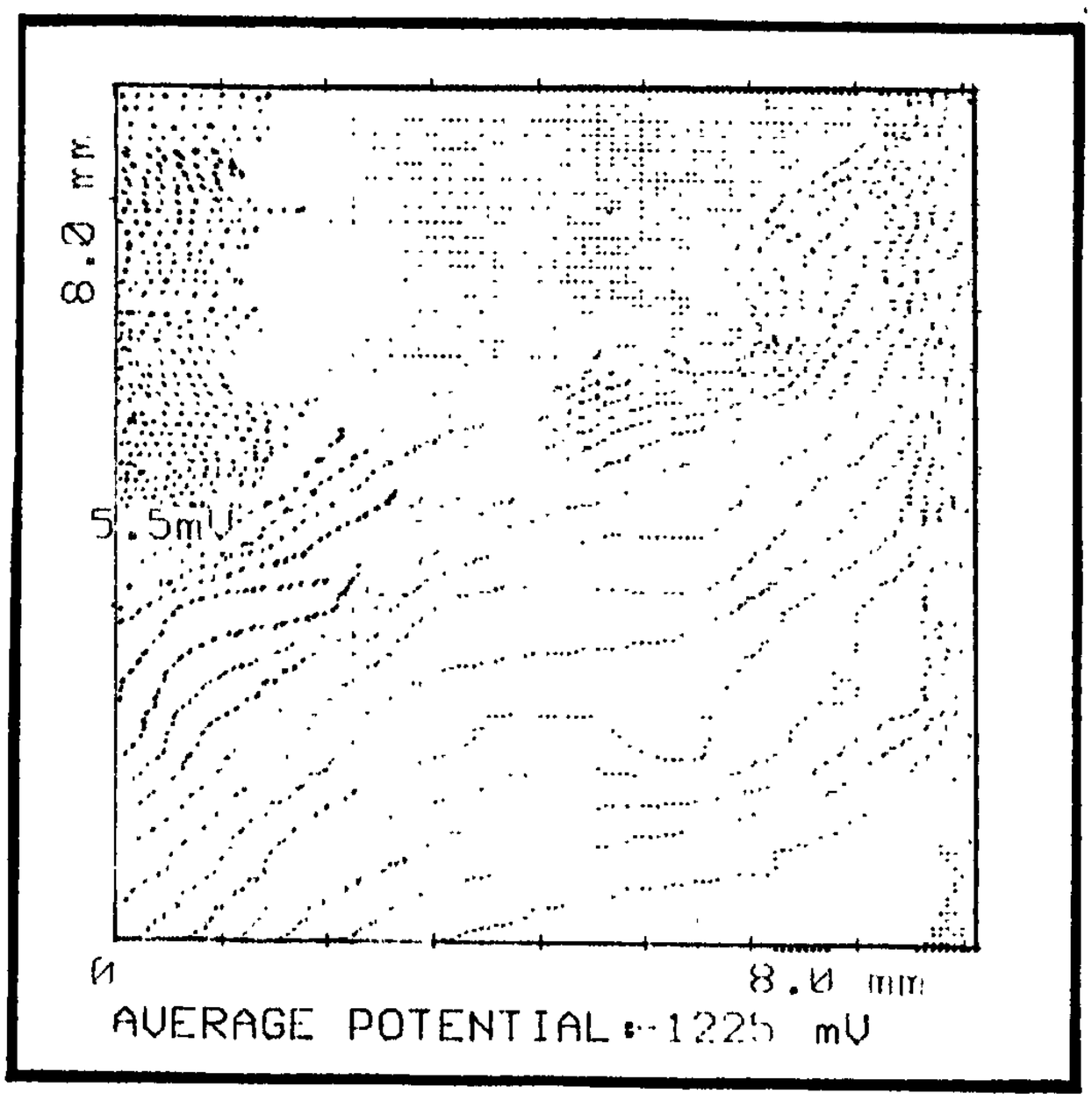

(b) (i) Alloy 4, Electrolyte E with mercury, discharged at 73mA.

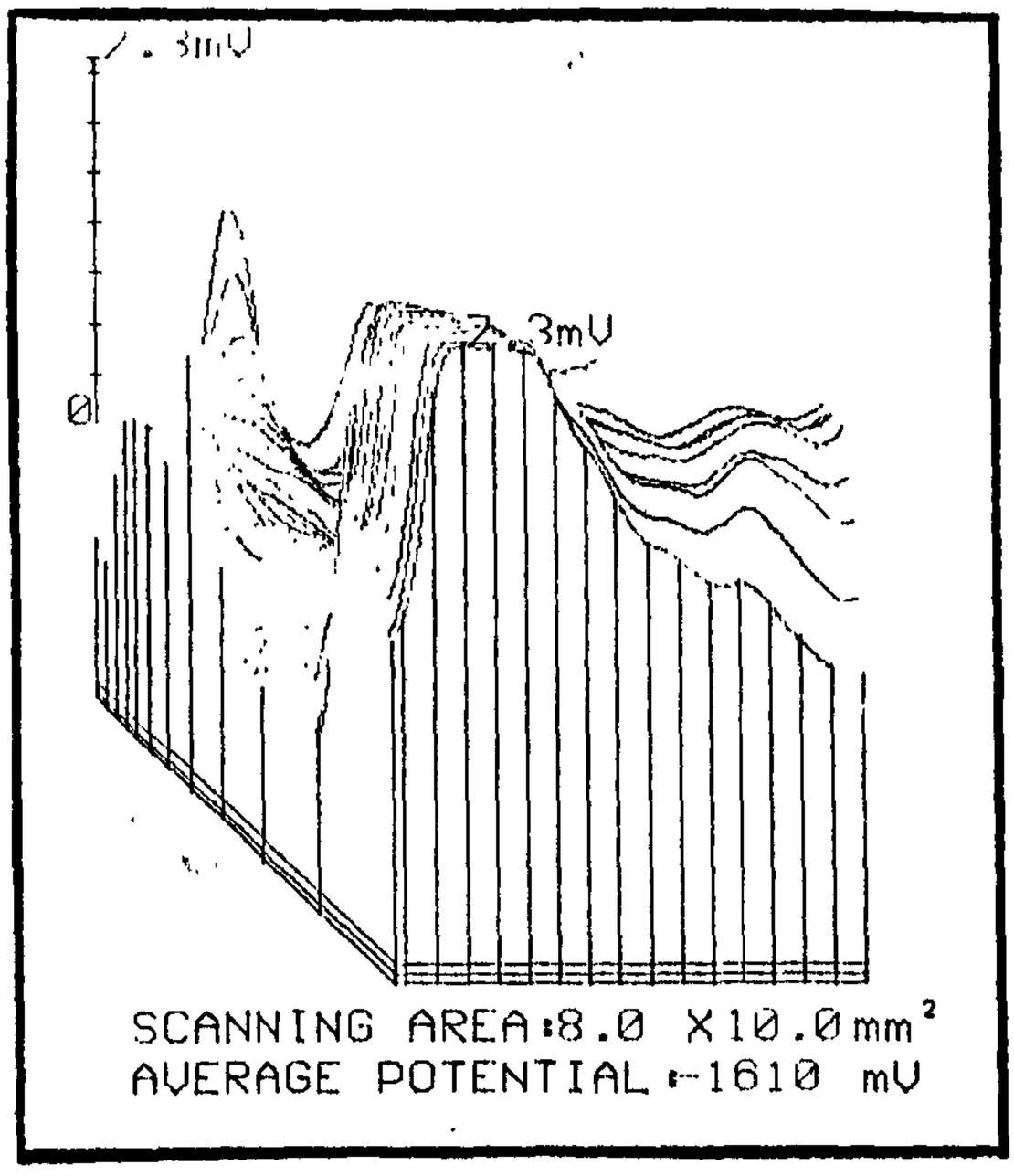

(ii) Equivalent potential diagram.

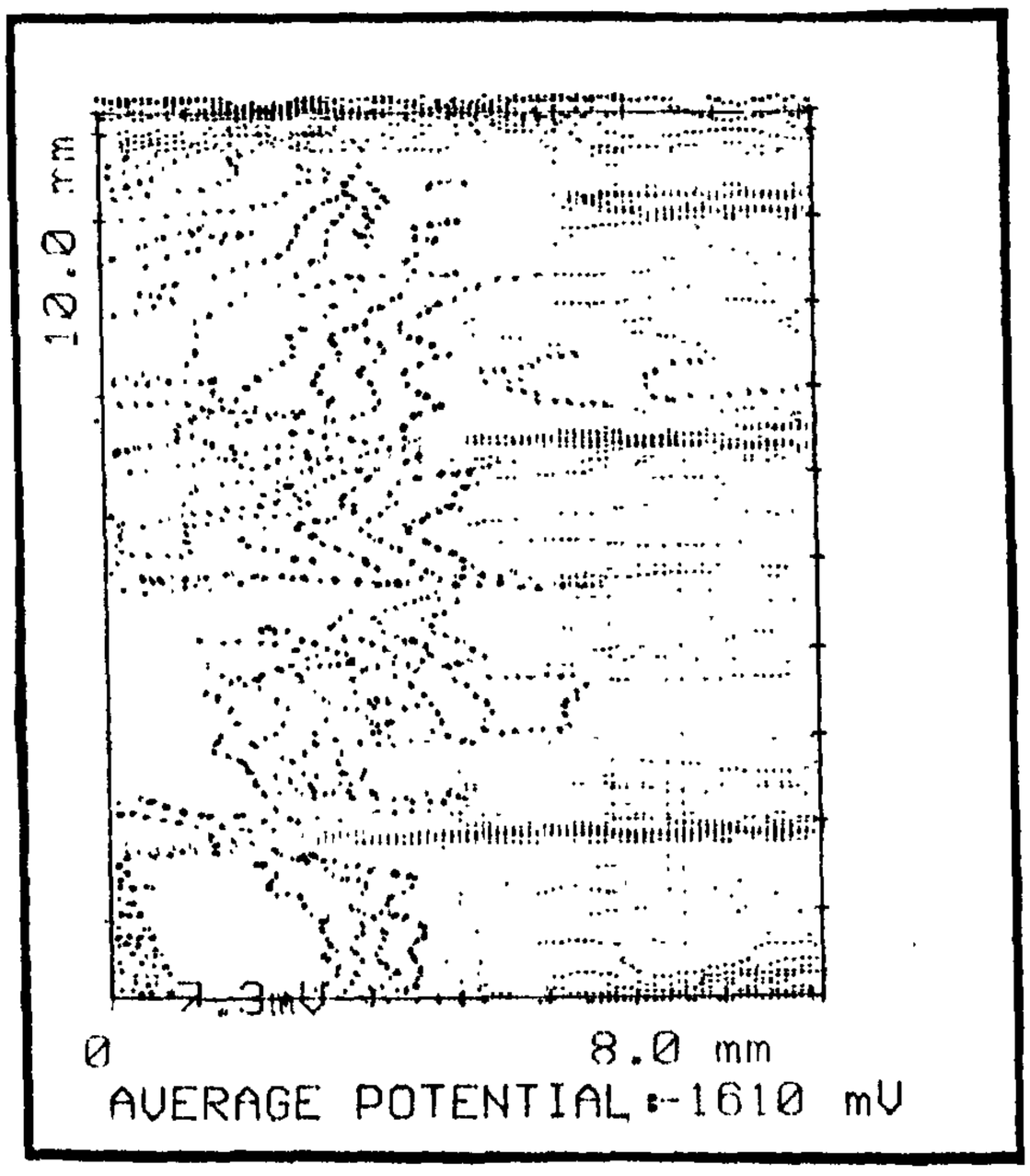

Alloy 2 was used in electrolyte E (saturated with mercury) in the system. The electrode was scanned at regular intervals of ten minutes and were recorded as t^0 to t^9, so ten scans were run in all over a period of ninety minutes. Four of the scans are shown in Figure 6.7 (a), (b), (c) and (d). After ten minutes (t^1), there is extremely little or no corrosion current. After thirty minutes (t^3), the equivalent current density peak is 0.2mV, this increases to 1.1mV after sixty minutes (t^6). After ninety minutes (t^9), there is considerable increase in corrosion current, and the current density peak in the most active microzone corresponds to a potential of 2.1mV.

Another interesting point here is that the area in Figure 6.7(c) which is flat and corresponds to approximately zero corrosion current after seventy minutes, is extremely active after ninety minutes in (d), and also the active area in (c) corresponds to the passive region in (d) after ninety minutes. Alloys 2,3 and 4 all have trace amounts of mercury present in the alloy (see Table 4.1 section 4.3). Comparison of Figure 6.7 (a), (b) (in electrolyte E saturated with mercury) and Figure 6.8 (electrolyte E no mercury added) at open circuit potential, shows the effect of the addition of mercury to the electrolyte. It can be seen that the corrosion current is not evenly distributed in Figure 6.8 though it is in Figure 6.7 (a) and (b).

The diagrams in Figure 6.9 show alloy 3 discharged at

constant current of 7mA in electrolyte E saturated with mercury. The scans were conducted at ten minute intervals. Figure 6.9 (a) and (b) compare the surface at t^0 and t^3 (i.e after zero and thirty minutes discharge). It is interesting to note that in (a)ii the passive regions of the electrode surface (marked ⟶ 1)are the most active after thirty minutes discharge in (b)ii. Also the active region in (a)ii (marked ⟶ 2) is the passive region in (b)ii. Thus the phenomenon observed at open circuit potential is seen during discharge.

On increasing the current the distribution is less uniform. This was found to be the case in almost all samples. Figure 6.10 (a) and (b) shows examples of alloy 3 and 4 discharged in electrolyte E saturated with mercury and electrolyte A saturated with mercury respectively.

The alloys were discharged at similar current density values and it can be seen from Figures 6.10 (b)ii and 6.11 (a) and (b) that alloy 2 has the most even distribution of current density. Equivalent potential diagrams for alloy 2 and alloy 4 show the relative uneven potential distribution on the latter.

6.5 Conclusions and Discussion.

The discharge process of aluminium alloys in alkaline media is not uniform, if this were the case then the technique employed to measure the current distribution on the

electrode surface would yield no results.

It has been known for some time [94, 95] that mercury has the effect of reducing hydrogen evolution in the discharge of aluminium in alkali media, thereby acting as corrosion rate control. It may have also been previously thought that mercury has the effect of uniformly distributing the current at open circuit potential, however, traditional electrochemical methods have not been able to show this as they measure only the total current. Use of a microzone scanning current measurement technique enables the current distribution to be understood. By using two microelectrodes to scan the surface,it can be seen that at open circuit potential, aluminium alloys in alkaline electrolytes without mercuric oxide additive, have a relatively high level of unevenly distributed corrosion current as compared to the behaviour of electrodes placed in mercury saturated electrolytes (see Figure 6.6).

Further studies were carried out at open circuit potential (see Figure 6.7). Scans were conducted at regular intervals of ten minutes and it was observed that at zero current, the corrosion current increased with time. This is in agreement with previous work carried out at The Chemical Energy Research Centre [96] which showed that hydrogen evolution increases with time. Quarshie [93] showed that the use of mercuric oxide as an electrolyte additive results in a thin film of mercury on the electrode surface. As the activation

overpotential of hydrogen on mercury is very high, the cathodic evolution of hydrogen is reduced considerably [97]. However after a certain time the hydroxide ions begin to diffuse through the mercury barrier to the aluminium surface where corrosion begins to occur at a greater rate.

Also noticeable in this experiment was the fact that the passive regions in Figure 6.7(c) become the active regions after a further twenty minutes in (d), and the active regions in (c) become passive in (d). These results show that a feature of the current distribution on aluminium alloys in alkaline electrolytes is continuous alternation between active and passive behaviour of the electrode surface.

A possible explanation for this change in distribution with time is that an active microzone is an area where the oxide layer has been eaten away and the current concentrates in that particular zone. However, at this active zone the concentration of local hydroxide ions decreases with time, as the concentration of local aluminium ions becomes higher. The build up of aluminium ions causes the site to become less active whereas in another microzone the hydroxide has eaten the oxide layer away and the site has become active. When this site becomes less active, the aluminium ions at the former site have dissolved into the bulk and the site becomes active again.

The comparison of Figures 6.7 (a), (b) and 6.8 shows the importance of the mercuric oxide as an electrolyte additive rather than an alloying material. Alloy 2 was placed in electrolyte E. In figure 6.8 however, there is no mercuric oxide in the electrolyte. It can be seen from these diagrams that the distribution of corrosion current is relatively uneven in Figure 6.8 as compared with Figure 6.7, which used the same electrolyte, though saturated with mercury.

Alloy 2 has mercury present as a trace additive. The result shows that the presence of mercury is more important in the electrolyte than the alloy, even though the solubility of mercury in the alkaline solution is small.

On discharge of alloy 3 at 7mA over a period of thirty minutes in electrolyte E saturated with mercury, distribution diagrams Figure 6.9 were obtained. These diagrams illustrate the fact that the current distribution changes with time when current is flowing. Again the alternating in competition of active and passive regions can be seen, with the extremely active region in Figure 6.9(a)ii being passive in (b)ii and vice versa. This is important as the total result from this behaviour is that a more uniform discharge of aluminium occurs, thus enhancing the efficiency of utilisation of the alloy.

Another noticeable conclusion that can be drawn from the

results is that the higher the discharge current, the more uneven is the current distribution. Figure 6.10 shows this point.

The final conclusion that can be drawn from the in situ electrode discharge measurements, is that alloy 2 shows the most even current distibution. A comparison of Figure 6.11 and 6.10(b)ii exhibits this. Thus the efficiency of utilisation of the aluminium is increased.

In general, the microzone current distribution measurement technique has revealed interesting information of the role of mercuric oxide as an electrolyte additive. These results agree with the conclusion that Quarshie [93] obtained that the use of mercuric oxide as an electrolyte additive significantly reduces corrosion. However, the results have also shown that use of this additive also uniformly distributes the current.

That the current density distribution is not uniform may have been previously assumed. This experimental technique proves this conclusively at both open circuit potential and during discharge. The experiments also show that the current distribution becomes more uneven with increasing current values. Finally, the results also suggest the superiority of alloy 2 over other alloys, as regards a more even distribution of current.

CHAPTER 7.

USE OF ELLIPSOMETRY TO STUDY THE SENSITIVITY OF SURFACE STRUCTURE TO ALLOY COMPOSITION.

Aluminium air cells require a short period before full power output is achieved. This is due to the presence of the protective oxide film on aluminium, which is broken down by the electrolyte on contact. Preliminary ellipsometry experiments were performed to investigate the oxide film, and to determine if the various alloying elements affected the thickness of this layer, thereby increasing or decreasing the period prior to full power output.

7.1 Introduction to Ellipsometry [98, 99, 100].

Ellipsometry is a technique which measures the change in state of elliptically polarised light upon reflection at a surface, in order to obtain information about that surface. This method is sensitive to films as thin as a monolayer when they are oxides.

Optical reflection may be best understood in terms of the wavelike properties of light. In order to define a monochromatic light beam it is necessary to know the frequency, amplitude, direction of propogation, electric vectors and magnetic field vector (though it is not so necessary to consider the last named).

The electric vector associated with the wave oscillates in a plane as the wave propogates and the intensity of the light is proportional to the electric field amplitude. Reflection of light from a surface is more efficient for rays having

certain particular orientations with respect to the physical surfaces involved, and therefore the reflected beams are partially polarised because a particular direction of oscillation predominates. A careful processing of the beam can result in a plane polarised beam in which the rays have the same angle for the plane of electric field oscillation.

If the polarisation is parallel to the plane of incidence then the beam is said to be 'p' polarised, likewise if the beam is perpendicular to the plane of incidence the beam is said to be 's' polarised. If a linearly polarised beam is reflected from a surface it is found that the parallel and perpendicular components undergo different changes in amplitude and phase. This means that individual pairs of rays are in phase upon incidence but out of phase upon reflection see Figure 7.1. This means that the resultant electric field traces out as a spiral as the wave propogates. The projection of the spiral is an ellipse, the light is elliptically polarised, and the parallel and perpendicular components are reflected with different efficiencies and phase shifts. The difference in phase angle between the fast and slow components is given by Δ , and the ratio of the electric field amplitude is given by ;

$$(7.1) \qquad \frac{Ep}{Es} = \tan \psi$$

Measurement of Δ and ψ is achieved by using an

Figure 7.1 Phase Difference Upon Reflection of Plane of Incidence Causing the Electric Field Vector to Trace Out as a Spiral.

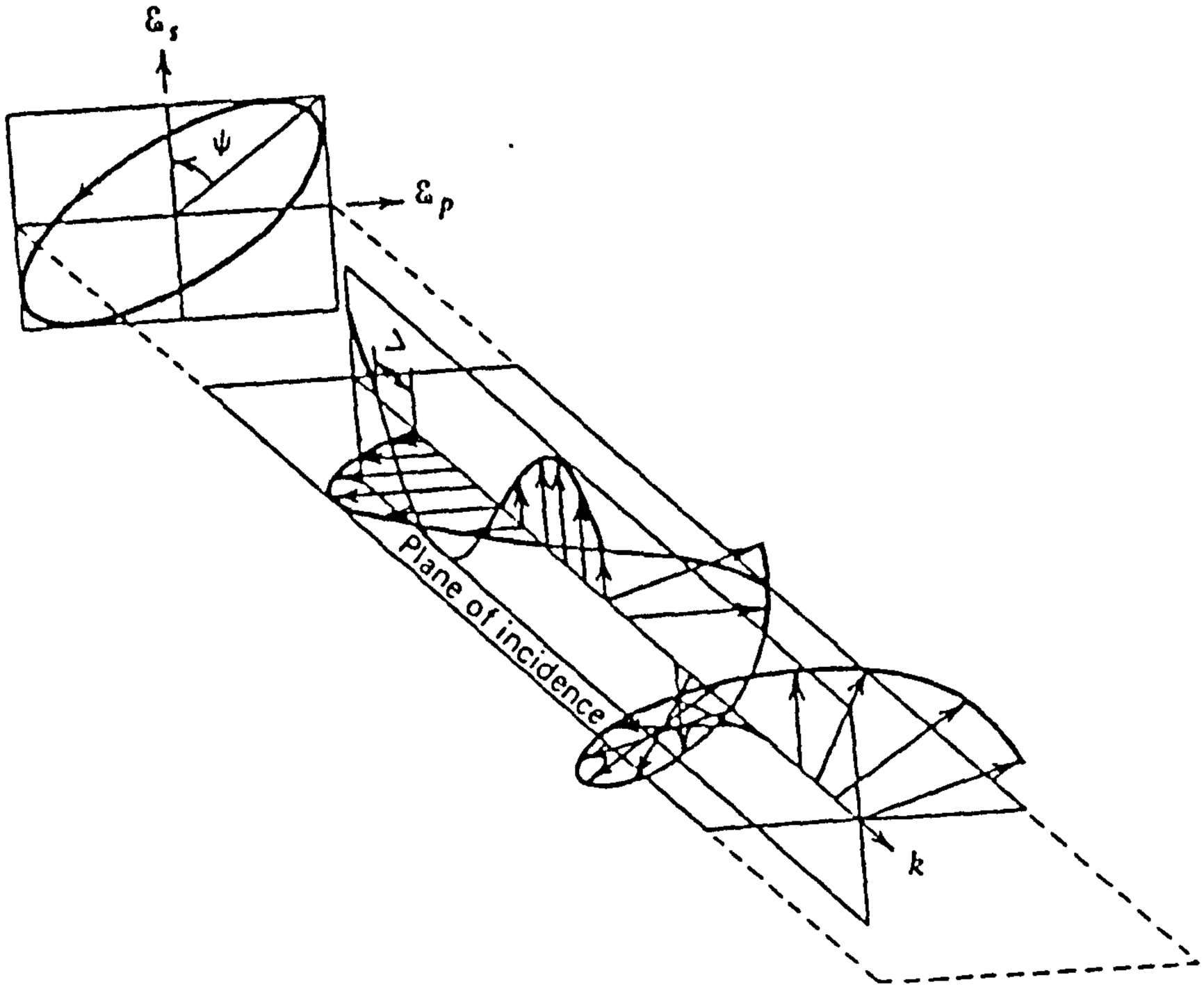

ellipsometer. The ellipsometer relies on a null balance to calculate values for Δ and ψ .

7.2 Components of an Ellipsometer.

Readings of an ellipsometer are those of a cylindrical polariser compensator and analyser, each being mounted and the scale being marked in degrees. The procedure involves obtaining a reflection from the surface at the required angle of incidence keeping the compensator fixed at 45^{o} to the plane of incidence and the polariser and analyser rotated to produce extinction. The two readings of polariser and analyser represent Δ and ψ respectively. A typical ellipsometer can be seen in Figure 7.2.

7.3 Reflection at a Film Covered Surface.

The thickness of the oxide layer present on the substrate (d), and the refractive index for that oxide layer (n_1), are in this case, unknown values. In these circumstances a series of n_1 values are chosen and corresponding values are evaluated from the experimental ellipsometric data. These calculations result in error terms of different magnitudes, and the range of n_1 and d within the corresponding errors $\delta\,\Delta$ and $\delta\,\psi$ are then determined.

If it is assumed that the sample film and base will absorb light to a certain extent, the complex refractive index can be represented as follows ;

Figure 7.2 Components of an Ellipsometer.

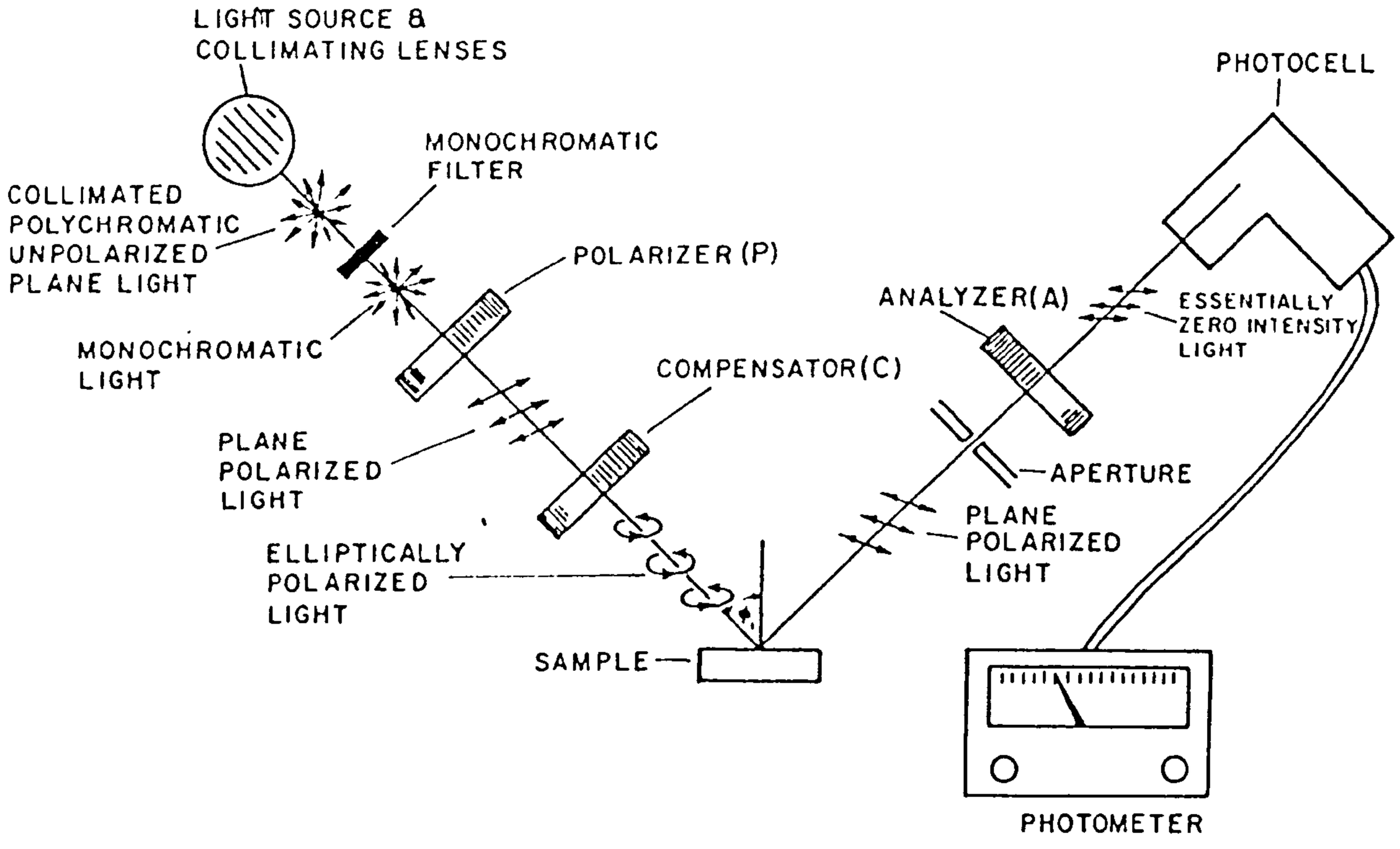

(7.2) $N_1 = n_1 - jk_1$

(7.3) $N_2 = n_2 - jk_2$

where N = complex refractive index

n = refractive index.

The angles of incidence and refraction and refractive indices for oxide layer, substrate and immersion medium are given in Figure 7.3. According to Snell's law , the values of the constants in Figure 7.3 are related by ;

(7.4) $n_o \sin\phi_o = N_1 \sin\phi_1 = N_2 \sin\phi_2$

where ϕ_1 and ϕ_2 are angles of refraction.

The Fresnel reflection coefficients for the parallel and perpendicular vibrations for reflected and transmitted vectors may be expressed as follows ;

(7.5) $$r_{0,1}(p) = \frac{N_1 \cos\phi_o - n_o \cos\phi_1}{N_1 \cos\phi_o + n_o \cos\phi_1}$$

(7.6) $$r_{0,1}(s) = \frac{n_o \cos\phi_o - N_1 \cos\phi_1}{n_o \cos\phi_o + N_1 \cos\phi_1}$$

(7.7) $$r_{1,2}(p) = \frac{N_2 \cos\phi_1 - N_1 \cos\phi_2}{N_2 \cos\phi_1 + N_1 \cos\phi_2}$$

Figure 7.3 Angles of Incidence and Refraction and Refractive Indices for Oxide Layer, Substrate and Immersion Medium.

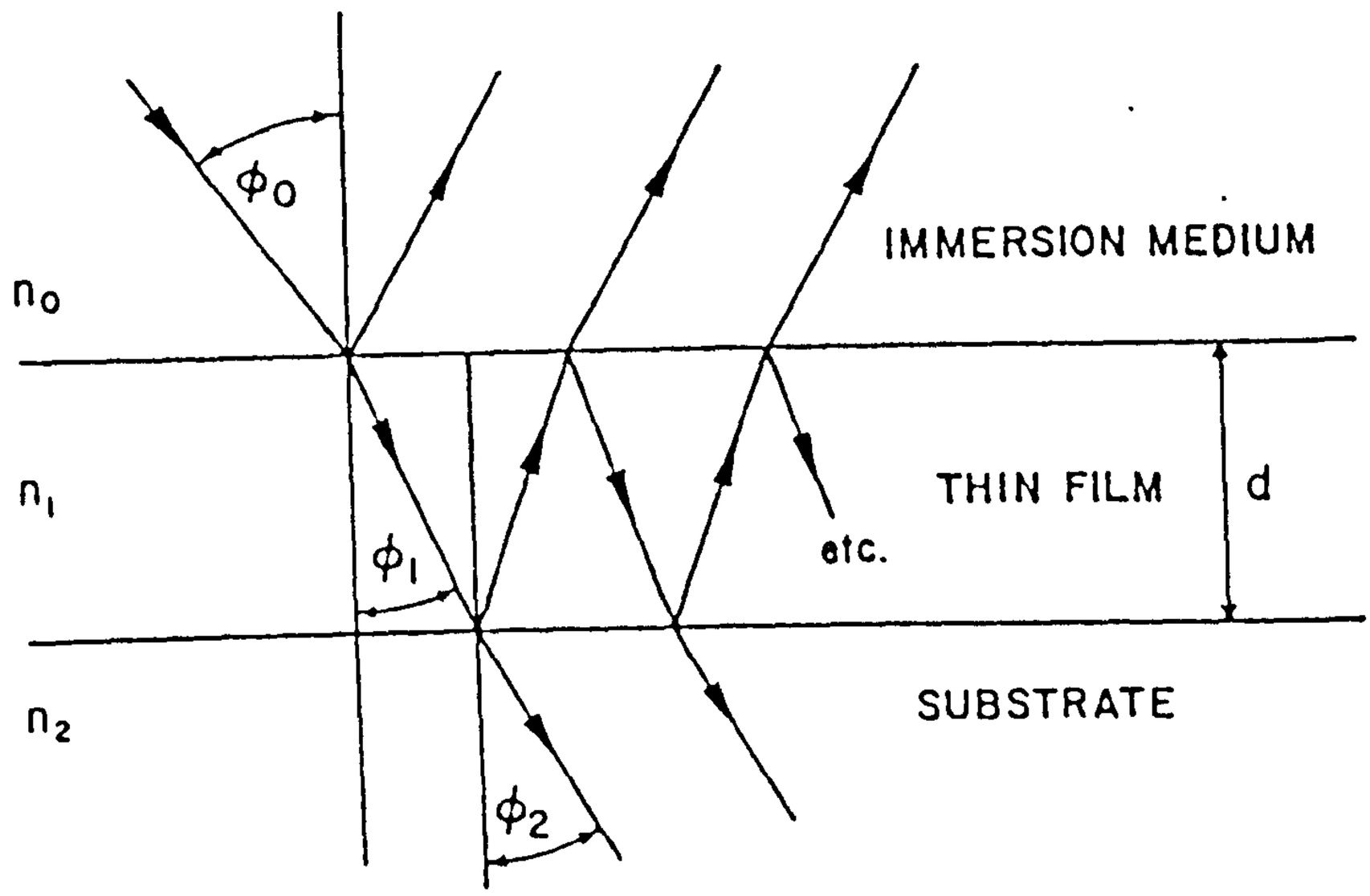

$$(7.8) \qquad r_{1,2}(s) = \frac{N_1 \cos\phi_1 - N_2 \cos\phi_2}{N_1 \cos\phi_1 + N_2 \cos\phi_2}$$

The total reflection coefficients Rp and Rs are given by;

$$(7.9) \qquad Rp = \frac{r_{0,1}(p) + r_{1,2}(p)\, e^{-j\phi}}{1 + r_{0,1}(p)\, r_{1,2}(p)\, e^{-j\phi}}$$

$$(7.10) \qquad Rp = \frac{r_{0,1}(s) + r_{1,2}(s)\, e^{-j\phi}}{1 + r_{0,1}(s)\, r_{1,2}(s)\, e^{-j\phi}}$$

$$(7.11) \quad \text{where} \quad \phi = \frac{4\pi d}{\lambda_o} N_1(\cos\phi_1)$$

This leads to the basic formula for ellipsometric characterisation of a surface film and metal ;

$$(7.12) \qquad \frac{Rp}{Rs} = \tan\psi\ e^{j\Delta} = x + jy$$

or

$$(7.13) \qquad \Delta = \arctan(y/x)$$

$$(7.14) \qquad \psi = \arctan\left(\sqrt{x^2 + y^2}\right)$$

Therefore the ratio of the parallel and perpendicular reflection coefficients of the electric vector are related to the variables Δ and ψ . The parameters involved in the above equations are as follows ;

n_o = refractive index of solution

N_1 = complex refractive index of film

N_2 = complex refractive index of substrate

k_1, k_2 = absorbtion constants

ϕ_o = angle of incidence

ϕ_1, ϕ_2 = refractive angles

λ = wavelength

d = thickness of film

Δ, ψ = values read from ellipsometer.

The unknown parameters are N_1, N_2, k_1, k_2, and d. The index of refraction of solution n_o is independently detected by other means. N_2 and k_2 can be calculated directly from the value of Δ and ψ when measuring at zero film thickness, (i.e. when applied voltage = zero). At this point it is assumed that k_1, N_1 and d = zero. In the actual experiment it is difficult to obtain a surface with no oxide film as aluminium is too reactive a metal.

For films of finite thickness, n_2 and k_2 can be calculated as shown in the following equations. As we assume that at 0V the thickness of the oxide film is zero, the values of Δ and ψ recorded at that potential are regarded as the functions for a film free surface.

$$(7.15)\quad n_2^2 - k_2^2 = \sin\phi_o\left[1+ \frac{\tan^2\phi_o(\cos^2 2\bar{\psi} - \sin^2 2\bar{\psi}\sin^2\bar{\Delta})}{(1+\sin 2\bar{\psi}\cos\bar{\Delta})^2}\right]$$

and

$$(7.16)\quad 2n_2k_2 = \frac{\sin^2\phi_o \tan^2\phi_o \sin 4\bar{\psi}\sin\bar{\Delta}}{(1+\sin 2\bar{\psi}\cos\bar{\Delta})^2}$$

where $\bar{\psi}$ and $\bar{\Delta}$ are the functions for a film free surface.

If the angle of incidence (ϕ_o), film thickness, refractive indices of film and substrate are known, the expected values of Δ and ψ can be calculated. This is achieved by calculating in the following order, the angle of refraction in the film and substrate (ϕ_1 and ϕ_2 respectively), the Fresnel coefficients Rp and Rs and the thickness d of the film by computer. These calculated values can then be substituted in the expressions for the reflection coefficients, the ratio of which leads to values of Δ and ψ.

Once the refractive index of the substrate is calculated from equations 7.15 and 7.16, plots can be made of Δ vs. ψ for various values of film refractive index over a series of thickness values.

If the film refractive index is a complex number, then there are three unknowns (thickness d and the real and imaginary parts of the refractive index). In this situation the real part of the refractive index is assumed and the thickness and absorbtion coefficients of the film are calculated from the assumed value by computer. These are calculated over a wide range of values for the real part of the refractive index and then the experimental Δ vs. ψ plot is compared with the computed plot obtained from the assumed values. The curve with the best fit is assumed to be at the correct value of

n_1.

In the case of relatively thin films where $d << \lambda$, the exponential term in equation 7.12 can be expanded in a Taylor series in d/λ so that limitingly ;

$$(7.17) \qquad \Delta f = \bar{\Delta} - \alpha d$$

$$(7.18) \qquad \psi f = \bar{\psi} + \beta d$$

where subscript f refers to the film of finite thickness. In equations 7.17 and 7.18 and B are defined by ;

$$(7.19) \quad \alpha = \frac{4\pi}{\lambda_o} \frac{(1/(n_1^2) - 1)(\cos^2\phi_o - a)(\cos\phi_o \sin^2\phi_o)}{(\cos^2\phi_o - a)^2 + a_1^2}$$

and

$$(7.20) \quad \beta = \frac{2\pi}{\lambda_o} a_1 \frac{(1/(n_1^2) - 1)(1 - n_1^2\cos^2\phi_o)(\cos\phi_o \sin^2\psi \sin^2\phi_o)}{(\cos^2\phi_o - a)^2 + a_1^2}.$$

where

$$(7.21) \quad a = \frac{n_2^2 - k_2^2}{(n_2^2 + k_2^2)^2}$$

and

$$(7.22) \quad a_1 = \frac{2n_2k_2}{(n_2^2 + k_2^2)^2}$$

where n_2 and k_2 refer to the refractive properties of the substrate, and n_1 to those of the thin film.

7.4 Experimental Procedure.

The investigation of the surface structure of the four aluminuium alloys was carried out using a TC-2 Ellipsometer (Xian Radio Factory). Each alloy had an exposed surface area of approximately 25mm x 30mm, which had been polished to a fine finish using metal polishing liquid (Bondaglass Voss Ltd.) The alloy was held firmly in place during the course of the experiment by a perspex plate, see Figure 7.4.

The cell arrangement was then fitted onto the electrolyte container so that the exposed aluminium and the platinum counter electrodes were below the level of the solution. The electrodes were connected to a potentiostat.

The cell system was placed on an adjustable platform which formed a part of the ellipsometer instrument. The aluminium alloys were anodised in 3% tartaric acid, following a paper given by Dell'Oca [101]. Initial readings of Δ and ψ were taken at 0V and then at various increasing potential values. Five minutes was allowed before each reading so as to allow the potential to become stable.

Figure 7.4 The Electrode Arrangement.

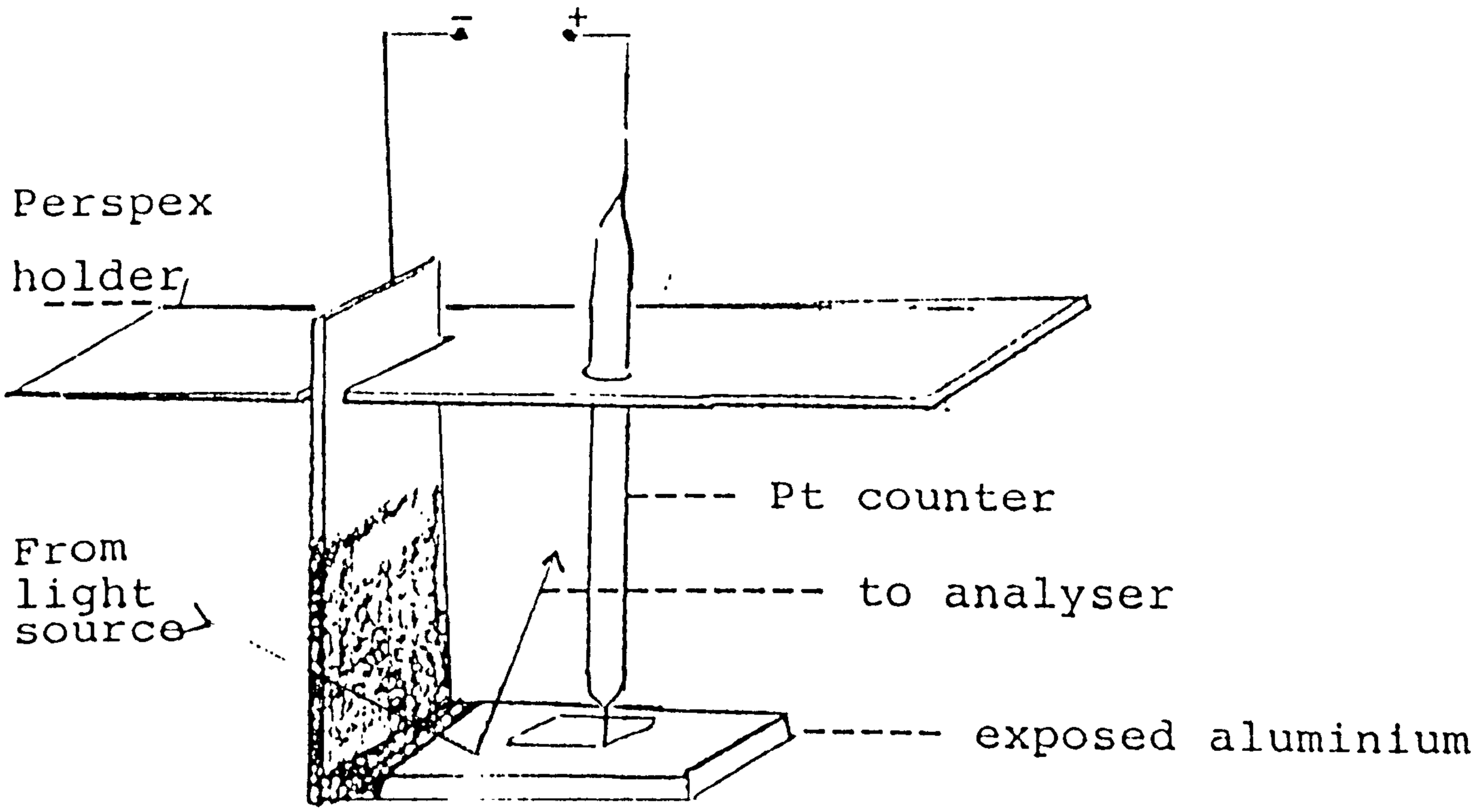

7.5 Results.

Figure 7.5 represents alloy 2 and shows the conventional Δ vs. ψ plot of ellipsometry. The experimental points begin at point A which theoretically represents the film free surface. As the alloy is anodised and further measurements taken, the experimental points on the graph trace out an elliptically shaped curve in an anticlockwise direction. The curve drawn in Figure 7.5 represents the " best fit" to the experimental data and represents a refractive index of 2.05 for the oxide layer.

The d values inserted at each point on the curve were calculated by using the McCrackin computer program [102]. This program enabled the best fit curve to be drawn from the experimental results and allowed a value of n_1 and thickness d at the various points on the curve to be calculated. Table 7.1 gives the computer printout of the experimental points and the points from estimating values of N_1, N_2 and k_2 for the best fit curve.

Figures 7.6 and 7.7 show negative straight line plots. These figures represent alloys 3 and 4 respectively. The results indicate that alloys 3 and 4 show thin film formation on anodisation in the tartaric acid electrolyte. n_1 was calculated mathematically from the theoretical equations. Figure 7.8 represents the behaviour of alloy 1. No curve was obtained for this alloy from ellipsometric analysis. The

Figure 7.5 Ellipsometry Results for Anodisation of

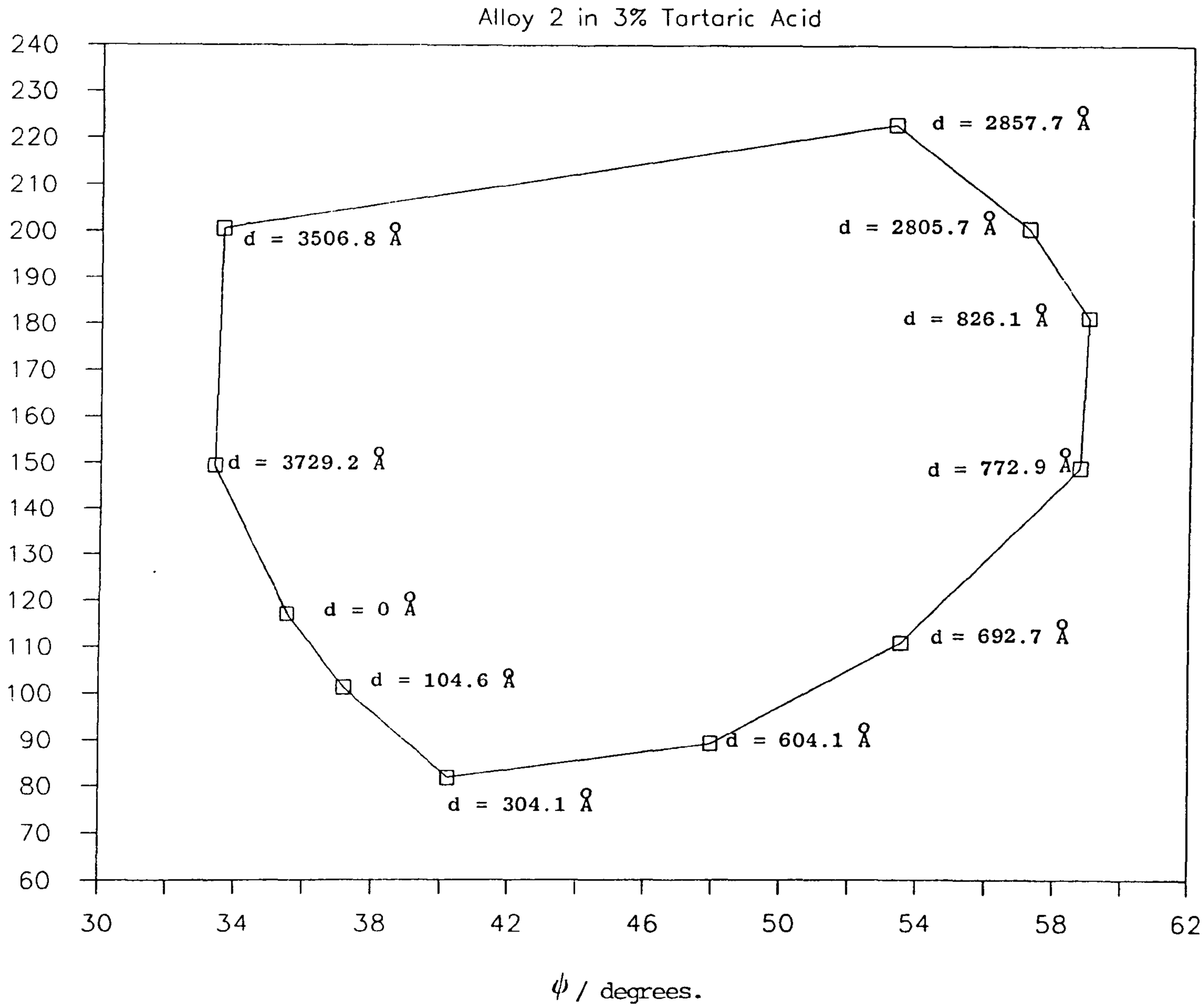

Table 7.1 Computerised and Experimental Values for Δ and Ψ.
Also given - best fit n_1, k_2.

```
THIS IS NO:  2
N=1.337          N1=2.05516433   K1=0
N2=2.02841646    K2=-4.97105012  THE SUM. OF SQUARE DEVIATION U=  344.806177
POINT  0         DELTA= 0        PASI=  0
POINT  1         DELTA= 100      PASI=  33.25
POINT  2         DELTA= 82       PASI=  40
POINT  3         DELTA= 92       PASI=  48
POINT  4         DELTA= 110      PASI=  56
POINT  5         DELTA= 150      PASI=  62
POINT  6         DELTA= 180      PASI=  60
POINT  7         DELTA= 200      PASI=  55
POINT  8         DELTA= 220      PASI=  44
POINT  9         DELTA= 200      PASI=  35
POINT  10        DELTA= 150      PASI=  32
POINT0           D=0             DELTA=117.124544
PSI=35.5037864
POINT1           D=104.651937    DELTA=101.149537
PSI=37.154809
POINT2           D=304.075849    DELTA=81.6998819
PSI=40.1992366
POINT3           D=504.075849    DELTA=89.0925303
PSI=47.953043
POINT4           D=692.722502    DELTA=110.967874
PSI=53.5070583
POINT5           D=772.951971    DELTA=148.892036
PSI=56.7189092
POINT6           D=926.067853    DELTA=181.414733
PSI=59.9237889
POINT7           D=2805.73706    DELTA=200.676301
PSI=57.1813874
POINT8           D=2857.71866    DELTA=223.049139
PSI=53.2782614
POINT9           D=3506.75687    DELTA=200.544772
PSI=33.5755581
POINT10          D=3729.17045    DELTA=149.358421
PSI=33.3680459
```

Figure 7.6 Ellipsometry Results for Anodisation of Alloy 3 in 3% Tartaric Acid

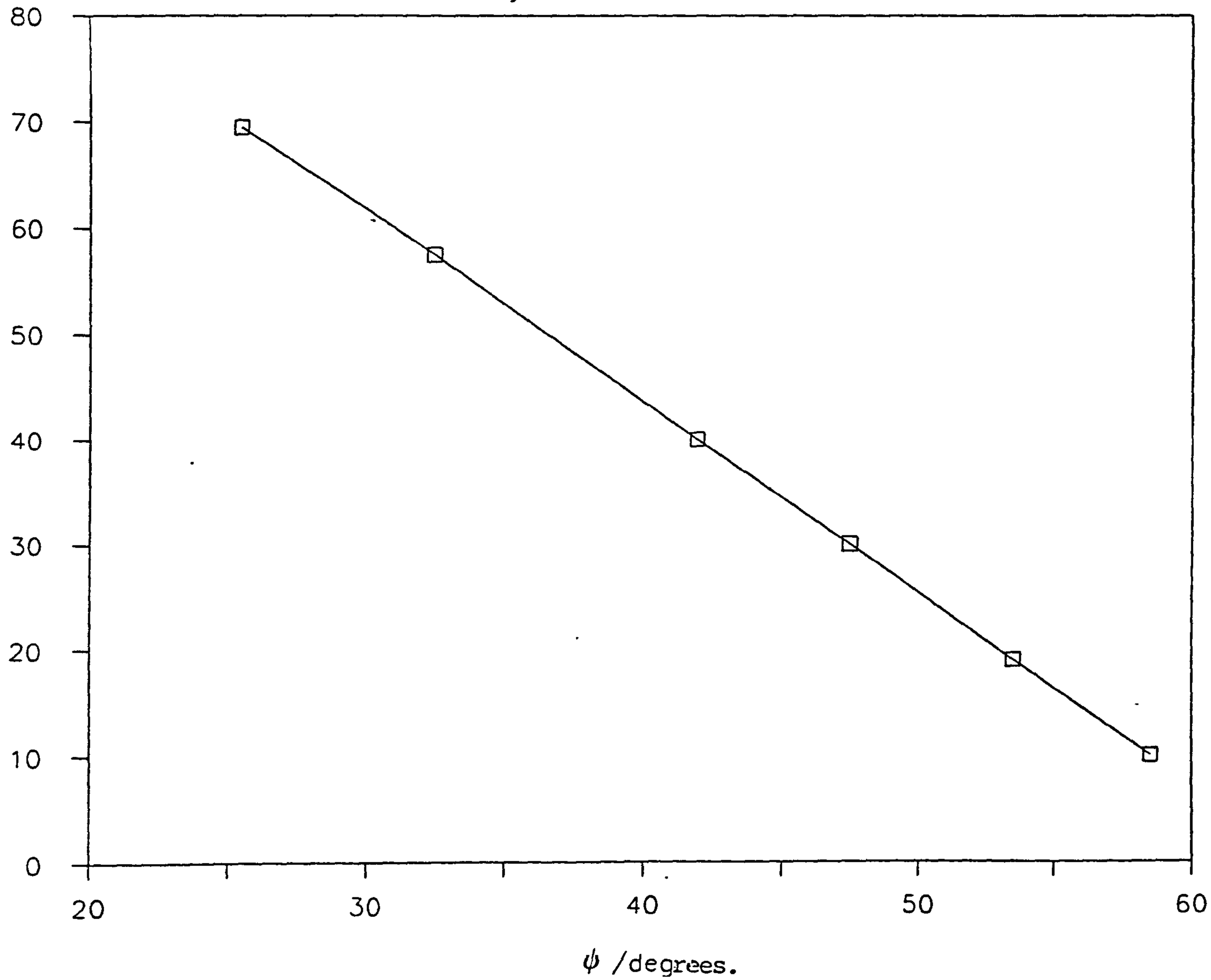

Figure 7.7 Ellipsometry Results for Anodisation of

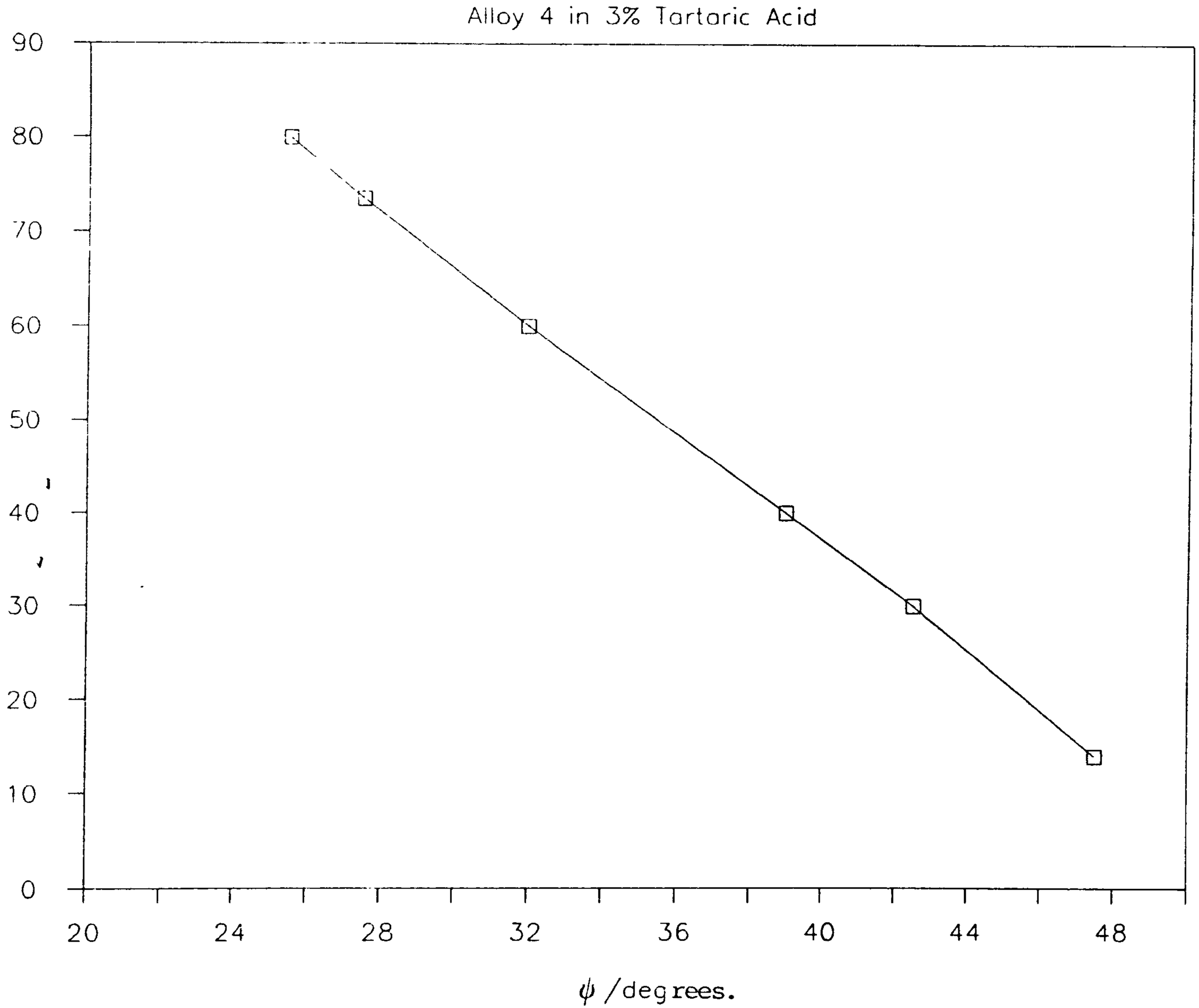

Figure 7.8 Ellipsometry Results for Anodisation of Alloy 1 in 3% Tartaric Acid

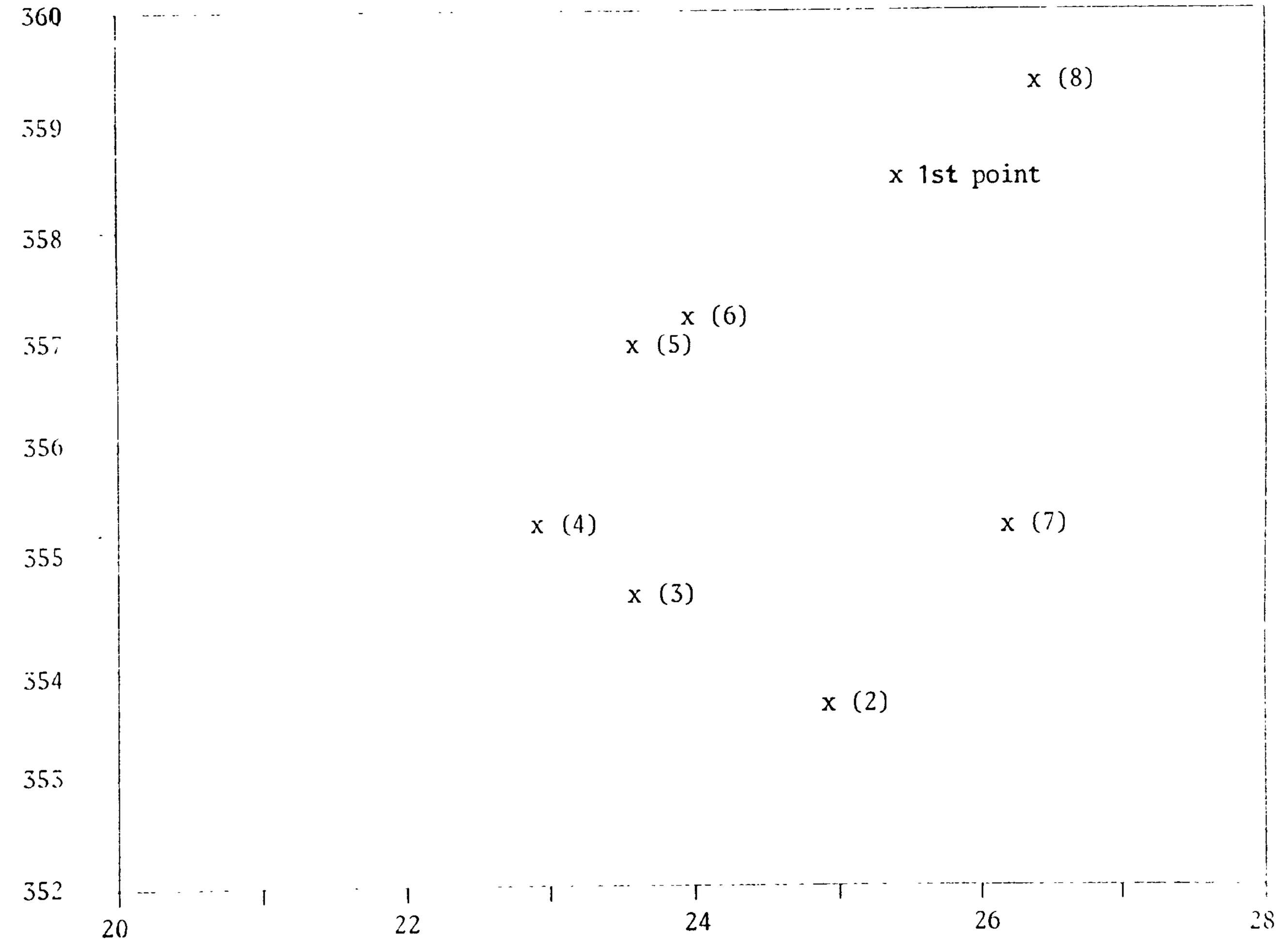

* It was pointed out by the examiners that these results must be regarded with some suspicion, as a refractive index of 1.08 is unlikely as it is approaching the refractive index of air. Values quoted by Dell'Oca et al [101] are in the region of 1.3-6.5. The value obtained for alloy 3 is clearly outside this range and therefore there is some doubt as to the validity of these results.

results indicate a constantly changing n_1 value.

Table 7.2 Refractive Index of Oxide Layer for Various Alloys.

Alloy	Refractive Index of Oxide Layer
1	Not Constant
2	2.05
3	1.08 *
4	1.87

7.6 Conclusions.

The four alloys were examined in a tartaric acid electrolyte. Ideally this work should be continued using a low concentration alkaline electrolyte. It is difficult to reproduce the exact conditions of a functioning aluminium air cell, as the concentration of the electrolyte used, (ca. 40 wt%) would result in gas bubbles which would affect the experiment. However, low concentration alkaline solution could be used and the behaviour of the alloys further investigated.

Results from the experiments performed show that the four alloys behave differently under ellipsometric analysis in 3% tartaric acid. Alloy 2 exhibits thick oxide layer formation. This suggests first the formation of a barrier film [103] followed by porous oxide growth. Alloys 3 and 4 do not

behave as alloy 2, there being a thick oxide layer formed. There appears to be no thick porous oxide growth. Alloy 1 was difficult to analyse due to no observable curve being obtainable on plotting Δ vs. ψ data. This suggested that the refractive index for the forming oxide layer was not constant.

These results suggest that the structure of the aluminium surface is extremely sensitive to to the composition of the alloy. Even though the the w/w % of trace metals added to the aluminium in each case is very small, the effect on the surface structure is considerable.

CHAPTER 8.

FULL CELL TESTS.

8.1 Introduction.

Full cell tests were performed on alloys 1-4 using electrolytes A, B, and E. The purpose of these tests was to analyse which alloy in which electrolyte gave the best performance under the stated conditions. Quarshie claimed[93] that with an alloy Q4, a cell with limited electrolyte could operate up to 50% longer with a mixed electrolyte than with potassium hydroxide. As one of the main aims of this work was to extend the examination of the mixed electrolyte to a further range of commercially available alloys, it was decided to use capacity values, period of cell operation and power output data as the characteristics on which to compare the performances of each alloy in the various electrolytes.

The full cell system employs an aluminium alloy anode, an air (oxygen) cathode and an alkaline electrolyte. Previous work at City University [104, 105, 106, 107, 108, 109] has enabled long life, low cost and high performance teflon bonded air electrodes to be prepared. These air electrodes were prepared as described in section 3.2.4. The aluminium anodes were prepared as described in section 3.2.1.

8.2 Capacity Analysis of Full Cells.

8.2.1 Experimental Procedure.

The full cell apparatus was as shown in Figure 8.1 a) and b), and the cell was discharged to passivation using the circuit as shown in Figure 8.2. The total area of air electrode was 9.68cm^2 and the geometrical area of aluminium electrode electrode employed was 2.5cm^2. The electrolyte volume was limited to 2.5cm^3. The potentiostat was converted to the galvanostatic mode and the cells discharged at 100mA/cm^2. A chart recorder was used to measure the potential across each full cell and the data plotted on voltage vs. time graphs. Each alloy was discharged in each electrolyte several times and an average of the data calculated and plotted.

8.2.2 Results.

The results of the experiment are shown in Figures 8.3, 8.4 and 8.5. Under the limiting electrolyte conditions, the capacities were calculated for each alloy and a table of the results obtained is given.

Figure 8.1 Full Cell System.

a) The Air Electrode.

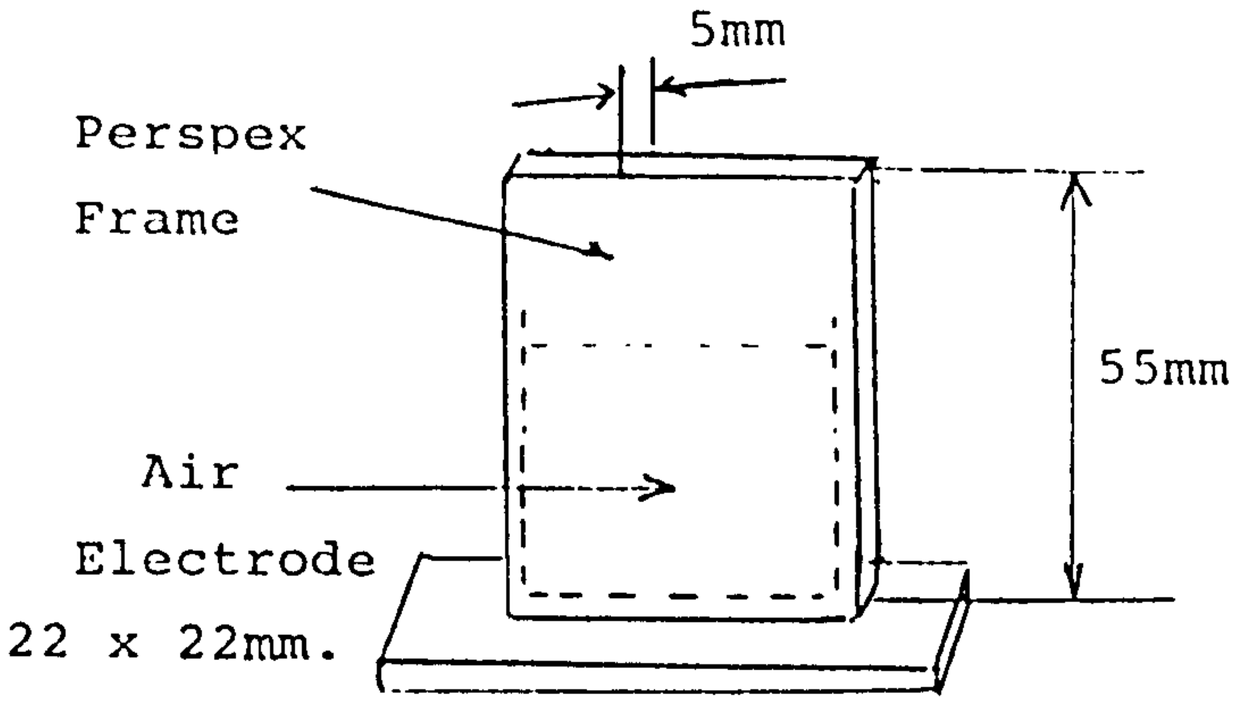

b) The Aluminium Alloy Electrode.

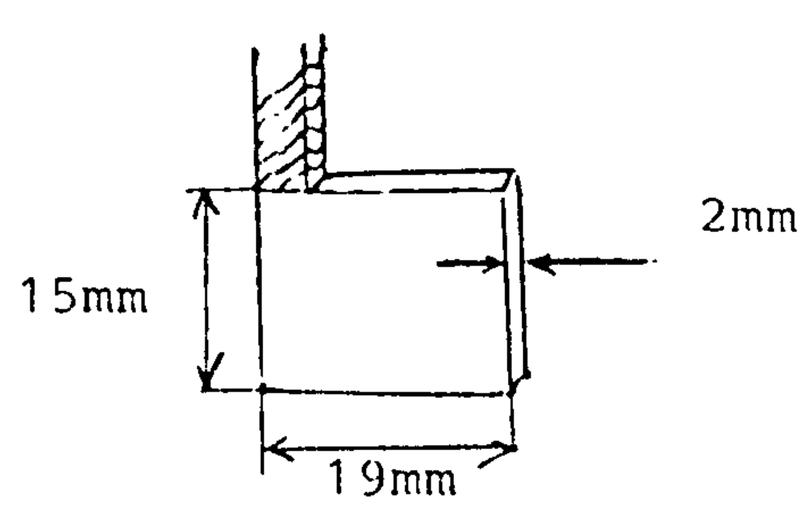

Figure 8.2 Circuit for Cell Discharge.

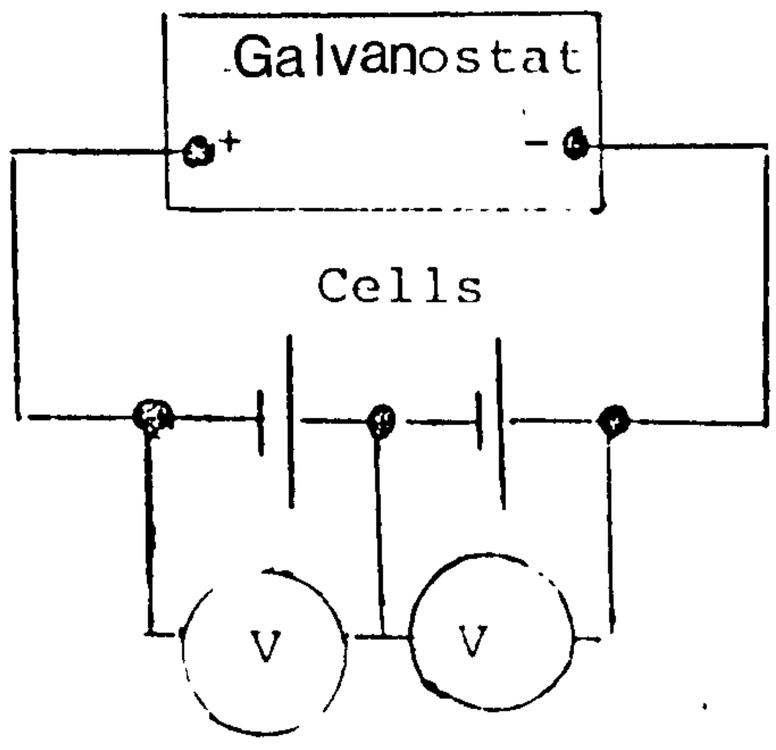

Figure 8.3

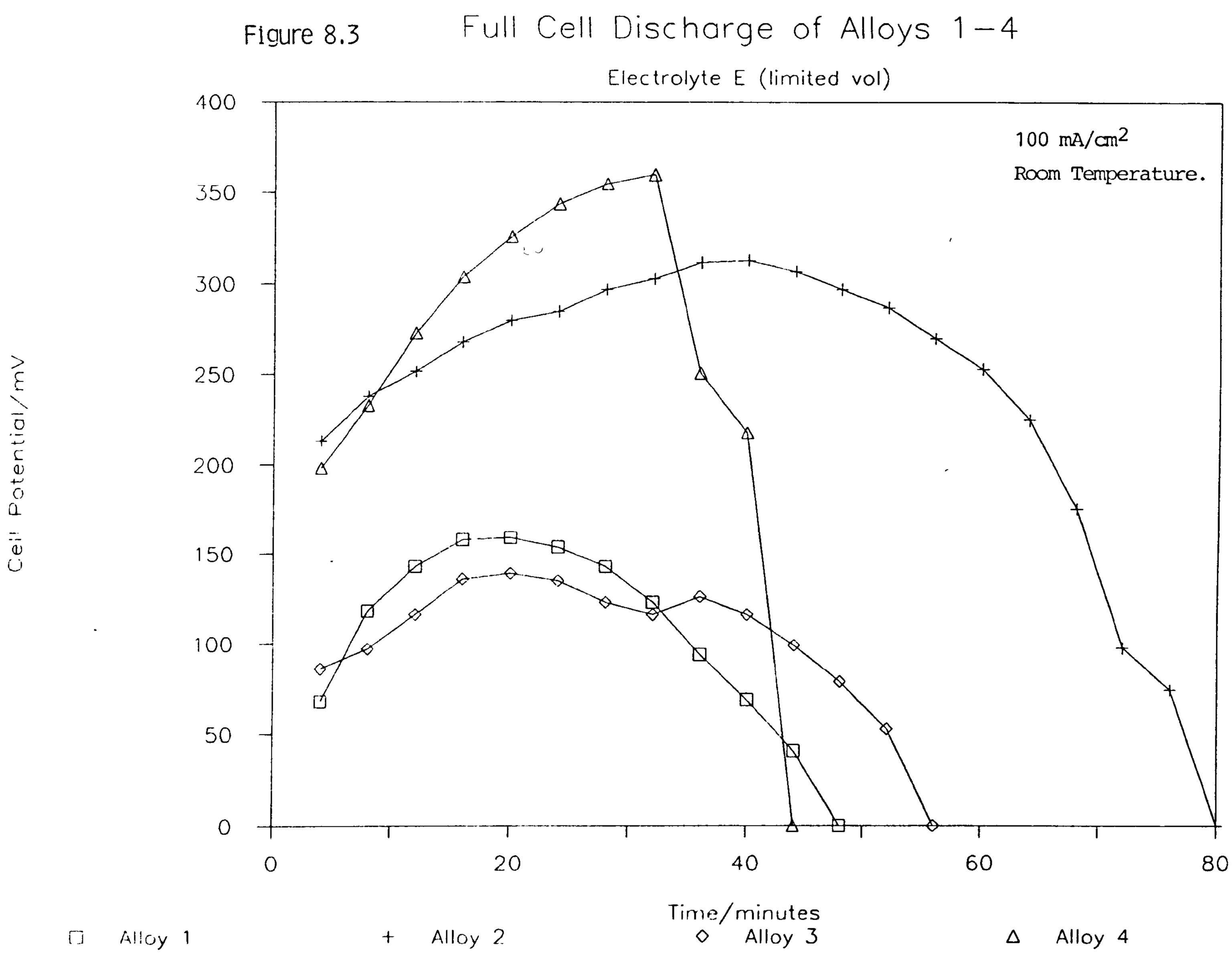
Full Cell Discharge of Alloys 1–4
Electrolyte E (limited vol)
100 mA/cm2
Room Temperature.
Cell Potential/mV
400
350
300
250
200
150
100
50
0
0
20
40
60
80
Time/minutes
Alloy 1
Alloy 2
Alloy 3
Alloy 4

Figure 8.4 Full Cell Discharge of Alloys 1–4

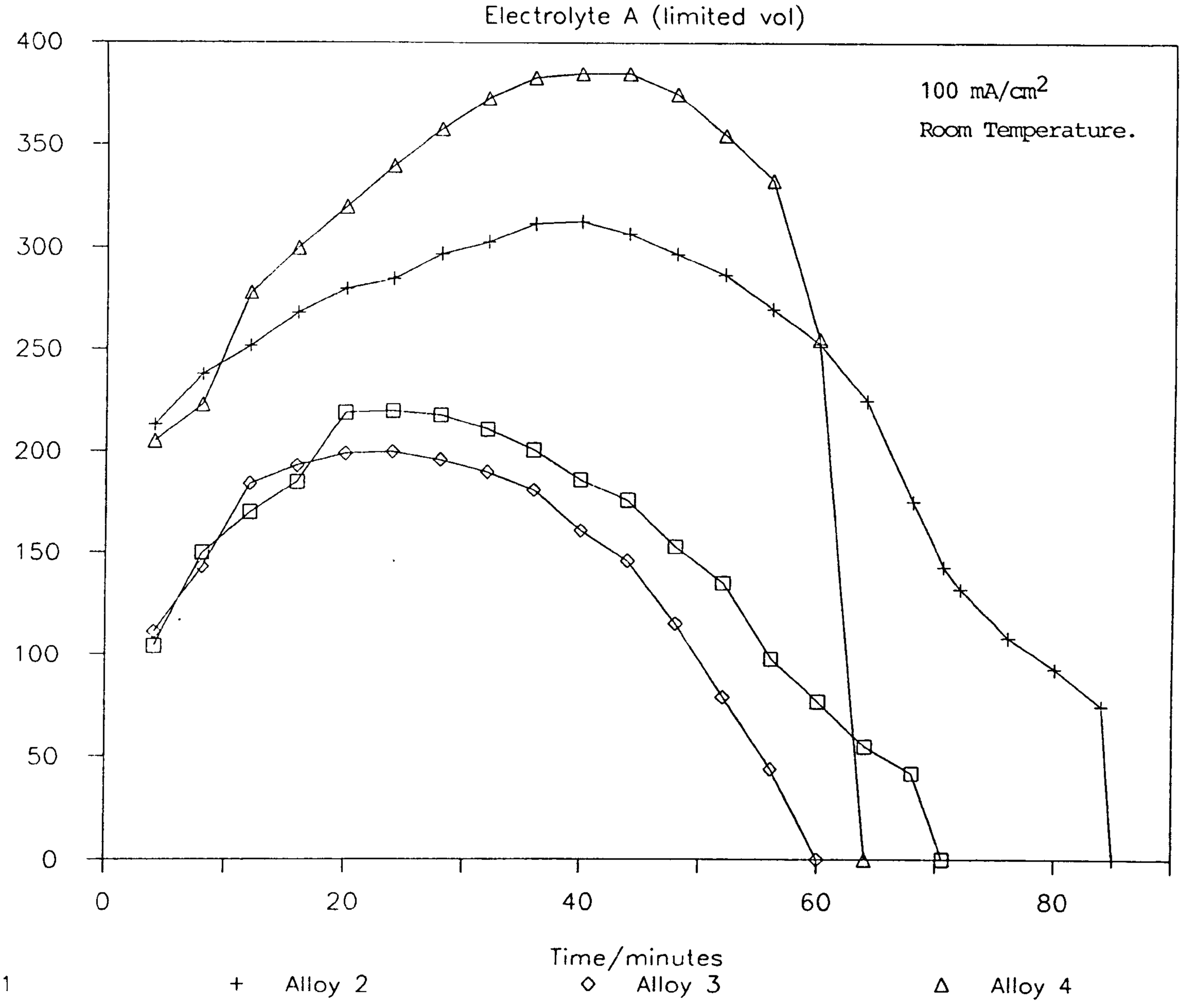

Figure 8.5 Full Cell Discharge of Alloys 1–4

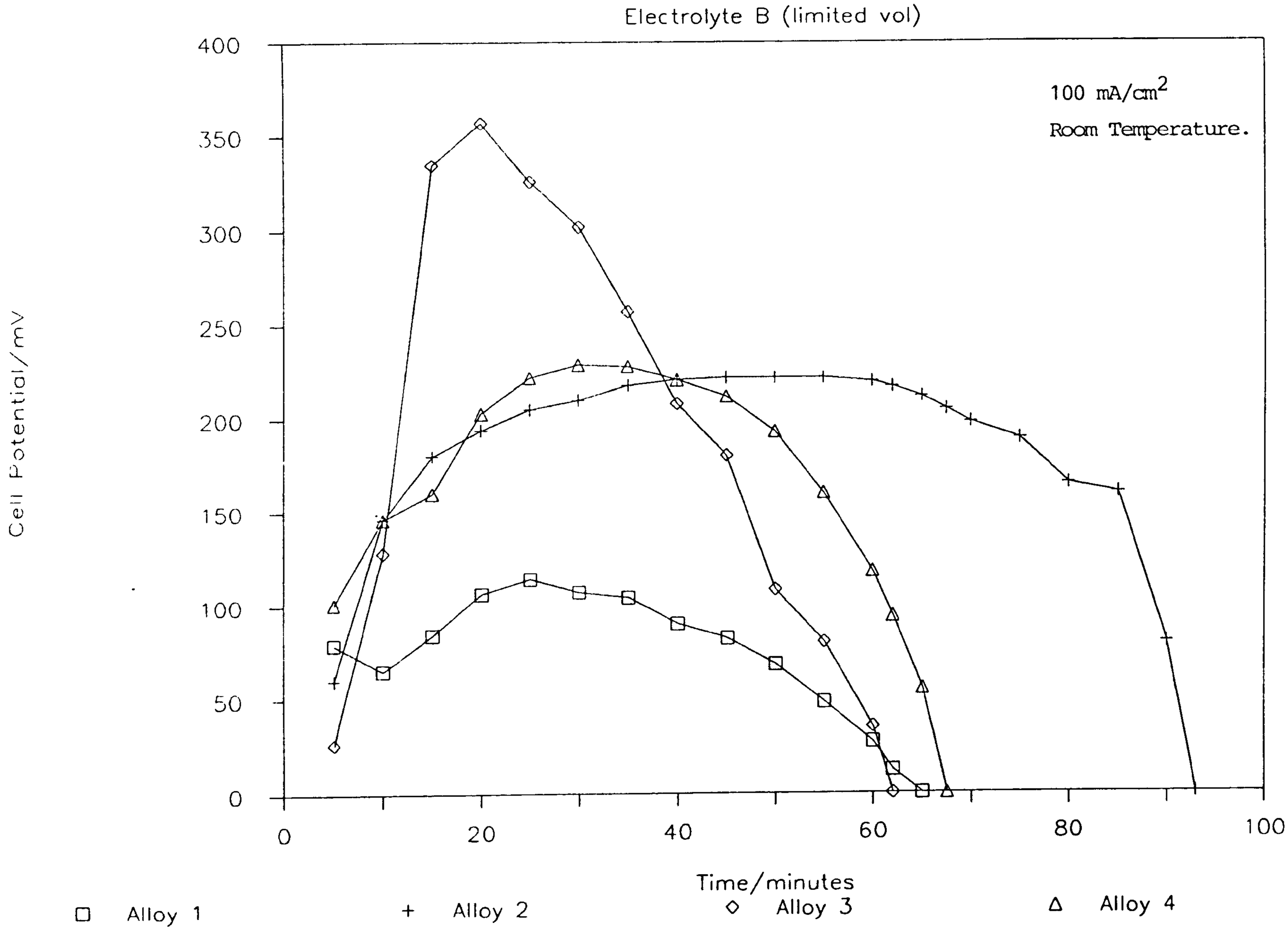

Table 8.1 Capacity in Ah of Alloys 1-4 in Electrolytes A,B and E.

Alloy	Electrolyte A	B	E
1	0.70	0.68	0.48
2	0.80	0.93	0.72
3	0.62	0.62	0.55
4	0.63	0.67	0.44

8.3 Power Output Analysis of Full Cells.

8.3.1 Experimental Procedure.

In order to calculate power output from the full cell, the cell was discharged over a constant load and the potential recorded versus time on a chart recorder. The cell was of dimensions as shown in Figure 8.6 and the load was 5 ohms. The circuit for the experiment is given in Figure 8.7. Each alloy was discharged in electrolytes A, B and E. On initial runs of the experiment it was soon realised that some of the electrolyte was being lost to evaporation. Calculations revealed that amounts being lost were not consistent.

Therefore it was decided to attempt to solve the problem practically, and so a glass side arm was inserted into the cell as shown in Figure 8.6. As the aluminium anode was immersed in the electrolyte the level of the solution in the side arm was marked. The electrolyte was maintained at the same level by `topping up' the electrolyte with water via a syringe. By this method, evaporation of water from the electrolyte was accounted for.

8.3.2 Results.

Typical results are given in the voltage vs. time and power vs. time plots in Figures 8.8-8.15. Table 8.2 gives typical values for the periods of cell life for alloys 1-4 in each electrolyte. The percentage increase in operating life from use of electrolyte B over that of electrolyte E for each alloy, is given in the far right hand column. It is significant that in the case of every alloy cell operating life is longer when used with mixed electrolyte B. Table 8.3 gives the power output calculated from experimental data obtained. The percentage increase in power output from use of electrolyte B over that of electrolyte E of alloys 1-4 are given in the far right hand column. Alloys 2 and 3 exhibit a significant increase in power output from using electrolyte B, however, alloys 1 and 4 do not.

Figure 8.6 Design of Cell.

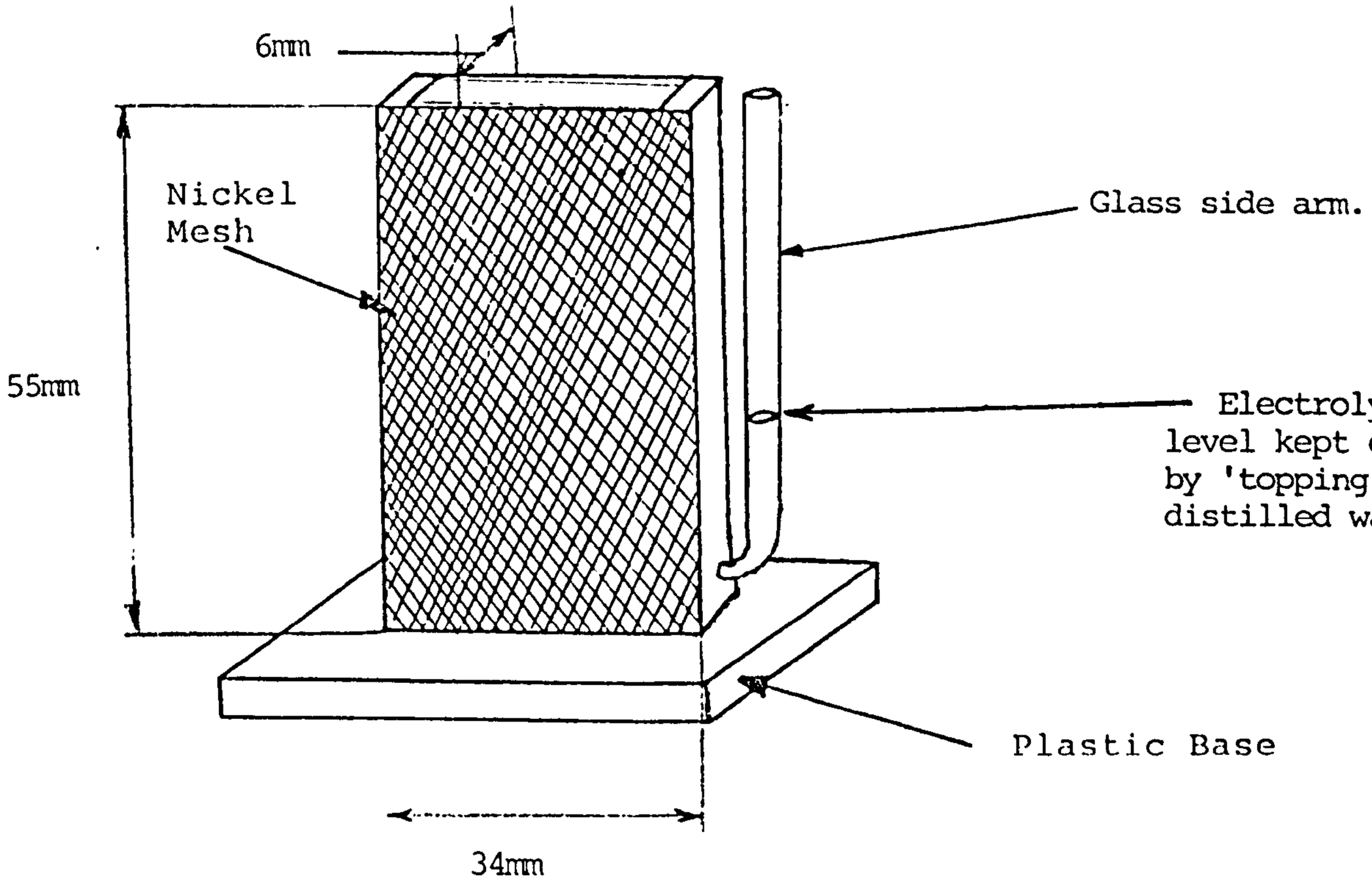

Figure 8.7 Discharge Circuit for Power Output Analysis of Full Cells.

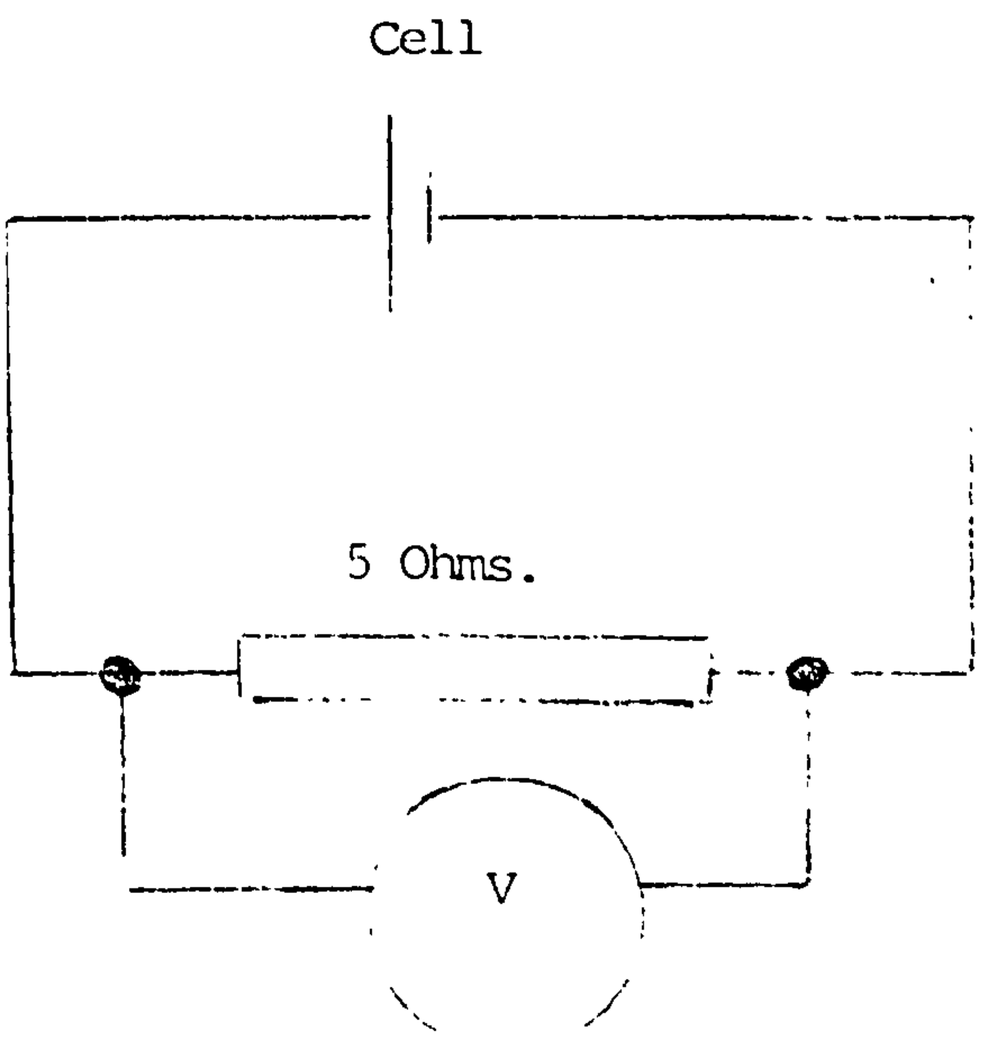

Figure 8.8

Full Cell Tests Alloy 1

Electrolytes A, B & E

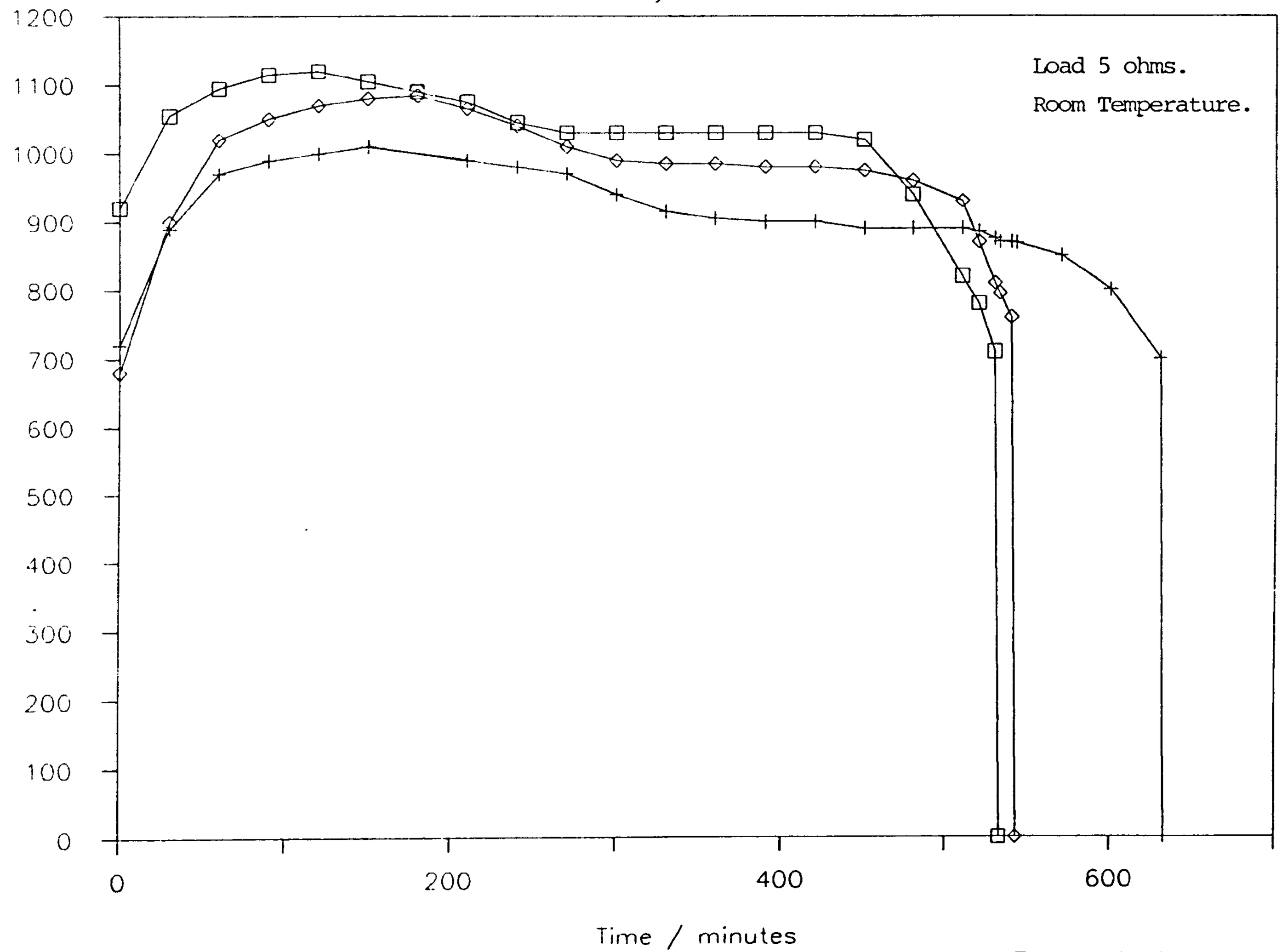

Figure 8.9

Full Cell Tests Alloy 1

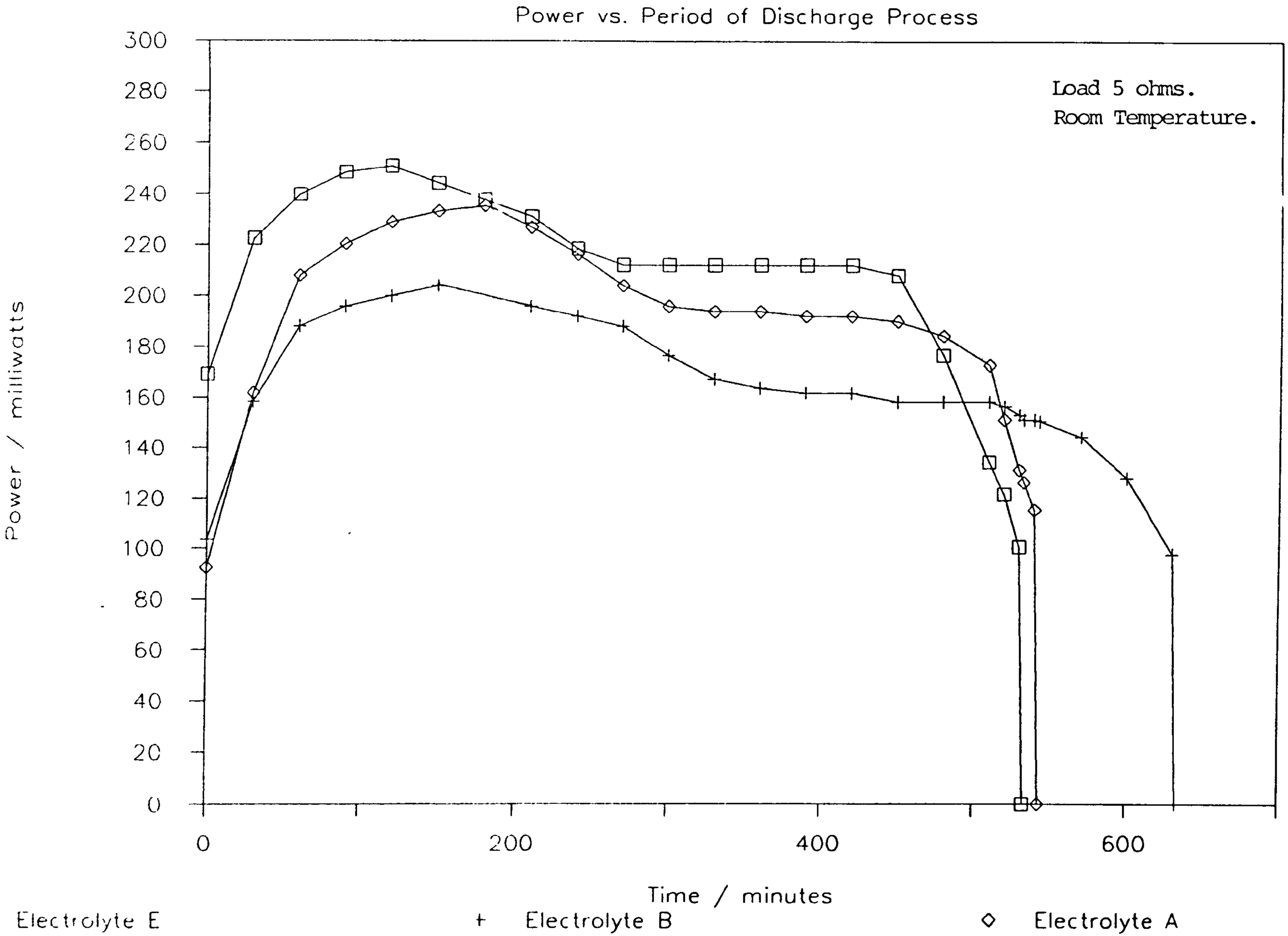

Figure 8.10

Full Cell Tests Alloy 2

Electrolytes A, B & E

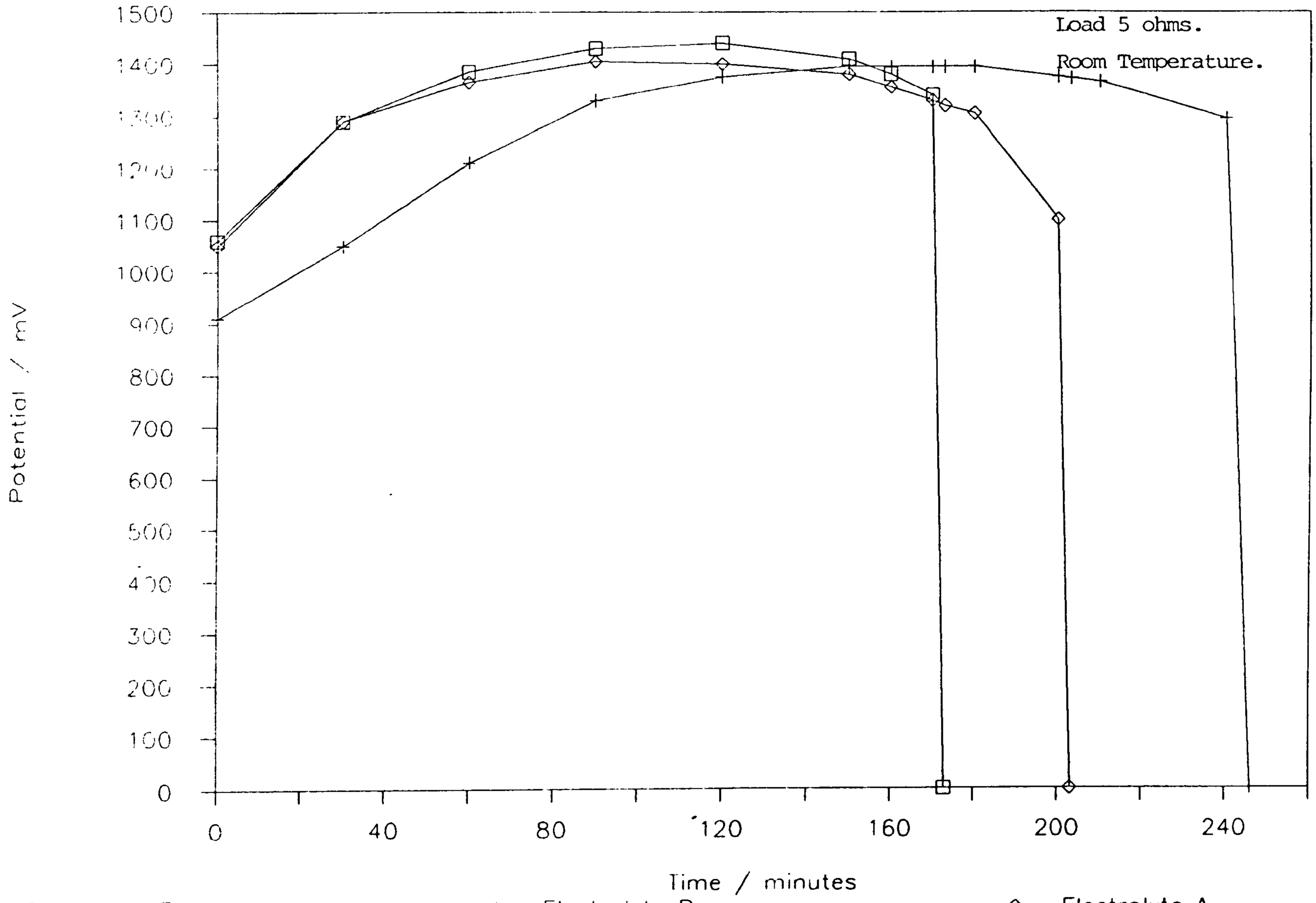

Figure 8.11 Full Cell Tests Alloy 2

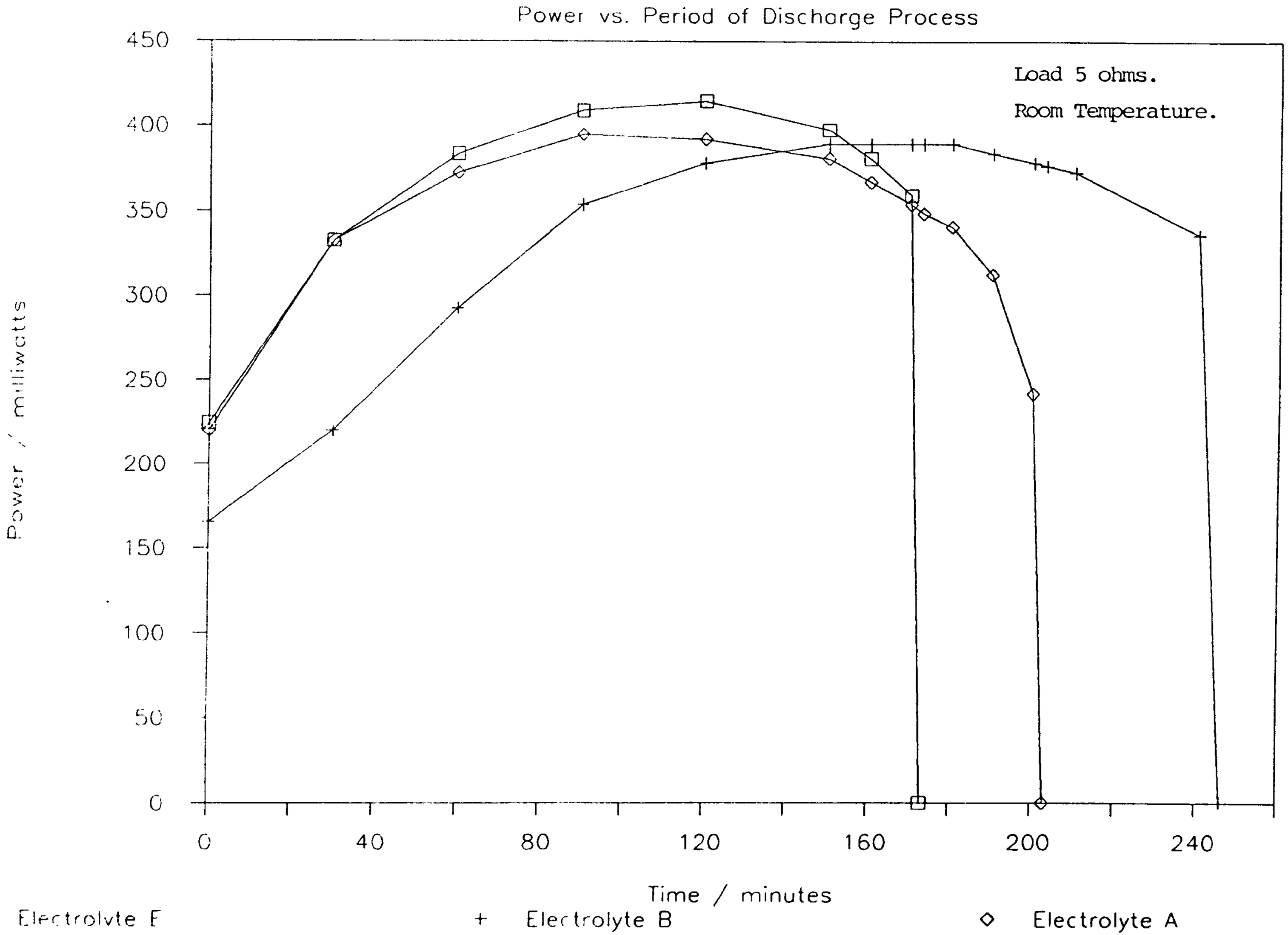

Figure 8.12

Full Cell Tests Alloy 3

Electrolytes E, B and A

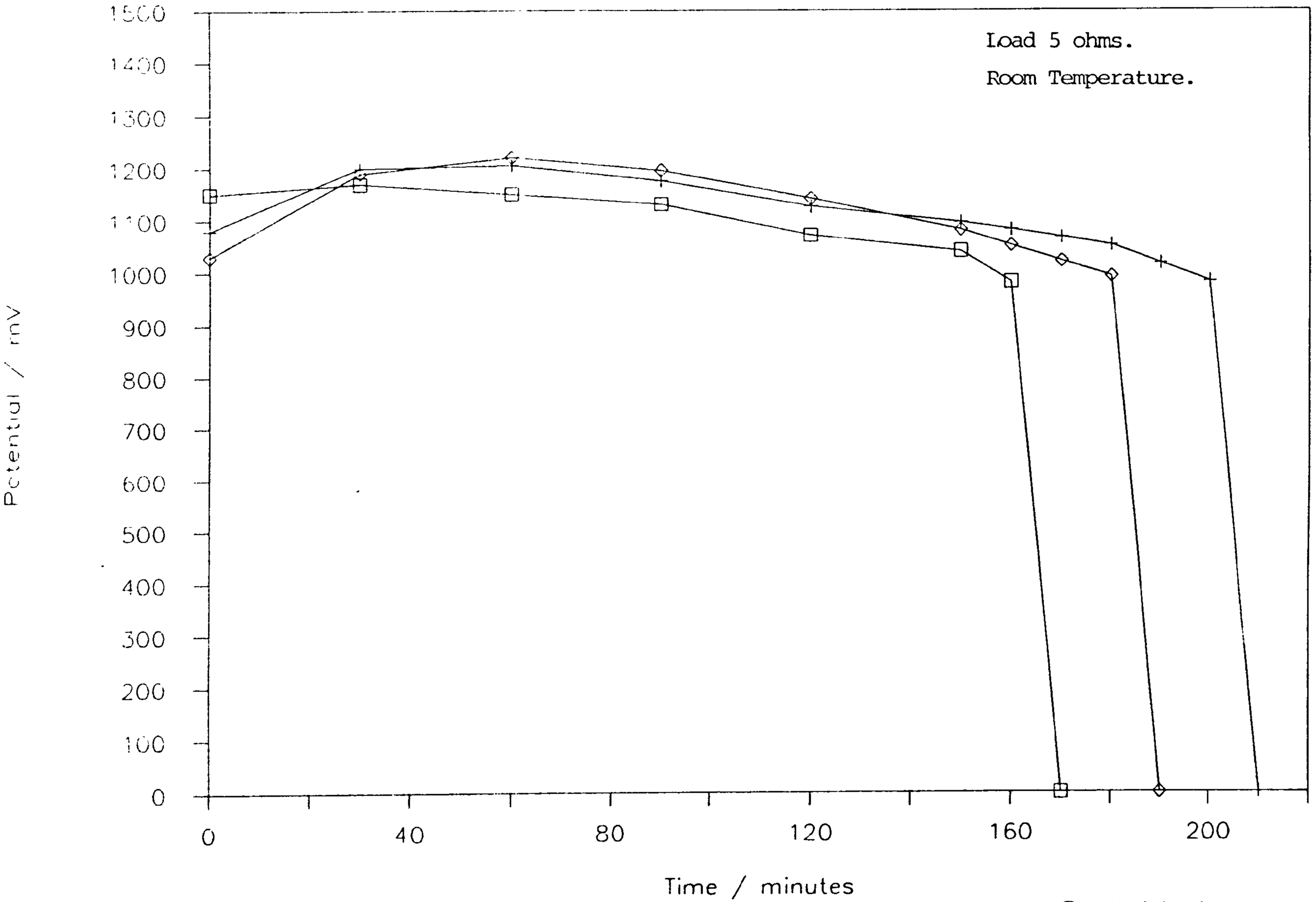

Figure 8.13 Full Cell Tests Alloy 3

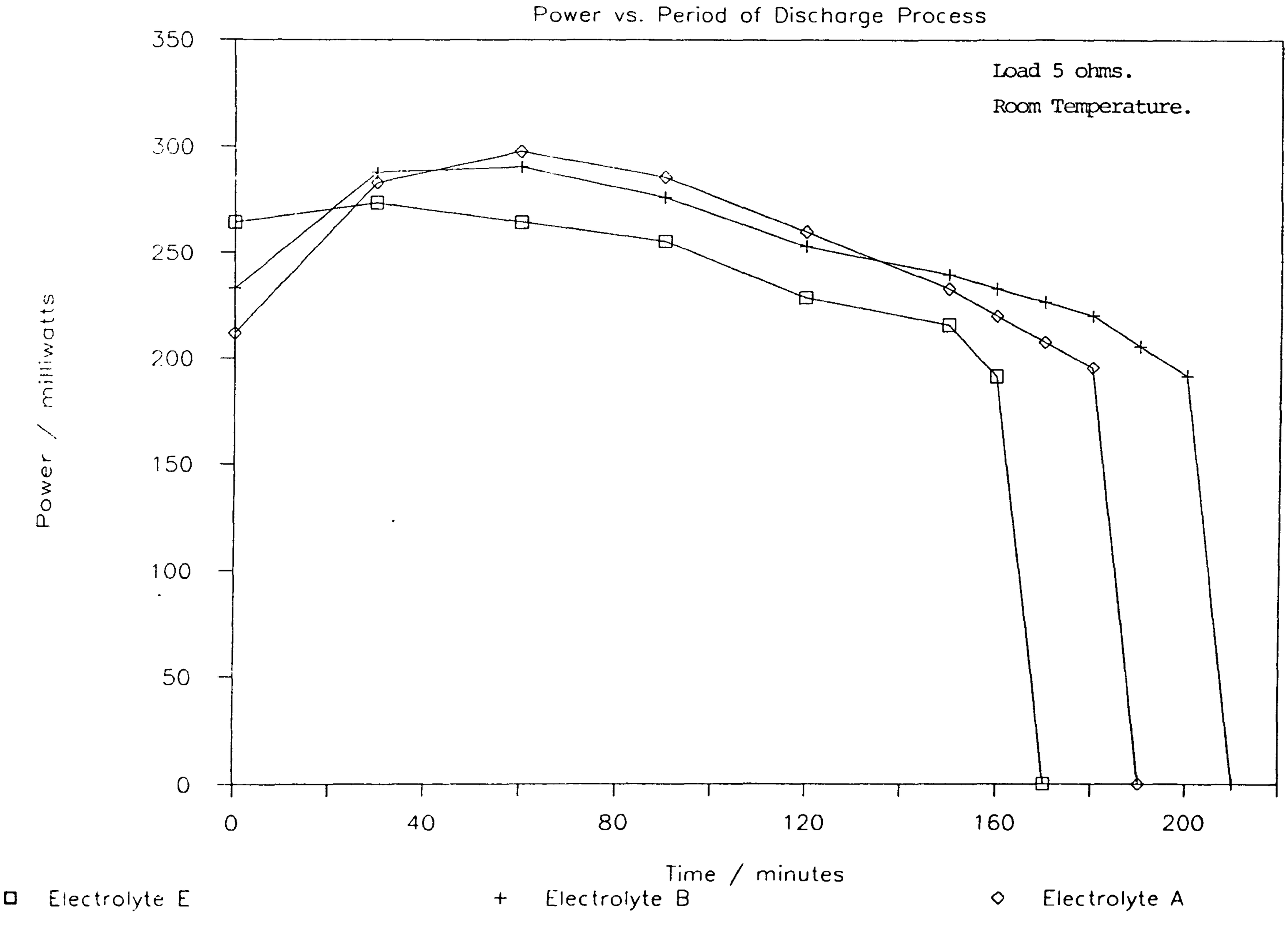

Figure 8.14 Full Cell Tests Alloy 4

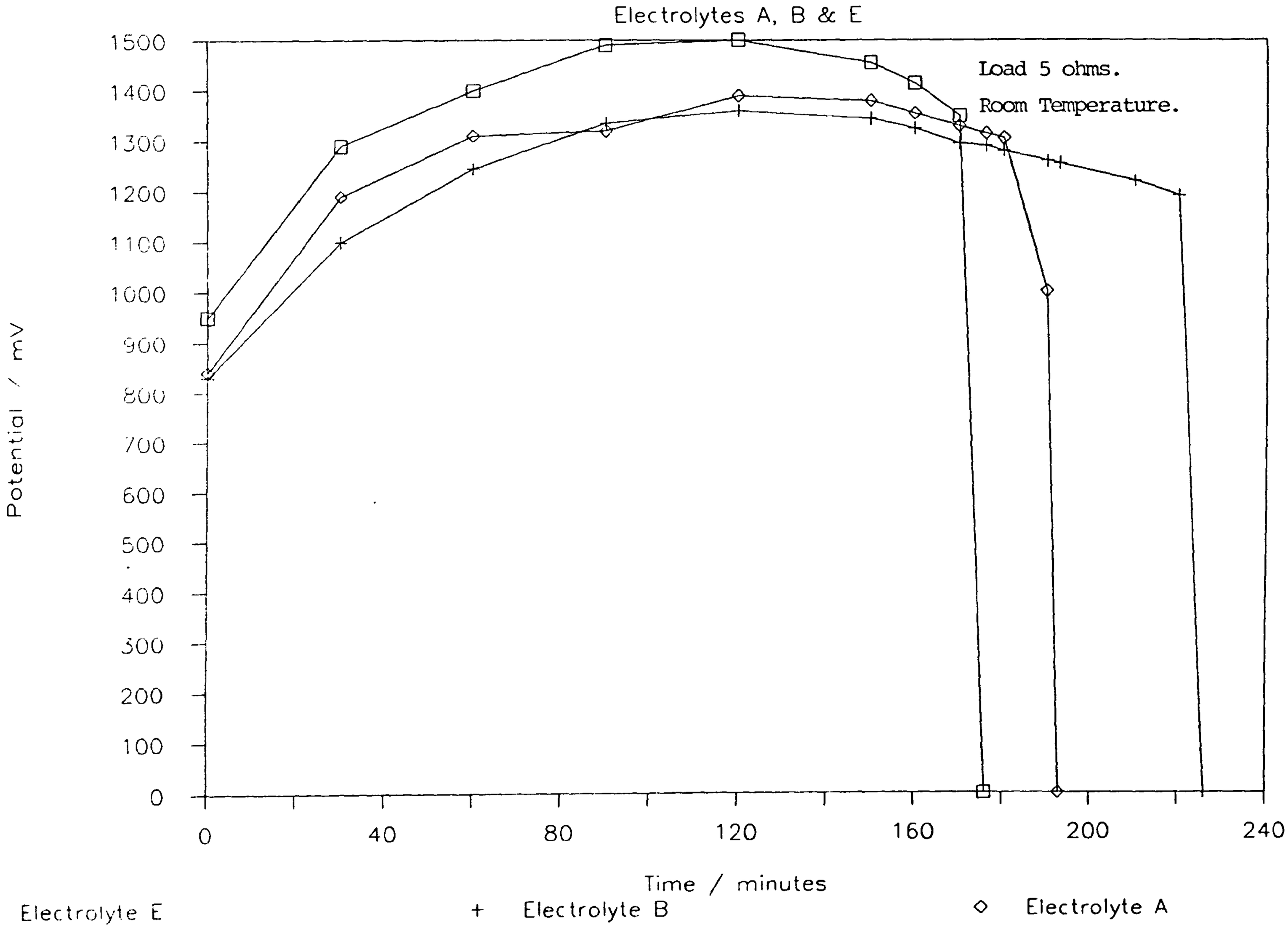

Figure 8.15 Full Cell Tests Alloy 4

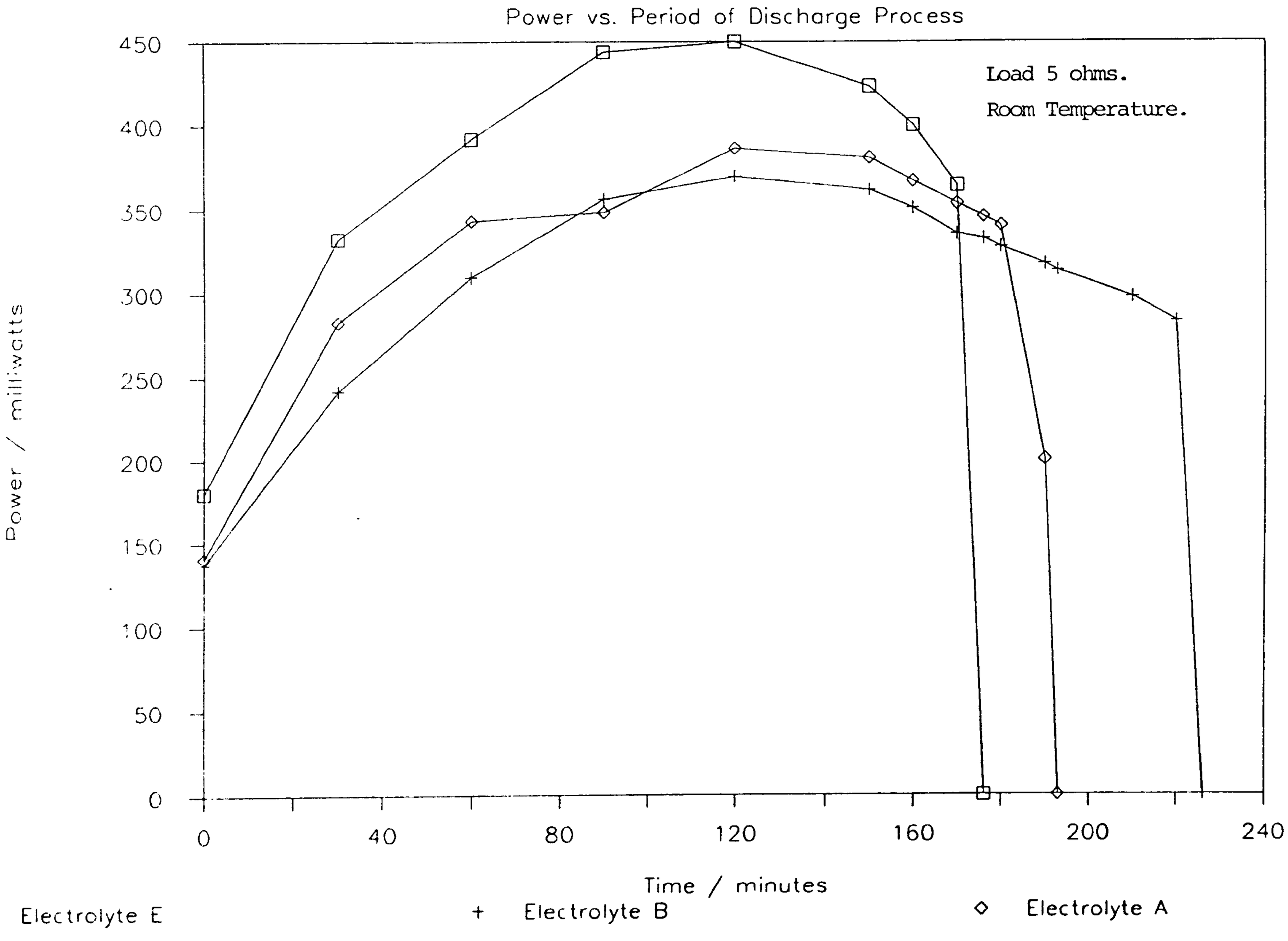

Table 8.2 Typical Results for Cell Operating Life (minutes) of Alloys 1-4 in Electrolytes A, B and E.

Alloy	Electrolyte A	Electrolyte B	Electrolyte E	Percentage Increase in Operating Life of Electrolyte B Compared to E.
1	541	633	533	19
2	203	246	173	42
3	190	213	170	25
4	193	226	176	28

Table 8.3 Typical Results for Full Cell Power Output (Wh) of Alloys 1-4 in Electrolytes A, B and E.

Alloy	Electrolyte A	Electrolyte B	Electrolyte E	Percentage Increase in Power Output of Electrolyte B Compared to E.
1	1.80	1.90	1.88	-
2	1.18	1.34	1.06	26
3	0.81	0.89	0.69	28
4	1.07	1.19	1.14	5

8.4 Conclusions.

From the capacity analysis results we observe that on discharge at 100mA/cm^2, every alloy gives better performance in electrolyte B rather than electrolyte E. It was also found that in all experiments cell operating life was longer for mixed electrolytes A and B than for electrolyte E. This can be related to the fact that the mixed electrolyte has a greater solubility for aluminate ions, and also the nature of the structure of the reaction product. Whilst the results do show the longer operating life obtained from use of the mixed electrolyte, it is noticeable that the increase in cell life is not quite as great as what might be expected from the dramatic increase in solubility of aluminate that is observed. This may be explained by the growth of hydroxide precipitation during operation of the cell affecting the result. A prototype model could include for example, a circulating electrolyte which constantly flows through the cell, thereby removing this problem. Under such circumstances it is likely that the cell performance would improve.

As for the alloys themselves it seems certain that the small quantities of alloying elements play a significant role in the differing results. Alloy 2, which has the highest capacity values in electrolyte B, has a relatively high tin content. It seems likely from work done in previous

chapters that a layer of tin is formed on the electrode surface causing an anodic shift in potential. Alloy 1, which is the highest purity aluminium, performs well in mixed electrolytes, and contains different elements to alloy 2. Alloy 4, which contains exceptionally high quantities of tin has the third largest capacity value in electrolyte B, whereas alloy 3, with it s low corrosion characteristics (because of it s high titanium content and the absence of gallium) has the lowest value. In electrolyte E however, this alloy performs better than both alloys 1 and 4 as regards capacity.

The full cell power output results are interesting in that all alloys again ran for longer periods in mixed electrolytes than in electrolyte E by at least ca. 20%. However, on analysis of the results of the plots of power vs. time, the actual power output is only significantly greater (ca. 25%) in two of the four alloys. The increase in power output in alloys 2 and 3 are related to the fact that the cells are running for longer periods in the mixed electrolytes. However, even though the cell operating life is still longer for alloys 1 and 4 in the mixed electrolytes, there is no significant increase in power output values. This is due to the fact that there is a drop in potential with the use of the mixed electrolytes and these two alloys, which only becomes really apparent when power vs. time graphs are plotted. The explanation for this drop in potential is that the conductivity is lower in

the mixed electrolytes due to the conductivity of sodium hydroxide being lower than that of potassium hydroxide. This is shown by the fact that mixed electrolyte A, which has a higher proportion of potassium hydroxide, tends to have higher operating potentials than those for electrolyte B. However, it is the ability of alloys 2 and 3 to run for longer periods in electrolyte B, that results in the greater power output values.

CHAPTER 9.

CONCLUSIONS, APPLICATIONS FOR THE CELL AND SUGGESTIONS FOR FURTHER WORK.

9.1 Introduction.

The use of aluminium as a battery anode material is an extremely attractive idea, both for technological and economical reasons. Theoretically, aluminium can yield more energy by weight than any other metal other than lithium. It s relative abundance, smelters produce over thirteen million tonnes of aluminium every year, and it s low cost related to the fact that supply outstrips demand, are the basic reasons for it s financial attractiveness.

Because of the relatively low demand for the metal, (the main markets are transport and building and these have been depressed in recent years), aluminium companies are amongst the leaders in the search for new applications. The idea of coupling the metal with an oxygen electrode is attractive. The structure of the latter has been developed and improved over the last thirty years so as to produce cheap, high performance teflon bonded electrodes. The low mass of the air electrode coupled with the high energy, light weight aluminium leads to an extremely desirable high energy density system.

Development of this system however, first reported by Zaromb in the 1960's [110], has not been as rapid as perhaps might have been. This is because aluminium air, like all electrochemical cells, as well as having significant virtues also has disadvantages. The main reasons for this

relatively slow development of the system are considerable metallurgical and electrochemical problems [111]. The presence of a highly stable protective oxide film on the surface of the metal prevents the dissolution of aluminium, and for the system to work, this layer must be broken down. However, rapid breakdown of this layer can result in uncontrolled dissolution which is accompanied by evolution of hydrogen. Researchers turned to alloying aluminium with suitable elements which reduce hydrogen evolution and cause an anodic shift in potential. However, it is impossible to completely remove the problem of hydrogen evolution, even with the use of high hydrogen overpotential additives. Minimising this problem with alloying elements, and then removing the problem of hydrogen gas evolved, using suitable hydrogen oxygen recombination units [112], seems to be a feasible solution.

The problem in the alkaline cell of the precipitation during discharge of a fine white aluminium hydroxide which tends to clog the cell and reduce performance, can be overcome by using a mixed electrolyte of potassium and sodium hydroxide rather than the traditionally used potassium hydroxide. Also the covering of the active sites on the air electrode by this white precipitate can be prevented by regenerating the electrolyte by means of cyclones. Interesting work performed at City [113] has also shown that in situ deposition of active material on the cathode can be achieved.

The following section 9.2 summarises the work done for this project in attempts to overcome some of the previously stated problems of the system. In the proceeding section 9.3, some of the possible applications of the system are examined. The justification for any financial investment in the development of the aluminium air cell certainly depends on finding feasible applications for the system.

9.2 Conclusions of Work Done.

Quarshie [93] discovered that the use of a mixed electrolyte consisting of 1:1 50 wt/v% sodium hydroxide and 30 wt/v% potassium hydroxide dramatically increased the operating life of an aluminium air cell using alloy Q4. This was due to the quite dramatic increase in solubility of aluminate that was observed from use of the mixture as compared to 40 wt/v% potassium hydroxide electrolyte. One of the objectives of this work was to apply the electrolyte to other commercially available aluminium alloys and determine the effect on both half cell and full cell performance.

What is observed in half cell tests is that in all electrolytes at very low current densities (up to 10mA/cm^2) alloy 3 with it's low corrosion characteristics exhibits the most negative potential. However, on increasing the current density value up to ca. 150mA/cm^2 in mixed electrolyte and 250mA/cm^2 in electrolyte E, alloy 4 with it's high power

characteristics clearly has the most anodic potential. In electrolyte E alloys 1,2 and 3 can cope with much higher current density values of up to 400mA/cm^2, whereas in mixed electrolyte B, alloy 3 passivates soonest at less than 100mA/cm^2, whilst alloys 1 and 2 still give significantly higher negative potential values at current densities in the region of 250mA/cm^2.

This information reveals characteristics for each alloy. Depending on the requirements of a system a suitable alloy could be employed. For a low current density system alloy 3 is the most suitable anode material. At values of between ca. 20 and 150mA/cm^2, alloy 4 gives the best performance. At higher values alloys 1 and 2 can still operate.

The Tafel plots again reveal interesting information. The highest exchange current density values are obtained for alloy 2 in the mixed electrolyte, followed by alloy 4 in mixed electrolyte B. Both these alloys contain significant quantities of tin. The Tafel slopes themselves show a dramatic change in slope from the kinetically controlled region to the diffusion influenced region when using a mixed electrolyte. This is not observed when using electrolyte E. This may be explainable by the differing nature of the reaction product formed in the case of the mixed electrolytes A and B and that formed with the use of electrolyte E. It appears that the presence of sodium hydroxide results in this sharp change of Tafel slope and

also causes the formation of a granular precipitate.

The full cell results show that in the capacity analysis, use of mixed electrolyte results in greater values for all alloys, most significantly , alloy 2. Perhaps the most important data however, are the power output results obtained from discharge of full cells over a constant load. The first point to note is that all alloys ran for longer periods in mixed electrolytes than in potassium hydroxide. However, on actually calculating the power output values, it was shown that only alloys 2 and 3 showed a significant increase in power output. Alloys 1 and 4 give roughly similar power output values in mixed electrolyte B as in electrolyte E. This phenomenon can be explained by the fact that with alloys 1 and 4 in mixed electrolyte, the potential values recorded are markedly lower than in potassium hydroxide. This drop in potential, which probably arises because of the lower conductivity of the mixed electrolyte, becomes more significant on calculation of power output values. Thus it appears that not all alloys actually increase power output, though they do run for longer periods in mixed electrolytes. It is interesting to note that alloy 1 has the greater power output values in all electrolytes. It must be pointed out however, that these values also contain the results obtained towards the end of discharge where alloy 1 appears to tail away to zero potential, rather than the more abrupt end of operating life that is observed with alloys 2, 3 and 4. It is likely that in use, the cell

would have to be replaced or mechanically recharged well before passivation actually occurs, as the power output towards the end of discharge would be too low to enable equipment to function. However, alloys 1 and 2 again show the greatest values, and it would appear that these two are the better performance alloys.

Two alloys, numbers 1 and 4, were found to have very similar power output characteristics in both mixed and potassium hydroxide electrolytes. However, it would still be advantageous for any aluminium air system to employ a mixed electrolyte rather than potassium hydroxide. This is due to the nature of the reaction product. With potassium hydroxide, a fine white precipitate is obtained on passivation which completely smothers and clogs the full cell system. This precipitate is extremely difficult to remove, and it can end up covering the active sites on the air electrode thereby reducing cell efficiency. However, with a mixed sodium and potassium hydroxide electrolyte, a granular precipitate is observed, which is easily flushed out of the cell, thereby considerably reducing this problem. It is also possible that the presence of a granular precipitate contributes to the greater operating life of the full cell. The presence of a reaction product of this nature would allow diffusion of ions to and from the electrode surface for a longer period.

Work has also been carried out in attempts to reduce

wasteful hydrogen evolution. Quarshie [93] showed that mercuric oxide was the most effective corrosion inhibitor. The role of mercury in the discharge process was further examined using a novel microelectrode scanning system. Information obtained from use of this equipment proved that the presence of minute quantities of mercury in the electrolyte cause an even distribution of current on the electrode surface, thus increasing anodic efficiency. Previous researchers may have thought that this was the case, but traditional electrochemical techniques deal with total current rather than the microzone current that the microelectrode scanning system is concerned with.

Finally, some preliminary experiments were carried out on the various aluminium alloys using ellipsometry. Initial investigations involved the anodisation of the alloys in tartaric acid, and revealed interesting information about the surface of the alloys. It appears that the trace elements added to the aluminium significantly affect the surface structure.

The objective of this work was to apply the mixed electrolyte to various aluminium alloys and to examine the effect. Also, another objective was to look at some of the problems of the aluminium air cell and attempt to find feasible solutions. Work by Quarshie [93] helped solve some of these problems, discovering an improved electrolyte and an electrolyte additive which acts as a corrosion inhibitor.

This work has also attempted to explain why the suggested solutions results in improved performance.

9.3 Applications for Aluminium Air Cells.

A major potential use for aluminium air cells are as power sources for portable equipment. This is because of the low weight of the system and it s ability to provide high power output. Typical applications are as power sources for computers, television cameras, videos, power tools and submersibles. (An excellent review of the use of aluminium air for powering submersibles is given by Quarshie [93]). Generally speaking, all portable equipment using electrical power are potential users of aluminium air.

Another area in which aluminium air could penetrate the present market is as back up emergency sources. Electrical failure can cause major inconveniences and standby power is often an important requirement. In certain circumstances it is essential to have an effective and reliable back up supply to provide lighting for e.g. operating theatres in hospitals, telephone exchanges and underground trains. There are obviously many other areas which would require a reliable emergency power source and the law demands that public places have to have adequately lit emergency exits, and fire alarms which have to be connected to a back up supply should a mains failure occur. Currently, nickel cadmium and lead acid battery packs provide the emergency

power. The following comparison between a nickel cadmium and aluminium air cell, indicates that it is quite feasible to assume that aluminium air could penetrate this market.

A standard type of emergency lighting for interior use is the 8 Watt fluorescent emergency light with a discharge duration of three hours. R.S. Components provide an emergency light system containing a 4.8V nickel cadmium battery pack, (model no. 565793). The battery cost is £14.08, and the necessary acompanying battery charger costs £30.20 (model no. 59991067), giving a total cost of £44.28. Nickel cadmium and aluminium air cells are compared in Table 9.1.

Table 9.1 A Comparison of Al- Air and Nickel Cadmium Cells.

Type of Cell	Aluminium Air (Primary or Mechanically Rechargeable)	Nickel Cadmium (Secondary)
Cathode	Oxygen Reduction	Nickel Oxide
Anode	Aluminium	Cadmium
Electrolyte	Alkaline	Alkaline
Energy Density (Wh/kg)		
Theoretical	8000	235
Actual	400-800	ca.25
Discharge Potential(V)	1.2 - 1.6	1.0 - 1.3

Economic Analysis of the Aluminium Air Cell.

Table 9.2. gives the necessary data required to calculate the manufacturing cost of an aluminium air cell required to run an 8 Watt fluorescent emergency light for a three hour period.

Table 9.2 Characteristics of Cell Providing 8W.

Power Required = 8W

Discharge Period = 3h

Cell Potential = 1.25V.

Current Density = 100mA/cm2

Anodic Efficiency = 90%

Energy Required = Power x Time = 24Wh

Capacity Required = Energy/Voltage = 20Ah

Electrochemical Equivalent of Aluminium = 2.98Ah/g

At 90% Efficiency Mass of Aluminium Required

= 20Ah/(2.98 x 0.9) = 7.46g

A 20Ah rated cell required for three hours would discharge at a current of 6.67A. As the current density rating of the air electrode is 0.1A/cm^2, this means that an air electrode of total area 66.7cm^2 would be required. A cell casing

would therefore consist of two air electrodes ca.5.7 cm x 6cm pasted onto a larger perspex frame, and assuming that the optimum distance between the electrodes is 0.5cm, the volume of electrolyte required would be 17.5cm^3.

The system is found to give best performance with a mixed electrolyte of 50% NaOH and 30% KOH.

1cm^3 of electrolyte would contain 0.5g of NaOH and 0.3g KOH.

Thus the mass of NaOH in 17.5cm^3 of electrolyte = 8.75g

and the mass of KOH in 17.5cm^3 of electrolyte = 5.25g

Table 9.3. gives the approximate mass of material required for 1cm^2 of the air electrode. These values were calculated from the loading of material per cm^2.

Table 9.3 Mass of Air Electrode Materials.

Material	g/cm^2	Mass (g) Required for Cell of Total Area 66.7cm^3
Carbon	0.0945	6.30
PTFE	0.0495	3.30
Co_3O_4	0.0135	0.90
Ni	0.0928	6.19

Table 9.4. gives the cost of material as taken from the 'BDH Reagents, Diagnostics Fine Chemicals 87/88 Catalogue.' As costs are per kg of material , they have been halved to make a more realistic value because large scale manufacture of

aluminium air cells would result in the purchase of bulk raw materials at a lower cost. The total cost of these raw materials has been multiplied by four to give an estimate figure for the manufacturing costs.

Table 9.4 Cost of Raw Materials.

Material	£/kg	Mass Required for single cell g	Cost in Pence
Aluminum*	10	7.46	7.46
PTFE	30	3.30	9.90
Carbon	6.6	6.30	4.16
Co_3O_4	105	0.90	9.45
Nickel**	20(per m^2)	(66.7cm^2)	13.34
KOH	3.4	5.25	1.79
NaOH	2.8	8.75	2.45

Total Cost of Materials = 48.55p

Total Manufacturing Costs = 48.55p x 4

= £ 1.94

* Cost of aluminium from Incoform Ltd . Birmingham.

** Cost of nickel mesh from Bedford, Steer, End, Slough.

It is now necessary to make some further assumptions.

(i) One power failure occurs per year. Thus one aluminium air cell would be required a year giving a total of five cells

over a five year period.

(ii) The life of the nickel cadmium battery pack is taken as five years, the cost of recharging the cells is negligible.

(iii) The selling price is taken as the manufacturing cost times 250%, since manufacturing profit is ca. 50% of manufacturing costs, and retail profit is ca. 100% of manufacturing costs.

(iv) The cost of a hydrogen oxygen recombination unit is taken as £4.00 and can be reused with each new aluminium air cell. (Hydrocap retail their hydrogen oxygen recombination unit in the United States for ca. $4.00.)

The cost of running an aluminium air battery for a five year period taking the above assumptions into account is calculated as follows.

Selling Price of Aluminum Air = Manufacturing Cost x 250%.

= £ 1.94 x 2.5

= £ 4.85.

Cost of five Aluminum Air cells = Selling Price + Cost of H_2/O_2 Unit.

= (£ 4.85 x 5) + £ 4.00

= £ 28.25

Cost of Nickel Cadmium Cell = Price of Battery + Charger Pack

= £ 14.08 +£ 30.20

= £ 44.28.

The economic analysis shows that the cost of the aluminium air system for the purpose of emergency lighting could cost approximately 35% less than the nickel cadmium packs presently used.

Summary.

The intention of the latter part of section 9.3 was to highlight one potential use of the aluminium air system to show that full scale manufacture is economically feasible. As the system is so flexible, cell design would depend to a large extent on the potential use. Some of the main advantages that this system has over existing commercially available electrochemical cells are listed below ;

(i) Uses cheap and readily available materials.

(ii) Infinite capacity of air electrode.

(iii) Aluminium has an exceptionally high energy density.

(iv) Low mass of cell system.

Due to the abundance of aluminium ore, and its high energy

density, a great deal of effort and money has been spent in the research and development of prototype aluminium air systems. Since the early 1980's considerable progress has been made. Alcan in 1986 produced a battery which was used to power a golf cart and have made claims that by the year 2000, we will have conventional cars powered by aluminium air. Volume for volume, aluminum consumed in a battery releases four times as much energy as gasoline burnt in an engine, and does not produce pollutants as byproducts of use.

There are problems still to be overcome eg, reducing corrosion current, evaporation of the electrolyte etc., but the intense research of the last decade or so has resulted in prototype models of the battery becomming available on the market. As manufacturers become more aware of the benefits of the system, they will begin to look for further applications for this technology. It appears that the next ten years will be an exciting period regarding the progress of electrochemical power sources with the aluminum air system playing a crucial role in high energy density applications.

9.4 Suggestions for Further Work.

It is likely that aluminium anodes can be further optimised by varying the quantities of the elements Zn, Ga, In, Bi, Pb and Sn. Greater anodic potentials will be achieved if the

quantities of those elements which form cathodic sites on the aluminium electrode, i.e. Fe, Cu and Si, can be further reduced.

Further investigations can also be carried out using the microelectrode scanning system. It would be interesting to obtain various aluminium alloys e.g. aluminium - gallium, aluminium - indium and aluminium - tin, and study the effect of the individual elements on the distribution of current on the electrode surface. Using this technique it is possible to determine the most effective additive for even distribution of current on the aluminium surface.

There is a great deal of work that can be performed using ellipsometry. Originally the intention was to first experiment with tartaric acid ele ctrolyte, and then move onto study the behaviour of the various alloys in electolytes A, B and E. Lack of time on the instrument unfortunately prevented this this from being completed, but the results indicated different behaviour from the four alloys in tartaric acid, which suggests that it might be worth following this idea up. Work of this nature could lead to more information on film thickness, relating to the slow start up of the aluminium air cell.

Further study must also be made into the dramatic increase in solubility obtained from the use of mixed sodium and potassium hydroxide electrolyte to that of pure potassium

hydroxide. The explanation for this behaviour is still at present, unclear. However, further investigations could focus on the solubility of sodium aluminate in potassium hydroxide and potassium aluminate in sodium hydroxide and comparisons made to the solubility of potassium aluminate in potassium hydroxide and sodium aluminate in sodium hydroxide.

With these suggestions it is clear that there is a considerable amount of work that can be still carried out on aluminium air systems. However, the next positive step forward in the work is the development of a prototype model, and analysis of such a model. With the experience and knowledge obtained at the Chemical Energy Research Centre significant advantages over similar prototypes could be achieved. If this prototype can be developed at a University research centre, and satisfactory results obtained, then the major areas of concern will be the engineering design drawbacks that are normally associated with the development stage.

Figure 9.1 The Aluminium Air Cell.

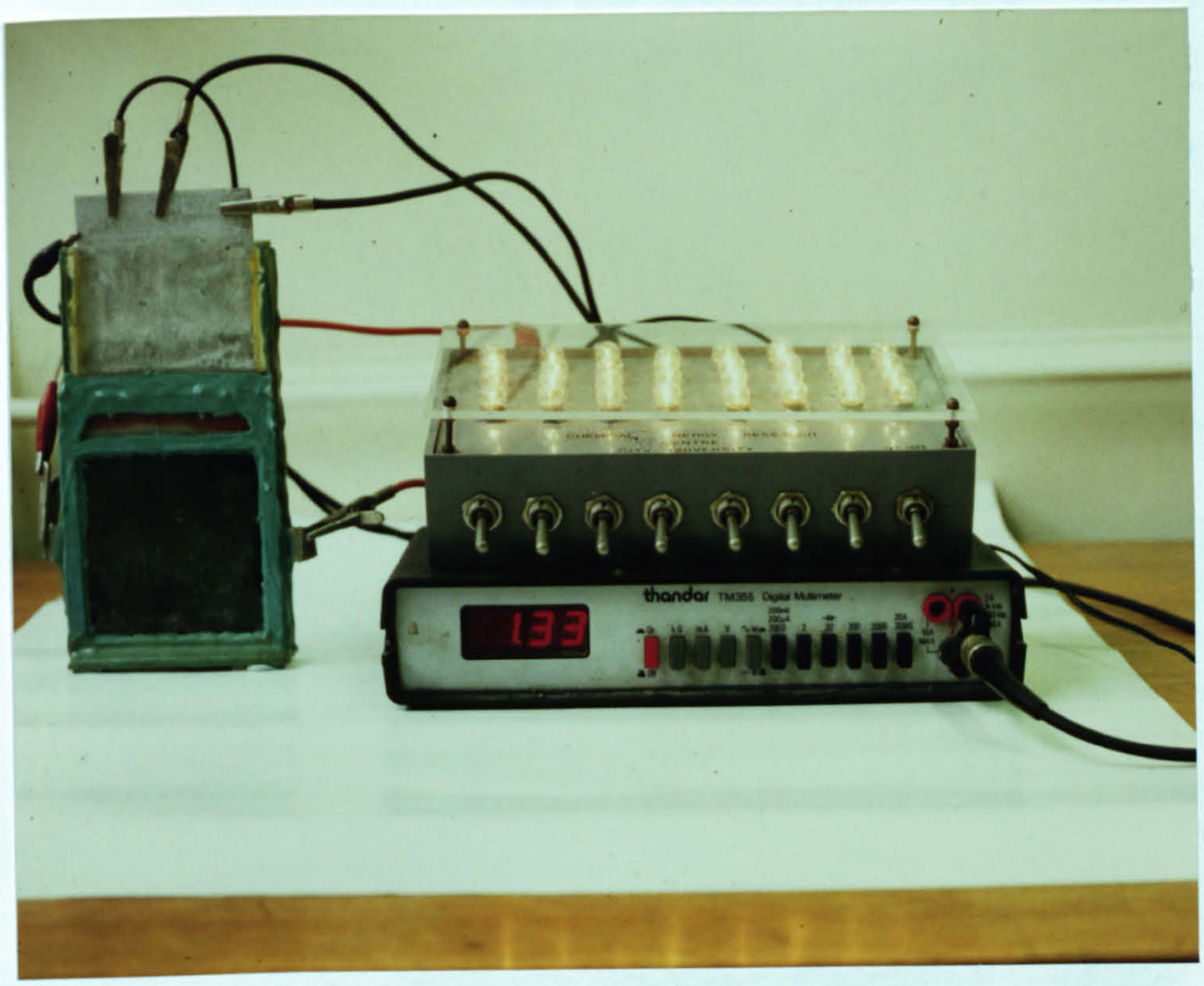

REFERENCES.

[1] Zecevic S., Gajic Lj., Despic A.R. & Drazic D.M., Electrochimica Acta, Vol.26, No.11, (1981), p1625.

[2] Tommasi D., Traite des Piles Electriques, Georges Carre, Paris, (1881), p131.

[3] Mennons M.A.F., U.K. Patent 296 (1858).

[4] Brown C.H., U.S. Patent 503567 (1893).

[5] Anderson E.L., U.S. Patent 706631 (1902).

[6] Anderson E.L. & Noble J., U.S. Patent 759740 (1904).

[7] Vince C.H., U.K. Patent 399561 (1933).

[8] Pennock A.G. & Lee S., U.K. Patent 437536 (1935).

[9] Sargent D.E., U.S. Patent 2554447 (1951).

[10] Ruben S., U.S. Patent 2638489 (1951).

[11] Quarshie R.L., PhD Thesis, City University, (1985).

[12] Bockstie L., Trevethan D. & Zaromb S., J. Electrochem. Soc. Vol.110, No.4, (1963), p267.

[13] Zaromb S., U.S. Patent 3513031 (1970).

[14] Scamans G., O'Callaghan B., Hamlen R. & Fitzpatrick N., 'Advances in the Development of Aluminium Air Batteries', 11th Power Sources Conference, Brighton, (1986).

[15] Hasvold O., 'Development of an Alkaline Aluminium Air Battery System at the Norwegian Defence Research Establishment' Presentation to the Society of Chemical Industry, Electrochemical Technology Group Symposium, Oct (1987).

[16] Fitzpatrick N. & Scamans G., 'Aluminium is a Fuel for Tomorrow' New Scientist 17th July (1986).

[17] Brown O.R. & Whitely J.S., Electrochimica Acta, Vol. 32, No. 4, (1987), p545.

[18] Nisancioglu K. & Holtan H., Electrochimica Acta, Vol.24, (1979), p1229.

[19] Tseung A.C.C., Lin Z.G. & Quarshie R.L., U.K. Patent No.18833, (1986).

[20] Glicksman R., J.Electrochem. Soc., vol.106, (1959), p457.

[21] Brown O.R. & Whitley J.S., Electrochimica Acta, vol. 32, No.4, (1987), p545.

[22] Hori Y., Takao J. & Shomon H., Electrochimica Acta, vol 30, No.9, (1985), p1121.

[23] Belitskus D., J.Electrochem Soc., vol. 119, (1972), p295.

[24] Despic A.R., Drazic D.M., Purenovic M.M. & Cikovic N. J. Applied Electrochem., 6, (1976), p527.

[25] Despic A.R., Drazic D.M., Zecevic S.K. & Atanasoski R.T. Electrochimica Acta, vol. 26, (1981), p173.

[26] Hori Y. , Takao J. & Shomon H., Electrochimica Acta, vol 31, No.5, (1986), p555 .

[27] Zaromb S., J. Electrochem. Soc., vol.109, (1962), p1126.

[28] Schumm B., J. Electrochem. Soc., vol.123, (1976), p1696.

[29] Redding J.T.& Newport J.J., Materials Protection,(1966), 12, p15.

[30] Stevanovic R.M., Despic A.R.& Drazic D.M., Electrochimica Acta, Vol.33, (1988), p397.

[31] Vincent C.A. et al., Modern Batteries, Edward Arnold, (1984), p90.

[32] Jiang S.P., PhD Thesis, City University, (1987).

[33] Hanbook of Chemistry and Physics, 67th Edition, CRC Press p D-153, (1986-87).

[34] As reference [11].

[35] Crow D.R., Principles & Applications of Electrochemistry. Chapman and Hall, London (1979), p183.

[36] Salvin W., Atomic Absorption Spectroscopy, Interscience, New York (1968).

[37] Vogel's Textbook of Quantitative Inorganic Analysis, 4th Edition, Longman, New York (1978), p810.

[38] West A.R., Solid State Chemistry and it's Applications, Wiley & Sons, (1984), p64.

[39] Edited by Chatham A.K. & Day P., Solid State Chemistry Techniques, Oxford Science Publications (1987), p86.

[40] Edited Windawi H. & Ho F., Applied Electron Spectroscopy for Chemical Analysis, Wiley & Sons (1982), Chapter 1.

[41] As reference [39], p45.

[42] ASTMA Powder Diffraction File, Alphabetical Index of Inorganic Compounds, TCPDS International Centre for Diffraction Data, Pensylvania, U.S.A. (1978).

[43] Ives D.J.G. & Janz G.J., Reference Electrodes, Academic Press, New York (1961), p335.

[44] Elbeik S. & Tseung A.C.C., Internal Report, City University, (1986).

[45] Delahay P., New Instrumental Methods in Electrochemistry Interscience Publishers, New York (1954), p36.

[46] Bevan H.L., PhD Thesis, City University, (1970).

[47] Lin C.G., PhD Thesis, Xiamen University.

[48] Modern Electrochemical Experiments, vol.2, Xiamen Electrochemistry Group, Xiamen University, to be published.

[49] Yeager E. & Sankind A., Techniques of Electrochemistry

vol.1, Wiley, (1972), p395.

[50] Bullman G., PhD Thesis, City University, (1972).

[51] Cahoon N.C. & Heise G.W., The Primary Battery, Vol.2, Wiley and Sons, (1976), p171.

[52] As reference [20].

[53] Reding J.T. & Newport J.J., U.S. Patent No.3337332, (1967).

[54] As reference [24].

[55] As reference [26].

[56] As reference [17].

[57] Scamans G., Chemistry and Industry, 17th March (1986).

[58] Bohnstedt W., J. Power Sources Vol.5, (1980), p245.

[59] Scamans G. & Fitzpatrick N., New Scientist, 17th July (1986), p34.

[60] Brown C.H., U.S. Patent No.503567, (1893).

[61] Heise G.W., Schumacher E.A. & Cahoon N.C., J. Electrochem Soc. Vol. 94, (1948), p99.

[62] Moden J.R. & Perkons G., U.S. Patent No.4107406, (1977).

[63] Pryor M.J., Keir D.S. & Sperry P.R., U.S. Patent No.3180728, (1965) (a).

[64] Pryor M.J., Keir D.S. & Sperry P.R., U.S. Patent No.3186836, (1965) (b).

[65] Pryor M.J., Keir D.S. & Sperry P.R., U.S. Patent No.3189486, (1965) (c).

[66] Pryor M.J., Keir D.S. & Sperry P.R., U.S., Patent No.3240029, (1966) (a).

[67] Pryor M.J., Keir D.S. & Sperry P.R., U.S. Patent No.3240688, (1966) (b).

[68] Pryor M.J., Keir D.S. & Sperry P.R., U.S. Patent No.3250649, (1966) (c).

[69] Pryor M.J., Keir D.S. & Sperry P.R., U.S. Patent No.3282688, (1966) (d).

[70] Pryor M.J., Keir D.S. & Sperry P.R., U.S. Patent No.3368952, (1968) (a).

[71] Pryor M.J., Keir D.S. & Sperry P.R., U.S. Patent No.3368958, (1968) (b).

[72] Rutemiller H.C., U.S. Patent No.3227644, (1966).

[73] Rutemiller H.C., U.S. Patent No.3418240, (1968).

[74] As reference [29].

[75] Mance A., Cerovic A. & Mihajlovic A., J. Applied Electrochem., Vol. 14, (1984), p459.

[76] Pryor M.J., Keir D.S. & Sperry P.R., J. Electrochem. Soc. Vol.114 No.8, (1967), p777.

[77] Pryor M.J., Keir D.S. & Sperry P.R., J. Electrochem. Soc. Vol.116 No.3, (1969), p319.

[78] Sakano T. & Toda K., U.S. Patent No.3172760, (1965).

[79] Schreiber C.F., U.S. Patent No. 3537963 (1970).

[80] As reference [22].

[81] Tuck C.D.S., Hunter J.A. & Scamans G.M., Alcan Int. Ltd. Banbury, Oxon. `The Electrochemical Behaviour of Al-Ga Alloys in Neutral and Alkaline Electrolytes.'

[82] Kirk Othmer, Encyclopaedia of Chemical Technology, 3rd Edition, vol 23, p98.

[83] Scamans G.M., O'Callaghan B., Hamlen R. & Fitzpatrick N., Power Sources Conference, Vol.11, Edited by Pearce L.J., (1986).

[84] Hasvold O., `Development of Alkaline Al-Air Battery System' Presentation at SCI Symposium, Belgrave Square, London. 13th October 1987.

[85] Denaro A.R., Elementary Electrochemistry, Butterworths, (1971).

[86] As reference [83].

[87] Drazic D.M., Despic A.R., Zecevic S., Atanackovic M. & Illiev I., Power Sources 7, (1978), p353.

[88] As reference [11].

[89] Principles of Instrumental Analysis, Skoog D.A., 3rd Edition, Saunders College Publishers, (1985), p294.

[90] Basic Instrumental Analysis, Pease B.F., Van Nostrand, (1980), p164.

[91] As reference [48].

[92] As reference [47].

[93] As reference [11].

[94] Bockstie L.,Trevethan D.R.& Zaromb S., J.Electrochem.Soc. Vol.110 No.4, (1963), p267.

[95] Rohrman F.A., U.S. Patent 2758082 (1956).

[96] Lin Z.G., Discussion of Work Performed at City University in 1982.

[97] As reference [22].

[98] Instrumental Methods in Electrochemistry., Southampton Electrochemistry Group, Ellis Horwood Ltd. (1985), p327.

[99] Bard A.J. & Faulkner L.R., Electrochemical Methods Fundamentals and Applications, Wiley & Sons,(1980), p583.

[100] Principles of Ellipsometry, Muller R.H., Advances in Electrochemistry and Electrochemical Engineering, Edited

by Delahay P. & Tobias C.N., Vol.9, (1973), p167.

[101] Dell'Oca C.J. & Fleming P.J., J.Electrochem.Soc., Vol.123 No.10, (1976), p1489.

[102] McCrackin F.C., Passaglia E., Stromberg R.R. & Steinberg H.L., J. Res. Natl. Bur. Stds., A. Phys. and Chem., 67A, (1963), p363.

[103] Heber K.V., Electrochimica Acta Vol. 23, (1978), p127.

[104] Tseung A.C.C., Rasiyah P. & Hibbert D.B., British Patent Application No. 804483, (1980).

[105] Yeung K.L.K. & Tseung A.C.C., J. Electrochem. Soc., 125, (1978), p878.

[106] King W.J.& Tseung A.C.C., Electrochimica Acta, 19,(1974). p201.

[107] Tseung A.C.C., Hobbs B.S.& Tantram A.D.S., Electrochimica Acta, 15, (1970), p473.

[108] Vassie P.R. & Tseung A.C.C., Electrochimica Acta, 20, (1975), p759.

[109] Tseung A.C.C., J. Applied Electrochem., 15, (1985), p575.

[110] As reference [13]

[111] As reference [14]

[112] Tseung A.C.C., Ho T.M. & Elbeik C., H_2/O_2 Recombination Device. British Patent Application No. 85.28126, (1985).

[113] Tseung A.C.C., Jiang S.P., Chen Y. & You J.K., British Patent Application No. 88.154943 (1988).